

THE SYNTHESIS AND CHARACTERIZATION OF A VARIETY OF
BIOLOGICALLY RELEVANT CAGED PHENOLS AND CATECHOLS

by

DUNCAN MCLAIN

(Under the Direction of Timothy M. Dore)

ABSTRACT

Spatio-temporal release of biologically relevant small molecules provides exquisite control over the activation of receptors and signaling pathways. This can be accomplished via a photochemical reaction that releases the desired small molecule in response to irradiation of light. A series of small molecules (serotonin, capsaicin, VNA, octopamine, tyrosine, dopamine, epinephrine, and norepinephrine) that contain either a phenol or catechol moiety were caged using either BHQ or CyHQ. In all cases the CyHQ caged compounds proved sensitive toward 1PE and 2PE processes with quantum efficiencies of 0.2 – 0.4 upon irradiation at 365 nm and two photon cross sections of 0.15 – 0.31 GM when irradiated at 740 nm. All but two compounds, BHQ-dopamine and BHQ-estradiol were found to be sensitive to both 1PE and 2PE with quantum efficiencies of 0.30 – 0.40 and two photon cross sections of 0.40 – 0.60 GM. CyHQ-epinephrine and CyHQ-norepinephrine possessed a novel photodegradation pathway that was analyzed through radical trapping experiments and product studies.

INDEX WORDS: Caged compounds, two photon excitation, dopamine, neurotransmitters, catechols, phenols.

THE SYNTHESIS AND CHARACTERIZATION OF A VARIETY OF
BIOLOGICALLY RELEVANT CAGED PHENOLS AND CATECHOLS

by

DUNCAN MCLAIN

B.S. Kennesaw State University, 2008

A Dissertation Submitted to the Graduate Faculty of The University of Georgia in Partial

Fulfillment of the Requirements for the Degree

DOCTOR OF PHILOSOPHY

ATHENS, GEORGIA

2014

© 2014

Duncan McLain

All Rights Reserved

THE SYNTHESIS AND CHARACTERIZATION OF A VARIETY OF
BIOLOGICALLY RELEVANT CAGED PHENOLS AND CATECHOLS

by

DUNCAN MCLAIN

Major Professor:	Timothy M. Dore
Committee:	George F. Majetich
	Robert S. Philips

Electronic Version Approved:

Maureen Grasso
Dean of the Graduate School
The University of Georgia
May 2014

DEDICATION

I don't think I would have gotten anywhere near as far in life as I have were it not for my parents. My path to maturity and responsibility was a remarkably long and difficult one, and they put up with a lot from me on my way there.

ACKNOWLEDGEMENTS

I would like to thank the lab members I've worked with both past and present: Adam Rea, Kyle Harris, Robert Kutlik, Stephen Flynn, Adna Muliawan, Mark Bernard, Matt O'Conner, Magnus Widegren, Shahienaz Hampton, Idrees Mohammed, Louise Ashall, and Cyril Herbivo. It's you all that have made this job an enjoyable place to be. I would also like to especially thank the people who I've worked with on the CyHQ project, the conversations and results we shared have been invaluable in enabling me to finish my research. In addition to the members of my own lab, I would also like to thank James Lauderdale and the members of his lab for the collaborations we've had as well as the informative discussions about neuroscience and application of caging groups to biological systems.

I would also like to thank my PI, Tim Dore, and my committee members, George Majetich and Robert Phillips, for providing feedback and challenging my ideas and making me a better scientist.

TABLE OF CONTENTS

	Page
ACKNOWLEDGEMENTS	v
LIST OF TABLES	xi
LIST OF FIGURES.....	xii
CHAPTER	
1 Dopamine Expression and Function	1
Introduction.....	1
Dopamine Receptor Expression Patterns and Anatomy	1
Striatal Dopamine Neurons	2
Medium Spiny Neurons	6
Prefrontal Cortex.....	8
Molecular and Cellular Dopamine Signaling.....	9
Dopaminergic Signaling	9
GPCR Signaling and DARPP-32.....	9
MEK/ERK Signaling.....	11
PLC Signaling.....	12
G _{βγ} Signaling	13
Ion Channel Regulation	13
Modulation of Pre- and Postsynaptic Neurotransmitters	14
Modulation of Neural Microcircuitry	17

2	Application of Caged Neurotransmitters.....	20
	Introduction.....	20
	Caged Glutamate	21
	Caged GABA	23
	Caged Ca ²⁺	25
	Caged IP3.....	27
	Caged Monoamines	29
	Caged Vanilloids	31
	Summary	32
3	Synthesis and Photochemistry of Biologically Relevant Caged Phenols	33
	Introduction.....	33
	Synthesis of Caged Octopamines.....	35
	Synthesis of Caged Tyrosines.....	36
	Synthesis of Caged Estradiols	37
	Synthesis of Caged Vanilloids	38
	Synthesis of Caged Serotonin.....	39
	Photochemistry of Caged Octopamines.....	40
	Photochemistry of Caged Tyrosines.....	43
	Photochemistry of Caged Estradiols	45
	Photochemistry of Caged Vanilloids.....	46
	Photochemistry of Caged Serotonin.....	48
	Debromination Analysis Under IPE	50
	Summary	52

4	Synthesis and Photochemistry of Biologically Relevant Caged Catechols.....	53
	Introduction.....	53
	Synthesis of BHQ-dopamine	55
	Synthesis of CyHQ-dopamine	56
	Synthesis of CyHQ-epinephrine and CyHQ-norepinephrine	57
	Photochemistry of Caged Dopamine.....	57
	Photochemistry of CyHQ-epinephrine and CyHQ-norepinephrine	61
	Summary.....	65
5	Experimentals	66
	General.....	66
	Synthesis of MOM-CyHQ-oMs (34)	67
	Synthesis of MOM-BHQ-octopamine (<i>N</i> -Boc) (35)	69
	Synthesis of MOM-CyHQ-octopamine (<i>N</i> -Boc) (36)	71
	Synthesis of BHQ-octopamine (37).....	73
	Synthesis of CyHQ-octopamine (38).....	75
	Synthesis of MOM-BHQ-tyrosine (<i>N</i> -Boc) (CO ₂ Me) (39).....	77
	Synthesis of MOM-CyHQ-tyrosine (<i>N</i> -Boc) (CO ₂ Me) (40).....	79
	Synthesis of BHQ-tyrosine (41).....	81
	Synthesis of CyHQ-tyrosine (42).....	83
	Synthesis of MOM-BHQ-estradiol (43).....	85
	Synthesis of MOM-CyHQ-estradiol (44).....	88
	Synthesis of BHQ-estradiol (45).....	90
	Synthesis of CyHQ-estradiol (46).....	92

Synthesis of MOM-CyHQ-VAA (47).....	94
Synthesis of MOM-CyHQ-VNA (48).....	96
Synthesis of MOM-CyHQ-capsaicin (49).....	98
Synthesis of CyHQ-VNA (50).....	100
Synthesis of CyHQ-VAA (51).....	102
Synthesis of CyHQ-capsaicin (52).....	104
Synthesis of MOM-CyHQ-serotonin (<i>N</i> -Boc) (53).....	106
Synthesis of CyHQ-serotonin (54).....	108
Synthesis of MOM-BHQ-dopamine (<i>N</i> -Boc) (63).....	110
Synthesis of BHQ-dopamine (64) and (65).....	113
Synthesis of MOM-CyHQ-dopamine (<i>N</i> -Boc) (66).....	117
Synthesis of CyHQ-dopamine (67) and (68).....	119
Synthesis of CyHQ-epinephrine (69).....	122
Synthesis of CyHQ-norepinephrine (70).....	125
Determination of quantum efficiency for one-photon photolysis	128
Determination of dark hydrolysis rate.....	130
Determination of molar absorptivity coefficient	131
Determination of fluorescence emission intensity.....	132
Determination of two-photon uncaging cross-section	133
REFERENCES	136
APPENDICES	
A Synthesis of a Warhead Free AOMK.....	151
B Toward the Optimization of the Synthesis of CyHQ	156

C	Synthesis of BHQ-ATP Sodium Salt	160
D	Synthesis and Testing of a Human Ferrochelatase Ligand	163

LIST OF TABLES

	Page
Table 1 Photochemical properties of caged octopamine compounds	43
Table 2 Photochemical properties of caged tyrosine compounds	45
Table 3 Photochemical properties of caged estradiol compounds	46
Table 4 Photochemical properties of caged vanilloid compounds	49
Table 5 Photochemical properties of caged serotonin compounds.....	50
Table 6 Comparison of calculated pK_a to photolysis for BHQ caged phenols	61

LIST OF FIGURES

	Page
Figure 1 Dopamine pathways ⁵	2
Figure 2 Striatal inputs and outputs ⁸	4
Figure 3 Dysregulation of neurotransmitter signaling in Parkinson's disease ²⁴	7
Figure 4 Activity of DARPP-32 signaling cascade(release requested) ³⁹	11
Figure 5 Selected caged glutamate compounds	22
Figure 6 Selected caged GABA compounds	24
Figure 7 Selected caged calcium compounds	26
Figure 8 Selected caged IP3 compounds	28
Figure 9 Selected caged monoamines	30
Figure 10 Selected caged vanilloids	31
Figure 11 BHQ-OAc and CyHQ-OAc.....	34
Figure 12 Synthesis of BHQ and CyHQ caged octopamine	36
Figure 13 Synthesis of BHQ and CyHQ caged tyrosine	37
Figure 14 Synthesis of BHQ and CyHQ caged estradiol.....	38
Figure 15 Synthesis of CyHQ caged VAA, VNA, and capsaicin	39
Figure 16 Synthesis of CyHQ caged serotonin.....	40
Figure 17 IPE Photolysis of BHQ-octopamine (left) and CyHQ-octopamine (right)	41
Figure 18 2PE Photolysis of BHQ-octopamine (left) or CyHQ-octopamine (right)	42
Figure 19 Bhc-octopamine	42

Figure 20 1PE Photolysis of BHQ-tyrosine (left) and CyHQ-tyrosine (right)	44
Figure 21 2PE Photolysis of BHQ-Tyrosine (left) and CyHQ-tyrosine (right)	44
Figure 22 o-CNV-tyrosine	44
Figure 23 1PE Photolysis of CyHQ-estradiol.....	45
Figure 24 2PE Photolysis of CyHQ-estradiol.....	46
Figure 25 Debromination of BHQ-estradiol.....	47
Figure 26 BHQ-VAA	47
Figure 27 1PE Photolysis of CyHQ-VAA	48
Figure 28 2PE Photolysis of CyHQ-VAA	48
Figure 29 BCMACM-capsaicin	49
Figure 30 BHQ- <i>O</i> -serotonin (60) and BHQ- <i>N</i> -serotonin (61).....	50
Figure 31 1PE Photolysis of CyHQ-serotonin.....	50
Figure 32 2PE Photolysis of CyHQ-serotonin.....	50
Figure 33 Debromination side reaction.....	51
Figure 34 Debromination of BHQ-OH as a function of optical irradiance	52
Figure 35 Comparison of rate of debromination and photolysis in BHQ-octopamine	52
Figure 36 o-NB-dopamine and RuBi-dopamine	55
Figure 37 Synthesis of BHQ-dopamine	56
Figure 38 Possible BHQ-dopamine isomers	57
Figure 39 Synthesis of CyHQ-dopamine	57
Figure 40 Synthesis of CyHQ-epinephrine and CyHQ-norepinephrine	58
Figure 41 Photochemistry of BHQ-dopamine	59
Figure 42 Fluorescence emission spectra of BHQ-dopamine and BHQ-OAc standard...	60

Figure 43 BHQ caged phenols	61
Figure 44 IPE photolysis of CyHQ-dopamine	62
Figure 45 2PE photolysis of CyHQ-dopamine	62
Figure 46 IPE photodegradation of CyHQ-epinephrine	63
Figure 47 Overlaid uHPLC absorbance traces of epinephrine and primary photoproduct	64
Figure 48 Photolysis of CyHQ-epinephrine	65
Figure 49 Potential primary photoproducts	65
Figure 50 Proposed CyHQ-epinephrine photolysis mechanism	67
Figure 51 Representative AOMK	152
Figure 52 Synthesis of warhead free AOMK	153
Figure 53 Caging Scaffold	156
Figure 54 Alternative HQ attempts	156
Figure 55 HQ formation from acetaldehyde.....	157
Figure 56 Original CyHQ formation.....	158
Figure 57 Microwave formation of CyHQ	159
Figure 58 Synthesis of BHQ-ATP	160
Figure 59 ¹ HNMR in D ₂ O of BHQ-ATP TEA Salt (black) Na Salt (red)	161
Figure 60 P2X receptor activation with BHQ-ATP, each red dot (left) corresponds to an electrophysiological response (right)	162
Figure 61 Synthesis of Corrole	164

CHAPTER 1

Dopamine Expression and Function

Introduction

Monoamines are a class of neurotransmitters and neuromodulators characterized by the presence of a phenethylamine moiety. Included in this class of compounds are the catecholamines: dopamine, epinephrine, and norepinephrine. They are formed by the metabolism of tyrosine and further specific processing inside the neuron. Catecholamines have been implicated in a wide variety of neuronal signaling processes including, growth and differentiation, long term potentiation,ⁱ learning and reward behavior, and modulation of glutamatergic and GABAergic signaling.¹

Dopamine Receptor Expression Patterns and Anatomy

Dopamine receptors (abbreviated D1-D5) are expressed broadly throughout the brain and periphery organs and tissues. In the brain dopamine receptors are expressed at high density in the nigrostriatal,ⁱⁱ mesolimbic,ⁱⁱⁱ mesocortical,^{iv} and frontal cortex areas (Figure 1 shows the major dopaminergic projection),^v they are also expressed at much lower levels in the hippocampus,^{vi} cerebellum,^{vii} thalamic^{viii} and hypothalamic^{ix} areas.

ⁱ Long lasting enhancement of signal between two neurons implicated in learning and memory formation

ⁱⁱ Major dopamine pathways, responsible for connecting the substantia nigra and the striatum

ⁱⁱⁱ Major dopamine pathway, responsible for connecting the ventral tegmental area (VTA) to the prefrontal cortex

^{iv} Major dopamine pathway, connects the VTA to the cerebral cortex in particular the frontal lobes.

^v One of four major lobes in the brain associated with reward, attention, short-term memory, planning, and motivation.

^{vi} Consolidates transformation of short-term memory to long-term memory, also involved in spatial navigation

^{vii} Involved in motor control and cognitive functions including attention, language, and regulating fear and pleasure responses

Receptors have also been found in the retinal areas (D1, D2, and D4)² and the pituitary (D2)³ and all of the receptor subtypes have been observed in the kidneys, adrenal glands, sympathetic ganglia, gastrointestinal tract, blood vessels, and heart.⁴

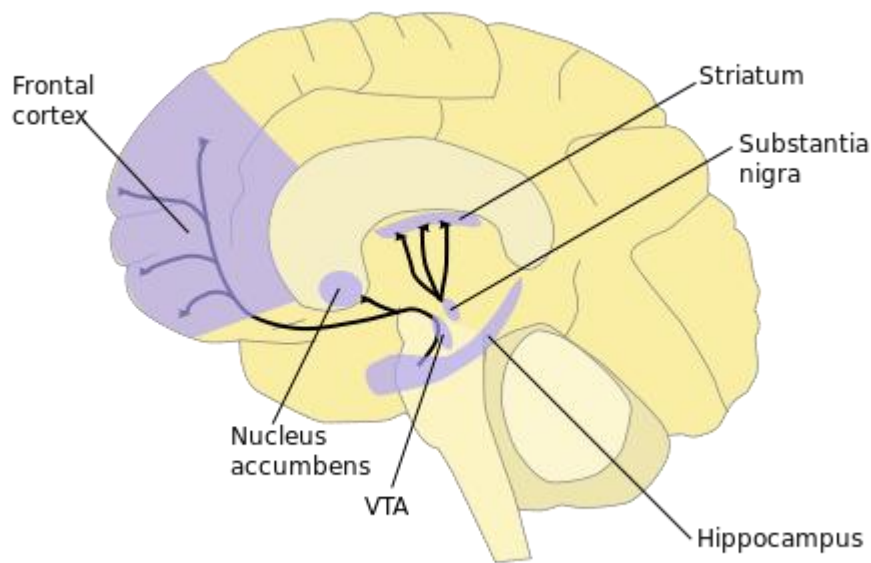


Figure 1 Dopamine pathways⁵

Striatal Dopamine Neurons

One of the more prominent dopamine systems, elucidated by histochemical analysis, is a group of midbrain dopamine neurons which project into the striatum^x and nucleus accumbens.^{xi6} These projections are organized into three distinct areas: the

^{viii} Relays sensory and motor signals to the cerebral cortex

^{ix} Links the nervous system to the endocrine system

^x Coordinates motivation with body movement, primarily inhibits unwanted behaviors and small voluntary movements

^{xi} Each hemisphere possesses its own nucleus accumbens with differing morphology and function, plays an important role in pleasure and fear, as well as the placebo effect.

ventral tegmenta,^{xii} the substantia nigra par compacta,^{xiii} and the retrorubal area (illustrated in Figure 2),^{xiv} however there is minimal anatomical difference between dopamine neurons in the three areas. Together they form a continuous system where axonal projections provide input into all parts of the striatum and nucleus accumbens. This, in turn, leads to a homogeneous distribution of dopamine neurons in the striatum with little to no clear cytoarchitectural^{xv} distinction observable between dopamine neurons in the three areas. In contrast to the homogeneity of distribution and cytoarcheticture are the underlying neural circuits that provide the functional organization found in the basal ganglia.⁷ This leads to a difficulty in determining the function of striatal dopamine neurons based on gross anatomical features and as a result there is a limited understanding of the specific nature, and number of potential subtypes of striatal dopamine neurons.

^{xii} Part of the mesolimbic system, involved in cognition, motivation, and drug addiction

^{xiii} Subset of the substantia nigra, involved in reward coding and reinforcement as well as being implicated in behavioral aspects of drug addiction

^{xiv} Midbrain projection responsible for eating and social aversion behaviors

^{xv} Cytoarchitecture refers to the arrangement and organization of somatic compartments and receptors within a specific neuron

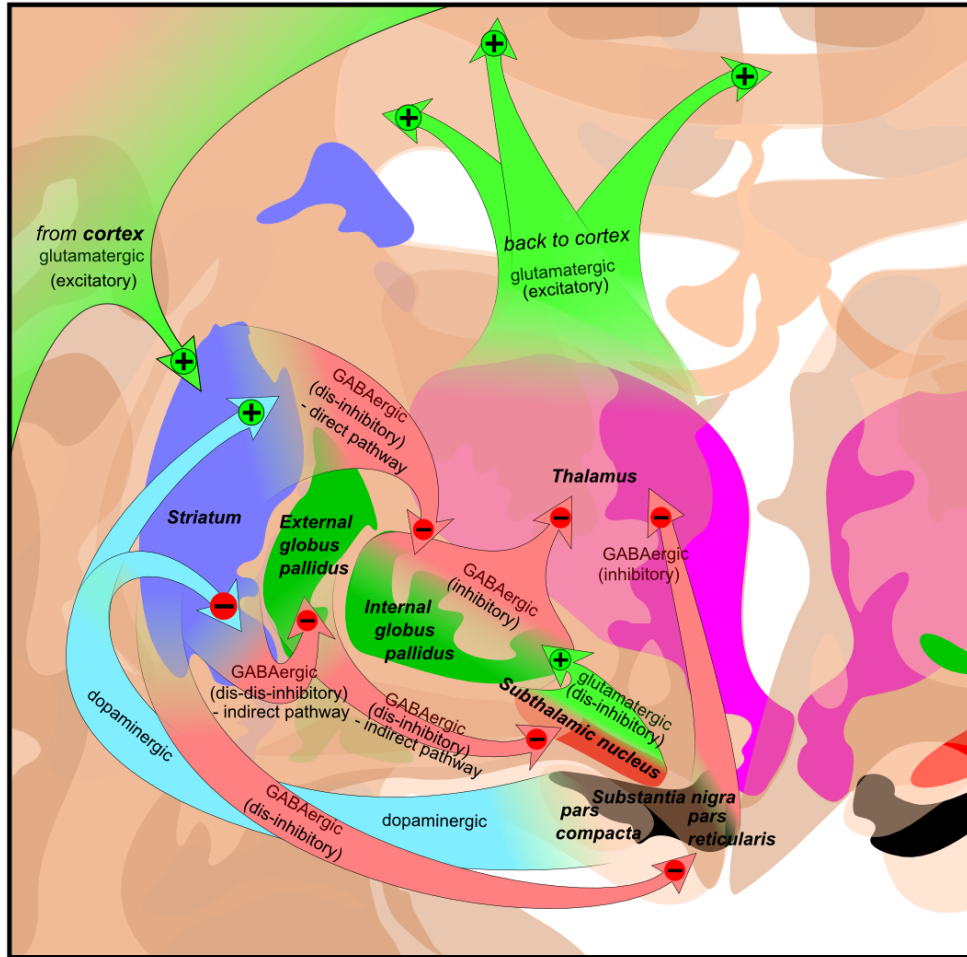


Figure 2 Striatal inputs and outputs⁸

Dopamine neurons in the striatum share some rather unique anatomical features in respect to other types of neurons. Firstly, the axonal length is around 47 cm abnormally long in comparison to the inhibitory interneurons^{xvi} whose length is 7mm. As a consequence, dopamine axons account for about 5% of the total volume of the striatum.⁹ Secondly, the number of dopamine neurons is relatively small, only around 12,000,¹⁰ when compared to the number of spiny neurons^{xvii} (around five million¹¹), and a tiny fraction of the overall number of neurons in the striatum. Finally, there is an abnormally

^{xvi} Refers to a locally projecting neuron that displays inhibitory activity primarily through GABA signaling
^{xvii} Subtype of inhibitory neuron accounting for 90-95% of the neurons in the basal ganglia, plays a key role in controlling body, limb, and eye movements

high level of arborization^{xviii} in the dendrites^{xix}: estimates have placed the number of synapses contained by striatal dopamine neurons at between 200,000 and 300,000 synapses.¹² This puts the number of synapses 3 to 4 orders of magnitude higher than other types of striatal neurons: spiny neurons are estimated to contain 300¹³ and fast spiking neurons^{xx} contain around 5000 synapses.¹⁴ The extensive arborization of a small subset of neurons provides the entirety of dopaminergic signaling in the striatum and gives rise to a number of questions regarding how and where axon potentials are propagated through the dendritic arbor.

Compartments within the striatum develop in response to early postnatal innervations^{xxi} of dopamine. This innervation dissipates rapidly as development progresses and gives way to the homogeneous distribution discussed above. Left behind is a network of patches, where innervation occurred, and matrix, where innervation did not occur.¹⁵ Axonal tracing studies have demonstrated that dopamine neurons in the substantia nigra target selectively, but not specifically the patch or matrix compartments based on dorsal vs. ventral origination respectively.¹⁶ Deep layer 5 corticostriatal neurons selectively innervate striatal patch compartments which then innervate the substantia nigra, while superficial layer 5 corticostriatal neurons innervate the matrix compartments which innervate primarily GABAergic neurons in the basal ganglia.¹⁷ This bifurcation of signal leading from patch and matrix compartments enables the

^{xviii} Term that denotes the level of dendrite branching within a neuron

^{xix} Branched projection of a neuron that propagates stimulation from adjacent axonal projections to the soma where the signal is then sent to the axon

^{xx} Fast spiking neurons tend to be inhibitory and are characterized by fast transient bursts of activity

^{xxi} stimulations

propagation of sensory signaling to the substantia nigra and the integration of sensory information with executive function^{xxii} in the basal ganglia.

Two major projections of glutamatergic activity occur in the striatum, one set is derived from the thalamus and the other is derived from the cortex. Recent immunocytochemical experiments have demonstrated that the number of thalamic (25%) and cortical (37%) projections are on the same order of magnitude.¹⁸ Further analysis of the synaptic contacts between cortical and thalamic termini showed that 96% of cortical termini and 72% of thalamic termini made contact with dendritic spines^{xxiii} and that these contacts were apposed by dopaminergic neurons 20% and 27% of the time respectively.¹⁹ These percentages are true for all areas of the striatum studied and indicate that the modulation of glutamatergic signaling by dopamine is likely not a specific result of location but rather a result of circuit level distribution and the density of dopaminergic neurons.

Medium Spiny Neurons

Medium spiny neurons (MSNs) are GABAergic neurons that make up 90% of the basal ganglia^{xxiv} and are made up of two major subtypes of neurons based on their axonal projections: direct and indirect. Direct neurons are named due to the fact that they directly innervate the substantia nigra, and indirect neurons are named because they indirectly innervate a number of different neural areas by acting on the globus pallidus.^{xxv,20} The neurons that form the direct and indirect pathways intermingle and

^{xxii} Umbrella term for regulation of cognitive processes such as reasoning, problem solving, and planning and execution

^{xxiii} Small protrusion on a dendrite that receives input from a single synapse of an axo

^{xxiv} Made up of varied subcortical neurons implicated in the control of routine behaviors and procedural learning

^{xxv} Works with cerebellum to coordinate inhibitory and excitatory activity to control subconscious movement behaviors

overlap with respect to origination in the patch or matrix areas; direct and indirect neurons are differentiated on a functional level by analyzing levels of GABA binding and the expression of various associated cofactors that result from GABAergic signaling.²¹ Later studies confirmed the differential expression of direct and indirect neurons by noting the segregation of D1 to the direct pathway and D2 to the indirect pathway.²² Differentiation of D1 and D2 receptors to direct and indirect MSNs provides a base for understanding movement disorders; such as Parkinson's, whereby disruption of dopaminergic signaling in either set of neurons results in a cascade of activation or deactivation of GABAergic signaling that leads to uncontrolled motor activity (Figure 3 provides a schematic representation of the discussed dysregulation).²³

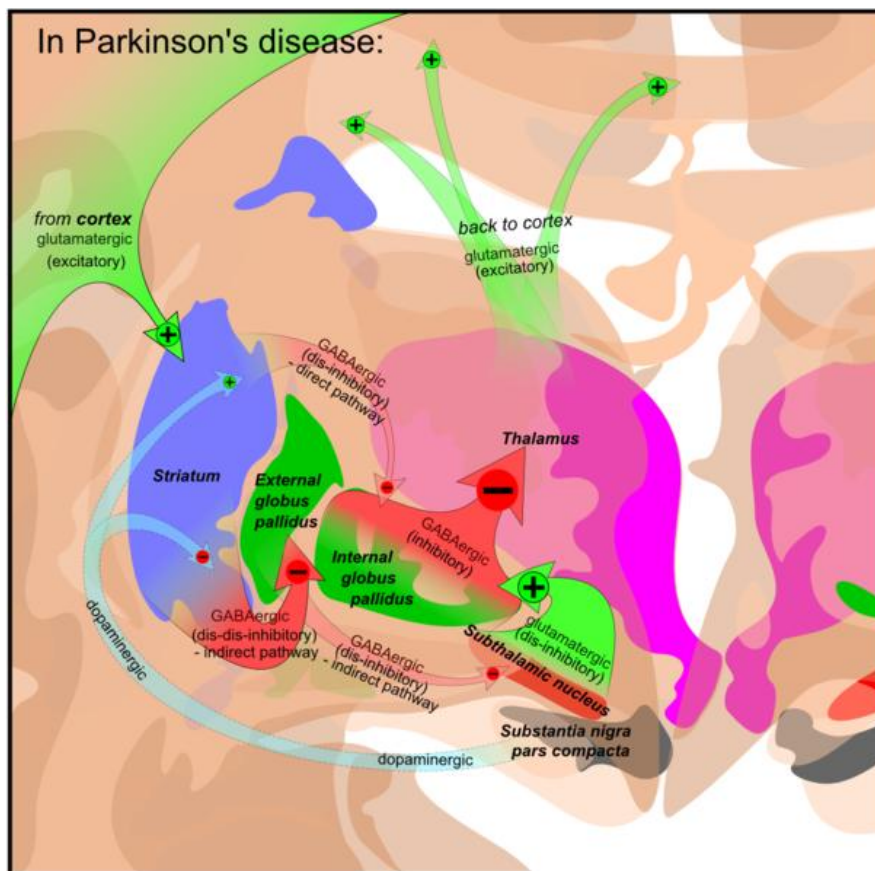


Figure 3 Dysregulation of neurotransmitter signaling in Parkinson's disease²⁴

Prefrontal Cortex

The prefrontal cortex (PFC) is involved in the regulation of thought, action, emotion, and is considered essential for human cognition.²⁵ The complexity of executive function that occurs in the PFC is a function of the diverse array of dopamine projections to various cortical and subcortical regions as well as the ability of these projections to innervate both excitatory and inhibitory neurons.²⁶ In contrast to dopamine neuron organization and distribution in the striatum, the prefrontal cortex consists of specialized, interconnected subregions.²⁷ Dopamine neurons in the PFC are also significantly structurally different from those of the striatum, in particular dopamine neurons form a bilaminar pattern^{xxvi} in the upper and deeper cortical layers, but lack the arborization found in the striatum.²⁸ Instead dopamine neurons in the PFC form varicosities, spots of vessel enlargement, about 40% of which form active synapses while the rest are thought to contribute to extrasynaptic dopamine signaling.²⁹

Synaptic dopamine in the PFC is primarily released onto dendritic spines and selectively targets the distal dendrites of pyramidal neurons^{xxvii}.²⁹ These synapses often contain both dopaminergic and glutamatergic neurons and are similar in function to the three component synapses found in the striatum.³⁰ The presence of both dopamine and glutamate at a single synapse enables both direct and indirect modulation of repeated excitatory activity between pyramidal neurons by synaptic dopamine release. The other method of dopamine signaling in the PFC involves extrasynaptic release; this occurs either through diffusion out of the synapse or through direct action on the dendritic stem. Extrasynaptic release of dopamine is hypothesized to occur due to the presence of both

^{xxvi} A bilayer of thin plates of neurons

^{xxvii} Primary excitatory neurons in the cerebral cortex, source of extensive investigation into neurotransmitter signaling

dopamine receptors and the dopamine transporter (DAT) along nonsynaptic portions of the dendrite.³¹ However, both the precise nature of signaling involved in extrasynaptic release of dopamine as well as synaptic diffusion of dopamine are poorly understood.

Molecular and Cellular Dopamine Signaling

Dopaminergic Signaling

Dopamine was first discovered as a metabolite of tyrosine in 1957 by Carlsson and coworkers, and from that point on has attracted considerable scientific interest. Immunostaining experiments, done in the 1960's identified four major dopaminergic projections in the mammalian brain: the nigrostriatal, mesolimbic, mesocortical, and tuberoinfundibular.^{xxviii,6} Along with immunostaining, early pharmacological work identified two distinct subtypes of dopamine receptors, termed D1-like^{xxix} (D1L) and D2-like (D2L) based upon their ability to activate or inhibit adenylyl cyclase (AC) respectively.³² Later genetic cloning experiments demonstrated the presence of five specific dopamine receptors labeled D1-D5, two of which activated AC (D1 and D5),³³ and three of which inhibited AC (D2, D3, and D4).³⁴

GPCR Signaling and DARPP-32

D1-like Dopamine receptors (D1R) function primarily as G-protein coupled receptors (GPCRs) and are expressed postsynaptically and stimulate cAMP production through the dissociation of the $G_{\alpha s}$ subunit and subsequent binding of adenylyl cyclase (AC); this activation leads to phosphorylation of downstream targets including protein kinase A (PKA). D2-like receptors (D2R) are expressed both pre- and postsynaptically

^{xxviii} Major dopamine pathway that connects the hypothalamus with the median eminence and is heavily involved in the regulation of endocrine system

^{xxix} Initially only two receptor subtypes were known D1 and D2, later experiments identifying other subtypes with overlapping expression and activity led to the designation D-like to indicate the combined action of the different dopamine receptors

and inhibit cAMP production through the dissociation of the $G_{\alpha i}$ subunit and subsequent binding to AC. This dual activation and inhibition allows dopamine to play both an activating and inhibitory role on PKA.¹

One of the primary targets of neuronal PKA, and one of significant scientific interest is the 32kDA dopamine and cAMP-regulated phosphoprotein (DARPP-32). DARPP-32 is predominantly expressed in MSNs and acts as a signal integrator involved in modulating cell signaling in response to a number of neurotransmitters and growth factors by inhibiting phosphoprotein 1 (PP1).³⁵ DARPP-32 is phosphorylated on threonine 34 in response to PKA activation by D1R and dephosphorylated in response to PKA inhibition by D2R. It can also be phosphorylated in response to increased Ca^{2+} levels resulting from activation of phospholipase C (PLC).³⁶ The phosphorylation state of DARPP-32 allows D1R to additionally activate PKA by inhibiting PP1 and D2R to deactivate PKA by activating PP1. The phosphorylation state of a number of ionotropic glutamate and GABA receptors is maintained by the equilibrium of PKA and PP1.³⁷ The ability to modulate glutamate and GABA receptor activity through phosphorylation has been implicated in the regulation of synaptic plasticity and long-term potentiation. DARPP-32 also integrates cyclin-dependent kinase 5 (CDK5) by phosphorylation at threonine 75, which indicates that dopamine might play a role in regulating neuronal growth and differentiation signals (the DARPP-32 signaling cascade is illustrated in Figure 4).³⁸

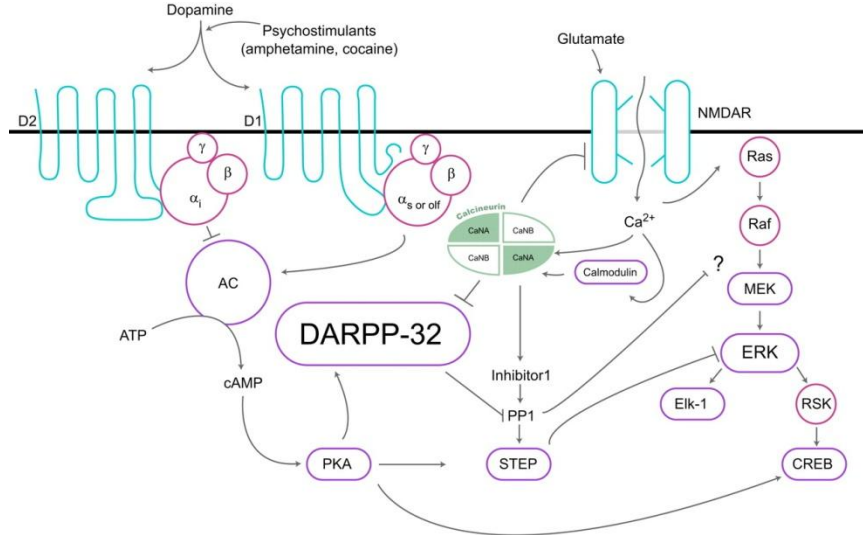


Figure 4 Activity of DARPP-32 signaling cascade (release requested)³⁹

MEK/ERK^{xxx} signaling

The downstream signaling network that is regulated by cAMP provides a mechanism for context-dependent dopamine signaling; for example many dopamine signaling responses would only occur with recent or concurrent activation of a different type of receptor. These context-dependent signaling events have been termed coincidence detectors and play an important role in the regulation of synaptic plasticity. MAP kinases (MAPKs) have been shown to act as coincidence detectors^{xxxii} that integrate dopamine signaling with that of other neurotransmitters.⁴⁰ Both D1R⁴¹ and D2R⁴² have been shown to regulate MAPK 1 and 2, with pharmacological inhibition of D2Rs by haloperidol^{xxxiii} being responsible for upregulating ERK 1 and 2 phosphorylation levels

^{xxx} Prominent intracellular signaling cascade involved in cell growth, differentiation, and gene regulation

^{xxxii} Coincidence detectors refers to the situation specific nature of signaling i.e. different contexts create different signaling results

^{xxxiii} Antipsychotic medication commonly used to treat schizophrenia acts as an inverse agonist of the D2, D3, and D4 receptors (Halodol)

while both pharmacological and genetic studies have demonstrated that D1 is essential for ERK activity in striatal MSNs.⁴³

N-Methyl-D-aspartate (NMDA) receptor^{xxxiii} activation leads to the phosphorylation of MEK, but in the absence of D1 signaling ERK is dephosphorylated by striatal-enriched tyrosine phosphatase (STEP) and no change in ERK activity has been observed.⁴⁴ In the presence of D1 signaling, PP1 is inhibited by increased phosphorylation of DARPP-32 which leads to inhibition of STEP, thus resulting in an increase in ERK activity.⁴⁵ This coregulation of ERK signaling by NMDA and D1 has been hypothesized as a route for the development of behavioral responses to drug abuse. Still, due to the precise nature and constrained spatial and temporal factors relating to coactivation of dopamine and other cellular signaling events, many of these coincidence regulators remain unknown.

PLC signaling

Calcium flux in neurons occurs through both extracellular and intracellular sources, with voltage gated channels and NMDARs being the primary source for extracellular calcium, and the endoplasmic reticulum being the primary storage for intracellular calcium.⁴⁶ Activation of intracellular calcium release comes primarily from triggering inositol 1,4,5-tris-phosphate (IP3) receptors, a downstream target of phospholipase C (PLC). DRs have demonstrated two models for upregulating PLC; D5 transfected into HEK293 cells induced significant calcium flux, whereas D1 transfected cells exhibited no change in calcium flux, and D1/D2 cotransfected cells have induced similar calcium flux changes.⁴⁷ Coexpression of D1 and D2 has been demonstrated by

^{xxxiii} NMDA is a specific agonist of the NMDA receptor (NMDAR). NMDAR is an ionotropic glutamate receptor with a voltage dependent activation due to extracellular channel blockage by Mg²⁺ ions

immunohistological studies, and a study of rat pyramidal neurons utilizing a CFP tagged D1 and YFP tagged D2 receptor demonstrated significant FRET based signaling.⁴⁸ The exact mechanism by which D5 regulates calcium flux is unknown as is the physiological significance of coexpression of D1/D2.

G_{βγ} signaling

G_{βγ}^{xxxiv} subunits separate from the G_α subunits following receptor activation and D2 regulated G_{βγ} has been shown to increase intracellular calcium levels in MSNs. D2 responsive G_{βγ} has also been shown to reduce the level of L-type calcium signaling^{xxxv} and regulate the activity of N-type calcium signaling^{xxxvi}. These subunits are also involved in the regulation of potassium flux through modulating G-protein coupled inwardly rectifying potassium channels^{xxxvii} (GIRKs).⁴⁹

The activity of the G_{βγ} complex acting on N-type calcium receptors enables an additional signaling complexity through modulating available pools neurotransmitters at the presynaptic termini and potentially contributing to presynaptic plasticity. G_{βγ} by acting on L-type calcium receptors acts postsynaptically through recruiting phospholipase A and C and modulating synaptic expression of receptors through downstream gene regulation.

Ion channel regulation

D1 and N-type calcium channels are coexpressed and colocalized in the prefrontal cortex. A recent study demonstrated the ability of the second intracellular loop of D1 to

^{xxxiv} G_{βγ} is a dimeric protein complex containing beta and gamma subunits that when released from the G protein complex enable signal transduction

^{xxxv} Refers to long lasting, postsynaptic, inward directing, calcium current that is involved in gene expression, synaptic efficiency, and cell survival.

^{xxxvi} Refers to presynaptic calcium signaling that is involved in synaptogenesis and neurotransmission

^{xxxvii} Fluxes potassium ions back into the neuron, enables neuron to return to resting state polarization.

directly interact with the C-terminus of the N-type calcium channel Cav2.2 and activation of D1 can lead to a dimerization event the results in the internalization of Cav2.2.⁵⁰ The C-terminus of D1 also interacts with two distinct intracellular portions of the NMDA receptor NR1 and NR2; these interactions are facilitated by the synaptic scaffolding protein (PSD-95) which can bind to both NMDAR and D1.⁵¹ The binding of D1 NMDA and PSD-95 anchors D1 to the cell membrane, and changes in the subcellular environment can preferentially cause binding of PSD-95 to NMDAR and thus facilitate internalization of D1.⁵² D1 NMDA interaction with NR1 results in the recruitment of calmodulin and PI3K and the activation of a cell signaling cascade, while the interaction with NR2 results in the inhibition of NMDA based currents.⁵³

Dopamine receptors can modulate the activity of ion channels directly through protein-protein interactions. These receptors can also act indirectly through $G_{\beta\gamma}$ subunits or through intermediary signaling proteins like DARPP-32. This complexity of regulation indicates that the role dopamine, and the dopamine receptors play, is determined by a wide array of potential signaling states and environments. Investigation into the multiplicity of signaling possibilities that dopamine is capable of generating will most likely proceed from a precise spatial and temporal dissection of those states and environments.

Modulation of pre- and postsynaptic neurotransmitters

As discussed above there are a wide variety of mechanisms through which dopamine may affect cellular signaling events. This is uniquely relevant, and difficult to study pharmacologically, in regards to presynaptic modulation of neurotransmitter release. Dopamine is classically considered a neuromodulator, this means that its role in

neural signaling stems from the ways in which it is capable of modulating the strength, duration, and intensity of the neurotransmitters glutamate and GABA. This modulation can occur at both synaptic and extrasynaptic points, result in different signaling motifs depending on whether the signal was proximal or distal to the soma, and perform in either a complementary or oppositional manner depending upon the precise spatial location of the signal itself.⁵⁴ Neuromodulation of any given synapse occurs by influencing either the pre- or post-synaptic neuron. One of the more important ways that presynaptic neurons are modulated is by changing the release probability of a given neurotransmitter. This presynaptic modulation can result from either direct action on the presynaptic neuron or through release of a retrograde signaling molecule^{xxxviii} from the postsynaptic neuron.

Dopamine has been implicated in regulating the release probability of both glutamatergic and GABAergic neurons. In accord with the classical understanding of dopamine^{xxxix} D2-like receptor activation leads to a decrease of glutamate release onto SPN's in both dorsal and ventral striatum.⁵⁵ D2-like receptors have also been shown to decrease GABA release onto pyramidal neurons,⁵⁶ SPNs,⁵⁷ and striatal interneurons.⁵⁸ D1-like receptors have also been shown to reduce GABA release onto fast-spiking interneurons⁵⁹ and SPNs, but only in the ventral striatum.⁶⁰ There are some notable exceptions to this view, however. The D2 receptor agonist quinpirole was shown to increase GABA release in one third of synaptic connections between fast spiking interneuron projections onto SPNs in nucleus accumbens and decrease GABA release in another third of said connections.⁵⁷ In addition, dopamine differentially affects GABA

^{xxxviii} Signaling molecule that is released postsynaptically and travels to the presynaptic termini

^{xxxix} D2 receptors being generally deactivating through inhibition of adenylyl cyclase most activation of D2 receptors leads to a decrease of signal.

signaling in the cortex by enhancing signaling from non fast-spiking neurons and depressing GABA release from fast-spiking neurons.⁶¹ The molecular mechanisms involved in dopamine's modulation of presynaptic neurons are poorly understood due to technical issues associated with probing presynaptic signaling cascades.⁵⁴ Nonetheless there are a few lines of research indicating that dopamine acts to inhibit voltage gated calcium channels $Ca_{v2.1}$ and $Ca_{v2.2}$; these channels are primarily responsible for initiating neurotransmission in the CNS and are a likely substrate for understanding the presynaptic effects of dopamine. In addition to direct modulation of neurotransmitter release, dopamine has been shown to modulate activity of cholinergic interneurons and can promote the postsynaptic release of adenosine and endocannabinoids^{x1} which can influence presynaptic neurons.⁶²

Modulation of postsynaptic neurons by dopamine is more thoroughly understood and occurs primarily through targeting NMDA and AMPA^{xii} receptors (AMPAr). Bath application of D1 agonists has shown that D1 receptor activation can potentiate extrasynaptic NMDA function, most likely through trafficking and phosphorylation of the NMDA receptor itself, though there is some disagreement over the identity of the intracellular effectors involved.⁶³ Identifying if and how dopamine modulates synaptic NMDAr activity has been more difficult. D1-like receptors have been shown to potentiate evoked NMDAr responses through PKA and PKC pathways in the prefrontal cortex,⁶⁴ while D-2 like receptors have been shown to reduce PKA mediated NMDAr response.⁶⁵ Co-application of D1-like⁶⁶ or D2-like⁶⁷ agonists in the presence of exogenous NMDA have been shown to attenuate the evoked response. Additionally D-4

^{x1} A group of lipid based neuromodulators involved in appetite, pain-sensation, mood, and memory

^{xii} α -amino-3-hydroxy-5-methyl-4-isooxazolepropionic acid

receptor activation suppresses NMDAR activity through a PKA-dependent receptor internalization.⁶⁶ Taken together, these data indicate that dopamine is able to both activate and deactivate NMDAR through either D1-like or D2-like receptors depending upon the identity and spatial location of the neuron in question. D1 agonists have shown to promote a PKA dependent phosphorylation of the AMPAR, while D2 receptor agonists promote the dephosphorylation of AMPAR through PP1.⁶⁸ In addition D2-like receptor agonists have been demonstrated to reduce the evoked response of AMPAR activation.⁶⁷ D1 receptor activation in cultured neurons has been shown to increase surface AMPAR expression.⁶⁹ It is important to note that dopamine signaling alone is insufficient to recruit AMPARs to postsynaptic terminals,⁷⁰ this is likely due the fact that AMPAR surface expression and lateral diffusion are governed by two distinct regulatory pathways.⁷¹

Modulation of microcircuits

One of the emergent properties of neural connectivity is the creation of microcircuitry, which is the connection of two or more neurons that are capable of modulating their own activity through a feedback or feed forward loop. These circuits are prominent in the cortico-striatal and thalamo-cortical regions of the brain and help to modulate a wide variety of behavioral systems.

The simplest striatal microcircuit is formed by the interaction of glutamatergic cortical pyramidal neurons and SPNs; the synapses are formed exclusively on the dendritic portion of the SPN and rise to a peak density 50 μm from the soma and drop in density rapidly.⁷² Individual cortical neurons connect to only one SPN, although most do so at multiple points.⁷³ An SPN requires a spatially regulated activation of cortical

neurons to overcome its highly negatively charged resting state potential (-90 mV)⁷⁴ at which point it reaches an up-state that lasts several hundred milliseconds and begins a spiking behavior that is independent from activation.⁷⁵

The neuromodulatory effect of dopamine for corticostriatal microcircuits is consistent with previous examples: D2 activation impedes up-state activation^{xlii} and reduces the spiking behavior when reached, while D1 activation accomplishes the reverse.⁷⁶ The process by which this occurs is not entirely understood, but some pieces are known. In the somatic regions where spiking behavior is generated, D2 activation reduces inward depolarizing currents^{xliii} through voltage gated calcium and sodium channels while increasing the influx of potassium ions through potassium channels^{xliv}.⁴⁹ D2 receptor activation also reduces presynaptic glutamate release, although whether dopamine acts pre- or postsynaptically is not yet known.⁷⁷ D1 activation as mentioned performs almost the exact opposite role, where D1 activation increases PKA activity, which in turn activates voltage gated calcium channels and inhibits somatic potassium currents.⁷⁸ In addition, D1 receptor activation decreases the opening of small conductance potassium channels which limit the rate of spiking in up-state SPNs.⁷⁹

A less direct way of modulating SPN activity is through a feed forward corticostriatal circuit where fast spiking, parvalbumin positive GABAergic interneurons receive glutamatergic input from pyramidal neurons and convey this activity to the SPN.⁸⁰ The inhibitory activity of GABAergic neurons provides a feedforward inhibition

^{xlii} Up-state, and the corresponding down-state refer to the observation that there are two sub-threshold resting states for a given neuron, one that is more negatively charged (down-state) and one that is less negatively charged (up-state). This arises either from intrinsic properties or because the network the neuron is in imposes this bistability.

^{xliii} Occurs through the influx of sodium and calcium ions through their respective ion channels

^{xliv} Potassium and chloride inhibit depolarization due to the resting potential of potassium being ~ -75 mV

circuit that is hypothesized to contribute to action selection by suppressing the SPN activity associated with unwanted actions.⁸¹ The role dopamine plays in this circuit is more straightforward as dopaminergic projections, primarily expressing D2 receptors, from the Globus Pallidus project heavily into the GABAergic interneurons.⁸² D2 receptor agonists have been shown to depress GABAergic inputs to fast spiking interneurons,⁸³ and it is likely that this contributes to reducing the gating effect observed in the movement disorder dystonia.

In contrast to the feedforward inhibition circuit is the feedback corticostriatal circuit formed by the connection of at least two SPNs. The regulation of this microcircuit is distinct in that there is a baseline level of dopamine always present that works to increase the lateral integration of signals, and transient elevations or depressions of dopamine concentration either increases or decreases the level of lateral inhibition, respectively.⁸⁴

Dopamine as a neuromodulator is crucial for regulating a number of complex autonomic and voluntary behavioral processes. It has been heavily implicated in both reward and decision making and the dysregulation of dopamine release has been hypothesized as the physiological underpinning of a number of psychological diseases including schizophrenia and substance addiction. These complex behavioral and physiological phenomena undoubtedly arise from the complex interplay of cellular signaling events described above and the ability to tie together behavioral events with their synaptic antecedents would be invaluable.

Chapter 2

Application of Caged Neurotransmitters

Introduction

The study of neuroscience is complicated by the sheer number of possible interactions both at the single synapse level, where individual receptors can be affected by a wide variety of primary and secondary messengers, and neurons themselves can be effected by feedback and feedforward circuits to the extent that one neuron is capable of modulating its own activity. The sheer complexity of the systems involved combined with the sub-millisecond temporal resolution of membrane depolarization have made it complicated to isolate which effects are involved in the generation, modulation, and propagation of signals inside the brain.⁸⁵ The ability to isolate variables and study them with exquisite spatial and temporal resolution is thus a major hurdle to generating a complete understanding of synaptic and circuit level neuroscience. To that end, a number of small molecule probes have been generated, notably among them two photon responsive caging groups that can release primary and secondary messengers on microsecond timescales and with femtoliter spatial resolution.⁸⁶

Caged compounds release a biological effector in response to light irradiation. This means of activation is orthogonal to other biological processes and is particularly useful in both tissue slice and tissue culture experiments because the desired effector can be released without complicating factors arising from the uncaging method. Brain slices and neuronal cell cultures are both commonly used to examine the role of individual

synapses and small recurrent neural circuits. Bath application of the caged compound followed by light irradiation induces a physiological response. The light used determines the spatial resolution of activation, lamps are used to induce global activation of the sample in question, a one photon laser will provide sub micrometer resolution in the XY plane, and a two photon laser will provide sub femtoliter spatial resolution. Due to the light intensities typically required for photolysis laser irradiation is typically accomplished a short distance away from the neural process being studied.

Caged Glutamate

Glutamate is the primary excitatory neurotransmitter in the CNS and the ability to activate neurons at the cell or synapse is a highly desired tool for dissecting neural circuits. It is therefore not surprising that a significant amount of research has gone into making photolabile probes for glutamate receptors with both one and two photon sensitivity. A number of labs have synthesized versions of caged glutamate and attempted to apply them to biological systems (Figure 5). Thompson's lab generated a nitro-coumarin caged glutamate **1**⁸⁷ and utilized it to study the dendritic compartmentalization of potassium conductances.⁸⁸ Kao and coworkers generated a carboxy-nitrobenzyl caged glutamate **2**⁸⁹ and used it as a proof of principle to examine localized calcium flux in the sarcoplasmic reticulum. The *para*-hydroxyphenacyl (pHP) caged glutamate **3** was synthesized by Kandler and coworkers,⁹⁰ but, unfortunately, the pHP caging group possesses only limited two photon sensitivity and so it has only been examined under one photon excitation. Furuta et. al. synthesized a bromo-hydroxycoumarin caged glutamate **6** that demonstrated good two photon sensitivity and used it in a proof of concept to map intact neuronal slices for glutamate sensitivity.⁹¹

Acyl-nitroindole (NI) caged glutamate **4**⁹² was the first generation of the widely used nitroindole scaffold but has received less attention than its counterpart methoxy-nitroindole (MNI) **5** due to its relatively lower sensitivity to 2PE.⁹³ Despite its reduced activity NI glutamate has been utilized to probe a number of complex signaling phenomena including: an uncommon inhibitory activity by metabotropic glutamate receptors (mGluR) in layer 4 cortical neurons,⁹⁴ distinct signaling profiles for intracortical layer 4 vs. layer 6 neurons,⁹⁵ and a biphasic calcium spike in rat purkinje neurons^{xlv} mediated by mGluR1^{xlvi}.⁹⁶

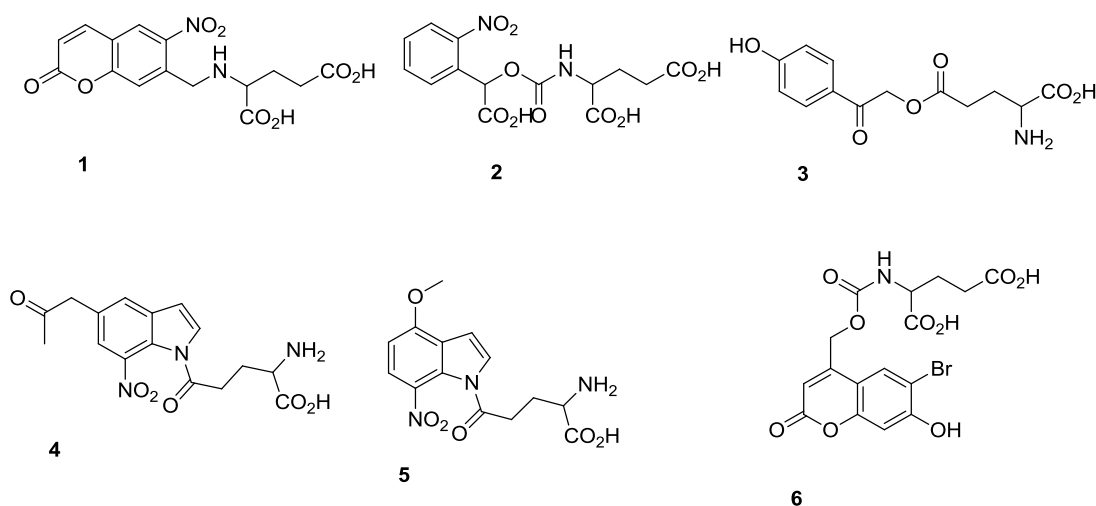


Figure 5 Selected caged glutamate compounds

By far the two most commonly encountered two photon sensitive caged glutamate is MNI-glutamate (**5**). MNI-glutamate was developed after a systematic investigation into the substituent effects of the original NI-glutamate that led to a fourfold increase in

^{xlv} Inhibitory neurons in the cerebellum and are the sole output of all the motor coordination from the cerebellar cortex

^{xlvi} Activation of mGluR1 leads to activation of the phospholipase C pathway

sensitivity toward two photon excitation.⁹² MNI-glutamate has been used to ascertain glutamate clearance rates from hippocampal CA1 astrocytes,⁹⁷ to study the channel opening kinetics⁹⁸ and glutamate occupancy time⁹⁹ of mGluR1, to examine the distribution of glutamate receptors in cortical¹⁰⁰ and hippocampal pyramidal neurons,¹⁰¹ to examine epileptic neural activity,¹⁰² synaptic plasticity,¹⁰³ but perhaps the most prominent use of MNI-glutamate has been in mapping neural circuits.¹⁰⁴

None of the caged glutamates possess optimal biological or photochemical properties. **1** and **2** lack 2PE sensitivity, **1**, **2**, **4**, **5**, and **6** have slow release kinetics either due to a decarboxylation reaction required for full activity (**2** and **6**)¹⁰⁵ or the ~millisecond release of nitrobenzyl photolysis¹⁰⁶ (**1**, **4**, and **5**), in addition to those limitations, **4** and **5** display activity even in the dark. The extensive utilization of **5** stems primarily from its commercial availability, but despite its well studied drawbacks,¹⁰⁷ the advantages offered by 2PE mediated release of glutamate have been deemed worthwhile.

Caged GABA

If glutamate is the primary excitatory neurotransmitter in the CNS then GABA performs the opposite role as the primary inhibitory neurotransmitter in the CNS. However, when compared with caged glutamate, there has been significantly less progress in generating a caged GABA with good optical properties for two photon excitation. This lack of caging groups is due primarily to the difficulty of existing caging groups to rapidly and directly release amines and amides. There are, however, four notable exceptions to this (Figure 6); a diethylaminocoumarin (DEAC) caged GABA **7**,¹⁰⁸ a biphenyl nitrophenethyl GABA **8**,¹⁰⁹ a carboxy-nitroindole derivative **9**¹¹⁰ and an inorganic ruthenium bipyridinyl (RuBi) caged GABA **10**.¹¹¹ While all four compounds

demonstrated proof of principle biological activity only RuBi-GABA has been investigated further.^{112,113}

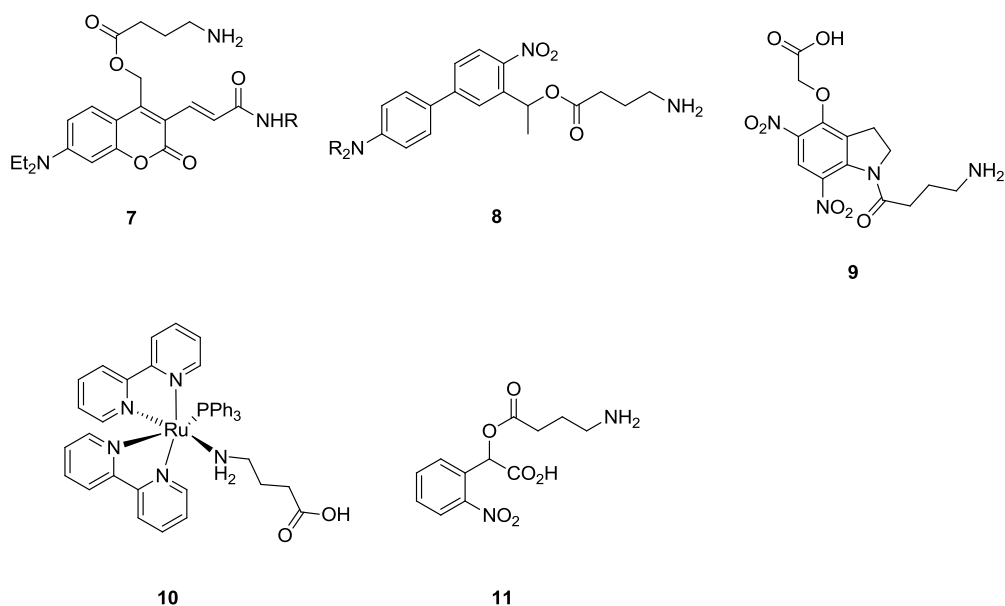


Figure 6 Selected caged GABA compounds

There has been more in depth study utilizing one photon responsive caged GABA, in particular CNB-GABA **11** synthesized by Hess and coworkers in 1994.¹¹⁴ Khirug et. al. demonstrated the presence of a negative charge gradient on the axonal initial segment of cortical principal neurons that depends heavily on localized distribution of chloride transporters.¹¹⁵ CNB-GABA has been used to suppress seizure like activity in rat brain slices,¹¹⁶ Dellal and coworkers demonstrated that localized GABA release in already depolarized cerebellar parallel fiber axons had an unexpected activating effect,¹¹⁷ and depression of calcium influx resulting from synaptic GABA spillover was measured.¹¹⁸

Both **7** and **10** exhibit good 2PE sensitivity and fast uncaging kinetics, however, the ester linkage for **7** renders the compound prone to dark state hydrolysis, the potential toxicity of the Ru scaffold in **10** is also of concern, but no definitive studies have been performed.

Caged Ca⁺²

Ca⁺² performs two major functions in the CNS. The first and most important is that upon activation of a neuron, ion channels open and allow calcium to flux into the neuron resulting in membrane depolarization and a concomitant neurotransmitter release. The second role calcium plays is through modulation of postsynaptic Ca⁺² concentration through direct binding to Ryanodine receptors or indirectly through the modulation of the PLC pathway.⁸⁵

In the late 1980's two labs independently developed caged calcium compounds (Figure 7), both based on the nitrobenzyl caging group: nitr-5 **12**¹¹⁹ developed by Tsien et. al. utilizing the BAPTA scaffold for Ca⁺² chelation, and DM-nitrophen **13**¹²⁰ developed by Davies and coworkers that utilized the EDTA scaffold for Ca⁺² chelation. The first true experiments involving caged Ca⁺² were simple in design, but demonstrated the powerful utility of these compounds, Tsien and coworkers were able to generate a dose response curve between released Ca⁺² and evoked K⁺ currents,¹²¹ while Zucker and Haydon were able to definitively answer the question of whether membrane potential altered neurotransmitter secretion by showing that it did not.¹²² Utilizing DM-nitrophen Zucker and coworkers revisited the nature of neurotransmitter secretion in relation to membrane polarization in crayfish motor neurons and found similar results, membrane polarization did not affect neurotransmitter release, but Ca²⁺ release near neurotransmitter

release sites did.¹²³ With these experiments in mind, Thomas and Almers utilized DM-nitrophen to probe rates of vesicle fusion in response to Ca^{2+} gradients, and found three distinct phases: one fast and two slow.¹²⁴ Further experiments with DM-nitrophen were able to elucidate the kinetics of the fast step ($17,000 \text{ s}^{-1}$),¹²⁵ the two slow steps ($7,000 \text{ s}^{-1}$ and 500 s^{-1}),¹²⁶ as well as the affinity ($7\text{-}21 \mu\text{M}$)¹²⁷ for Ca^{2+} of the fast step. Neher and coworkers used their previously developed methodology to then test retinal bipolar neurons and noted, interestingly, that there was only one phase of vesicle fusion; however, that phase was much faster ($1,200,000 \text{ s}^{-1}$).¹²⁸

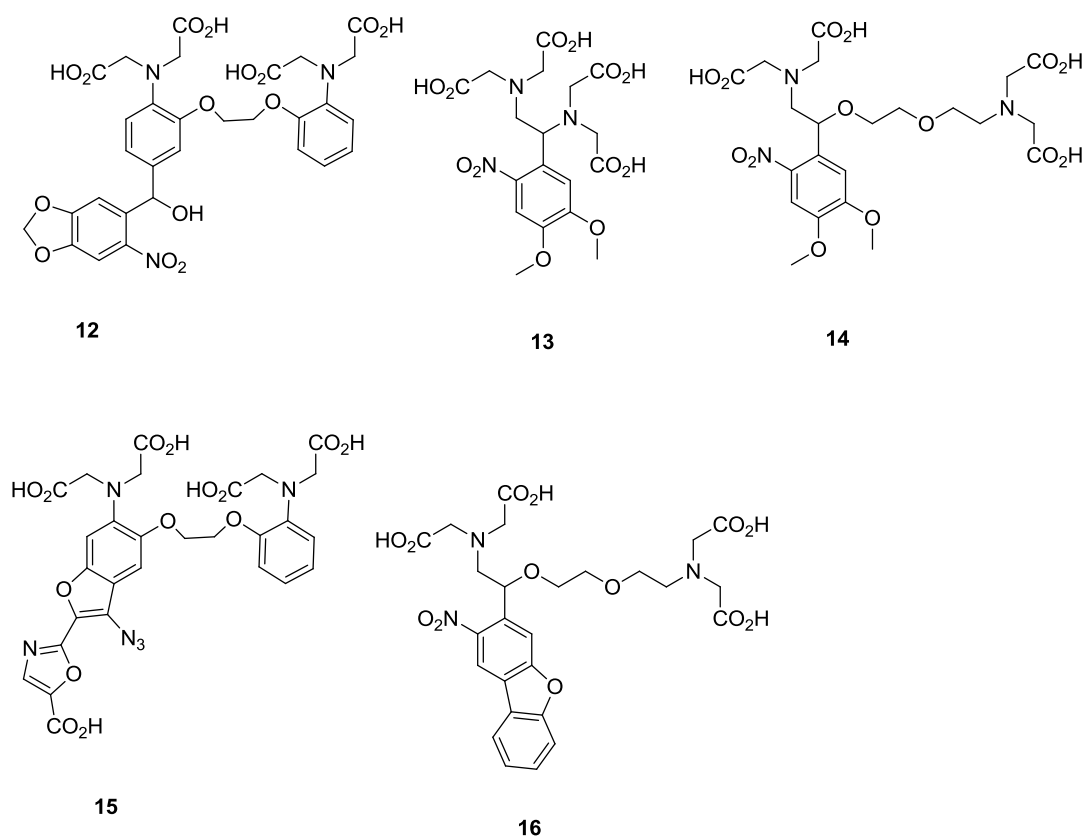
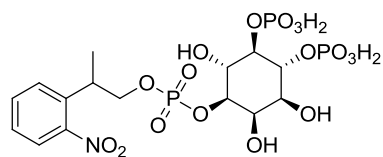


Figure 7 Selected caged calcium compounds

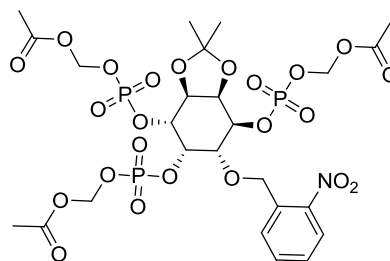
While both Nitr-5 and DM-nitrophen were successfully used to study a wide variety of neurological phenomena, neither cage was particularly well-suited for two photon mediated photolysis.⁸⁵ This necessitated the generation of a new series of compounds DMNPE **14**¹²⁹ based on a dimethoxynitrobenzyl scaffold, azid-1 **15**¹³⁰ based on the light driven fluorescence quenching of a flura-2 analogue, and NDBF **16**¹³¹ based on the nitrodibenzylfuran scaffold. Despite the favorable optical properties of both NDBF and azid-1 there has been limited application of these compounds in a two photon regime.

Caged IP3

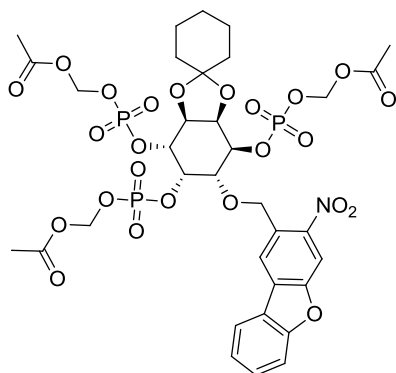
Inositol triphosphate (IP3) is a secondary messenger that acts primarily on the PLC pathway, and is capable of releasing intracellular stores of Ca^{2+} by activating IP3 receptors (IP3R) on the endoplasmic reticulum (ER). Due to several technical limitations regarding the release of caged Ca^{2+} ,⁸⁵ it may often prove more advantageous to trigger Ca^{2+} release through this indirect pathway. The first use of a caged IP3 was a nitrophenethyl derivative **17**¹³² (Figure 8) that the kinetics of examined smooth muscle contractions in response to laser flash photolysis. Due to the high hydrophilicity of the IP3 moiety, cell permeant variants have been developed **18**¹³³ that have been functionalized with AM and PM esters that are quickly hydrolyzed intracellularly. With this cell permeant variant, Wang et. al. were able to demonstrate a coincidence detector in purkinje cells that changes behavior based upon whether IP3 or Ca^{2+} release is triggered first.¹³⁴



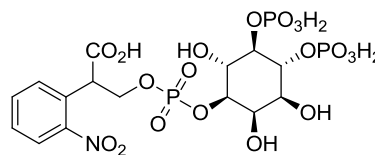
17



18



19



20

Figure 8 Selected caged IP3 compounds

Long-term depression (LTD) is an activity dependent reduction in the efficacy of neurons that can last multiple hours. This process can occur in many areas of the CNS, but is most prominently observed in the cerebellum. LTD, combined with its counterpart, long term potentiation (LTP), are thought to contribute to the selective strengthening and weakening of learning and memory. Tanaka et al. were able to show that intracellular release of Ca^{2+} via a cell permeant caged IP3 in conjunction with tetanic stimulation induces LTD in layer II/III cortical pyramidal neurons.¹³⁵ Kawato and coworkers also utilized a cell permeant caged IP3 in rat cerebellar purkinje cells to find that sustained increases in Ca^{2+} were correlated with an increase in the amount of IP3 required for subsequent Ca^{2+} release.¹³⁶

Davies and coworkers have also synthesized a caged IP3 based on the NDBF scaffold **19**¹³⁷ and utilized it to compare subcellular Ca²⁺ release in wildtype vs two mouse models of Alzheimer's disease. They noted that there were non-propagating astrocytic Ca²⁺ signaling events resulting from the localized activation of IP3 receptors and posited a possible connection between gliotransmission perturbation and Alzheimer's disease.¹³⁸ This hypothesis built off earlier work by Parker et. al. who utilized a carboxy-nitrobenzyl (CNB) caged IP3 **20** to demonstrate a link between Ca²⁺ hyperactivity and a presenilin 1 mutation in rat cortical neurons.¹³⁹

Caged Monoamines

As described in the previous chapter, monoamines play a complicated and often contradictory role in neurotransmission depending on a number of context-dependent cues that can depend on a myriad of variables. Despite the complexity of function of these neuromodulators, and the seemingly perfect fit that would exist with caging group technology, due to the precise spatial and temporal control over neuron activation, surprisingly little investigation has been undertaken.

Muralidharan and Nerbonne synthesized a series of adrenergic agonists caged with a nitrobenzyl group **21** and **22** (Figure 9),¹⁴⁰ but application of these compounds to biological systems has yet to occur. Hess and coworkers synthesized a carboxy-nitrobenzyl caged serotonin **23** and used it to investigate the kinetics of the 5-HT₃ receptor.¹⁴¹ Further investigation of the 5-HT₃ receptor showed that the commercially available antidepressant fluoxetine (Prozac) occupied a different regulatory site than nicotine or cocaine.¹⁴² There has been slightly more investigation into caged dopamine,

depolarization and action potential firing.¹⁴⁶ The primary advantage is the large conductance induced by TRPV1 activation which allows for modulation of membrane potential at low TRPV1 expression levels.¹⁴⁷ Miesenbock and coworkers synthesized a DMNB caged capsaicin **26** (Figure 10) and demonstrated the applicability of the system to activate single neurons in cell culture.¹⁴⁸ A number of other groups have synthesized caged vanilloids and demonstrated their applicability to biological systems **27** and **28**.¹⁴⁹ Kao et. al. later demonstrated that the DMNB caged capsaicin was sufficiently sensitive to two photon mediated photolysis to activate dissociated neurons.¹⁵⁰

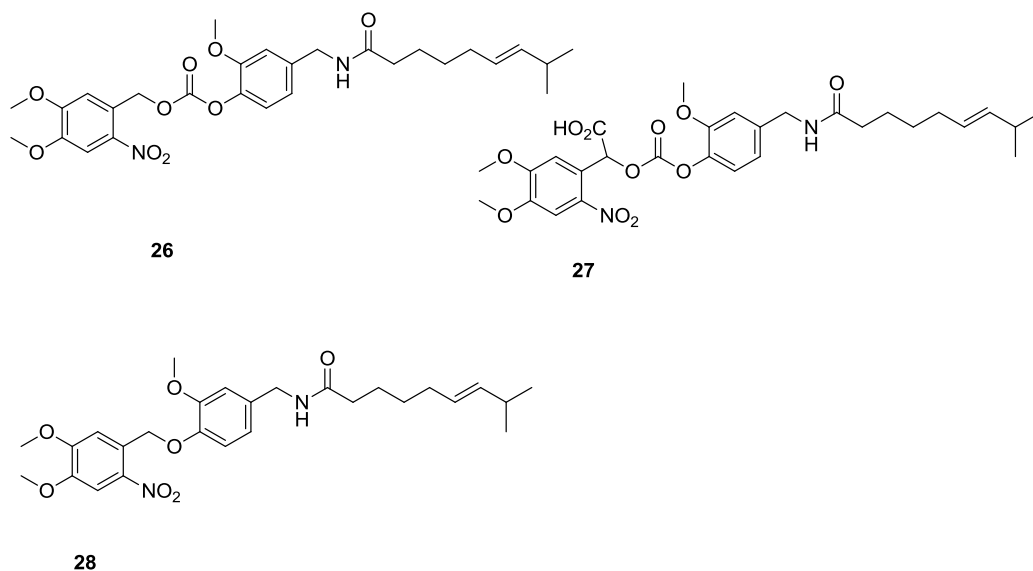


Figure 10 Selected caged vanilloids

Summary

Caged compounds are well situated to assist in dissecting the precise spatial and temporal signaling cues of neural circuits. They have demonstrated effectiveness in a number of applications ranging from the single synapse level to whole tissue activation. Despite these studies many caged compounds exhibit poor release kinetics, ranging from millisecond to second scale release, and low GM values. Improvements in the release

kinetics would allow further investigation into fast, sub microsecond, dynamic cellular processes. Increased GM values would enable 2PE uncaging on intracellular targets, a strategy that is currently limited by the high laser power required to affect uncaging.

Chapter 3

Synthesis and Photochemistry of Biologically Relevant Caged Phenols

Introduction

The phenolic functional group is a recurrent theme in biologically active small molecules, from basic building blocks such as the amino acid tyrosine to much more complex signaling molecules like estradiol. Phenols occupy a wide range of structure and an even wider range of function, and with any suitably complex signaling cascade the underlying processes give rise to an even greater array of potential outcomes. It is with this complexity in mind that investigation into the precise spatial and temporal regulation of these signaling cascades occurs.

One way to investigate the precise regulation of these processes is through the utilization of an orthogonal method to initiate or propagate specific steps in the desired process. Light is one such method and has found wide use in biological experiments. Optogenetic tools have placed membrane depolarization under the control of light and a retinal cofactor,¹⁵¹ photoaffinity labeling experiments have elucidated substrate/protein binding interactions,¹⁵² and a truly staggering number of fluorescent reporters have enabled the analysis of a variety of physiological states.¹⁵³

As described in chapter 2 there is another category of tools that can be activated via light: caged compounds. The identity and biological utility of caged compounds have been covered both here and elsewhere.^{85-86, 106, 146, 154} The applicability of caged compounds to a biological system is determined by certain parameters. For one photon

excitation (1PE) those parameters are the excitation wavelength, kinetics of photolysis, quantum efficiency, and the lack of undesired photochemical byproducts. For two photon excitation (2PE) the parameters are similar. Excitation wavelength, kinetics of photolysis, and the lack of undesired photoproducts are once again important however; the quantum efficiency parameter is replaced by the 2PE uncaging cross-section (GM), though this parameter is comparable in nature to one photon uncaging efficiency $(Q_u \cdot \epsilon)$.¹⁰⁶

Quantum efficiency is a relatively straightforward measurement that compares the ratio of photons that pass through a sample vs. the number of photons that are absorbed and trigger a photochemical reaction. The absorbance cross-section is similar to ϵ in that it represents the probability that a chromophore will simultaneously absorb two photons of light (reported in GM, $10^{-50} \cdot \text{cm}^4 \cdot \text{s} \cdot \text{photon}^{-1}$). Tsien and coworkers suggested that 0.10 GM was the threshold needed for biological application,⁹¹ this number is widely accepted in the field, although other researchers have placed it as high as 31 GM.¹⁵⁵

The Dore lab has demonstrated that both BHQ-OAc **29** and CyHQ-OAc **30** (Figure 11) undergo photolysis efficiently under both 1PE and 2PE,¹⁵⁶ BHQ has also demonstrated an ability to release phenols under 1PE and 2PE as well.¹⁵⁷ In this chapter, biologically relevant phenols caged with either the BHQ or CyHQ caging moiety will be discussed. A brief discussion on how a debromination side reaction is affected by optical irradiance is also included.

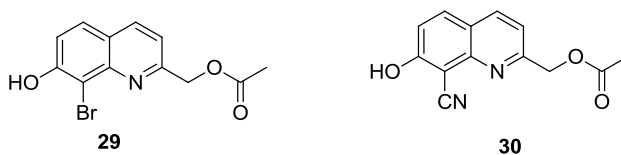


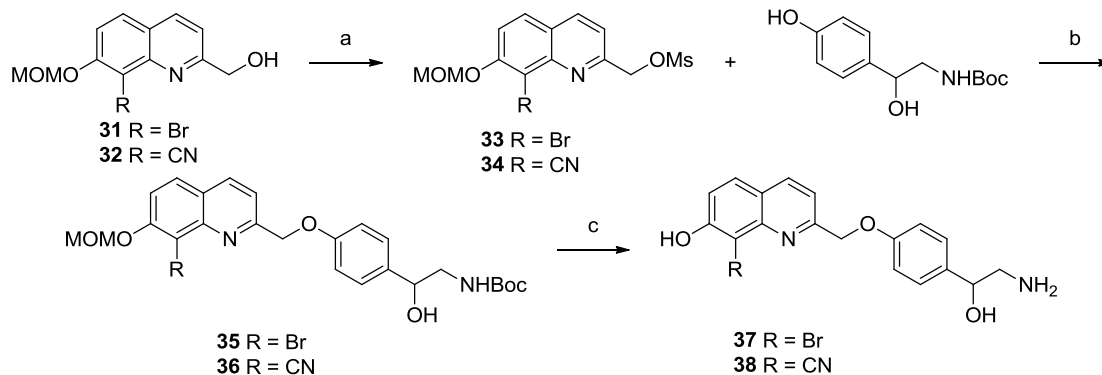
Figure 11 BHQ-OAc and CyHQ-OAc

Synthesis of Caged Octopamine

Drosophila melanogaster, fruit flies, are an extremely common neuroscience model animal due to their well understood and easily manipulated genome.¹⁵⁸ A larval fruit fly has around 10,000 neurons while an adult fruit fly possesses around 300,000 neurons,¹⁵⁹ far less than the approximately 100 million neurons of an adult human. This reduced complexity has allowed neuroscientists to make detailed neuronal maps of prominent sensory and behavioral pathways.¹⁶⁰ One of these pathways is the connection of olfactory neurons with reward behavior, however; limitations exist.¹⁶¹ The ability to precisely dissect the neural circuitry involved in integrating sensory cues with reward encoding in fruit flies may provide some insight into analogous circuitry in the human brain.

To accomplish this, we chose to cage octopamine. Octopamine is an insect neurotransmitter¹⁶² that has been prominently implicated in reward behaviors of fruit flies.¹⁶³ A caged octopamine with good optical properties would thus be able to generate spatially refined neural signals enabling precise knowledge of the role individual neurons play in integrating sensory data with reward behavior.

BHQ and CyHQ caged octopamine **37** and **38** were synthesized from the corresponding alcohol **31**¹⁶⁴ and **32**¹⁵⁶ respectively (Figure 12). Mesylation of the alcohols in THF provided the activated compounds **33**¹⁵⁷ and **34**. The mesylate was displaced with N-Boc protected octopamine in a nucleophilic substitution which resulted in the di-protected compounds **35** and **36** in low yield. Global deprotection with TMSCl in MeOH provided the desired compounds with good yield and high purity.



Reagents and conditions: (a) TEA, MsCl, THF, rt, 2 h, **31**: 73%, **32**: 35%; (b) Cs₂CO₃, acetone, rt, 18 h, **35**: 20%, **36**: 31%; (c) TMSCl, MeOH, 1 h, **37**: 36%, **38**: 80%

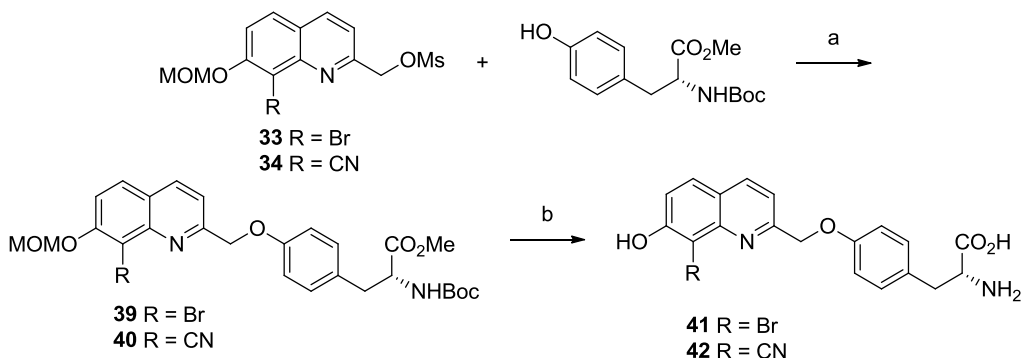
Figure 12 Synthesis of BHQ and CyHQ caged octopamine

Synthesis of Caged Tyrosine

A number of intracellular signaling cascades work through the phosphorylation and dephosphorylation of tyrosine residues. This on/off switching has attracted considerable interest, but has been difficult to study due to the complexity of orthogonally regulating the on/off state of individual enzymes. The ability to release site specific tyrosine residues with the application of light has demonstrated the utility of caging groups to enable control over signaling cascades.¹⁶⁵ However, there have been limited investigations into incorporating a caged tyrosine with sensitivity to 2PE. To address this shortcoming, we synthesized compounds **41** and **42**.

Initial attempts to synthesize BHQ and CyHQ caged tyrosine **41** and **42** utilizing N-Boc protected tyrosine resulted in coupling the ester rather than the phenol. The ester caged tyrosines exhibited poor dark stability, hydrolyzing in 4 h for the BHQ derivative and 16 h for the CyHQ derivative. This result was consistent with the hydrolytic stability observed for both **29** and **30**. With that result in mind a tyrosine protected at both the

carboxylate and amine functionalities was used. Starting from the activated compounds **33** or **34** (Figure 13), the mesylate was displaced with Boc-L-tyrosine methyl ester, in refluxing acetone with K_2CO_3 as a base to provide **39** or **40** with good yield. K_2CO_3 was used instead of Cs_2CO_3 due to the hygroscopicity of the latter base¹⁶⁶ and concern that in situ hydrolysis of the methyl ester would occur. Global deprotection with 4.5N HCl solution and heat provided the desired final compounds **41** or **42** in reasonable yield. Dark hydrolysis rates are more important in **41** and **42** than in most of the compounds synthesized due to the fact that the primary utility in a caged tyrosine is in its incorporation into proteins and the ability to block phosphorylation of tyrosine until irradiated with light.¹⁶⁷



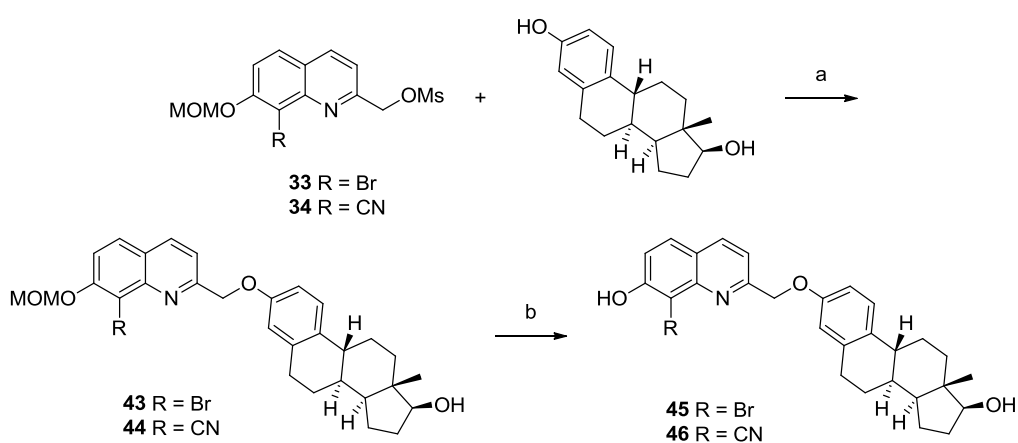
Reagents and conditions: (a) K_2CO_3 , acetone, reflux, 4 h, **39**: 69%, **40**: 77%; (b) 4.5N HCl, 65 °C, 1 h, **41**: 46%, **42**: 77%

Figure 13 Synthesis of BHQ and CyHQ caged tyrosine

Synthesis of Caged Estradiol

Estradiol has been implicated in both synaptogenesis¹⁶⁸ and neural plasticity.¹⁶⁹ The steroid also plays a prominent role in both gene regulation and expression.¹⁷⁰ Despite the potential utility in spatial and temporal control over either neuronal growth and plasticity, or gene regulation and expression, there have been no published attempts to cage estradiol.

To address this shortcoming, compounds **45** or **46** (Figure 14) were synthesized from the corresponding activated alcohols. Displacement of the mesylate with estradiol provided the protected precursors **43** or **44** in moderate yield. Due to a lack of additional sensitive functional groups compounds **45** or **46** were prepared utilizing standard methoxymethyl ether (MOM) deprotection conditions (95% TFA in DCM) to provide the desired products in good yield.



Reagents and conditions: (a) estradiol, Cs_2CO_3 , acetone, 18 h, **43**: 48%, **44**: 55%; (b) TFA, DCM, 1 h, **45**: 80%, **46**: 81%

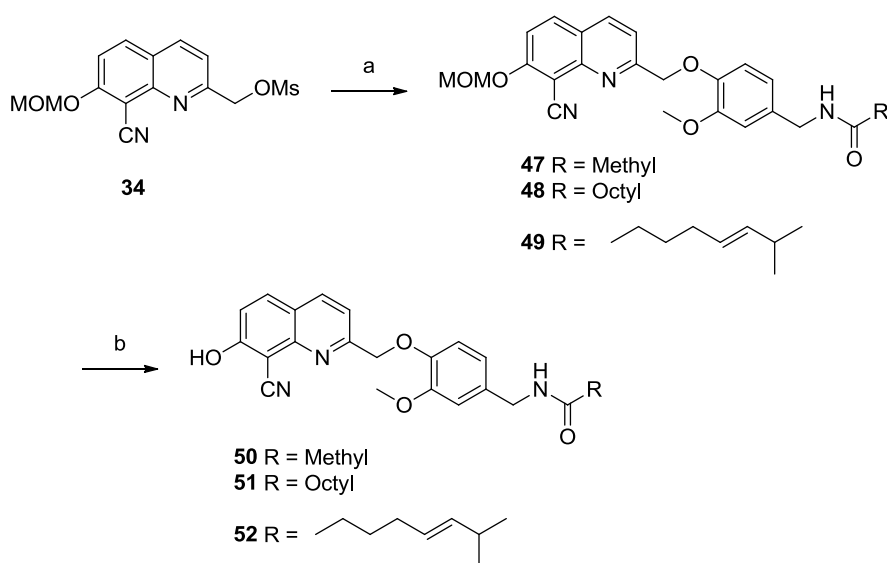
Figure 14 Synthesis of BHQ and CyHQ caged estradiol

Synthesis of Caged Vanilloids

Our lab had previously generated a series of vanilloid based BHQ caged transient receptor potential voltage ion channel (TRPV1) agonists.¹⁷¹ These compounds exhibited excellent 2PE sensitivity, however CyHQ displays a greater sensitivity to 1PE, and to complete the “toolkit” of photoactivatable TRPV1 compounds, a series of CyHQ caged vanilloids were synthesized. Compounds **51** and **52** (Figure 15) were synthesized for

their ability to activate heterologously expressed TRPV1, while **50** was synthesized as a water soluble analogue to probe the photochemistry in vitro.

MOM-protected CyHQ-OMs (**34**) was coupled to a series of vanilloids in THF and KOH, according to established lab protocols,¹⁷¹ and the protected precursors, **47**, **48**, or **49**, were synthesized in low yield. These compounds were then deprotected with standard MOM removal conditions to provide the desired caged vanilloids **50**, **51**, or **52** in moderate yield.



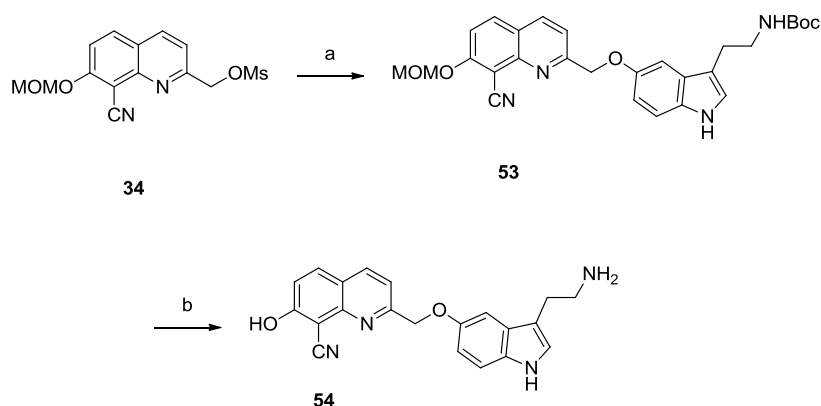
Reagents and conditions (a) vanilloid, THF, 1M KOH, 18 h, **47**: 24%, **48**: 32%, **49**: 37%; (b) TFA, DCM, 4 h, **50**: 57%, **51**: 57%, **52**: 17%

Figure 15 Synthesis of CyHQ caged VAA, VNA, and capsaicin

Synthesis of Caged Serotonin

A BHQ caged serotonin was synthesized previously in our lab and then utilized to study the left-right patterning of oocyte embryos.¹⁵⁷ Analogous to the reasons behind synthesizing **50**, **51**, and **52**, a CyHQ caged serotonin was a desired target.

Compound **53** (Figure 16) was synthesized from the activated alcohol **34** by displacing the mesylate with *N*-Boc-protected serotonin in acetone in moderate yield. Global deprotection with TMSCl in MeOH provided the desired compound **54**. Compound **54** was synthesized to expand upon the library of available caged serotonins synthesized in the Dore Lab, and to examine the role serotonin plays in embryonic development¹⁵⁷ and modulation of epileptiform activity.¹⁷²



Reagents and conditions: (a) Serotonin N-Boc, Cs₂CO₃, Acetone, 57%; (b) TMSCl, MeOH, 1 h, 63%

Figure 16 Synthesis of CyHQ caged serotonin

Photochemistry of Caged Octopamines

Compounds **37** and **38** were analyzed for their photochemical properties under both 1PE (Figure 17) and 2PE (Figure 18) for their use in biological systems. UV-Vis spectroscopy revealed that both compounds had λ_{max} near 370 nm, and extinction coefficients (ϵ) of 2500 and 5400 M⁻¹ cm⁻¹, respectively. Both compounds were then photolyzed under both 1PE and 2PE according to standard protocols.¹⁷¹ For 1PE photolysis, solutions of each compound were prepared in KMOPS buffer and then photolyzed with a LED set to 365 ± 10 nm. The photochemical reactions were analyzed

by uHPLC at various time points and peak areas were used to determine the extent of photolysis. For 2PE photolysis, solutions of each compound in KMOPS buffer were prepared and 20 μ L aliquots were removed and placed in a microcuvette and irradiated for various amounts of time with a Titanium:Sapphire (Ti:S) laser set to 740 nm. Each aliquot was removed in its entirety and analyzed by uHPLC to determine rates of photolysis. Rates of octopamine release were compared to a standard curve generated by serial dilutions of a known concentration of octopamine. Due to potential hydrolysis reactions that could occur in the absence of light it is necessary to determine the rate of that potential side reaction. Solutions of both compounds were prepared in KMOPS, placed in the dark at room temperature, and analyzed periodically by uHPLC to determine the extent of hydrolysis (both were stable to dark hydrolysis over 100 h).

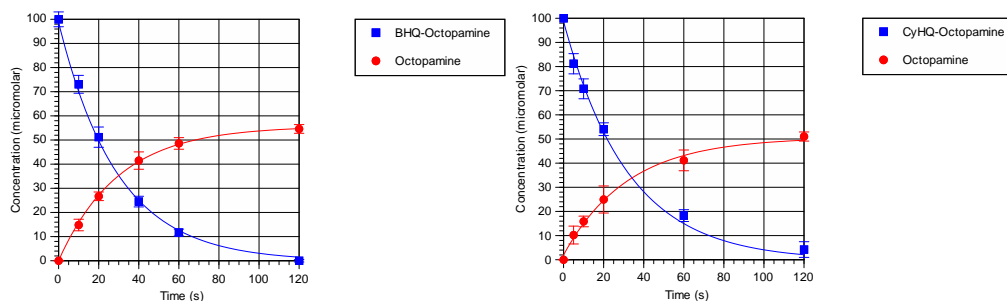


Figure 17 1PE Photolysis of BHQ-octopamine (left) and CyHQ-octopamine (right)

The photolysis curves demonstrate that both **37** and **38** are similarly sensitive to 1PE with quantum efficiency (Q_u) of 0.36 and 0.34 respectively. In comparison to the 1PE sensitivity, **37** is much more sensitive toward 2PE than **38** however both have a > 0.10 GM and are thus considered sufficiently sensitive to be used in 2PE experiments (the photochemical data are summarized in Table 1).

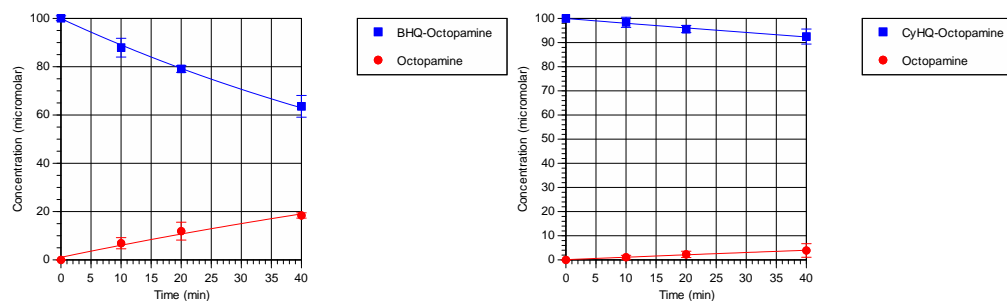


Figure 18 2PE Photolysis of BHQ-octopamine (left) or CyHQ-octopamine (right)

Compounds **37** and **38** exhibit good photochemical properties with regard to 1PE. Both compounds have similar Q_u values, although **38** has a much higher ϵ and thus is more sensitive to light ($Q_u \cdot \epsilon = 1900$ vs. 800). These values are in line with other published caged octopamines **55**¹⁷³ (Figure 19) synthesized by Haagen and coworkers. Compound **55** demonstrated a much higher ϵ at ~ 370 nm, but also demonstrated a much lower Q_u . Compound **55** was not evaluated for 2PE, but with the prevalence of Bhc caged compounds that exhibit 2PE sensitivity it is likely sensitive as well.¹⁰⁶ Compounds **37** and **38** also exhibit sensitivity toward 2PE that is in line with other BHQ and CyHQ caged compounds.

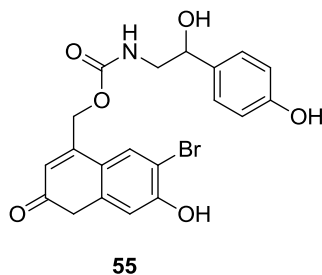


Figure 19 Bhc-octopamine

Table 1 Photochemical properties of caged octopamine compounds

Compound	λ_{\max} nm	ϵ $M^{-1}cm^{-1}$	Q_u	Sensitivity $Q_u \times \epsilon$	δ_u GM
BHQ-octopamine (37)	368	2500	0.34	850	0.49
CyHQ-octopamine (38)	372	5400	0.36	1944	0.18
Bhc-octopamine (55)	373	17150	0.16	2744	N/A

Photochemistry of Caged Tyrosines

Compounds **41** and **42** were analyzed by UV-Vis; both compounds reported a λ_{\max} around 370 nm and ϵ of 2600 and 4900 respectively. Samples of both compounds were prepared in KMOPS and photolyzed with a LED set to 365 ± 10 nm, and a Ti:S laser set to 740 nm. All photolysis reactions were analyzed by uHPLC and peak area was used to determine rates of photolysis (The photochemical data are summarized in Table 2). Both compounds exhibit similar 1PE curves (Figure 20), with **42** having a slightly higher Q_u of 0.38 vs. **41** with a Q_u of 0.32. Once again the BHQ caged compound demonstrates a much greater sensitivity toward 2PE (Figure 21) than does the CyHQ caged compound.

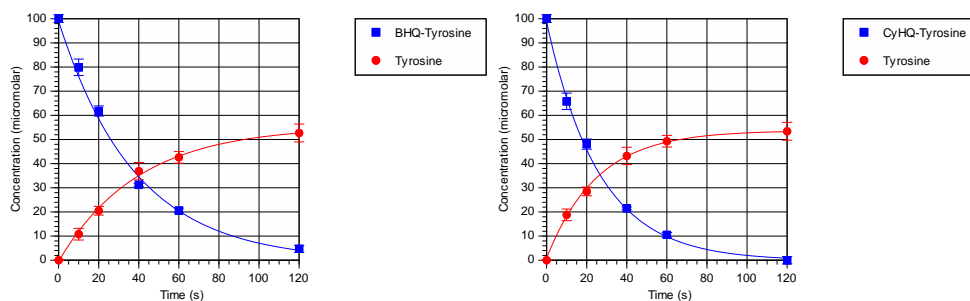


Figure 20 1PE Photolysis of BHQ-tyrosine (left) and CyHQ-tyrosine (right)

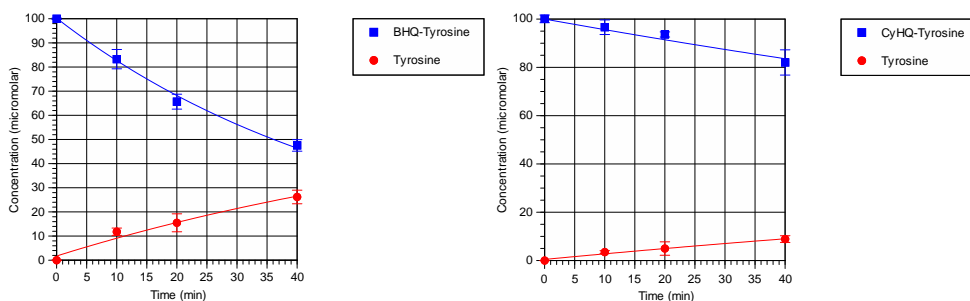
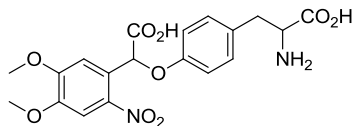


Figure 21 2PE Photolysis of BHQ-Tyrosine (left) and CyHQ-tyrosine (right)

Compounds **41** and **42** exhibit sensitivity toward both 1PE and 2PE that is in line with other reported BHQ and CyHQ caged compounds. Both **41** and **42** exhibit higher Q_u than the nitroveratryl caged tyrosine **56** (Figure 22) synthesized by Snaith and coworkers.¹⁷⁴ There have been no published reports of a 2PE sensitive caged tyrosine.



56

Figure 22 o-CNV-tyrosine

Table 2 Photochemical properties of caged tyrosine compounds

Compound	λ_{\max} nm	ϵ $M^{-1}cm^{-1}$	Q_u	Sensitivity $Q_u \times \epsilon$	δ_u GM
BHQ-Tyrosine (41)	366	2600	0.32	832	0.61
CyHQ-tyrosine (42)	371	4900	0.38	1862	0.36
o-CNV-Tyrosine 56	350	N/A	0.19	N/A	N/A

Photochemistry of Caged Estradiols

Compounds **45** and **46** were both analyzed for their sensitivity toward both 1PE and 2PE. UV-Vis analysis of the two compounds once again showed a λ_{\max} around 370 nm and ϵ of 2900 and 6200 $M^{-1}cm^{-1}$ respectively. Samples of both compounds were prepared in KMOPS and irradiated with a LED set to 365 ± 10 nm. Interestingly only **46** showed sensitivity toward 1PE (Figure 23) and 2PE (Figure 24) with a Q_u of 0.29 and 0.24 GM. Compound **45** showed only starting material and a single product **55**, as analyzed by uHPLC and LC-MS over the time course of photolysis (the photochemical data are summarized in Table 3).

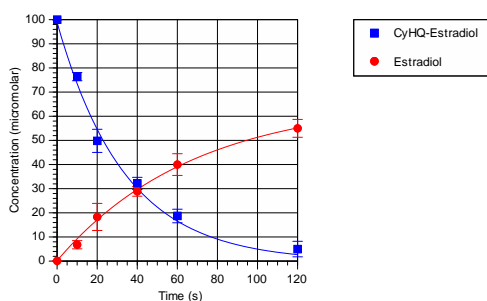


Figure 23 1PE Photolysis of CyHQ-estradiol

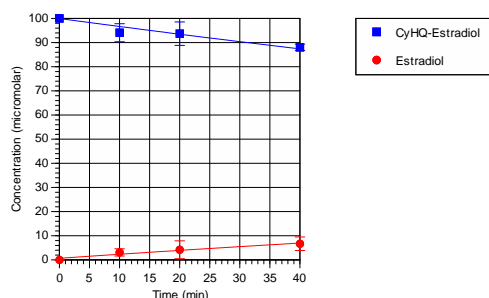


Figure 24 2PE Photolysis of CyHQ-estradiol

Table 3 Photochemical properties of caged estradiol compounds

Compound	λ_{\max} nm	ϵ $M^{-1}cm^{-1}$	Q_u	Sensitivity $Q_u \times \epsilon$	δ_u GM
CyHQ-estradiol (46)	373	6200	0.29	1798	0.24
BHQ-estradiol (45)	369	2400	N/A	N/A	N/A

It is possible that the product of the photochemical reaction of **45** is the debrominated structure **57** (Figure 25). Debromination of the BHQ scaffold has been observed previously and investigated to some extent,¹⁷⁵ however the results may not be directly comparable due to the difference between irradiation wavelengths, 254 nm ($112.5 \text{ kcal mol}^{-1}$) vs. 365 nm, ($78.3 \text{ kcal mol}^{-1}$) and the bond dissociation energy of an aryl carbon-bromine bond ($\sim 80 \text{ kcal mol}^{-1}$).¹⁷⁶ It is likely that debromination is a competitive pathway relative to photolysis, however in both studies the debrominated product was observed most abundantly when conditions disfavored photolysis, either through acidic or highly organic conditions.^{175, 177} A more detailed discussion of debromination will occur in the following sections.

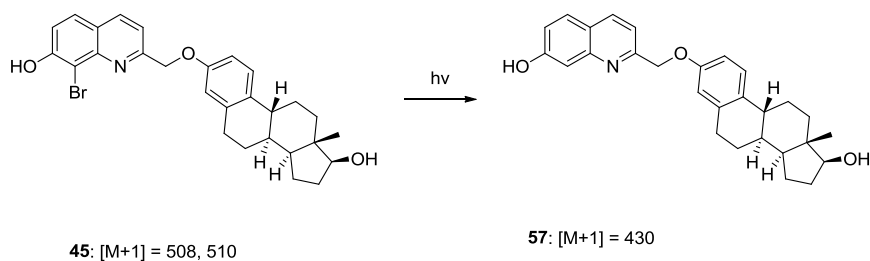


Figure 25 Debromination of BHQ-estradiol

Photochemistry of Caged Vanilloids

Compound **50** was synthesized to serve as a water soluble analogue to caged VNA **51** and caged capsaicin **52** due to issues with solubility in aqueous systems observed in the long alkyl chain vanilloids.¹⁷¹ Since the structural and electronic nature of **50** proximal to the uncaging site is similar to the biologically relevant compounds **51** and **52**, the only differences being the long alkyl chains, it should provide a reasonable insight into the uncaging kinetics of the relevant compounds. Analysis of **50** under both 1PE (Figure 27) and 2PE (Figure 28) showed that it was sensitive to photolysis under both methods. It is interesting to note that whereas **50** is much more sensitive toward 1PE than BHQ-VAA **58** (Q_u of 0.41 vs. 0.18) (Figure 26), it is much less sensitive toward 2PE, with a δ_u of 0.23 GM vs. 0.61 GM (the photochemical data are summarized in Table 4).¹⁷¹

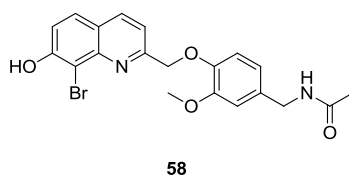


Figure 26 BHQ-VAA

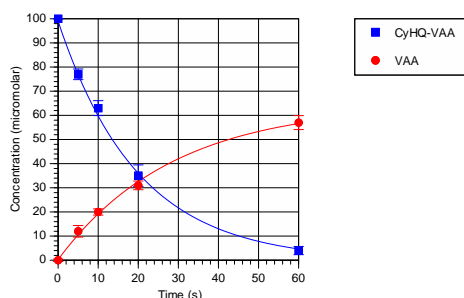


Figure 27 1PE Photolysis of CyHQ-VAA

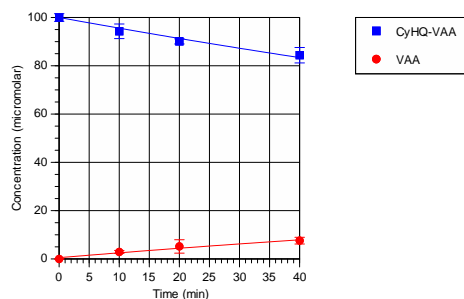


Figure 28 2PE Photolysis of CyHQ-VAA

Hagen and coworkers synthesized a biscarboxy-amino coumarin **59**^{149a} (Figure 29) with good optical properties for 1PE and high aqueous solubility. Compound **59** offers some advantages relative to the BHQ and CyHQ caged vanilloids due to its increased solubility in aqueous systems, however **59** is significantly less stable to dark hydrolysis (reported stability only over 24h) than either **58** (τ_{dark} 140 h) or **50** ($\tau_{\text{dark}} > 250$ h) which are stable to hydrolysis for either 5 days (**58**) or not hydrolytically sensitive (**50**). Compound **59** is significantly more sensitive to 1PE than **56** 2250 vs. 486, and slightly less sensitive than **50** (2829 vs. 2250). Compound **59** faces another important limitation, the carbonate linker renders the rate limiting step for release of capsaicin as the decarboxylation step, an event that is typically a quite slow first order process ($k_{\text{-CO}_2} = 10^{-3} \text{ s}^{-1}$).⁸⁹ 2PE sensitivity wasn't measured for **57** but based on analogous compounds a two photon cross-section of 0.2 – 0.3 GM¹⁰⁶ is reasonable. Thus while there is no single compound with optimal properties for both 1PE and 2PE the combination of CyHQ-

capsaicin for 1PE experiments and BHQ-Capsaicin for 2PE experiments should provide the most efficient toolset.

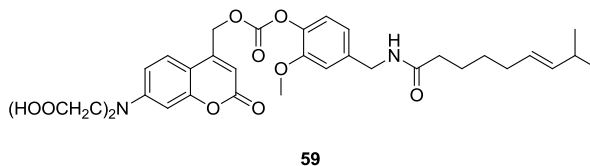


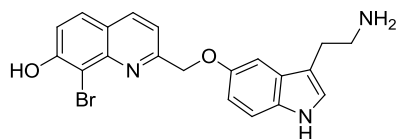
Figure 29 BCMACM-capsaicin

Table 4 Photochemical properties of caged vanilloid compounds

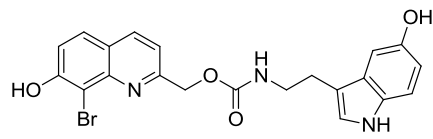
Compound	λ_{\max} nm	ϵ $M^{-1}cm^{-1}$	Q_u	Sensitivity $Q_u \times \epsilon$	δ_u GM
CyHQ-VAA (58)	368	6900	0.41	2829	0.24
BHQ-VAA (50)	370	2700	0.18	486	0.61
BCMACM-Capsaicin (59)	383	18750	0.12	2250	N/A

Photochemistry of Caged Serotonin

Compound **54** was analyzed by established protocols for sensitivity toward both 1PE and 2PE. It is worth noting that, as with the caged vanilloids, **54** showed a much greater sensitivity toward 1PE than either of the previously synthesized BHQ caged serotonins (Figure 30) **60** and **61**¹⁷¹ with a sensitivity of 2379 vs. 600 for **60** or 210 for **61**. The trend of opposite sensitivity for 1PE (Figure 31) and 2PE (Figure 32) held true in this case as the δ_u for **54** (0.23 GM) was lower than either **60** (0.50 GM) or **61** (0.42 GM) (the photochemical data are summarized in Table 5).



60



61

Figure 30 BHQ-*O*-serotonin (60) and BHQ-*N*-serotonin (61)

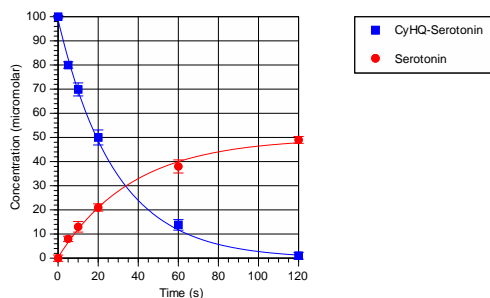


Figure 31 1PE Photolysis of CyHQ-serotonin

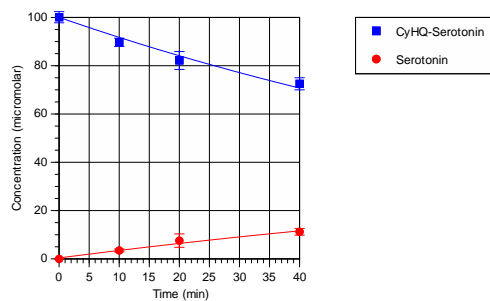


Figure 32 2PE Photolysis of CyHQ-serotonin

Table 5 Photochemical properties of caged serotonin compounds

Compound	λ_{\max} nm	ϵ $M^{-1}cm^{-1}$	Q_u	Sensitivity $Q_u \times \epsilon$	δ_u GM
CyHQ-O-5HT (31)	372	6100	0.39	2379	0.23
BHQ-O-5HT (60)	368	2000	0.30	600	0.50
BHQ-N-5HT (61)	370	2100	0.10	210	0.42

Debromination analysis under 1PE irradiation

Debromination is a side reaction in the photolysis of BHQ-X that is observed in 1PE experiments with all compounds synthesized in the lab to date (Figure 33). There is also a thermal debromination that occurs at temperatures above 115 °C in both DMF and DMAc (experimental observation). This pathway was first significantly observed in time resolved spectroscopy experiments and later confirmed by irradiation at 254 nm.¹⁷⁵ The amount of debromination that occurs was at that point unknown, but of sufficient concern that serious investigation into utilizing alternative previously developed caging groups, as well as next generation caging groups had begun. To address this concern, an investigation into the extent of debromination that is observed in the 1PE photolysis of BHQ caged compounds was performed.

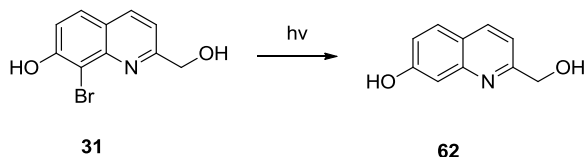


Figure 33 Debromination side reaction

1PE debromination was investigated by irradiating a 100 μM sample of **31** in KMOPS buffer with a LED set to 365 ± 10 nm at different optical power settings. Aliquots were removed at various time points and analyzed by uHPLC to create photolytic debromination curves (Figure 34). Compound **31** was chosen because photolysis of the C-O bond wouldn't complicate the analysis of the rate of debromination.

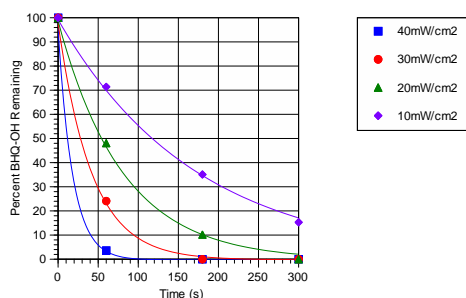


Figure 34 Debromination of BHQ-OH as a function of optical irradiance

Optical irradiance was chosen as the energy measurement rather than intensity due to the ease of calibration (for reference a typical photolysis experiment uses between 25 mW/cm² and 10 mW/cm²). Figure 34 clearly indicates that even at low power settings a significant portion of BHQ-OH is being converted to HQ-OH. Figure 35 shows a comparison of the rate of photolysis of a sample BHQ compound **37** vs. rates of debromination at 20 mW/cm² and 10 mW/cm² indicate that the debromination pathway is a significant portion of the overall photolysis mixture. HQ has demonstrated an ability to act as a caging group, although with much less efficiency than either BHQ or CyHQ, so this debromination side reaction doesn't render BHQ caged compounds photolytically inert.

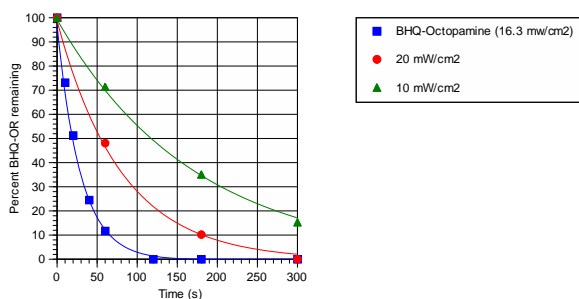


Figure 35 Comparison of rate of debromination and photolysis in BHQ-octopamine

The investigation into the debromination pathway under both IPE presented above provides some interesting results, and some potential areas for further

investigation. Debromination in 1PE appears to be a process that occurs on the base BHQ scaffold, and thus is likely observed to some extent for all BHQ-caged compounds. A comparison of the quantum efficiencies shows that **37** has a Q_u of ~0.34 while **31** has a Q_u for debromination of ~0.12. Thus a simple rationalization could be that for every 3 photolysis events there is 1 debromination event. However a more systematic investigation of the rates of debromination with a focus toward manipulating both the structural and electronic nature at and around the scissile C-O bond should provide much greater insight into what role, if any, the compound being caged plays in the debromination side reaction.

Summary

With one exception, BHQ-estradiol **45**, all of the phenols described in this chapter are sensitive to both 1PE and 2PE. For the compounds that displayed sensitivity to photolysis, the CyHQ caged compounds were approximately three to five fold more sensitivity to 1PE ($Q_u \cdot \epsilon$). In contrast to the 1PE sensitivity, the BHQ caged compounds exhibited a two to three fold higher sensitivity to 2PE (δ_u). The debromination reaction observed in initially during time resolved experiments¹⁷⁵ was verified to also be present at 365 nm. The extent of debromination was quantified with a Q_u of 0.12 which indicates that it is a significant contributor to the overall photolysis of BHQ caged compounds, but not the major pathway.

CHAPTER 4

Synthesis and Photochemistry of Biologically Relevant Caged Catechols

Introduction

Catecholamines are a class of compounds containing both a catecholic moiety and a side chain amine. Within this class are three molecules that possess important neuromodulatory activity: dopamine, epinephrine, and norepinephrine. Dopamine has been implicated in memory formation, executive function, and both conscious and autonomic motion(see chapter 1).¹⁷⁸ Whereas the adrenergics epinephrine and norepinephrine are more commonly associated with engaging fight or flight mechanisms,¹⁷⁹ heart rate and vasodilatations,¹⁸⁰ and modulating metabolic shifts,¹⁸¹ they have also been implicated in memory consolidation¹⁸² and emotional response.¹⁸³ There has been an increase of investigation into the broad spectrum activity of catecholamines as neuromodulators, but the precise mechanism(s) underlying the resultant behavioral phenomena are less well understood.

As mentioned in chapter 1, the dopaminergic system is complex. The expression patterns and cytoarchitectural features of dopaminergic neurons is dependent on the area of the brain involved.²⁰ Dopamine can perform both activating and inhibitory actions through modulation of adenylyl cyclase, phospholipase C, and it can also indirectly modulate MEK/ERK.¹ At tripartate synapses dopamine release is capable of modulating postsynaptic signaling directly through the above pathways, while presynaptic modulation can occur through the retrograde release of endocannabinoids.⁶² This

multiplicity of function, dependent on spatial and temporal orientation as well as on the state of the neuron(s) in question makes probing dopaminergic signaling experimentally difficult.

In order to accurately dissect dopaminergic signaling, several labs have synthesized versions of photoactivatable dopamine (Figure 36). Lee et. al. first synthesized nitrobenzyl caged dopamine in 1996 and in combination with cyclic voltammetry, which measures the voltage change as dopamine is oxidized and reduced, were able to assess dopamine release and clearance rates with 100-ms temporal resolution.¹⁴³ The nitrobenzyl cage suffers from two prominent drawbacks, the first and most prominent is the rate of release is dependent upon decomposition of the aci-nitro intermediate ($10^3 - 10^5 \text{ s}^{-1}$)¹⁸⁴ or upon acetal hydrolysis ($10^2 - 10^5 \text{ s}^{-1}$).¹⁸⁵ The second prominent drawback is the poor optical properties: low Q_u 0.01 – 0.05, low extinction coefficients at non-damaging wavelengths, and near complete insensitivity toward 2PE.¹⁸⁵ Etchinique and coworkers synthesized a RuBi caged dopamine with sensitivity toward 2PE (0.24 GM),¹⁴⁵ however the method relies on an earlier GM calculation based on action potential propagation in glutamatergic neurons,¹⁸⁶ an unreliable measurement at best.¹⁸⁷ Still RuBi dopamine represents the only published 2PE sensitive caged dopamine(Figure 36).

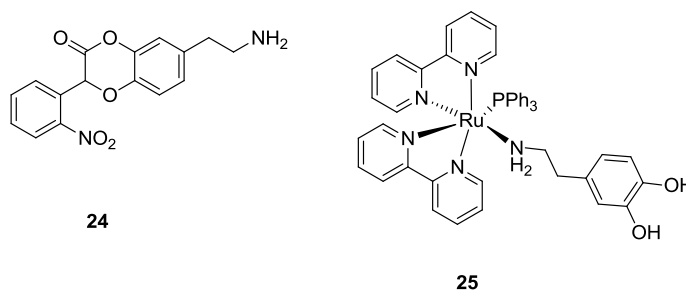
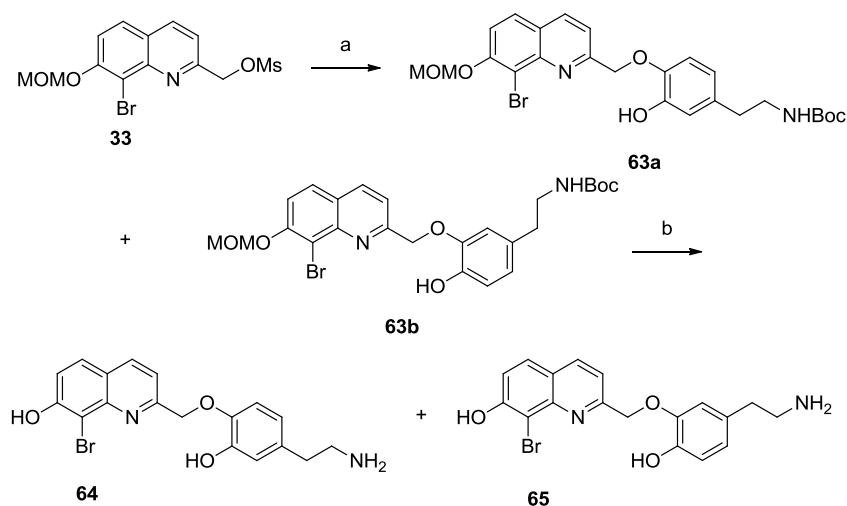


Figure 36 o-NB-dopamine and RuBi-dopamine

Synthesis of BHQ-dopamine

BHQ-dopamine **64** and **65** were first synthesized from the corresponding activated alcohol **33** (Figure 37) by coupling with N-Boc protected dopamine in THF with 1M KOH to provide a mixture of isomers that were co-purified to give **63**. The mixture was then globally deprotected with TMSCl in MeOH and HPLC purified to provide the single isomers **64** and **65** in a 1:1 ratio with low combined yield.



Reagents and conditions: (a) N-boc protected dopamine, 1M KOH, THF, rt, 18 h, 49%; (b) TMSCl, MeOH 36%

Figure 37 Synthesis of BHQ-dopamine

To assign isomeric identity to the mixture of **64** and **65** through space coupling was investigated. The nuclear Overhauser effect enables a determination of protons that are close enough in space to undergo cross-relaxation. 2DNMR (ROESY) experiments showed a clear through-space correlation between a_1 (5.31 ppm) and a_2 (6.88 ppm) and b_1 (5.32 ppm) and b_2 (6.92 ppm) (Figure 38).

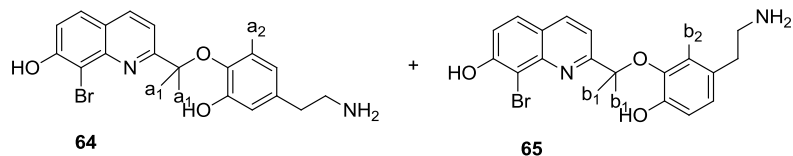
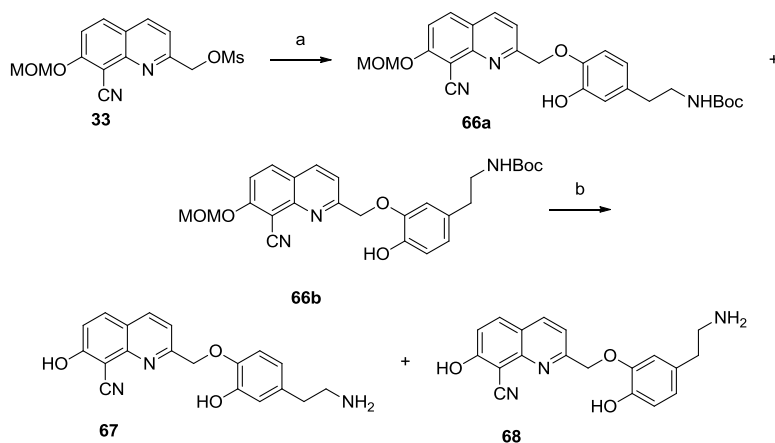


Figure 38 Possible BHQ-dopamine isomers

Synthesis of CyHQ-dopamine

Synthesis of **67** and **68** (Figure 39) from the corresponding activated alcohol **33** was accomplished by coupling *N*-Boc protected dopamine in acetone with Cs_2CO_3 , in low yield to provide **66** and then global deprotection with TMSCl in MeOH followed by HPLC purification to provide the final compounds. In contrast to the 1:1 product ratio that was observed with **64** and **65** an approximately 4:1 ratio was observed between **67** and **68**. The identity of each isomer was verified by 2DNMR and displayed results analogous to those observed for BHQ-dopamine.



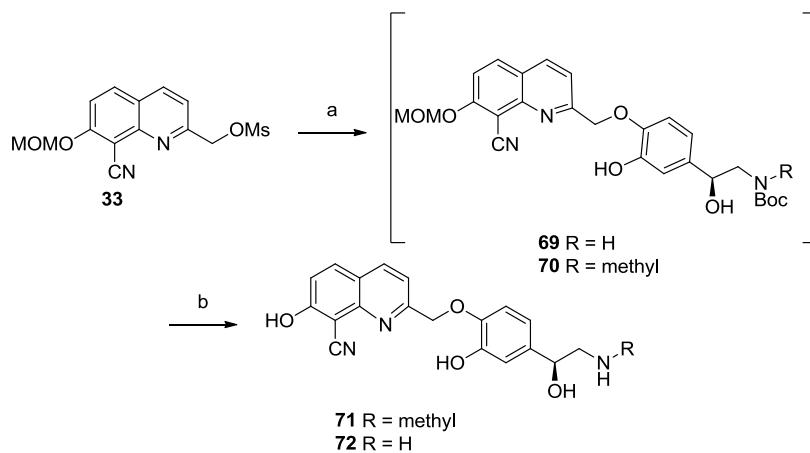
Reagents and conditions: (a) *N*-Boc protected dopamine, Cs_2CO_3 , acetone, rt, 18 h, 42%; (b) TMSCl, MeOH 31%

Figure 39 Synthesis of CyHQ-dopamine

The mono-functionalization of one of the phenolic groups of dopamine vs. another has not been widely attempted. Most attempts are difunctionalizations, however Fernandez et. al. observed a similar distribution ratio when they glycosylated dopamine *N*-Cbz with a 3:1 preference for hydroxyl group on C-3 of dopamine vs. the hydroxyl group on C-4 of dopamine.¹⁸⁸

Synthesis of Caged Epinephrine and Norepinephrine

Starting from the activated alcohol **33** (Figure 40), substitution with the desired catecholamine *N*-Boc protected norepinephrine to provide intermediate **69** or *N*-Boc protected epinephrine to provide intermediate **70**. Difficulty in purifying the intermediates **69** or **70** eventually resulted in telescoping the reaction from **33** to the desired catechol **71** or **72**, following global deprotection with trimethylsilyl chloride in methanol.



Reagents and conditions: (a) Epinephrine *N*-Boc, Cs₂CO₃, acetone, rt, 36 h (b) TMSCl, MeOH, **71**: 17%, **72**: 11%

Figure 40 Synthesis of CyHQ-epinephrine and CyHQ-norepinephrine

Photochemistry of Caged Dopamine

Attempts to photolyze compounds **64** and **65** as a mixture were unsuccessful (Figure 41). It was hypothesized that a photolytic event was occurring, but that instead of converting to the free alcohol **59** (pathway a), an isomerization event was occurring (pathway b).

To investigate this possibility isomers **64** and **65** were separated and individual samples were photolyzed by a LED set to 365 ± 10 nm as described in chapter 3. HPLC analysis of the results showed no isomerization occurred, and that the only product observed was ~5% abundance of the debrominated product after 5 minutes of irradiation.

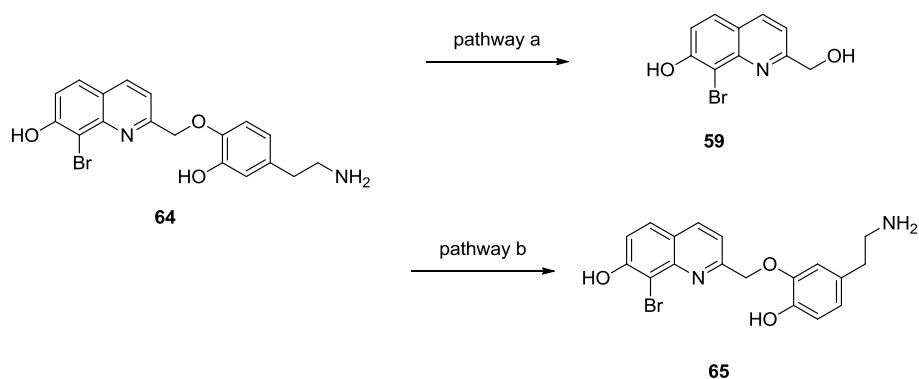


Figure 41 Photochemistry of BHQ-dopamine

The photolysis of BHQ caged compounds is hypothesized to occur through a triplet state intermediate.¹⁷⁵ This means that other photochemical processes that occur through the either a singlet or triplet excited state could be considered competing processes. Fluorescence is the radiative decay of a singlet excited state back to ground state energy, however a comparison of BHQ-dopamine (25 μ M) with BHQ-OAc (25 μ M) (Figure 42) demonstrates that their fluorescence emissions are within an order of magnitude, and it is unlikely that fluorescence alone is the major contributor to the lack of photolysis observed.

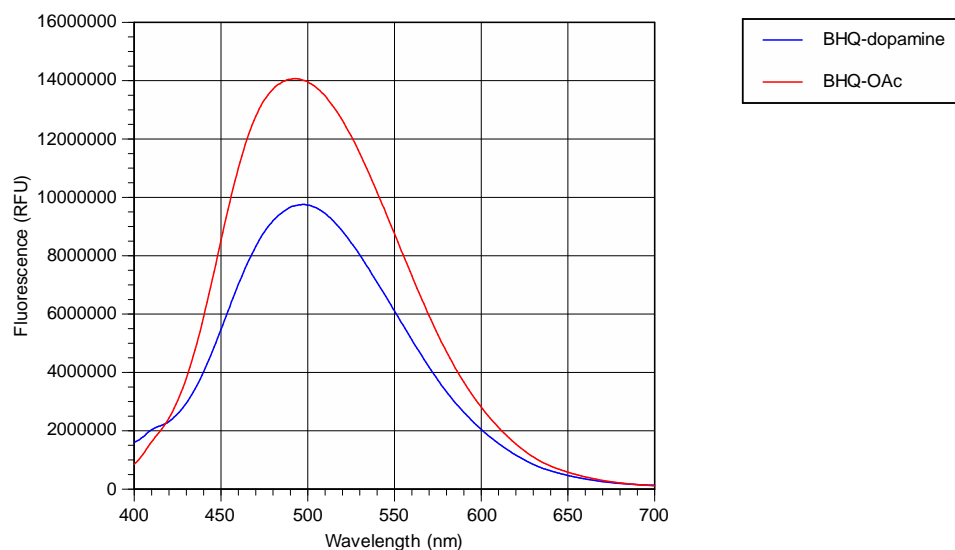


Figure 42 Fluorescence emission spectra of BHQ-dopamine and BHQ-OAc standard

Another factor to consider is the pK_a of the leaving group itself. Within the series of compounds containing either a phenol or catechol, a number of BHQ caged compounds have been generated (Figure 43). With the exception of **45** and **64/65**, all of the compounds listed release the desired compound with good optical properties and >50% yield (Table 6). An analysis of the pK_a of these leaving groups, calculated with advanced chemical development (ACD/LAB) V11.02 (through Scifinder) provides some insight into the lack of photolysis. ACD/LAB was chosen to provide a single consistent measurement of pK_a to avoid inconsistencies in experimental titrations. When analyzing a compound for potential utility in uncaging experiments, one of the parameters analyzed is the pK_a of the caged compound. This is done because the pK_a provides, indirectly, a measure of the leaving group ability of the protected compound, and leaving groups with high pK_a values tend to be photochemically inert.¹⁰⁶ Thus a simple explanation might be that both dopamine and estradiol are insufficiently good leaving groups to be uncaged with the BHQ caging group.

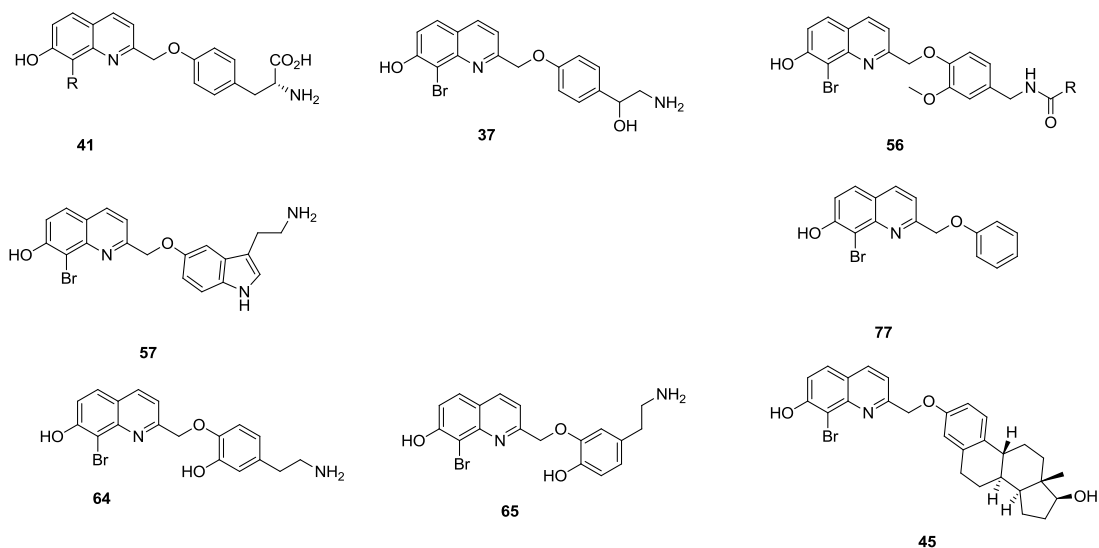


Figure 43 BHQ caged phenols

Table 6 Comparison of calculated pK_a to photolysis for BHQ caged phenols

Leaving Group	Calculated pK_a	Photolysis (y/n) (% yield of phenol)
Tyrosine	9.04	Yes (53%)
Octopamine	8.91	Yes (55%)
VAA	9.76	Yes (65%)
Serotonin	9.52	Yes (58%)
Phenol	9.86	Yes (57%)
Dopamine	10.11	No
Estradiol	10.27	No

The threshold for photolysis with the BHQ scaffold appears to be lower than what is observed with CyHQ. This is reflected by the fact that while photolysis of BHQ-dopamine and BHQ-estradiol produce no product, both CyHQ-dopamine and CyHQ-estradiol release the desired leaving group (Figure 44 and 45).

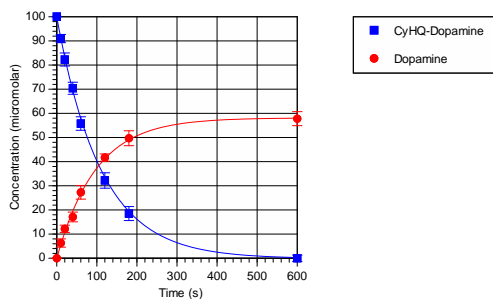


Figure 44 1PE photolysis of CyHQ-dopamine

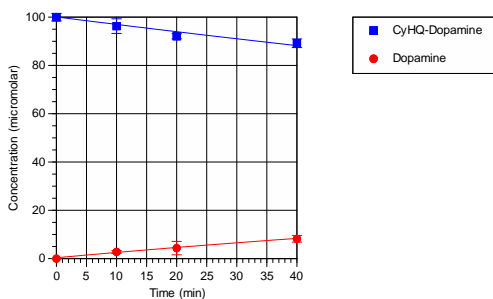


Figure 45 2PE photolysis of CyHQ-dopamine

The optical properties for CyHQ-dopamine are significantly lower than phenolic analogues,^{xlvii} with a Q_u of 0.18 and 1PE sensitivity of 936 and a δ_u of 0.15 GM. Compared to RuBi-dopamine, CyHQ-dopamine has a higher Q_u (0.18 vs. 0.085), as well as a higher 1PE sensitivity (936 vs. 417); however RuBi-dopamine is photolyzed at a much more benign wavelength 405 nm vs. 365 nm. The 2PE action cross sections are comparable; 0.15 δ_u for CyHQ-dopamine vs. δ_u 0.23 for RuBi-dopamine, but as mentioned previously the 2PE cross-section calculation of RuBi-dopamine is based on a comparative analysis of MNI-Glutamate generated action potentials.¹⁸⁹

^{xlvii} Compare Q_u for CyHQ-phenols of ~0.30 – 0.40 vs. 0.18 for CyHQ-dopamine and δ_u of 0.23 – 0.30 (CyHQ-phenol) vs. 0.15 (CyHQ-dopamine)

Photolysis of Epinephrine and Norepinephrine

A 100- μ M sample of **73** in KMOPS was prepared and irradiated with a LED at 365 ± 10 nm. Interestingly, while degradation of starting material proceeded fairly straightforwardly, no product generation was observed (Figure 46). Instead a photoproduct was generated that had been red-shifted ~ 20 -nm from 280 nm to ~ 300 nm (Figure 47) and had a retention time shift on the uHPLC from 1.64 minutes to 2.41 minutes.

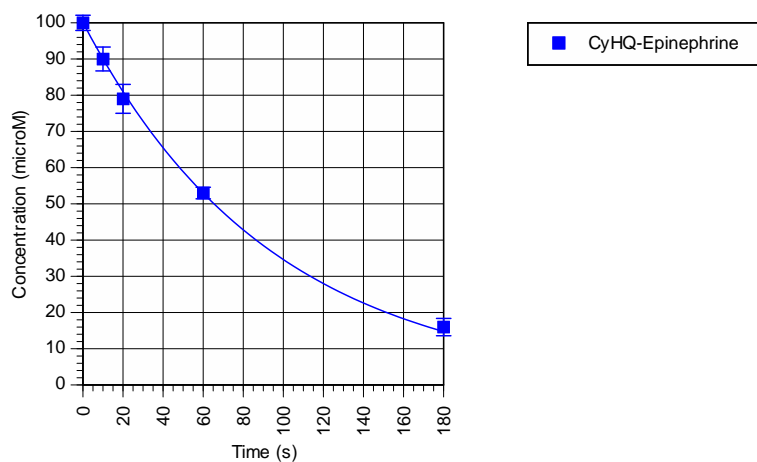


Figure 46 1PE photodegradation of CyHQ-epinephrine

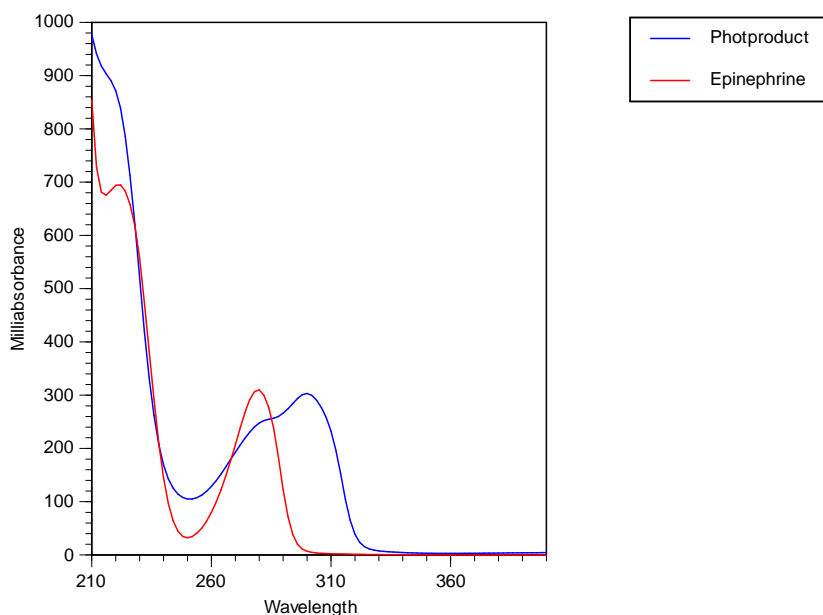


Figure 47 Overlaid uHPLC absorbance traces of epinephrine and primary photoproduct

To determine whether uncaging had occurred at all (Figure 48 pathway a or b), samples were analyzed by LCMS, and M+H was found for both starting material and CyHQ-OH. Next it was necessary to determine if the epinephrine was undergoing a further photochemical reaction to generate the observed photoproduct, however five minutes irradiation of a 100- μ M sample of epinephrine under the same conditions showed no change in peak area, UV absorbance spectra, or retention time shift between starting material and following irradiation. Dark hydrolysis analysis was also performed to determine whether CyHQ-OH was being released by a photochemical reaction or through hydrolysis of the starting material. The time constant of dark hydrolysis, τ_{dark} , was > 200 h, thus indicating that the CyHQ-OH generated during the photolysis experiment was indeed coming from a photochemical reaction. These data indicate that while some photochemical reaction was occurring (pathway b) that eventually led to the release of CyHQ-OH it wasn't the expected pathway a.

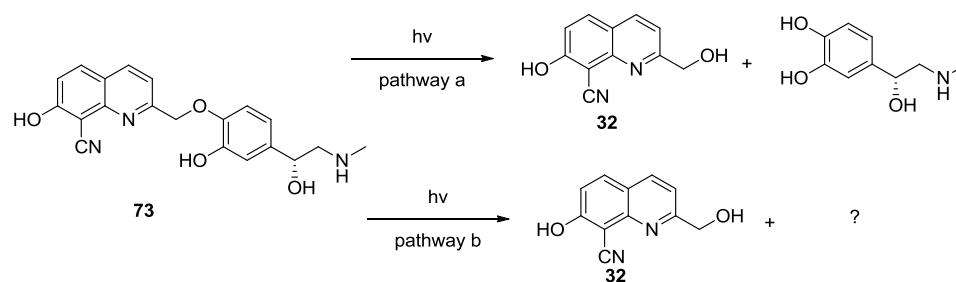


Figure 48 Photolysis of CyHQ-epinephrine

Photo-oxidation of catechols to quinones has been observed in literature,¹⁹⁰ however oxidation is not reported to occur above 290 nm. To test if epinephrine was being released and then subsequently photo-oxidized a 100- μ M sample of epinephrine either in the presence or absence of a 100- μ M sample of CyHQ-OH in KMOPS buffer 7.2 pH was irradiated for 10 min at 365 ± 10 nm. No photodegradation was observed in the absence of CyHQ-OH and $\sim 10\%$ degradation was observed in the presence of CyHQ-OH.

Further analysis of the LCMS data generated from the photolysis of **73** and photodegradation (irradiation of epinephrine in the presence of **32**) experiments showed trace amounts of $[M+H] = 164.1$ which could potentially correspond to either **78** or **79** (Figure 49). To determine which product formed, **78** was synthesized according to established protocols.¹⁹¹ The identity of **78** was verified by ^1H NMR and LCMS, and the retention time and UV trace matched up perfectly with the major observed photoproduct of the photolysis of CyHQ-epinephrine.

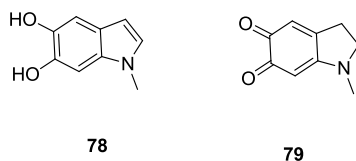


Figure 49 Potential primary photoproducts

The two electron oxidation of epinephrine from its catechol form to its quinone form is unlikely to occur while caged by CyHQ, but the literature around catechols offers an alternative possibility: the semiquinone. The one electron oxidation of epinephrine to its semiquinone form has a standard reduction potential (SRP) of 0.068 mV¹⁹² ~ 1/3 of the SRP for the oxidation of epinephrine to its quinone species.¹⁹³ The lifetime of the semiquinone radical ranges from microsecond to millisecond,¹⁹² significantly longer than the photolysis of BHQ, which is proposed to occur on the nanosecond timescale.¹⁷⁵ More interestingly is the fact that the semiquinone form of catechols are more acidic than the catechol form by 2 – 2.5 p*K_a* units.¹⁹² As stated previously the p*K_a* of the compound being caged is a good proxy for determining whether a compound can be photo-released or not, and such a drastic increase in acidity would shift epinephrine from p*K_a* ~ 10 to p*K_a* ~ 8, greatly increasing the likelihood of photolysis.

Figure 50 shows a potential reaction pathway. Step 1 is rationalized by the low one electron reduction potential: **74** absorbs a photon, exciting the compound into a singlet state which relaxes to a triplet state, and instead of photolyzing, a semiquinone radical is formed. The lifetime of the semiquinone radical is such that **81** could potentially absorb a second photon (step 2), and given the increased acidity of the semiquinone relative to the catechol, photolysis occurs. At this point the radical anion rapidly oxidizes to the quinone which then undergoes cyclization and dehydration to form the indole (step 3).

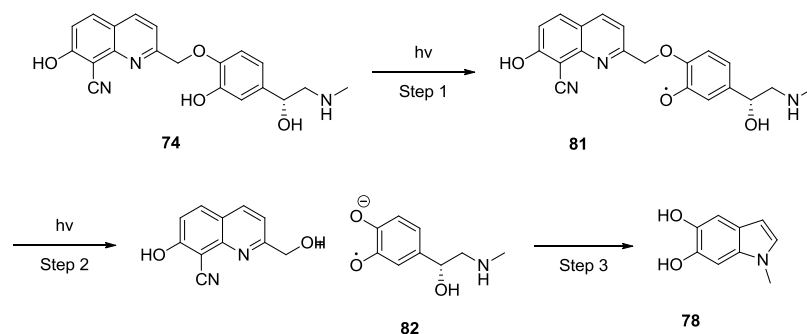


Figure 50 Proposed CyHQ-epinephrine photolysis mechanism

A sample of norepinephrine was prepared as described above for epinephrine, and the results indicate that the same reaction is occurring. Once again a ~20-nm red shift from 280 nm to 300 nm was observed, concurrent with a retention time shift of ~2 minutes. LCMS analysis showed the presence of CyHQ-OH and trace amounts of the analogous quinones.

Summary

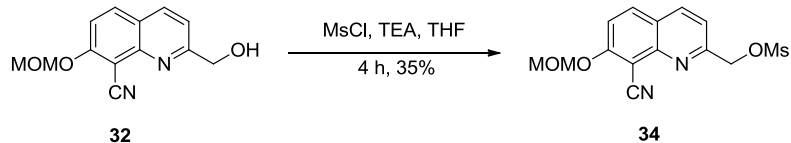
Catechols behave very differently than phenols do with respect to the photochemistry of the BHQ and CyHQ caging groups. While it is likely that dopamine is insufficient to act as a leaving group for the BHQ scaffold, it is sufficient for photorelease by CyHQ. The presence of undesired photoreactions in the adrenergic leads to the formation of a dihydroxyindole species as the major photoproduct.

Experimentals

General

Compounds **33**¹⁵⁷ and **79**¹⁹¹ were prepared according to known literature procedures. All other reagents and solvents were purchased from commercial sources and used without further purification. ¹H NMR and ¹³C NMR were recorded on Varian MercuryPlus 400 MHz and 500 MHz spectrometers or on a Bruker Avance III HD 600 MHz. UV spectra were recorded on a Cary 300 UV-Visible spectrophotometer (Varian) or a Cary 5000 UV-Vis-NIR spectrophotometer (Agilent). HPLC and uHPLC (analytical and preparative) was performed on an Agilent Infinity series system with an autosampler and diode array detector using Zorbax eclipse C-18 revers phase columns. HRMS was performed on an Agilent 6540 HD Accurate Mass QTOF/LC/MS with electrospray ionization (ESI) or a Micromass QTOF-Ultima with ESI. KMOPS buffer consisted of 100 mM KCl and 10 mM MOPS titrated to pH 7.2 with KOH. Flash chromatography was performed on an Isolera Spektra 4 with biotage SNAP cartridges packed with KP-SIL silica.

(8-Cyano-7-(methoxymethoxy)quinolin-2-yl)methyl methanesulfonate (34)

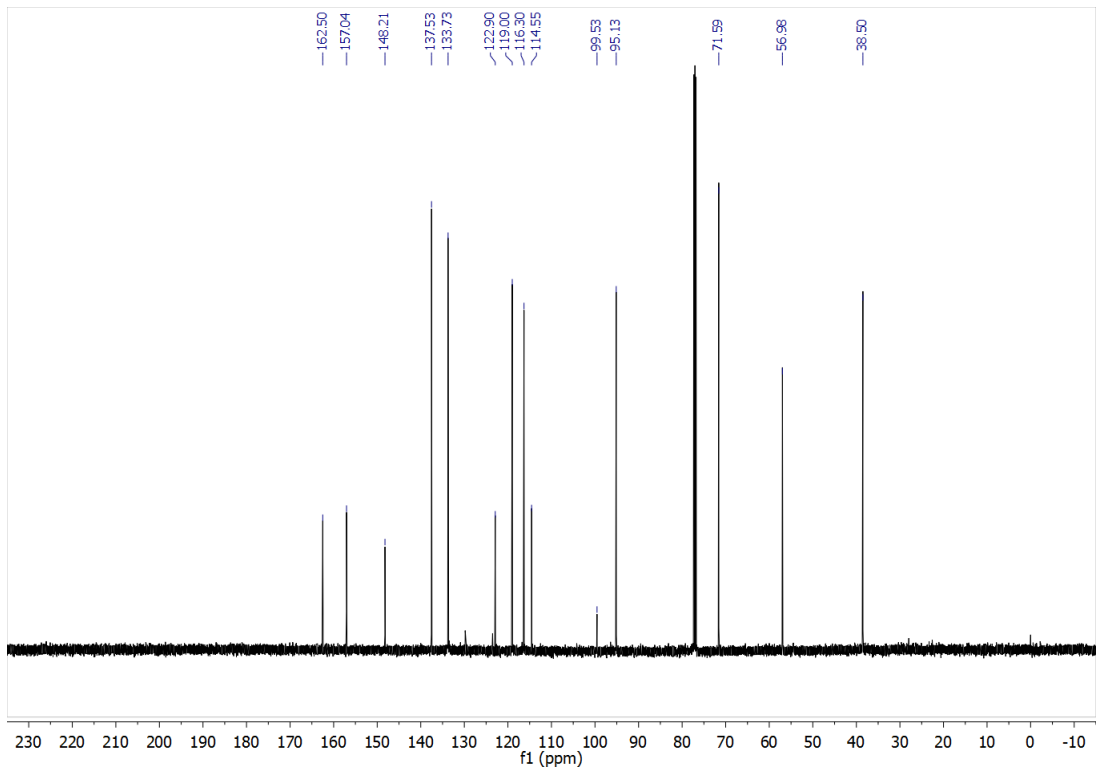
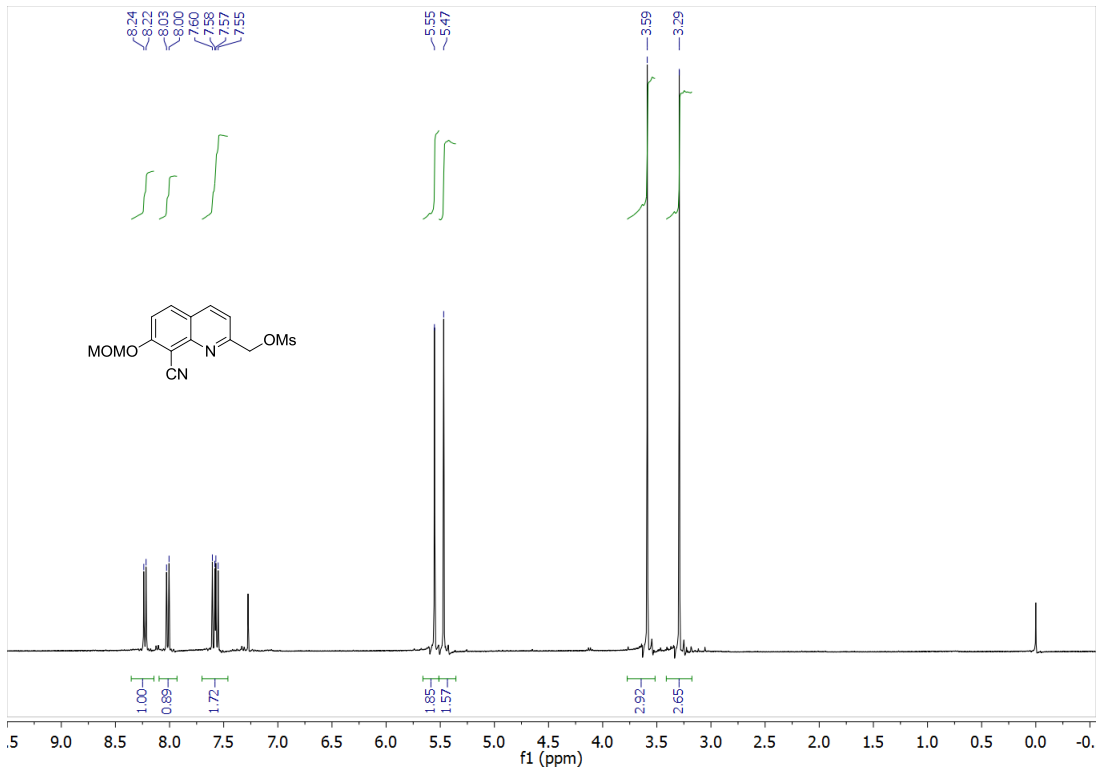


Compound **32** (0.31 g, 1.2 mmol) was stirred in THF (5 mL) and methanesulfonyl chloride (0.189 mL, 2.44 mmol) and TEA (0.51 mL, 3.7 mmol) were added. The reaction was monitored by uHPLC, and upon completion the reaction mixture was dried in vacuo onto celite and the crude product was purified via flash chromatography eluting with EtOAc/hexane (1:2) and dried to a white powder **34** (0.132 g, 0.408 mmol 35% yield).

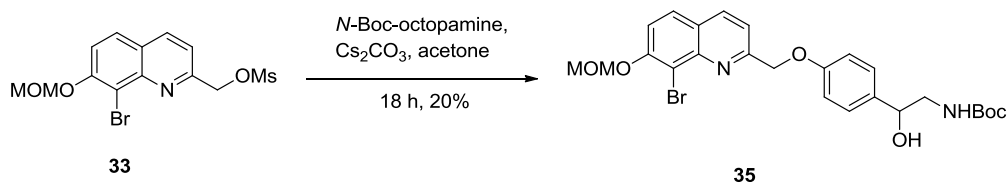
¹H NMR (400 MHz, chloroform-*d*) δ 8.23 (d, $J = 8.4$ Hz, 1H), 8.02 (d, $J = 9.2$ Hz, 1H), 7.58 (dd, $J = 12.6, 8.8$ Hz, 2H), 5.55 (s, 2H), 5.47 (s, 2H), 3.59 (s, 3H), 3.29 (s, 3H).

¹³CNMR (101 MHz, chloroform-*d*) δ 162.5, 157.0, 148.2, 137.5, 133.7, 122.9, 119.1, 116.3, 114.5, 99.5, 95.1, 71.6, 56.9, 38.5.

HRMS-ESI (m/z): $[M+H]^+$ calculated for $C_{14}H_{14}N_2O_5S$, 323.0696; found, 323.06966.



tert-Butyl (2-(4-((8-bromo-7-(methoxymethoxy)quinolin-2-yl)methoxy)phenyl)-2-hydroxyethyl)carbamate (35)

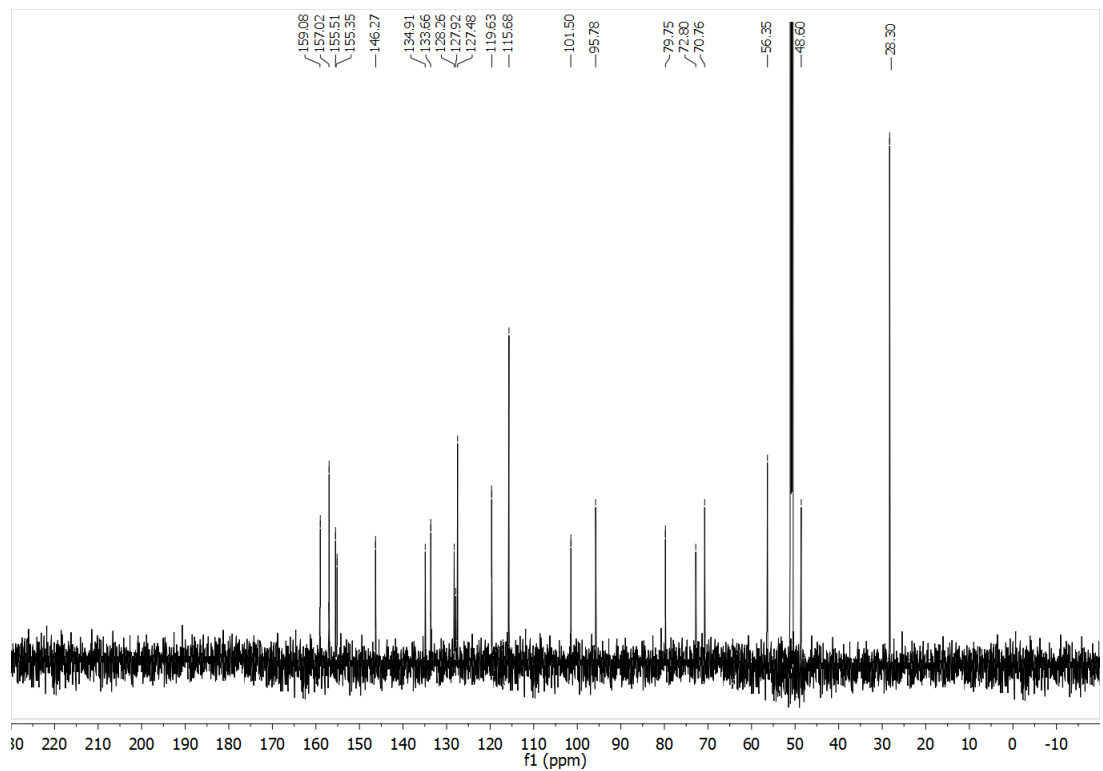
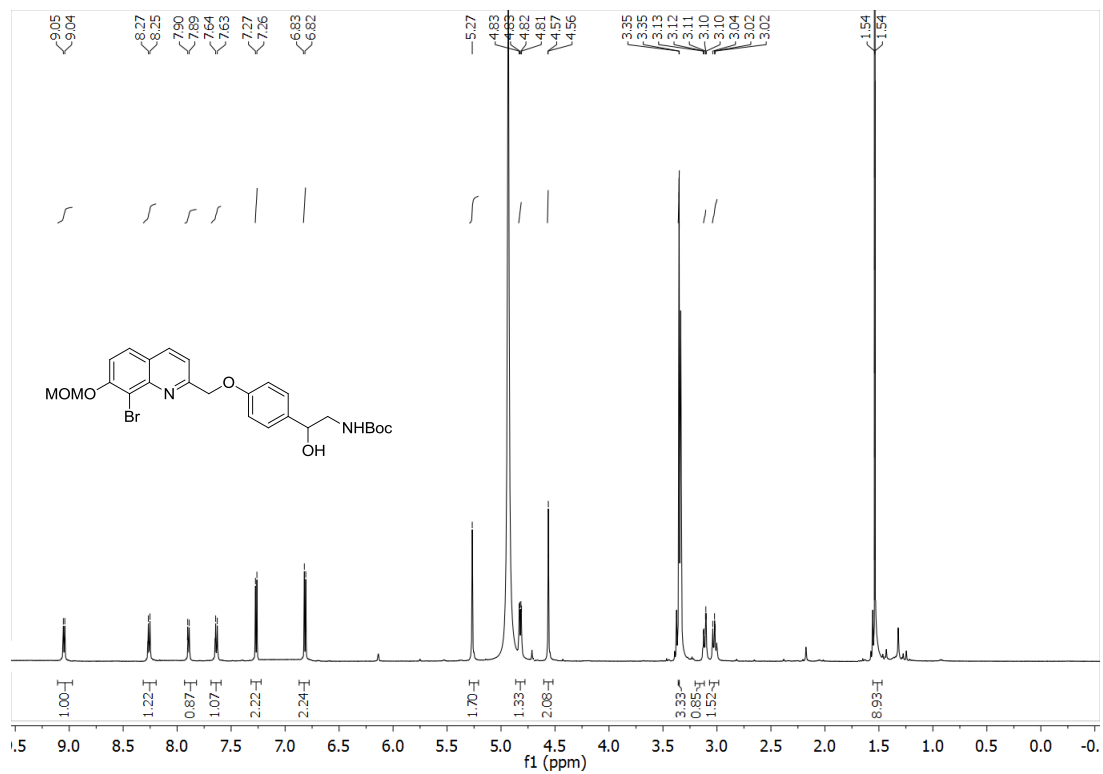


Compound **33** (0.035 g, 0.094 mmol) and *N*-Boc-octopamine (0.050 g, 0.20 mmol) were stirred in acetone (1 mL) and Cs₂CO₃ (0.075 g, 0.25 mmol) was added. The reaction was monitored by uHPLC and upon completion was diluted with brine, extracted with ethyl acetate, dried over anhydrous sodium sulfate, filtered, and concentrated in vacuo. The crude product was purified via flash chromatography eluting with EtOAc/hexane (1:1), which yielded **35** as a yellow solid upon drying (0.021 g, 0.039 mmol, 20% yield)

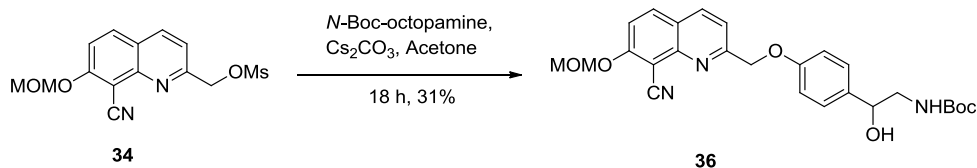
¹H NMR (600 MHz, methanol-*d*₄) δ 9.05 (d, *J* = 8.3 Hz, 1H), 8.26 (d, *J* = 9.0 Hz, 1H), 7.90 (d, *J* = 8.3 Hz, 1H), 7.64 (d, *J* = 9.0 Hz, 1H), 7.27 (d, *J* = 8.0 Hz, 2H), 6.82 (d, *J* = 8.0 Hz, 2H), 5.27 (s, 2H), 4.82 (dd, *J* = 9.8, 3.4 Hz, 1H), 4.57 (s, 3H), 3.35 (s, 3H), 3.27 – 2.70 (m, 2H), 1.54 (s, 9H).

¹³C NMR (125 MHz, methanol-*d*₄) δ 159.08, 157.02, 155.51, 155.35, 146.27, 134.91, 133.66, 128.26, 127.92, 127.48, 119.63, 115.68, 101.50, 95.78, 79.75, 72.80, 70.76, 56.35, 48.60, 28.30.

HRMS-ESI (*m/z*): [M+H]⁺ calculated for C₂₅H₂₉N₂O₆Br, 533.1282, 535.1262; found, 533.1285, 535.1263.



tert-Butyl (2-(4-((8-cyano-7-(methoxymethoxy)quinolin-2-yl)methoxy)phenyl)-2-hydroxyethyl)carbamate (36)

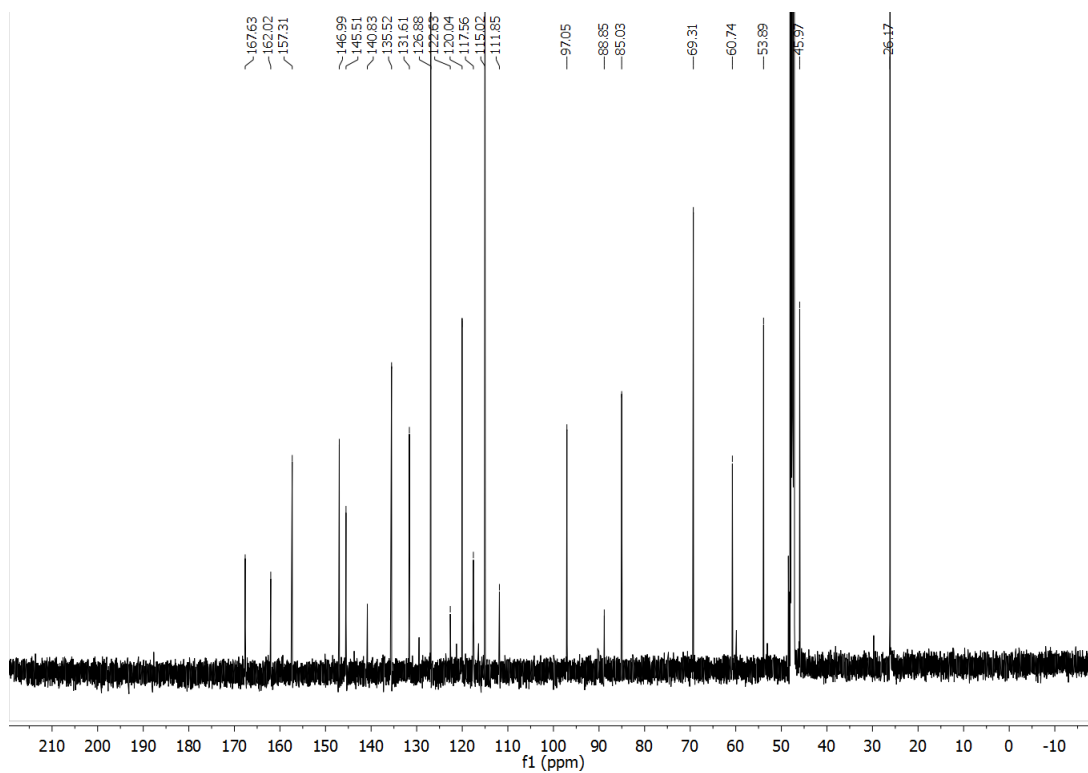
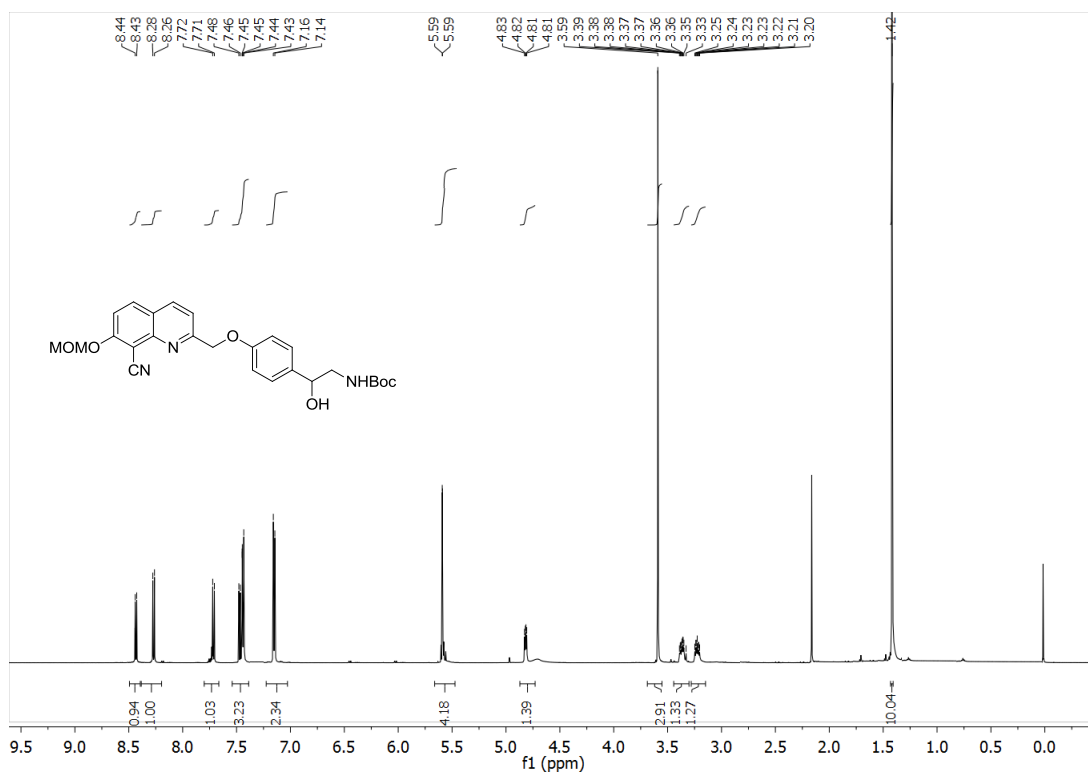


Compound **34** (0.050 g, 0.16 mmol) and *N*-Boc-octopamine (0.043 g, 0.17 mmol) were stirred in acetone (1 mL) and Cs₂CO₃ (0.10 g, 0.33 mmol) was added. The reaction was monitored by uHPLC and upon completion was quenched with brine, extracted with ethyl acetate, dried over anhydrous sodium sulfate, filtered, and was concentrated in vacuo. The crude product was purified via flash chromatography eluting with EtOAc/hexane (1:2), which yielded **36** as a yellow solid upon drying (0.025 g, 0.052 mmol, 31% yield)

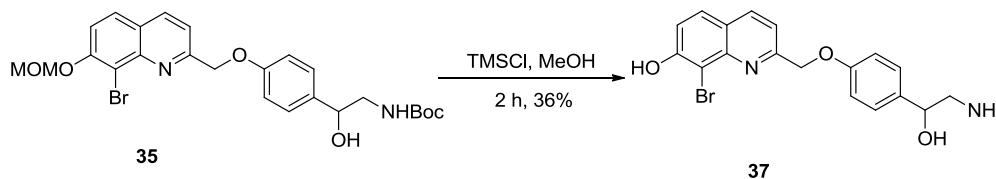
¹H NMR (600 MHz, methanol-*d*₄) δ 9.05 (d, *J* = 8.3 Hz, 1H), 8.26 (d, *J* = 9.1 Hz, 1H), 7.90 (d, *J* = 8.3 Hz, 1H), 7.64 (d, *J* = 8.9 Hz, 1H), 7.27 (d, *J* = 7.9 Hz, 2H), 6.82 (d, *J* = 7.9 Hz, 2H), 5.27 (s, 2H), 4.82 (dd, *J* = 11.9 Hz, 1H), 3.35 (s, 3H), 3.03 (dd, *J* = 10.2 Hz, 1H), 1.53 (s, 9H).

¹³C NMR (151 MHz, methanol-*d*₄) δ 167.63, 162.02, 157.31, 146.99, 145.51, 140.83, 135.52, 131.61, 126.88, 122.63, 120.04, 117.56, 115.02, 111.85, 97.05, 88.85, 85.03, 69.31, 60.74, 53.89, 45.97, 26.17.

HRMS-ESI (*m/z*): [M+H]⁺ calculated for C₂₆H₂₉N₃O₆, 480.2129; found, 480.21438.



2-((4-(2-Amino-1-hydroxyethyl)phenoxy)methyl)-8-bromoquinolin-7-ol (37)

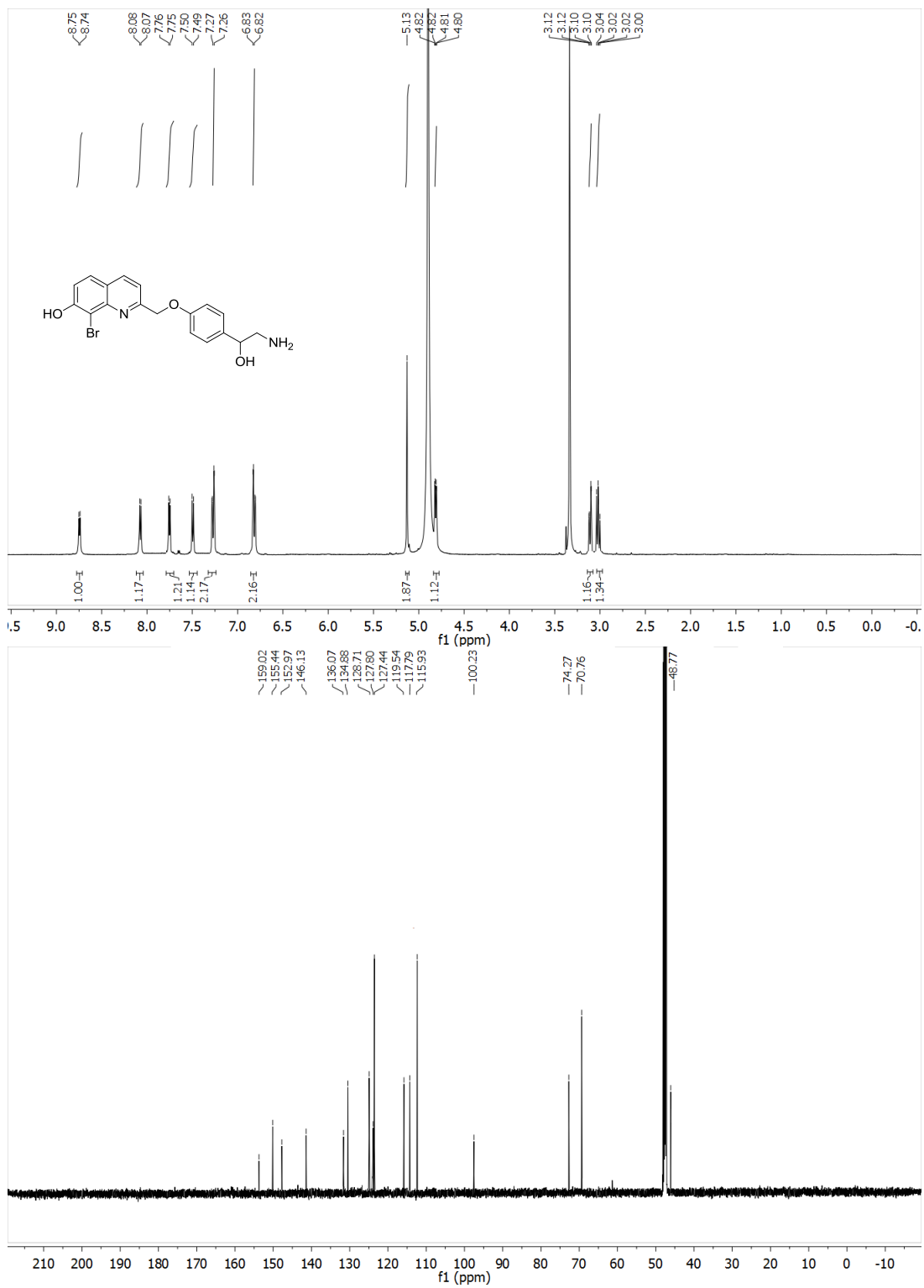


Compound **35** (0.063 g, 0.052 mmol) was dissolved in methanol (1 mL) and trimethylsilyl chloride (0.10 mL, 0.80 mmol) was added. The reaction was stirred in the dark and monitored by uHPLC. Upon completion, the reaction was concentrated in vacuo and purified by HPLC, 10 min gradient from 5% MeCN/95% H₂O (0.1% TFA) to 100% MeCN. Fractions containing only one peak were combined and concentrated in vacuo to provide **37** as a yellow oil (0.014 g, 0.036 mmol, 36% yield).

¹H NMR (600 MHz, methanol-*d*₄) δ 8.74 (d, *J* = 8.1 Hz, 1H), 8.07 (d, *J* = 8.7 Hz, 1H), 7.75 (d, *J* = 8.3 Hz, 1H), 7.49 (d, *J* = 8.9 Hz, 1H), 7.27 (d, *J* = 8.0 Hz, 2H), 6.82 (d, *J* = 7.9 Hz, 2H), 5.13 (s, 2H), 4.82 (d, *J* = 9.5 Hz, 1H), 4.81 (d, *J* = 9.6 Hz, 1H), 3.12 (t, *J* = 2.3 Hz, 1H), 3.03 (t, *J* = 2.1 Hz, 1H).

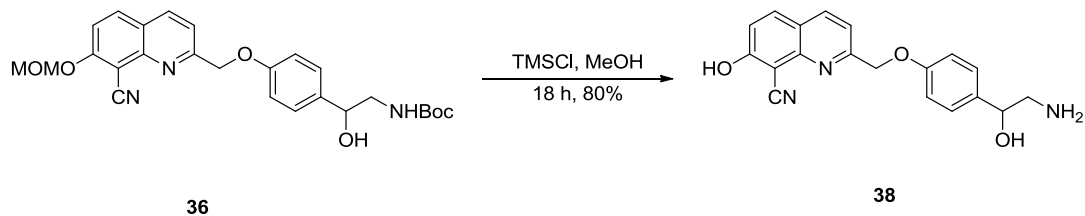
¹³C NMR (125 MHz, methanol-*d*₄) δ 159.02, 155.44, 152.97, 146.13, 136.07, 134.88, 128.71, 127.80, 127.44, 119.54, 117.79, 115.93, 100.23, 74.27, 70.76, 48.77.

HRMS-ESI (*m/z*): [M+H]⁺ calculated for C₁₈H₁₇N₂O₃Br, 389.0496, 391.0475; found, 389.04967, 391.04771.



2-((4-(2-Amino-1-hydroxyethyl)phenoxy)methyl)-7-hydroxyquinoline-8-carbonitrile

(38)

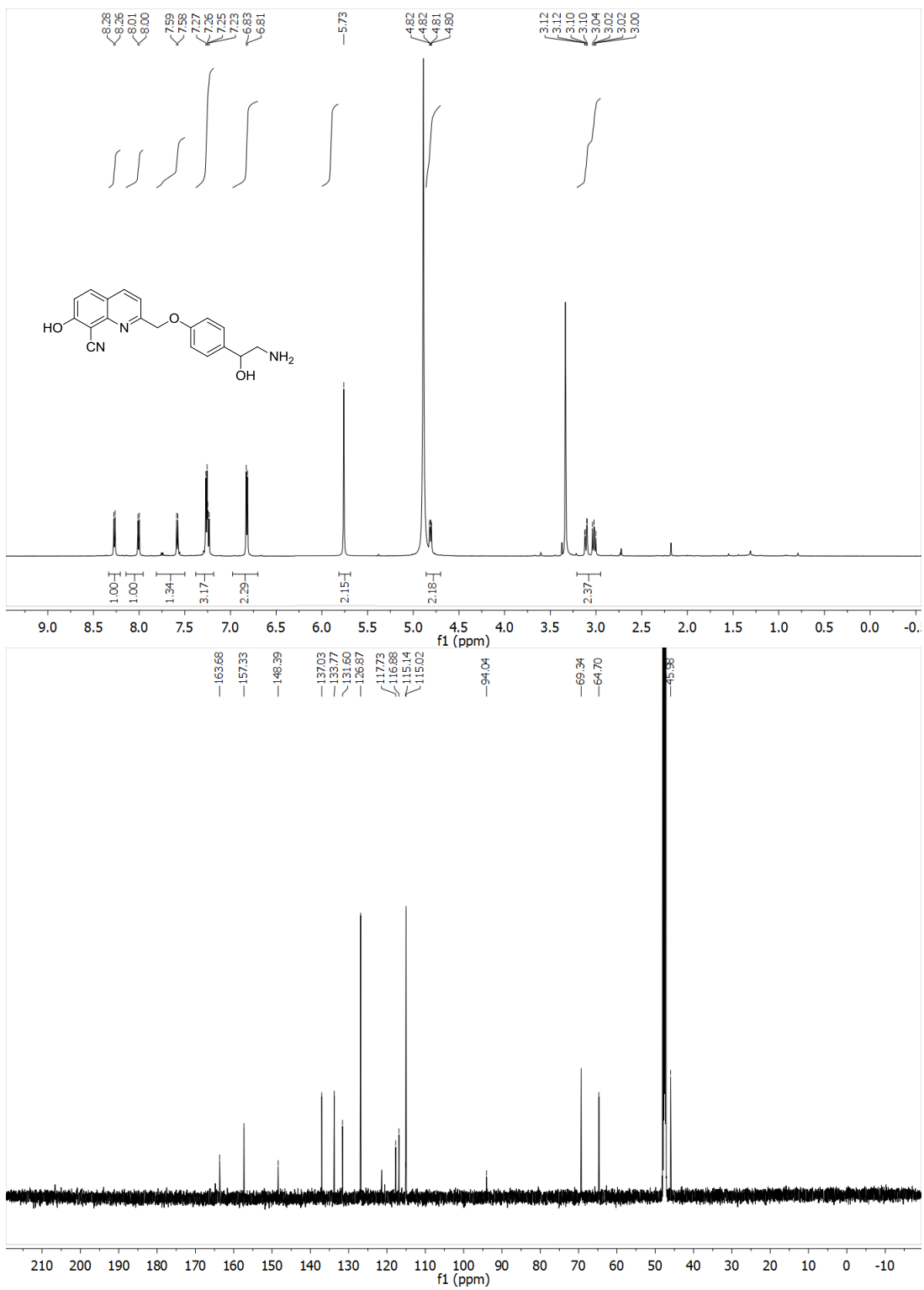


Compound **36** (0.025 g, 0.052 mmol) was dissolved in methanol (1 mL) and trimethylsilyl chloride (0.115 mL, 0.918 mmol) was added. The reaction was stirred in the dark and monitored by uHPLC. Upon completion, the reaction was concentrated in vacuo and purified by HPLC, 10 min gradient from 5% MeCN/95% H₂O (0.1% TFA) to 100% MeCN. Fractions containing only one peak were combined and concentrated in vacuo to provide **38** as a pale yellow solid (0.014 g, 0.042 mmol, 80% yield).

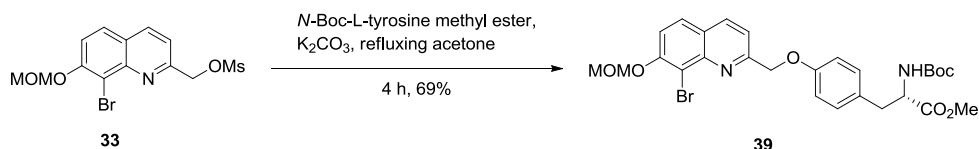
¹H NMR (600 MHz, methanol-*d*₄) δ 8.27 (d, *J* = 8.4 Hz, 1H), 8.01 (d, *J* = 9.1 Hz, 1H), 7.58 (d, *J* = 8.3 Hz, 1H), 7.26 (d, *J* = 8.5 Hz, 2H), 6.82 (d, *J* = 8.4 Hz, 2H), 5.03 (s, 2H), 4.81 (d, *J* = 6.5 Hz, 1H), 4.81 (d, *J* = 12.7 Hz, 1H), 3.12 (dd, *J* = 12.6 Hz, 1H), 3.02 (dd, *J* = 9.8, 12.6 Hz, 1H).

¹³CNMR (600 MHz, methanol-*d*₄) δ 163.6, 157.3, 148.4, 137.0, 133.7, 131.6, 126.8, 121.3, 117.7, 116.8, 115.1, 115.0, 94.0, 69.3, 64.7, 47.1, 45.9

HRMS-ESI (*m/z*): [M+H]⁺ calculated for C₁₉H₁₇N₃O₃, 336.1343; found, 336.13471



(S)-Methyl 3-(4-((8-bromo-7-(methoxymethoxy)quinolin-2-yl)methoxy)phenyl)-2-((tert-butoxycarbonyl)amino)propanoate (39)

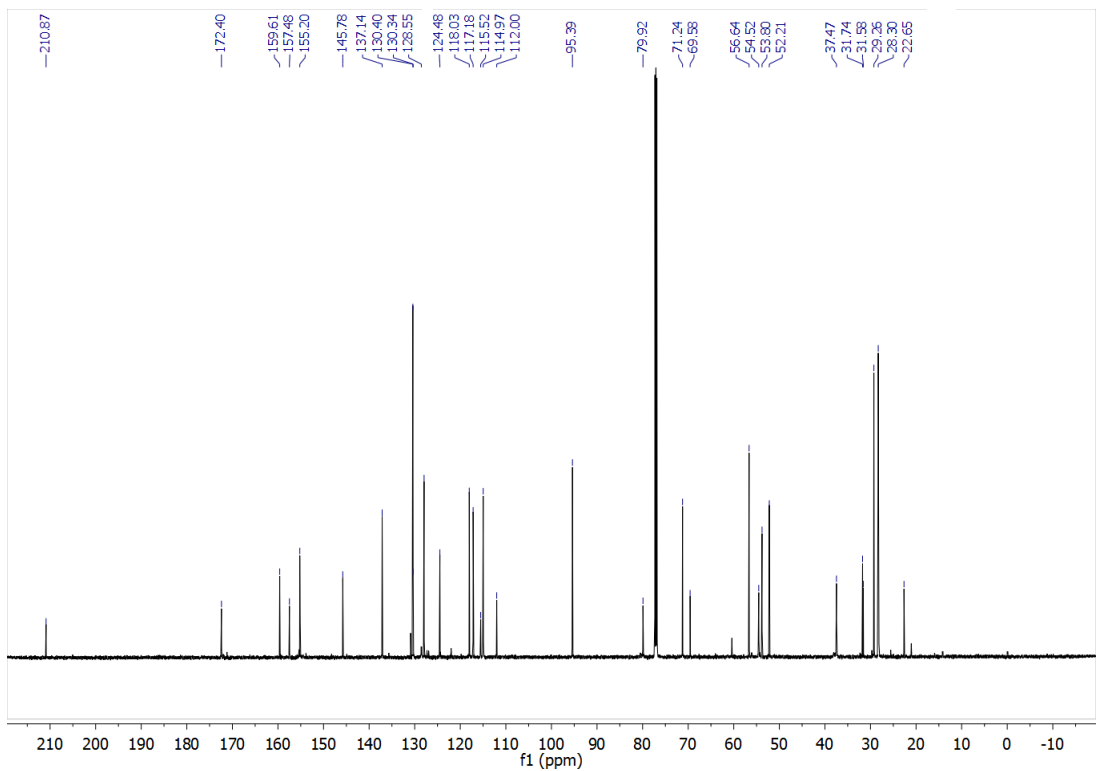
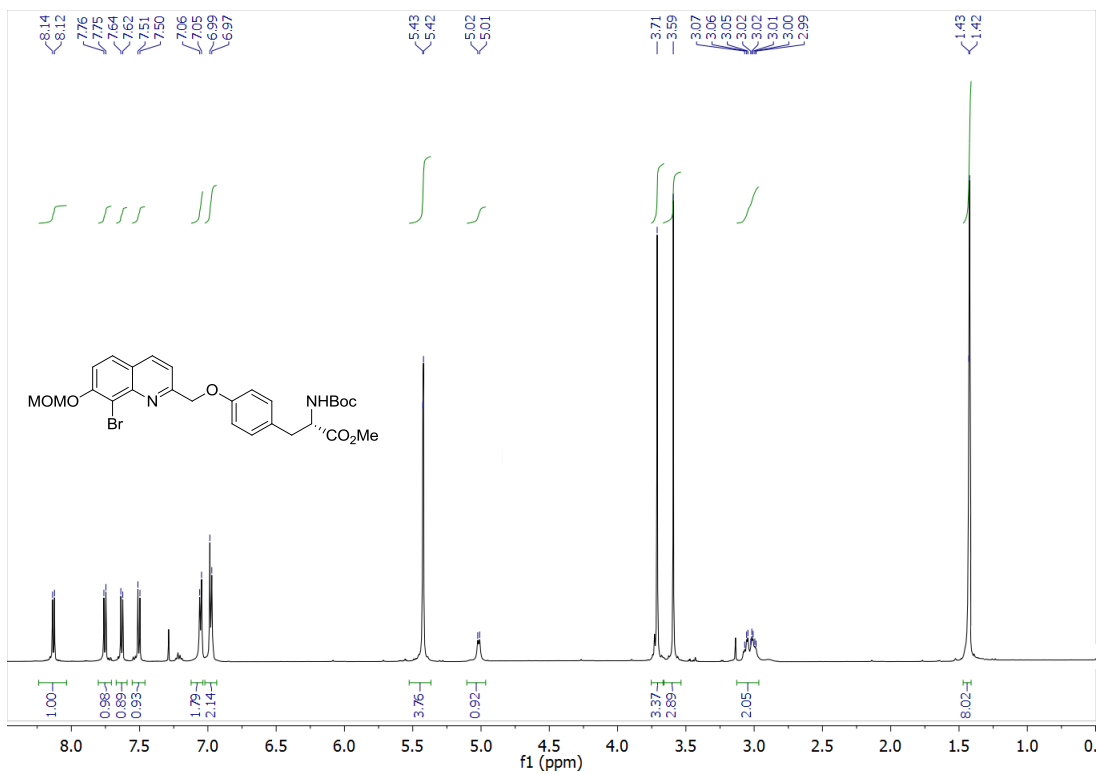


Compound **33** (0.085 g, 0.23 mmol), *N*-Boc-L-tyrosine methyl ester (0.090 g, 0.31 mmol), and K_2CO_3 (0.095 g, 0.69 mmol) were stirred in acetone (2 mL) and heated to reflux. The reaction was monitored by uHPLC, and upon completion the reaction mixture was loaded onto celite, dried in vacuo. The crude product was purified via flash chromatography eluting with EtOAc/hexane (2:3) and dried in vacuo to provide **39** as a yellow solid (0.089 g 0.16 mmol, 69% yield)

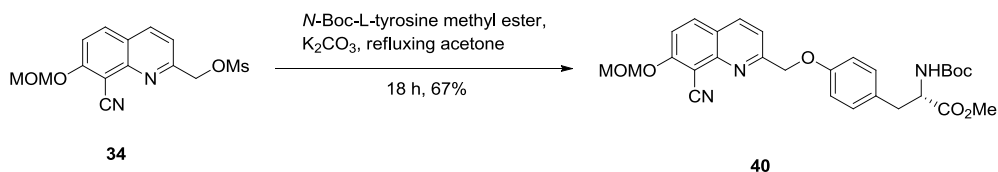
1H NMR (600 MHz, chloroform-*d*) δ 8.13 (d, J = 8.4 Hz, 1H), 7.75 (d, J = 9.0 Hz, 1H), 7.63 (d, J = 8.4 Hz, 1H), 7.50 (d, J = 9.0 Hz, 1H), 7.05 (d, J = 8.2 Hz, 2H), 6.98 (d, J = 8.6 Hz, 2H), 5.42 (d, J = 2.9 Hz, 4H), 5.02 (d, J = 8.3 Hz, 1H), 3.71 (s, 3H), 3.59 (s, 3H), 3.12 – 2.86 (m, 2H), 1.43 (d, J = 3.2 Hz, 9H).

^{13}C NMR (126 MHz, chloroform-*d*) δ 172.4, 159.6, 157.4, 155.2, 145.7, 137.1, 130.9, 128.5, 124.4, 118.0, 117.1, 115.5, 114.9, 112.0, 95.3, 79.9, 71.2, 69.5, 56.6, 54.5, 53.7, 52.2, 37.4, 31.7, 31.5, 29.2, 28.3, 22.6

HRMS-ESI (m/z): $[M+H]^+$ calculated for $C_{27}H_{31}N_2O_7Br$, 575.13944, 577.13734; found, 575.13934, 577.13773



(S)-methyl 2-((tert-butoxycarbonyl)amino)-3-(4-((8-cyano-7-(methoxymethoxy)quinolin-2-yl)methoxy)phenyl)propanoate (40)

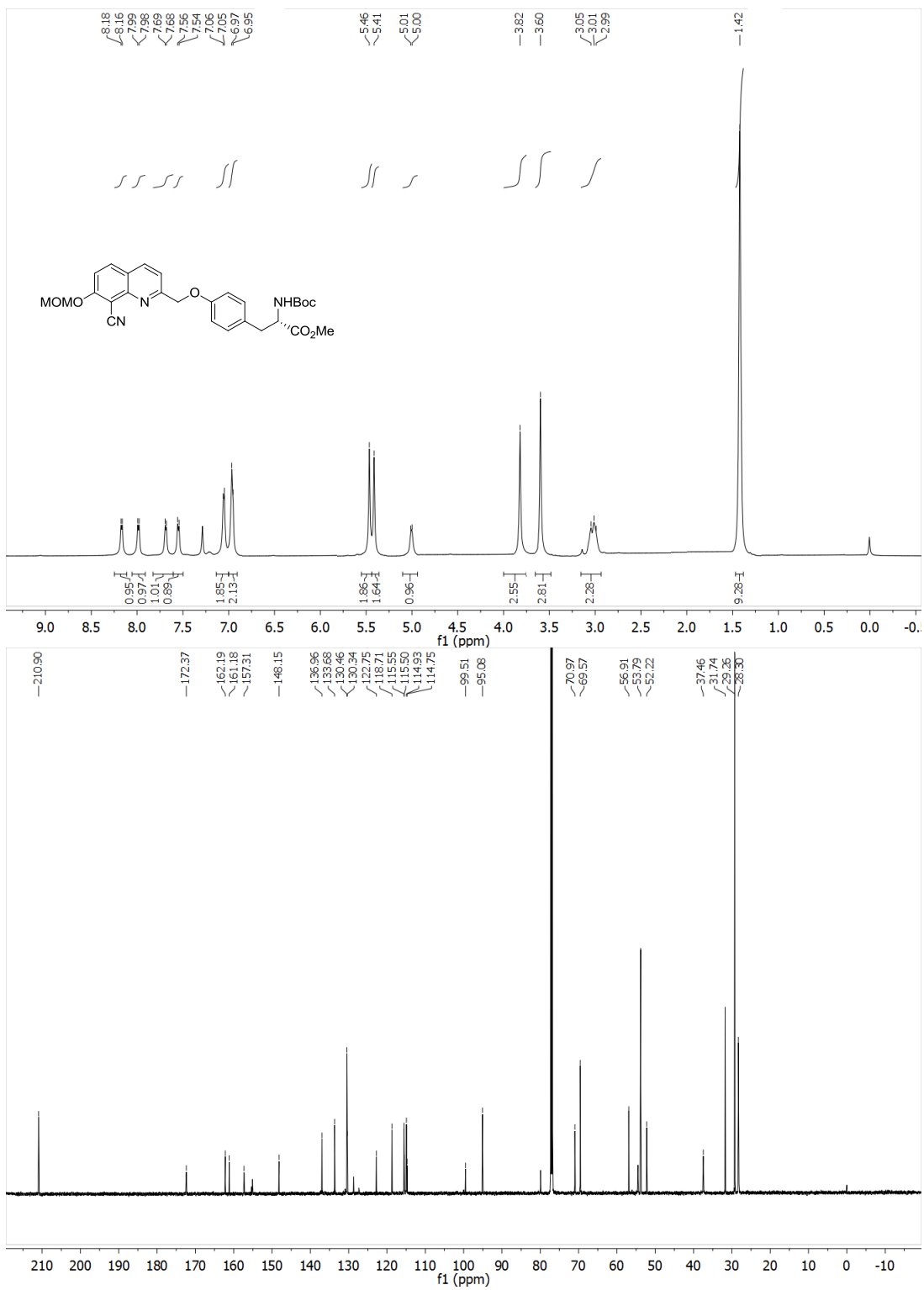


Compound **34** (0.025 g, 0.067 mmol), *N*-Boc-L-tyrosine methyl ester (0.025 g, 0.085 mmol), and K_2CO_3 (0.016 g, 0.12 mmol) were stirred in acetone (2 mL) and heated to reflux. The reaction was monitored by uHPLC, and upon the crude product was purified via flash chromatography eluting with EtOAc/hexane (1:2) and dried in vacuo to provide **40** as a yellow solid (0.031 g, 0.059 mmol, 67% yield)

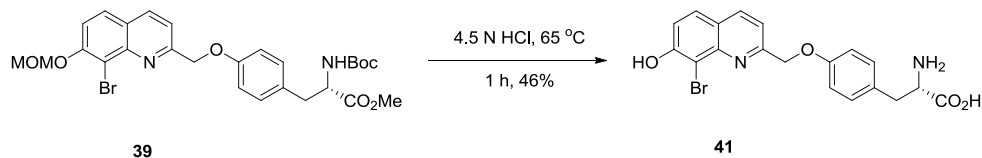
1H NMR (600 MHz, chloroform-*d*) δ 8.17 (d, $J = 7.6$ Hz, 1H), 7.99 (d, $J = 8.3$ Hz, 1H), 7.69 (d, $J = 7.5$ Hz, 1H), 7.55 (d, $J = 8.5$ Hz, 1H), 7.05 (d, $J = 5.7$ Hz, 1H), 6.97 (d, $J = 5.7$ Hz, 2H), 5.46 (s, 2H), 5.41 (s, 2H), 4.54 (m, 1H), 3.82 (s, 3H), 3.60 (s, 3H), 3.03 (m, 2H), 1.42 (s, 9H).

^{13}C NMR (126 MHz, chloroform-*d*) δ 172.3, 162.1, 161.1, 157.3, 155.3, 155.1, 148.1, 136.9, 133.6, 130.4, 128.7, 122.7, 118.7, 115.5, 114.9, 99.5, 95.0, 79.9, 70.9, 69.5, 56.9, 54.4, 53.7, 52.2, 37.4, 31.7, 29.2, 28.2

HRMS-ESI (m/z): $[M+H]^+$ calculated for $C_{28}H_{31}N_3O_7$, 522.2234; found, 522.22302



(S)-2-Amino-3-(4-((8-bromo-7-hydroxyquinolin-2-yl)methoxy)phenyl)propanoic acid (41)

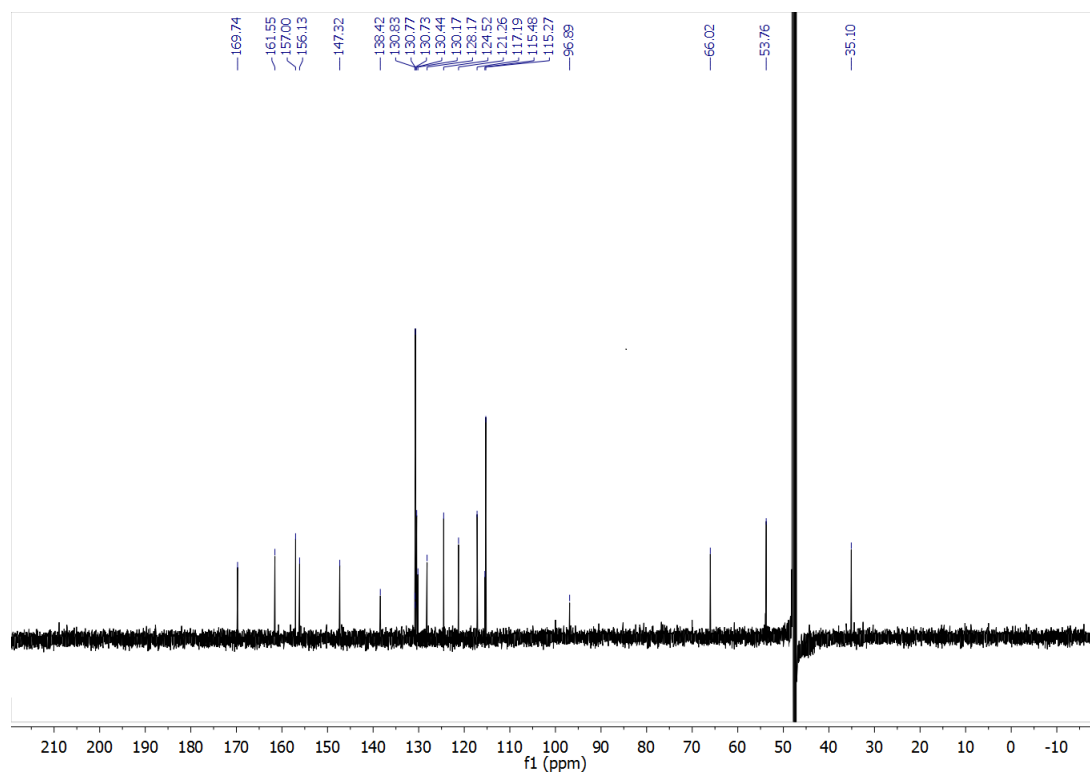
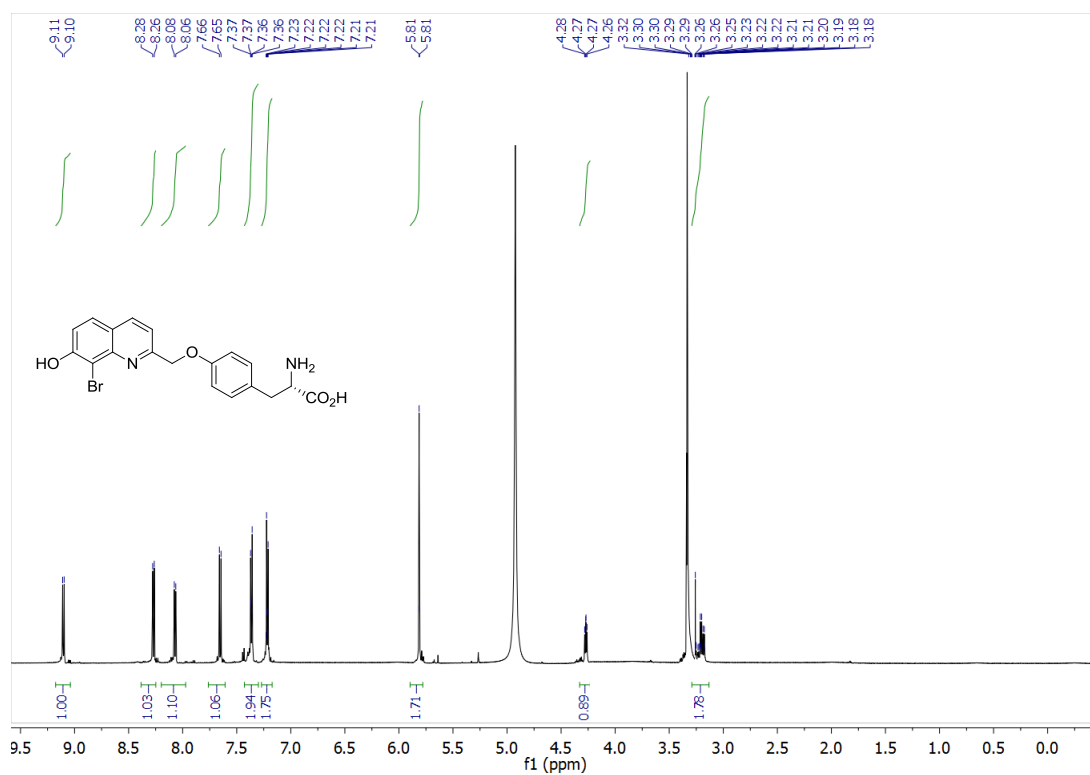


Compound **39** (0.045 g, 0.078 mmol) was stirred in 4.5N HCl_{aq} (2 mL) heated to an internal temperature of 65 °C. The reaction was monitored by uHPLC and upon completion was concentrated in vacuo. The crude product was purified via flash chromatography eluting with EtOAc/hexane (1:4) and dried in vacuo to yield **41** as a light orange solid (0.015 g, 0.036 mmol, 46% yield).

¹H NMR (600 MHz, methanol-*d*₄) δ 9.10 (d, *J* = 8.4 Hz, 1H), 8.27 (d, *J* = 9.0 Hz, 1H), 8.07 (d, *J* = 8.3 Hz, 1H), 7.65 (d, *J* = 9.0 Hz, 1H), 7.40 – 7.34 (m, 2H), 7.25 – 7.18 (m, 2H), 5.81 (s, 2H), 4.27 (dd, *J* = 7.4, 5.7 Hz, 1H), 3.33 – 3.11 (m, 2H).

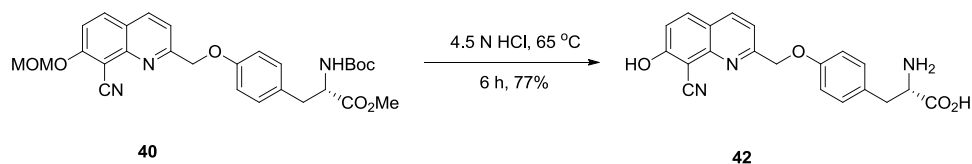
¹³C NMR (126 MHz, methanol-*d*₄) δ 169.74, 161.55, 157.00, 156.13, 147.32, 138.42, 130.83, 130.77, 130.73, 130.44, 130.17, 128.17, 124.52, 121.26, 117.19, 115.48, 115.27, 96.89, 66.02, 53.76, 35.10.

HRMS-ESI (*m/z*): [M+H]⁺ calculated for C₁₉H₁₇N₂O₄Br, 417.0445, 419.0424; found, 417.0446, 419.0427



(S)-2-Amino-3-(4-((8-cyano-7-hydroxyquinolin-2-yl)methoxy)phenyl)propanoic acid

(42)

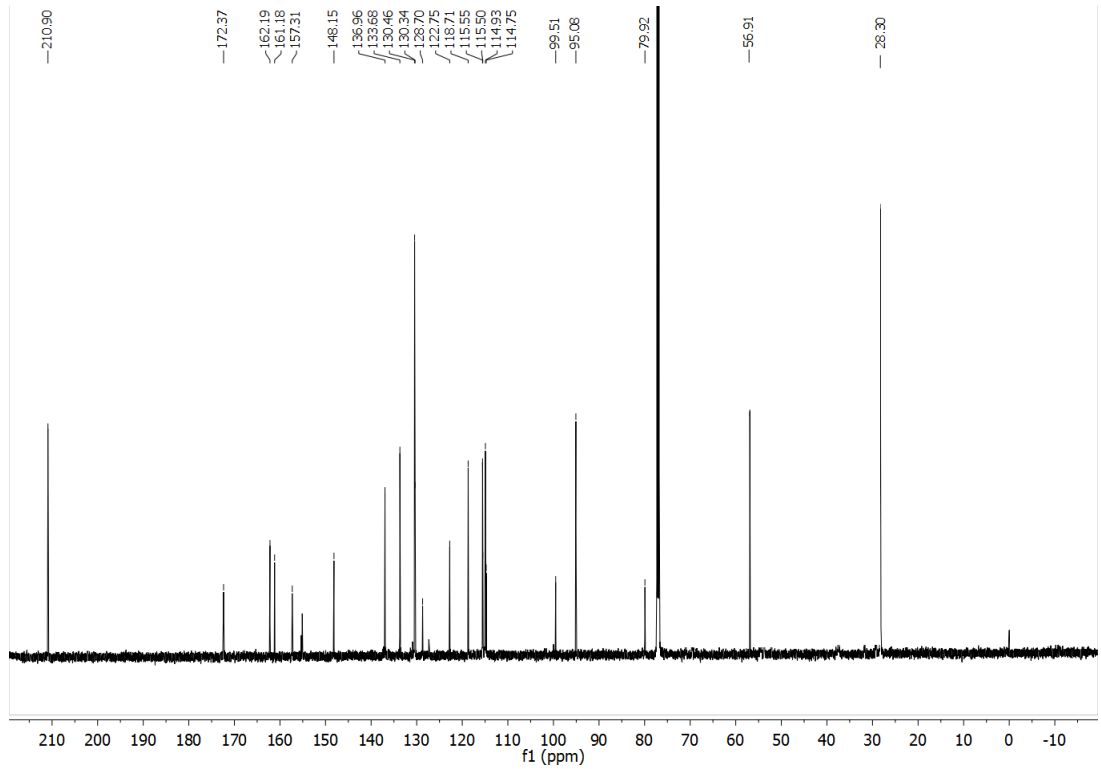
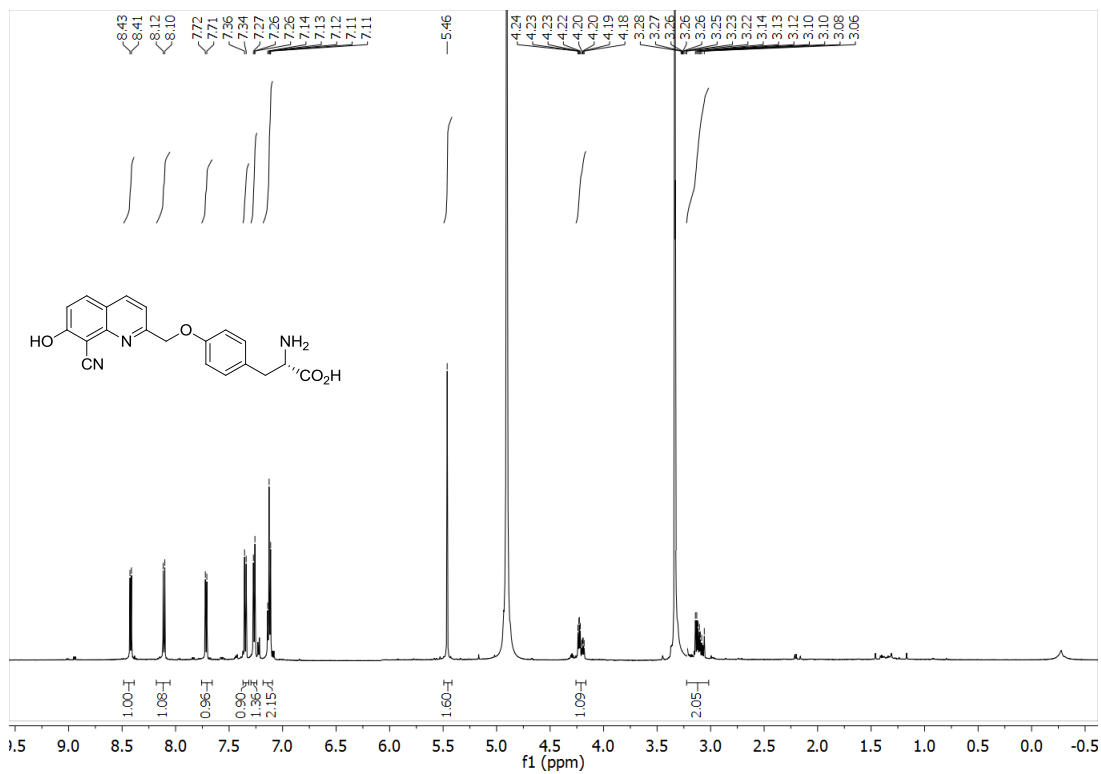


Compound **40** (0.015g, 0.029 mmol) was stirred in 4.5N HCl_{aq} (2 mL) and heated to an internal temperature of 65 °C. Reaction progress was monitored by uHPLC and upon completion was concentrated in vacuo and purified by reverse phase flash chromatography on C-18 capped silica MeCN/water (1:4) to yield a **42** as a light orange solid (0.008 g, 0.021 mmol, 77% yield)

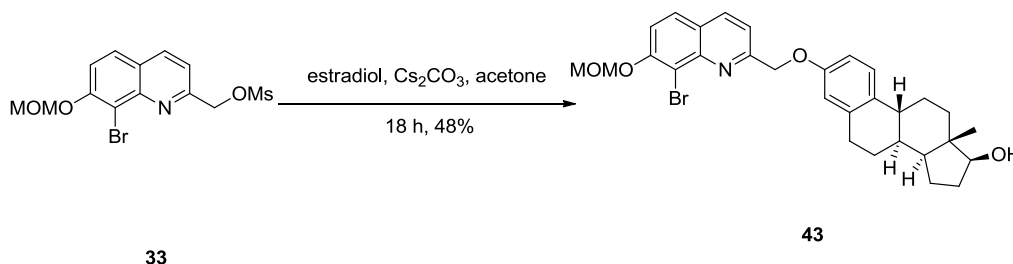
¹H NMR (600 MHz, methanol-*d*₄) δ 8.42 (d, *J* = 8.4 Hz, 1H), 8.11 (d, *J* = 9.1 Hz, 1H), 7.72 (d, *J* = 8.4 Hz, 1H), 7.35 (d, *J* = 9.1 Hz, 2H), 7.27 (d, *J* = 8.7 Hz, 2H), 5.46 (s, 2H), 4.23 (m, 1H), 3.14 (m, 2H).

¹³C NMR (126 MHz, methanol-*d*₄) δ 172.37, 162.19, 161.18, 157.31, 148.15, 136.96, 133.68, 130.46, 130.34, 128.70, 122.75, 118.71, 115.55, 115.50, 114.93, 114.75, 99.51, 95.08, 52.17, 28.30.

HRMS-ESI (*m/z*): [M+H]⁺ calculated for C₂₀H₁₇N₃O₄, 364.1292; found, 364.1330



(8*S*,9*R*,13*S*,14*S*,17*S*)-3-((8-Bromo-7-(methoxymethoxy)quinolin-2-yl)methoxy)-13-methyl-7,8,9,11,12,13,14,15,16,17-decahydro-6*H*-cyclopenta[*a*]phenanthren-17-ol
(43)

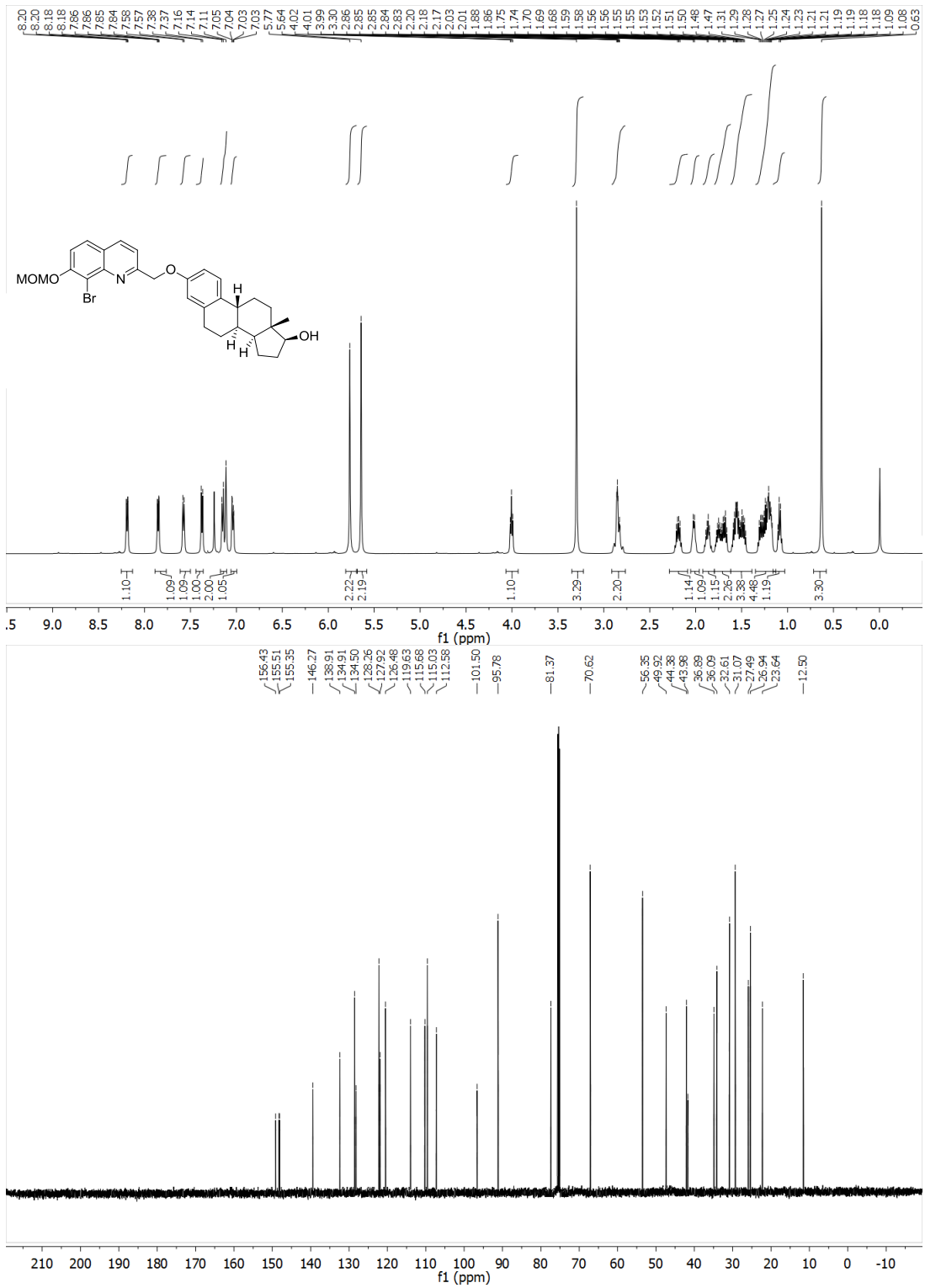


Compound **33** (0.030 g, 0.079 mmol) and estradiol (0.022 g, 0.079 mmol) were stirred in acetone (1 mL) and Cs₂CO₃ (0.051 g, 0.16 mmol) was added. The reaction was monitored by uHPLC, and upon completion was dried onto silica gel and the crude product was purified via flash chromatography eluting with EtOAc/hexane (1:3). The purified sample was dried in vacuo to provide **43** as a yellow solid (0.025 g, 0.45 mmol, 48% yield)

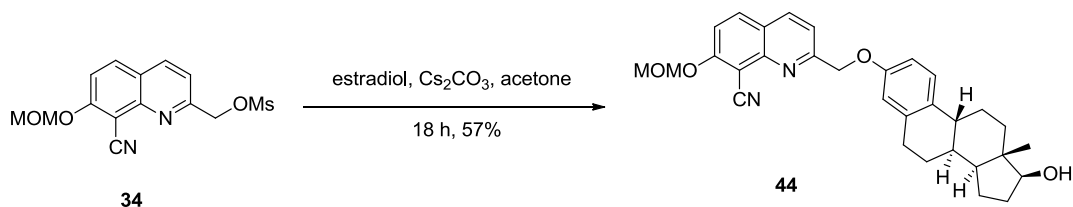
¹H NMR (600 MHz, chloroform-*d*) δ 8.21 – 8.17 (m, 1H), 7.89 – 7.76 (m, 1H), 7.58 (d, *J* = 7.5 Hz, 1H), 7.37 (d, *J* = 7.5 Hz, 1H), 7.17 – 7.11 (m, 2H), 7.04 (dd, *J* = 7.6, 2.0 Hz, 1H), 5.77 (s, 2H), 5.64 (s, 2H), 4.01 (t, *J* = 6.8 Hz, 1H), 3.30 (s, 3H), 2.84 (dt, *J* = 11.9, 3.8 Hz, 2H), 2.19 (dd, *J* = 13.1, 6.8 Hz, 1H), 2.02 (d, *J* = 7.2 Hz, 1H), 1.87 (q, *J* = 6.4 Hz, 1H), 1.72 (ddt, *J* = 32.6, 13.7, 6.6 Hz, 2H), 1.62 – 1.39 (m, 3H), 1.35 – 1.13 (m, 4H), 1.09 (t, *J* = 7.0 Hz, 1H), 0.63 (s, 3H).

¹³CNMR (125 MHz, chloroform-*d*) δ 156.43, 155.51, 155.35, 146.27, 138.91, 134.91, 134.50, 128.26, 127.92, 126.48, 119.63, 115.68, 115.03, 112.58, 101.50, 95.78, 81.37, 70.62, 56.35, 49.92, 44.38, 43.98, 36.89, 36.09, 32.61, 31.07, 27.49, 26.94, 23.64, 12.50.

HRMS-ESI (*m/z*): [M+H]⁺ calculated for C₃₀H₃₄N₁O₄Br, 552.1744, 554.1724;
found, 552.17438, 554.17251.



2-((((8*S*,9*R*,13*S*,14*S*,17*S*)-17-Hydroxy-13-methyl-7,8,9,11,12,13,14,15,16,17-decahydro-6*H*-cyclopenta[*a*]phenanthren-3-yl)oxy)methyl)-7-(methoxymethoxy)quinoline-8-carbonitrile (44**)**

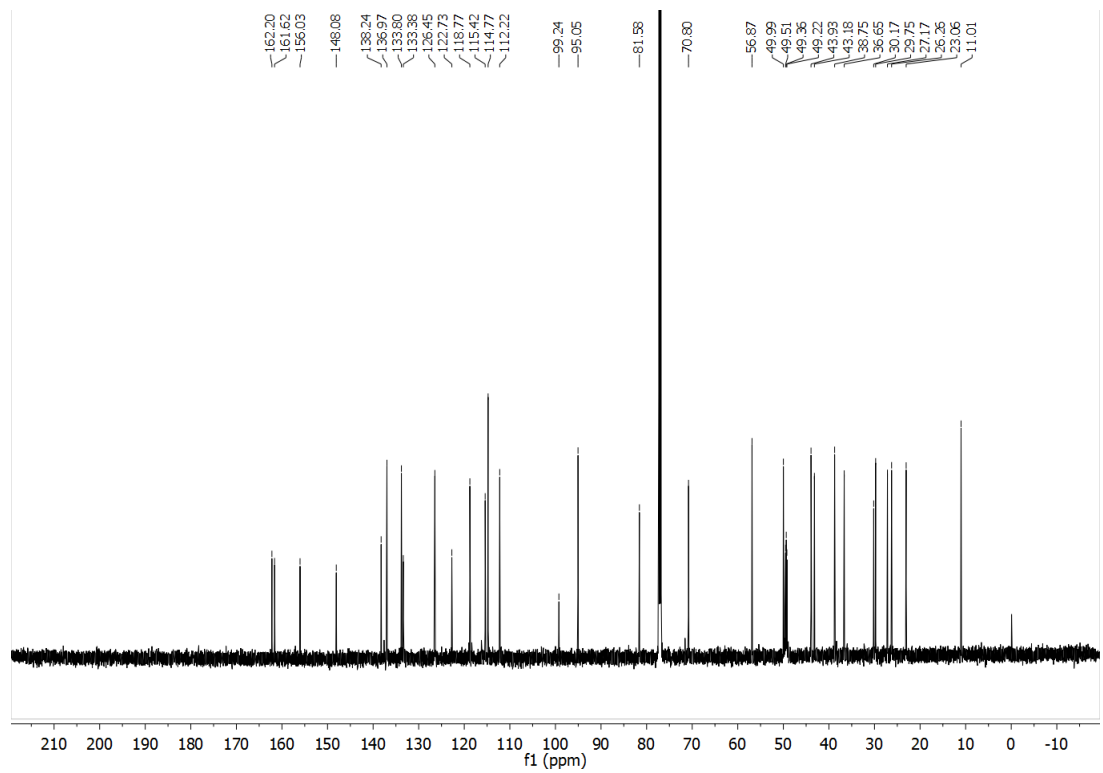
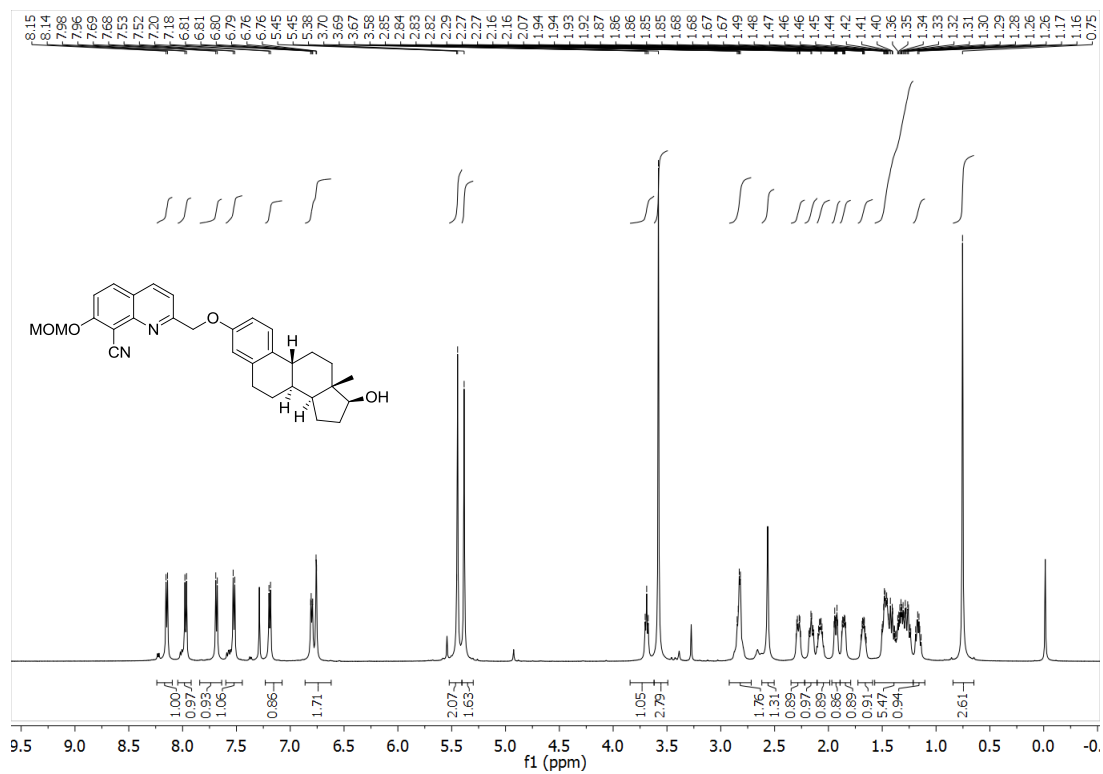


Compound **34** (0.045 g, 0.14 mmol) and estradiol (0.038 g, 0.14 mmol) were stirred in acetone (1 mL) and Cs₂CO₃ (0.091 g, 0.28 mmol) was added. The reaction was monitored by uHPLC, and upon completion was dried onto silica gel and the crude product was purified via flash chromatography eluting with EtOAc/hexane (1:4). The purified sample was dried in vacuo to provide **44** as a yellow solid (0.038 g, 0.076 mmol, 57% yield)

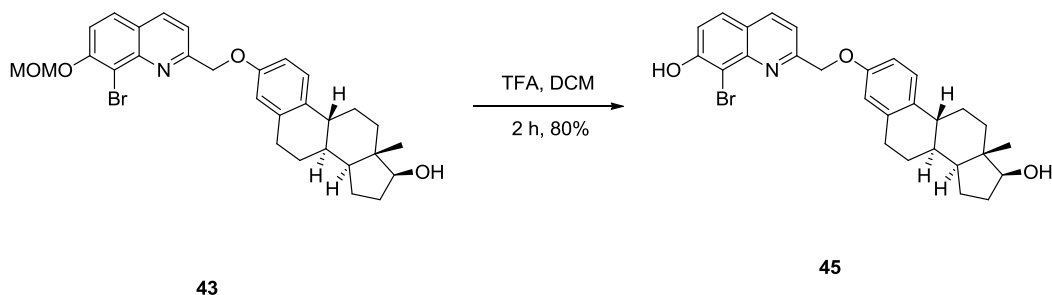
¹H NMR (600 MHz, chloroform-*d*) δ 8.15 (d, *J* = 8.4 Hz, 1H), 7.97 (d, *J* = 9.1 Hz, 1H), 7.68 (d, *J* = 8.4 Hz, 1H), 7.52 (d, *J* = 9.1 Hz, 1H), 7.19 (d, *J* = 8.5 Hz, 1H), 6.80 (d, *J* = 8.3 Hz, 1H), 6.76 (s, 1H), 5.45 (s, 2H), 5.36 (s, 2H) 3.69 (t, *J* = 8.4 Hz, 1H), 3.58 (s, 3H) 2.82 (d, *J* = 5.1 Hz, 2H), 2.56 (s, 1H) 2.28 (d, *J* = 10.9 Hz, 1H), 2.16 (t, *J* = 18.0 Hz, 1H), 2.08 (h, *J* = 18.7 Hz, 1H), 1.93 (d, *J* = 12.4 Hz, 1H), 1.87 (dd, *J* = 2.5 Hz, 1H), 1.68 (q, *J* = 3.8 Hz, 1H), 1.50-1.10 (m, 7H), 0.75 (s, 3H).

¹³CNMR (600 MHz, chloroform-*d*) δ 162.2, 161.6, 156.0, 148.0, 138.2, 136.9, 133.8, 133.3, 126.4, 122.7, 118.7, 115.4, 114.7, 112.2, 99.2, 95.0, 81.5, 70.8, 56.8, 49.9, 49.3, 43.9, 43.1, 38.7, 36.6, 30.1, 29.7, 27.1.

HRMS-ESI (*m/z*): [M+H]⁺ calculated for C₃₁H₃₄N₂O₄, 499.2591; found, 499.25291.



8-Bromo-2-((((8*S*,9*R*,13*S*,14*S*,17*S*)-17-hydroxy-13-methyl-7,8,9,11,12,13,14,15,16,17-decahydro-6*H*-cyclopenta[*a*]phenanthren-3-yl)oxy)methyl)quinolin-7-ol (45)



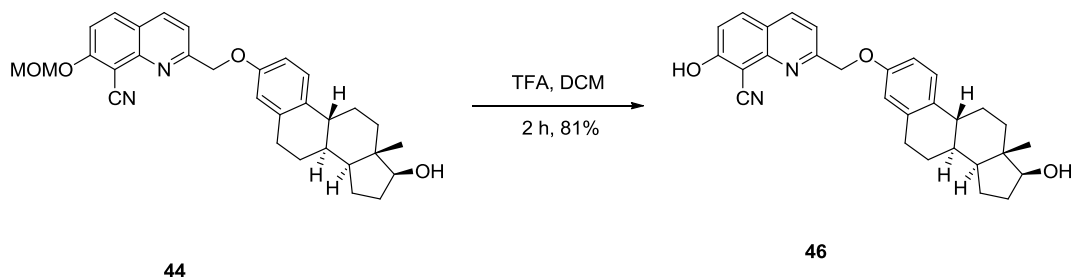
Compound **45** (0.038 g, 0.069 mmol) was stirred in dichloromethane (2 mL) and trifluoroacetic acid (0.026 mL, 0.34 mmol) was added. The reaction was monitored by uHPLC. Upon completion the reaction was concentrated in vacuo and purified through reverse phase chromatography Water/MeCN (2:3), fractions containing product were concentrated in vacuo to provide **45** as a pale yellow oil. (.028 g, 0.055 mmol, 80% yield)

¹H NMR (600 MHz, chloroform-*d*) δ 8.13 (dd, $J = 8.5, 1.9$ Hz, 1H), 7.72 (dd, $J = 8.9, 1.9$ Hz, 1H), 7.64 (d, $J = 8.7$ Hz, 1H), 7.34 (dd, $J = 8.9, 2.0$ Hz, 1H), 7.23 (d, $J = 8.7$ Hz, 1H), 6.88 – 6.84 (m, 1H), 6.82 (s, 1H), 5.42 (d, $J = 1.9$ Hz, 2H), 3.01 – 2.80 (m, 4H), 2.33 (d, $J = 13.4$ Hz, 2H), 2.26 – 2.07 (m, 3H), 1.96 (d, $J = 12.7$ Hz, 1H), 1.92 – 1.87 (m, 1H), 1.72 (d, $J = 9.9$ Hz, 1H), 1.55 – 1.15 (m, 12H), 0.80 (d, $J = 1.9$ Hz, 3H).

¹³C NMR (151 MHz, chloroform-*d*) δ 159.86, 156.28, 154.15, 145.28, 138.19, 137.13, 133.22, 128.31, 126.45, 123.66, 117.64, 117.48, 114.86, 112.31, 81.82, 71.10, 50.04, 49.89, 49.75, 43.97, 43.25, 38.80, 36.71, 30.53, 29.80, 27.22, 26.30, 23.12, 14.70, 11.06, 8.59.

HRMS-ESI (m/z): $[M+H]^+$ calculated for C₂₈H₃₀N₁O₃Br, 508.1482, 510.1462; found, 508.14873, 510.14653

7-Hydroxy-2-(((8*S*,9*R*,13*S*,14*S*,17*S*)-17-hydroxy-13-methyl-7,8,9,11,12,13,14,15,16,17-decahydro-6*H*-cyclopenta[*a*]phenanthren-3-yl)oxy)methyl)quinoline-8-carbonitrile (46)

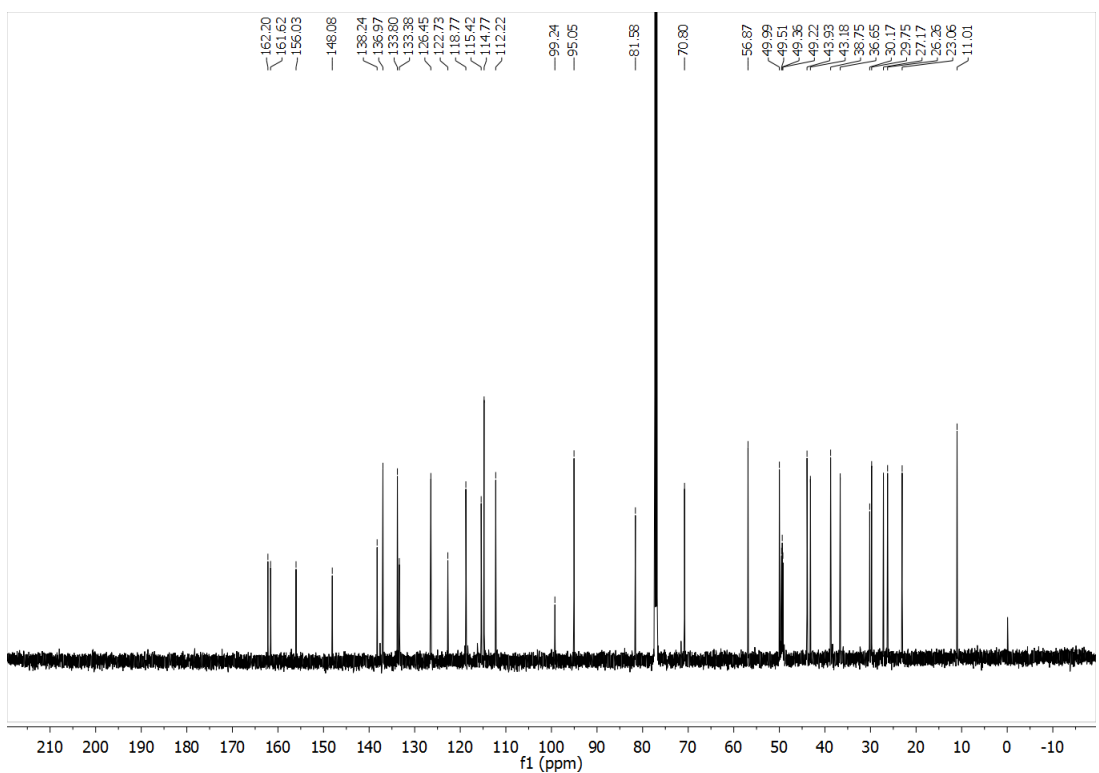
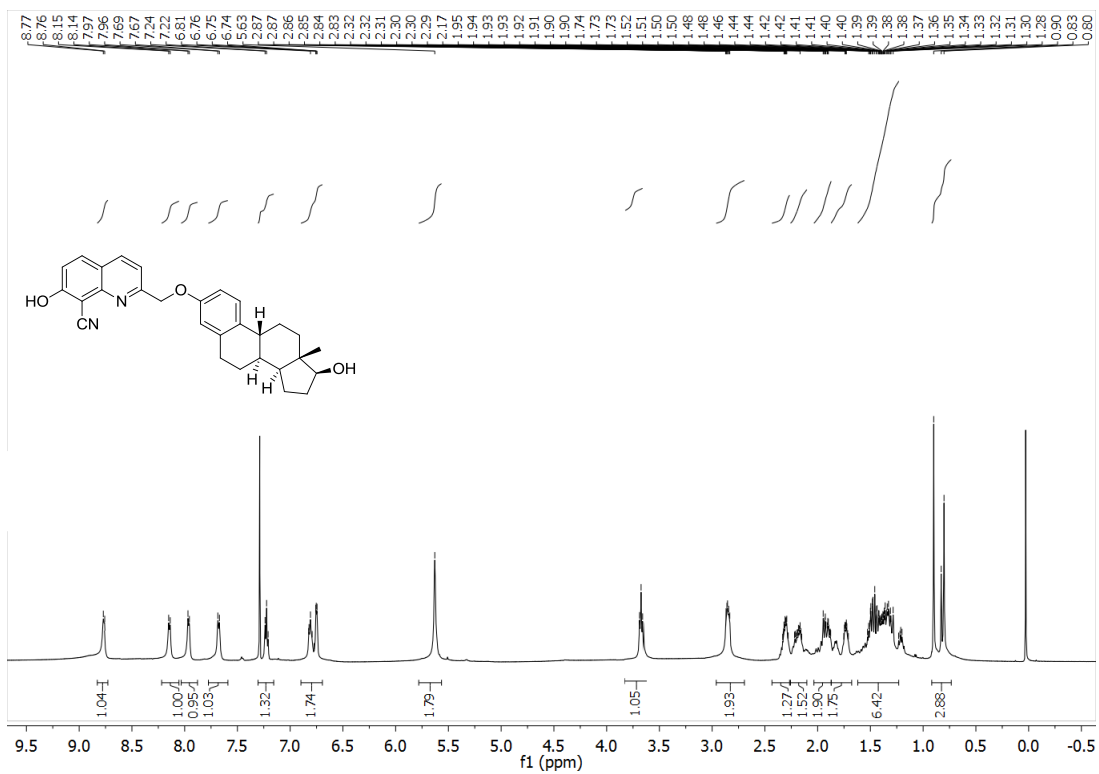


Compound **44** (0.050 g, 0.10 mmol) was stirred in dichloromethane (2 mL) and trifluoroacetic acid (0.023 mL, 0.30 mmol) was added. The reaction was monitored by uHPLC. Upon completion reaction the was concentrated in vacuo to provide **46** as a pale yellow oil. (0.037 g, 0.081 mmol, 81 % yield)

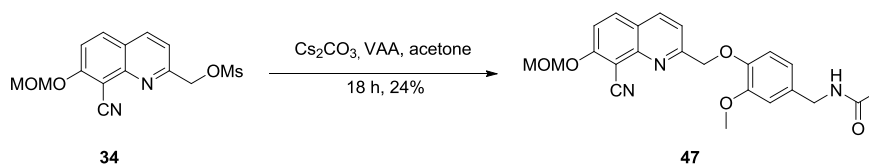
¹H NMR (600 MHz, chloroform-*d*) δ 8.76 (d, $J = 7.9$ Hz, 1H), 8.23 – 7.56 (m, 3H), 7.22 (t, $J = 8.6$ Hz, 1H), 6.99 – 6.54 (m, 2H), 5.63 (s, 2H), 3.84 (d, $J = 27.3$ Hz, 0H), 2.97 – 2.66 (m, 2H), 2.42 – 2.26 (m, 1H), 2.19 (ddd, $J = 19.5, 11.9, 4.4$ Hz, 1H), 2.01 – 1.83 (m, 1H), 1.83 – 1.69 (m, 1H), 1.65 – 1.17 (m, 4H), 1.00 – 0.65 (m, 3H).

CNMR: (151 MHz, chloroform-*d*) δ 169.5, 156.9, 154.5, 146.3, 138.6, 135.2, 134.4, 126.8, 122.8, 122.7, 117.7, 114.7, 112.0, 95.7, 86.7, 82.4, 66.9, 65.6, 55.0, 43.6, 43.3, 38.2, 36.5, 27.1, 26.9, 25.9, 23.1, 11.8, 11.0

HRMS-ESI (m/z): $[M+H]^+$ calculated for $C_{29}H_{30}N_2O_3$, 455.2329; found, 455.23283



***N*-4-((8-Cyano-7-(methoxymethoxy)quinolin-2-yl)methoxy)-3-methoxybenzylacetamide (47)**

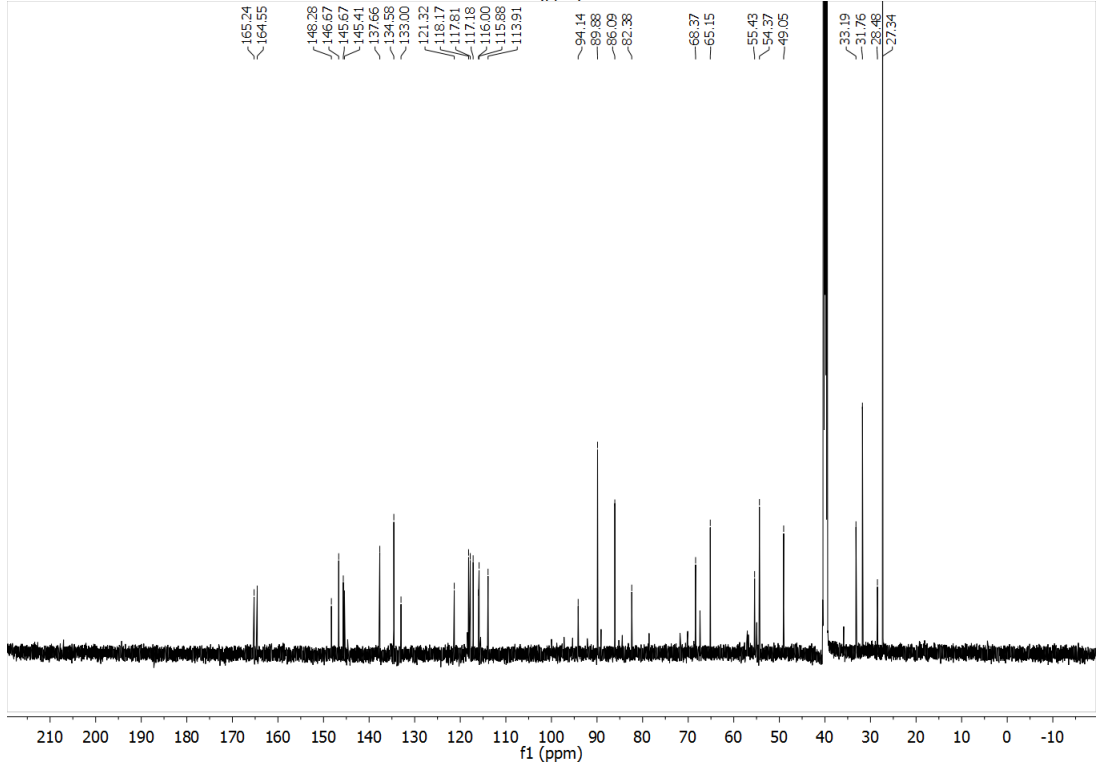
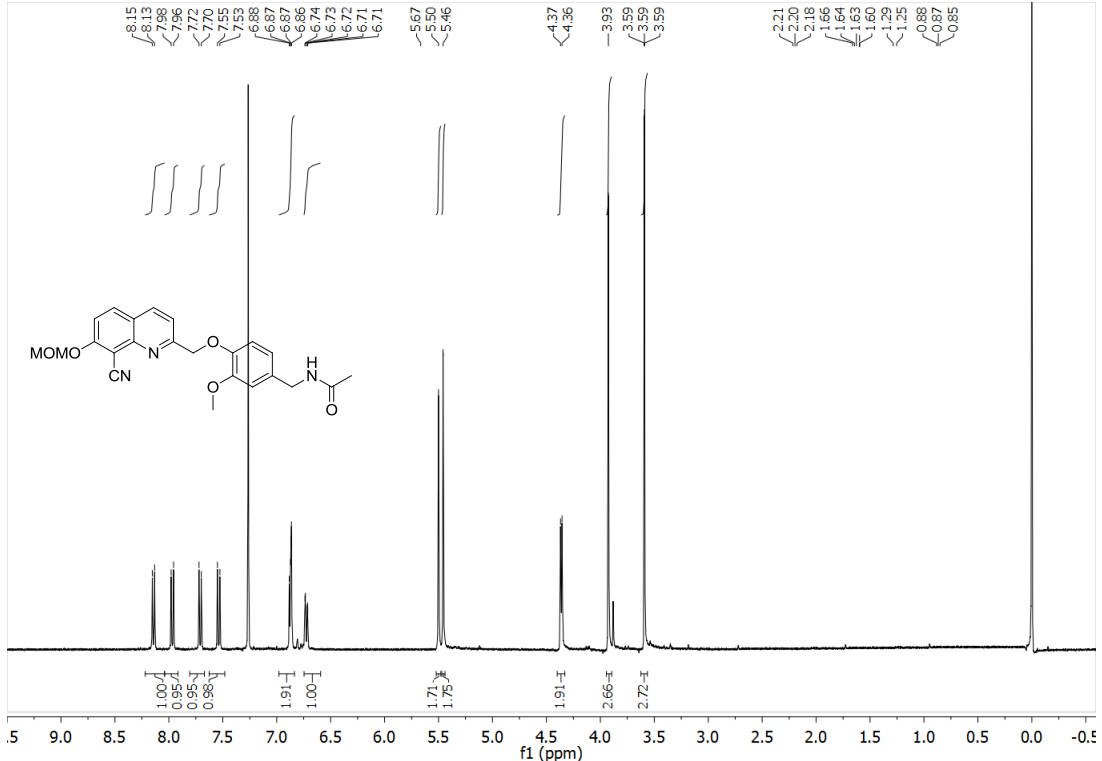


Compound **34** (0.045 g, 0.14 mmol) was dissolved in acetone (1 mL) and *N*-vanillyl acetamide (0.095 g, 0.32 mmol) and Cs_2CO_3 (0.091 g, 0.28 mmol) were added. The reaction was then stirred. The mixture was concentrated and the residue dissolved in CHCl_3 . The solution washed with water and brine, dried over MgSO_4 , filtered, and concentrated in vacuo. The crude product was purified via flash chromatography eluting with EtOAc/hexane (2:3). The solvent was removed in vacuo to provide MOM-CyHQ-VNA (0.014 g, 0.033 mmol, 24% yield):

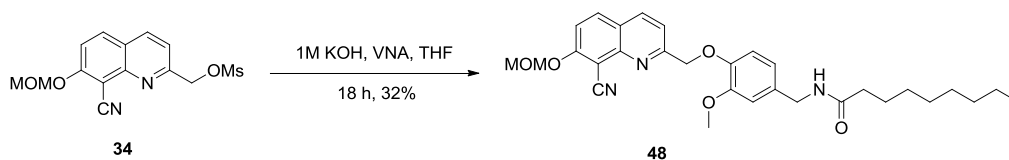
^1H NMR: (400 MHz, chloroform-*d*) δ 8.14 (d, $J = 8.5$ Hz, 1H), 7.97 (d, $J = 9.2$ Hz, 1H), 7.71 (d, $J = 8.5$ Hz, 1H), 7.54 (d, $J = 9.2$ Hz, 1H), 7.05 – 6.83 (m, 2H), 6.77 – 6.61 (m, 1H), 5.50 (s, 2H), 5.46 (s, 2H), 4.36 (d, $J = 5.7$ Hz, 2H), 3.93 (s, 3H), 3.59 (s, 2H).

^{13}C NMR: (151 MHz, methanol-*d*₄) δ 167.46, 162.10, 146.99, 145.35, 145.11, 144.20, 141.16, 135.44, 127.70, 122.56, 119.91, 119.61, 117.53, 115.36, 115.31, 111.99, 97.05, 89.08, 85.03, 60.92, 53.89, 40.84, 32.58, 26.18.

HRMS-ESI (m/z): $[\text{M}+\text{H}]^+$ calculated for $\text{C}_{23}\text{H}_{23}\text{N}_3\text{O}_5$, 422.1710; found, 422.1716



***N*-4-((8-Cyano-7-(methoxymethoxy)quinolin-2-yl)methoxy)-3-methoxybenzyl)nonanamide (48)**

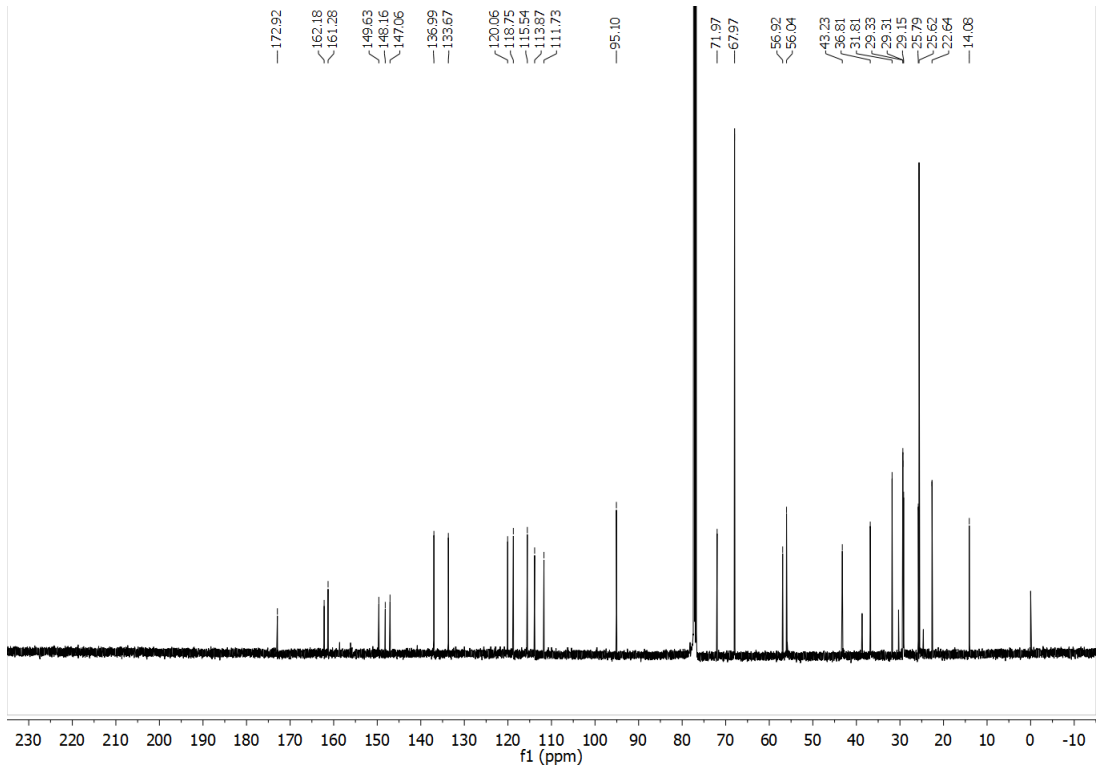
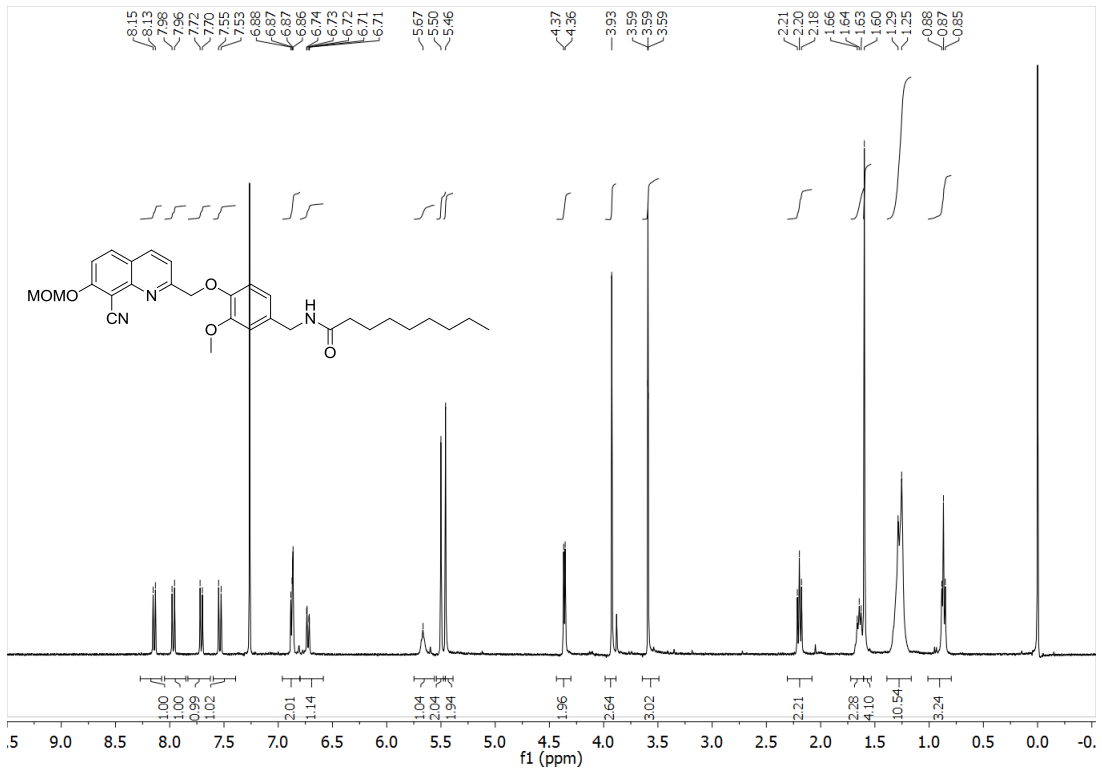


Compound **34** (0.10 g, 0.30 mmol) was dissolved in THF. *N*-vanillyl nonanamide (0.095 g, 0.32 mmol) and 1 M KOH (0.40 mL) were added and the reaction stirred overnight. The mixture was concentrated and the residue dissolved in CHCl₃. The solution washed with water and brine, dried over MgSO₄, filtered, and concentrated in vacuo. The crude product was purified via flash chromatography eluting with EtOAc/hexane (1:3). The solvent was removed in vacuo to provide **34** as a pale yellow oil (0.055 g, 0.11 mmol, 32% yield):

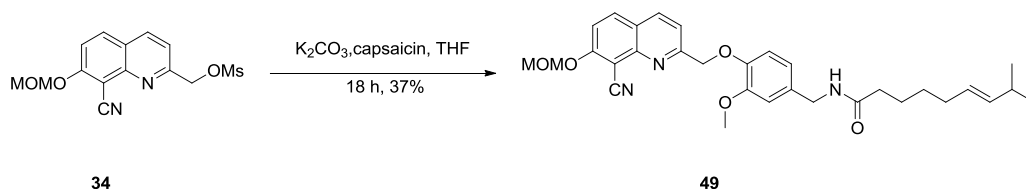
¹H NMR (400 MHz, chloroform-*d*) δ 8.14 (d, 1H), 7.97 (d, 1H), 7.71 (d, 1H), 7.54 (d, 1H), 6.88 (m, 2H), 6.72 (m, 1H), 5.78 (broad, 1H), 5.46 (s, 2H), 5.50 (s, 2H), 4.36 (d, 2H), 3.90 (s, 3H), 3.59 (s, 3H), 2.20 (t, 2H), 1.60 (m, 2H), 1.4 – 1.2 (m, 10 H), 0.84 (t, 3H);

¹³C NMR (126 MHz, chloroform-*d*) δ 172.92, 162.18, 161.28, 149.63, 148.16, 147.06, 136.99, 133.67, 120.06, 118.75, 115.54, 113.87, 111.73, 95.10, 71.97, 67.97, 56.92, 56.04, 43.23, 36.81, 31.81, 29.33, 29.31, 29.15, 25.79, 25.62, 22.64, 14.08.

HRMS-ESI (*m/z*): [M+H]⁺ calculated for C₃₀H₃₇N₃O₅, 520.2806; found, 520.28064



(E)-N-(4-((8-Cyano-7-(methoxymethoxy)quinolin-2-yl)methoxy)-3-methoxybenzyl)-8-methylnon-6-enamide (49)

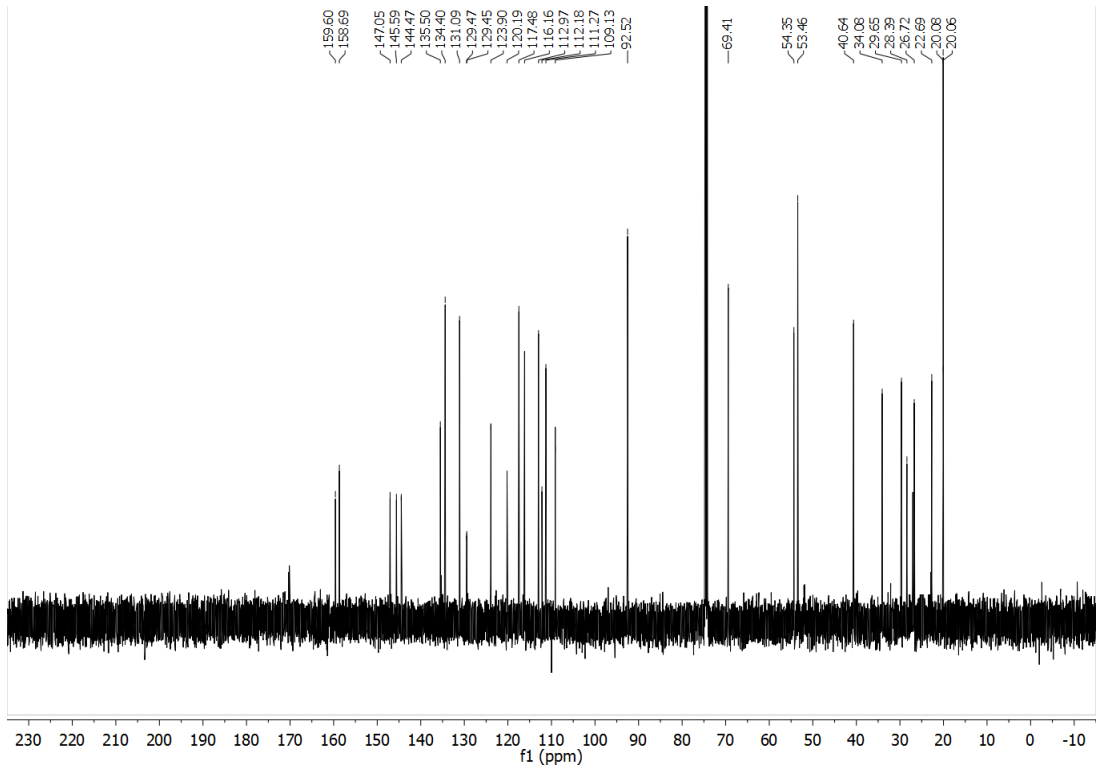
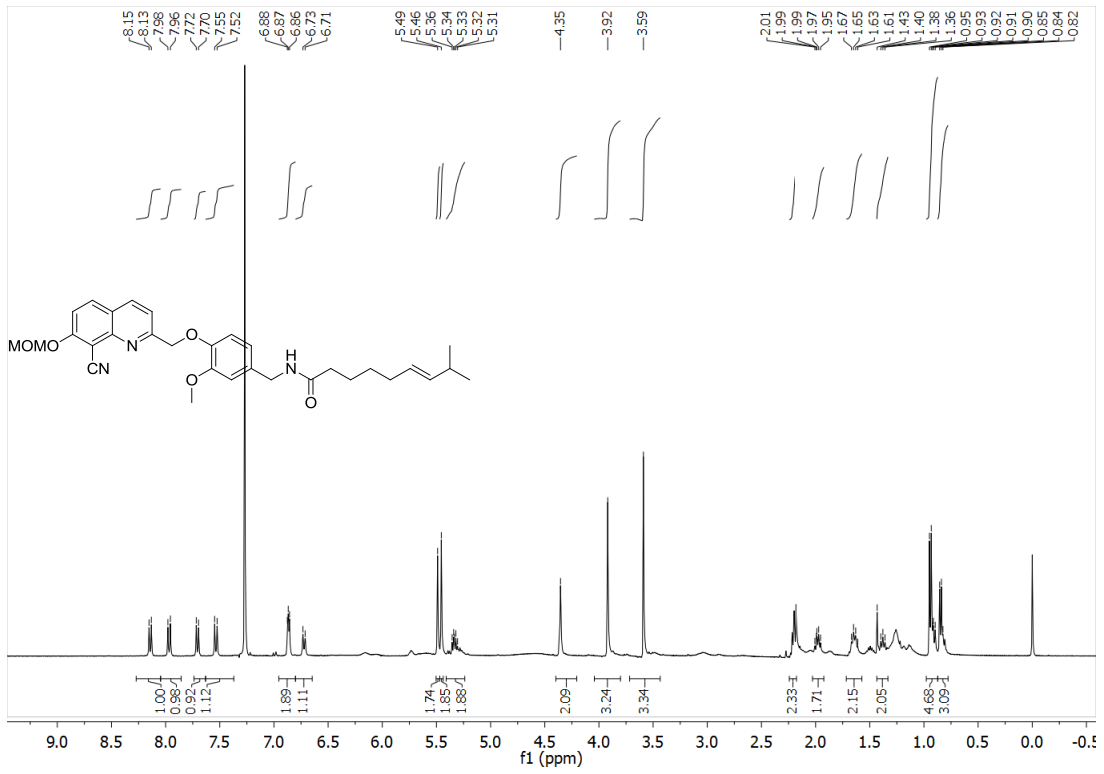


Compound **34** (0.092 g, 0.25 mmol) was dissolved in THF. Capsaicin (0.076 g, 0.25 mmol) and 1 M KOH (0.35 mL) were added and the reaction stirred overnight. The mixture was concentrated and the residue dissolved in $CHCl_3$. The solution washed with water and brine, dried over $MgSO_4$, filtered, and concentrated in vacuo. The crude product was purified via flash chromatography eluting with EtOAc/hexane (1:3). The solvent was removed in vacuo to provide MOM-CyHQ-capsaicin (0.054 g, 0.10 mmol, 37% yield):

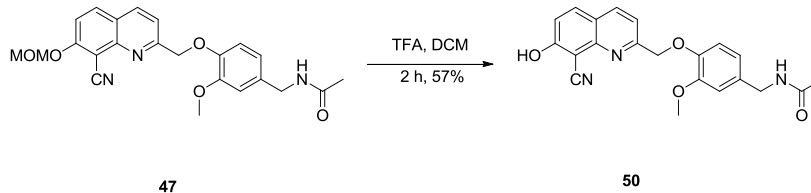
1H NMR (400 MHz, chloroform-*d*) δ 8.14 (d, 1H), 7.97 (d, 1H), 7.71 (d, 1H), 7.54 (d, 1H), 6.88 (d, 2H), 6.72 (d, 1H), 5.74 (broad, 1H), 5.49 (s, 2H), 5.46 (s, 2H), 5.33 (m, 1H), 4.36 (s, 2H), 3.92 (s, 3H), 3.59 (s, 3H), 2.20 (t, 2H), 1.65 (m, 2H), 1.4 – 1.2 (m, 8H), 0.94 (d, 3H), 0.85 (d, 3H);

^{13}C NMR ^{13}C NMR (126 MHz, methanol-*d*4) δ 159.60, 158.69, 147.05, 145.59, 144.47, 135.50, 134.40, 131.09, 129.47, 129.45, 123.90, 120.19, 117.48, 116.16, 112.97, 112.18, 111.27, 109.13, 92.52, 69.41, 54.35, 53.46, 40.64, 34.08, 29.65, 28.39, 26.72, 22.69, 20.08, 20.06.

HRMS-ESI (*m/z*): $[M+H]^+$ calculated for $C_{31}H_{37}N_3O_5$, 532.2806; found, 532.28058



***N*-4-((8-Cyano-7-hydroxyquinolin-2-yl)methoxy)-3-methoxybenzyl)acetamide (50)**

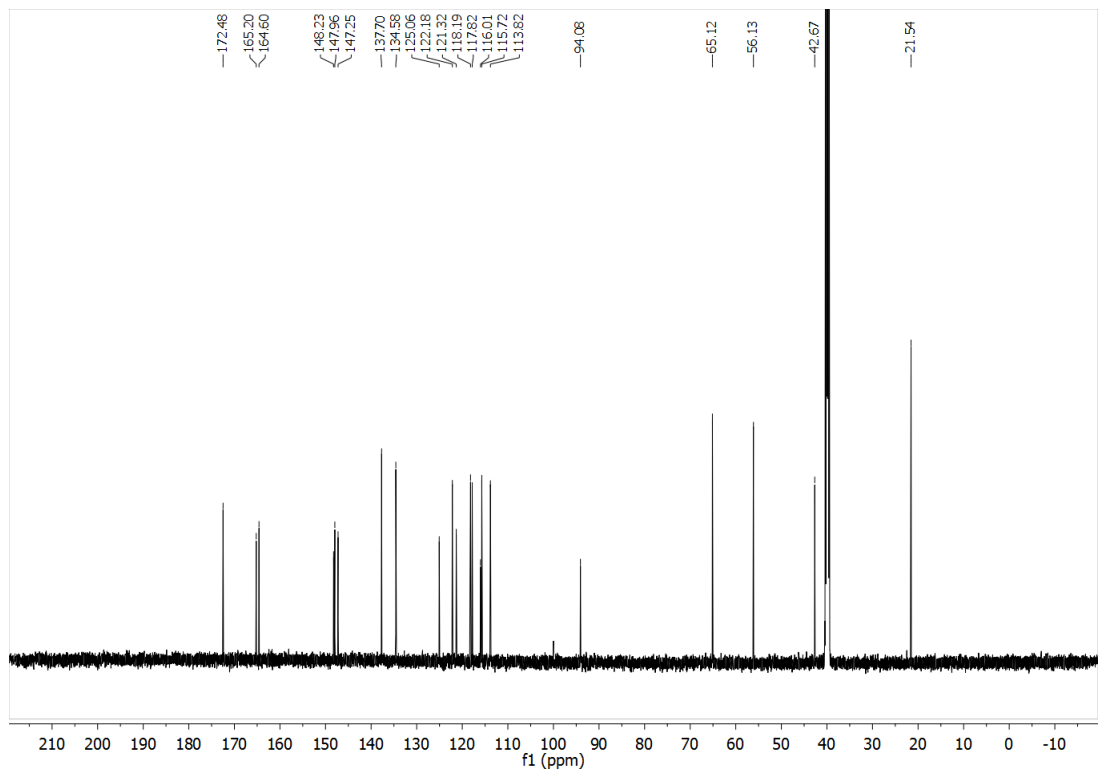
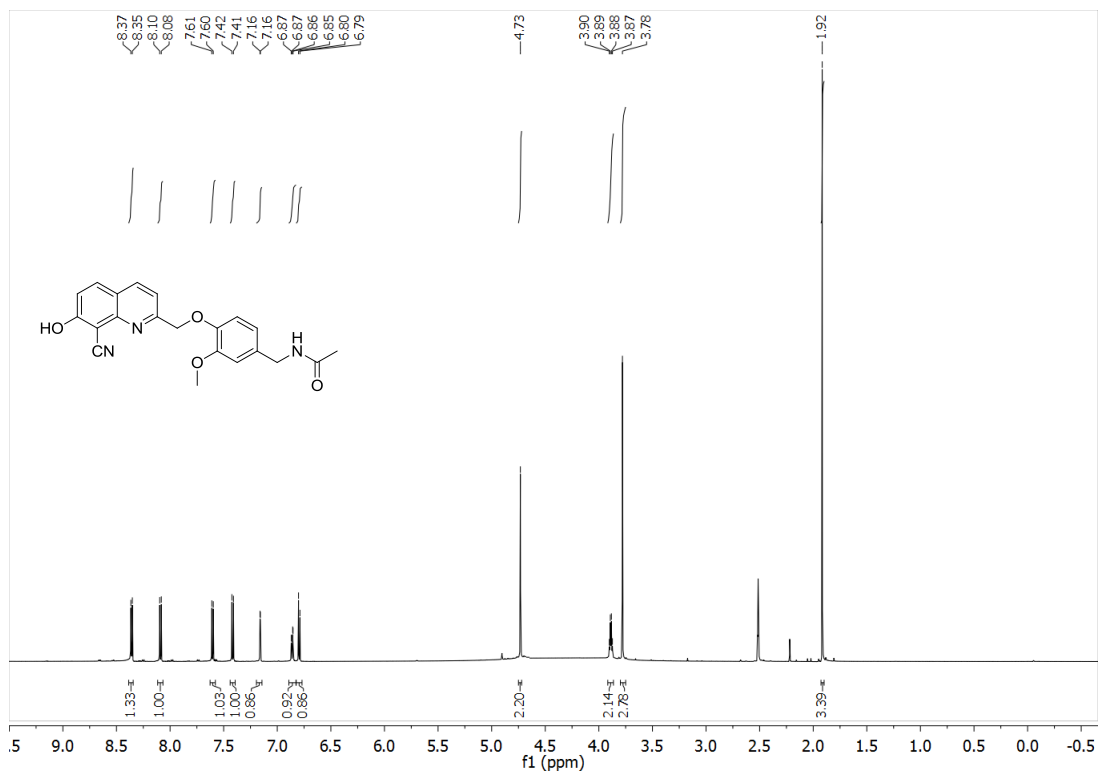


Compound **47** (0.020 g, 0.047 mmol) was dissolved in methylene chloride. Trifluoroacetic acid was added and the reaction stirred at rt for 2 h. The solvent was removed in vacuo and the residue purified by HPLC with 50% CH₃CN/50% H₂O (w/ 0.1 % TFA). Fractions containing only one peak were combined and concentrated to provide CyHQ-VNA (0.011 g, 0.029 mmol, 57% yield).

¹H NMR (600 MHz, DMSO-*d*₆) δ 8.36 (d, *J* = 8.4 Hz, 1H), 8.09 (d, *J* = 9.1 Hz, 1H), 7.60 (d, *J* = 8.4 Hz, 1H), 7.42 (d, *J* = 9.0 Hz, 1H), 7.16 (d, *J* = 2.0 Hz, 1H), 6.86 (dd, *J* = 8.1, 2.0 Hz, 1H), 6.80 (d, *J* = 8.0 Hz, 1H), 4.73 (s, 2H), 3.89 (q, *J* = 5.8 Hz, 2H), 3.78 (s, 2H), 1.92 (s, 3H).

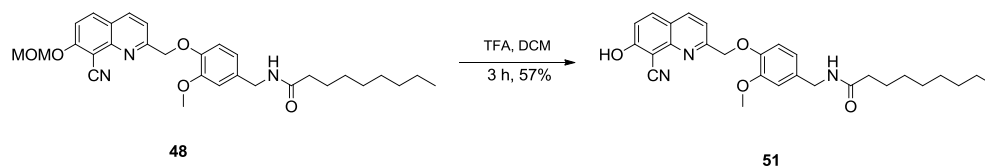
¹³C NMR (151 MHz, DMSO-*d*₆) δ 172.48, 165.20, 164.60, 148.23, 147.96, 147.25, 137.70, 134.58, 125.06, 122.18, 121.32, 118.19, 117.82, 116.01, 115.72, 113.82, 94.08, 65.12, 56.13, 42.67, 21.54.

HRMS-ESI (*m/z*): [M+H]⁺ calculated for C₂₁H₁₉N₃O₄, 378.1448; found, 378.14475.



***N*-4-((8-Cyano-7-hydroxyquinolin-2-yl)methoxy)-3-methoxybenzyl)nonanamide**

(51)

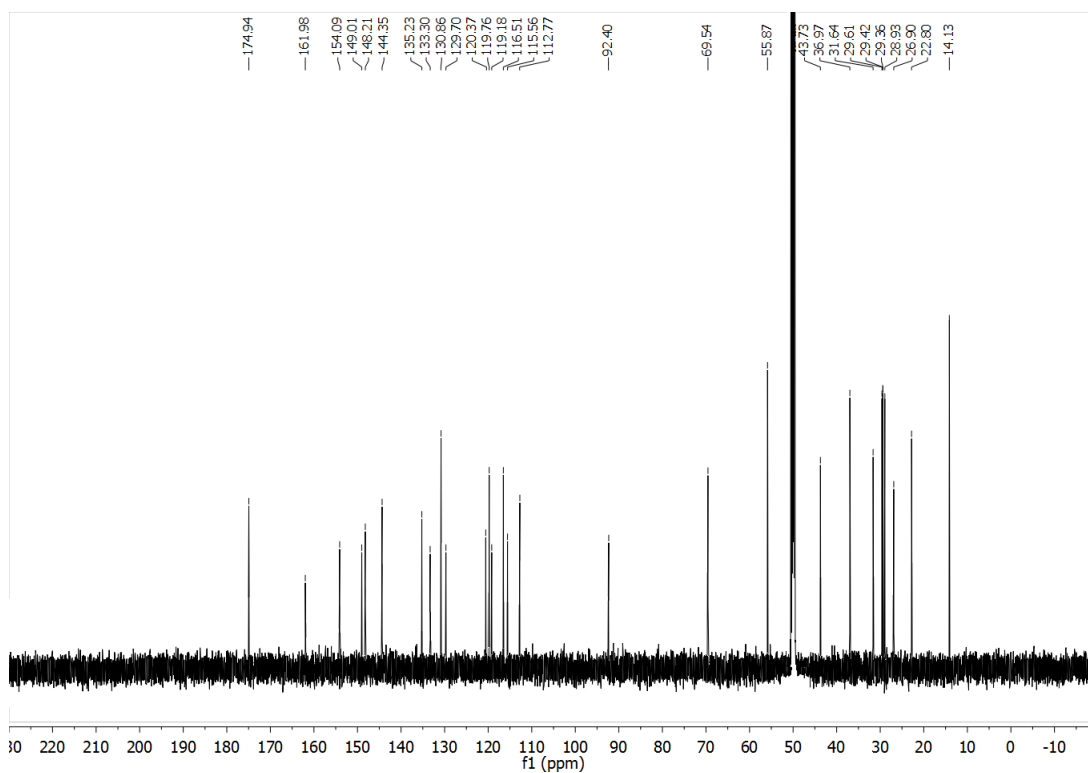
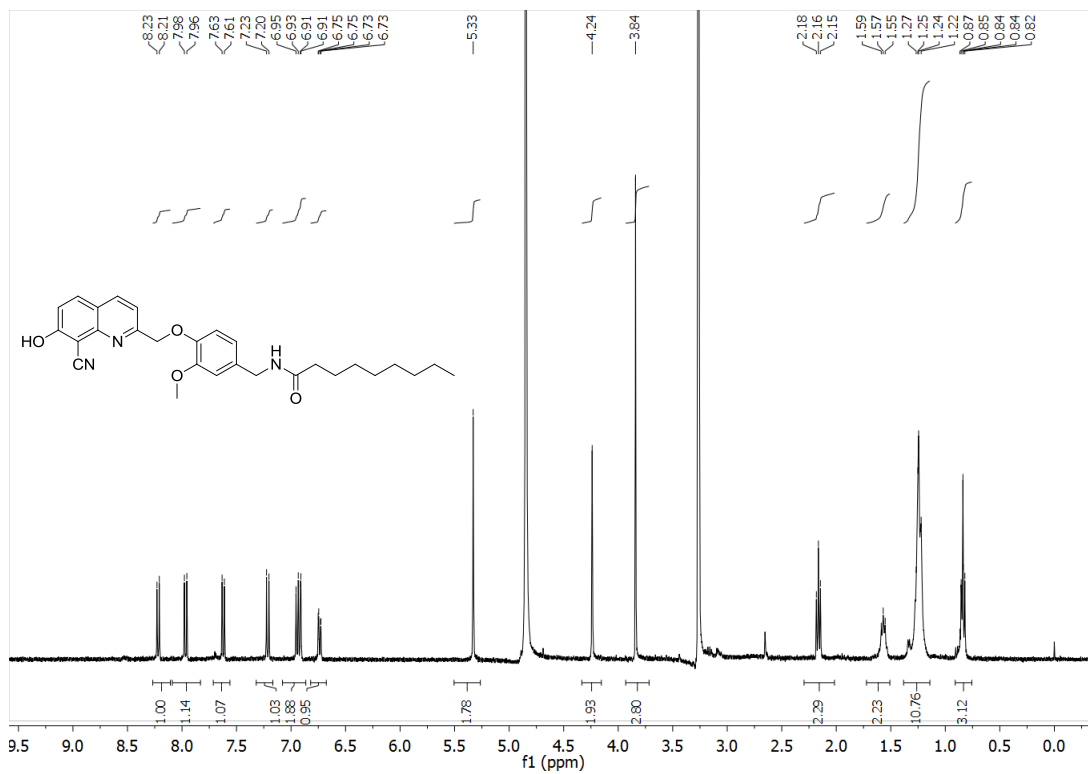


Compound **48** (0.055 g, 0.096 mmol) was dissolved in methylene chloride. Trifluoroacetic acid was added and the reaction stirred at rt for 2 h. The solvent was removed in vacuo and the crude product was purified via flash chromatography eluting with EtOAc/hexane (2:1) and dried in vacuo to provide **51** as a yellow solid. (0.029 g, 0.061 mmol, 57% yield).:

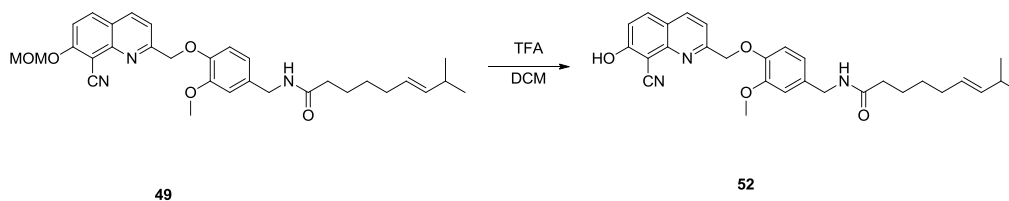
¹H NMR (400 MHz, methanol-*d*₄) δ 8.25 (d, 1H), 8.00 (d, 1H), 7.65 (d, 1H), 7.25 (d, 1H), 6.96 (m, 2H), 6.77 (d, 1H), 5.36 (s, 2H), 4.28 (m, 2H), 3.88 (s, 3H), 2.19 (t, 2H), 1.60 (m, 2H), 1.4 – 1.2 (m, 10 H), 0.84 (t, 3H);

¹³C NMR (125 MHz, methanol-*d*₄) δ 174.94, 161.98, 154.09, 149.01, 148.21, 144.35, 135.23, 133.30, 130.86, 129.70, 120.37, 119.76, 119.18, 116.51, 115.56, 112.77, 92.40, 69.54, 55.87, 43.73, 36.97, 31.64, 29.61, 29.42, 29.36, 28.93, 26.90, 22.80, 14.13.

HRMS-ESI (*m/z*): [M+H]⁺ calculated for C₂₈H₃₃N₃O₄, 476.2544; found, 476.25430



(E)-N-(4-((8-Cyano-7-hydroxyquinolin-2-yl)methoxy)-3-methoxybenzyl)-8-methylnon-6-enamide (52)

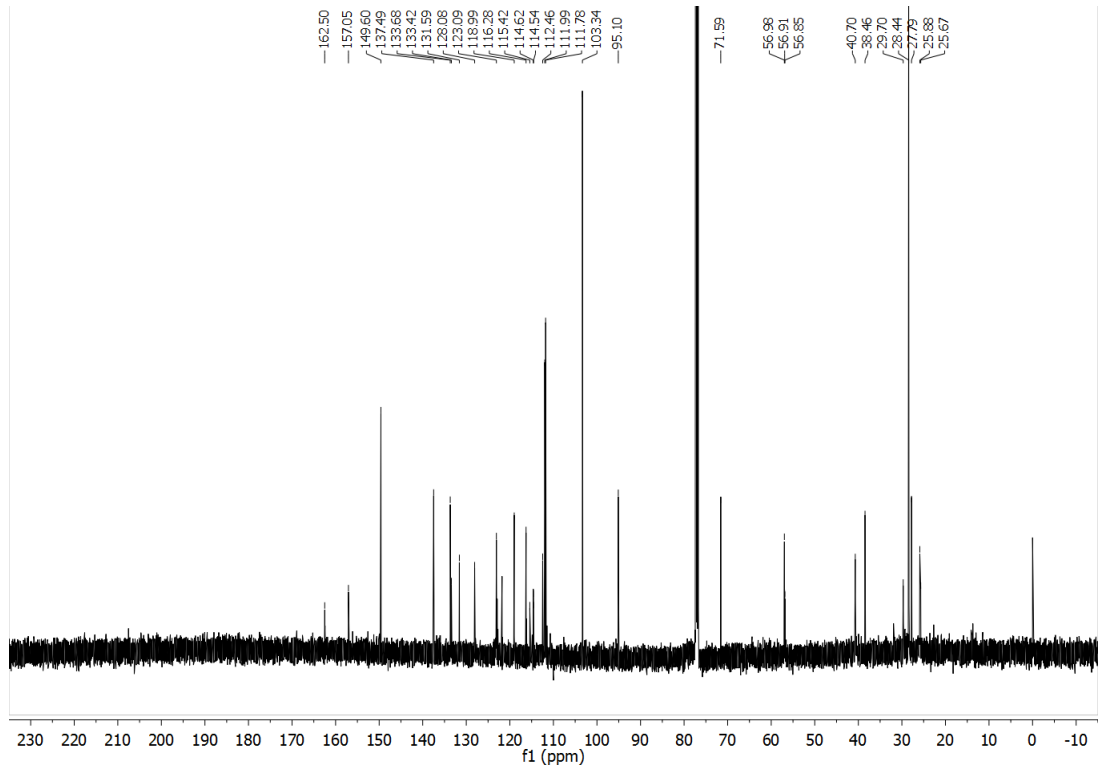
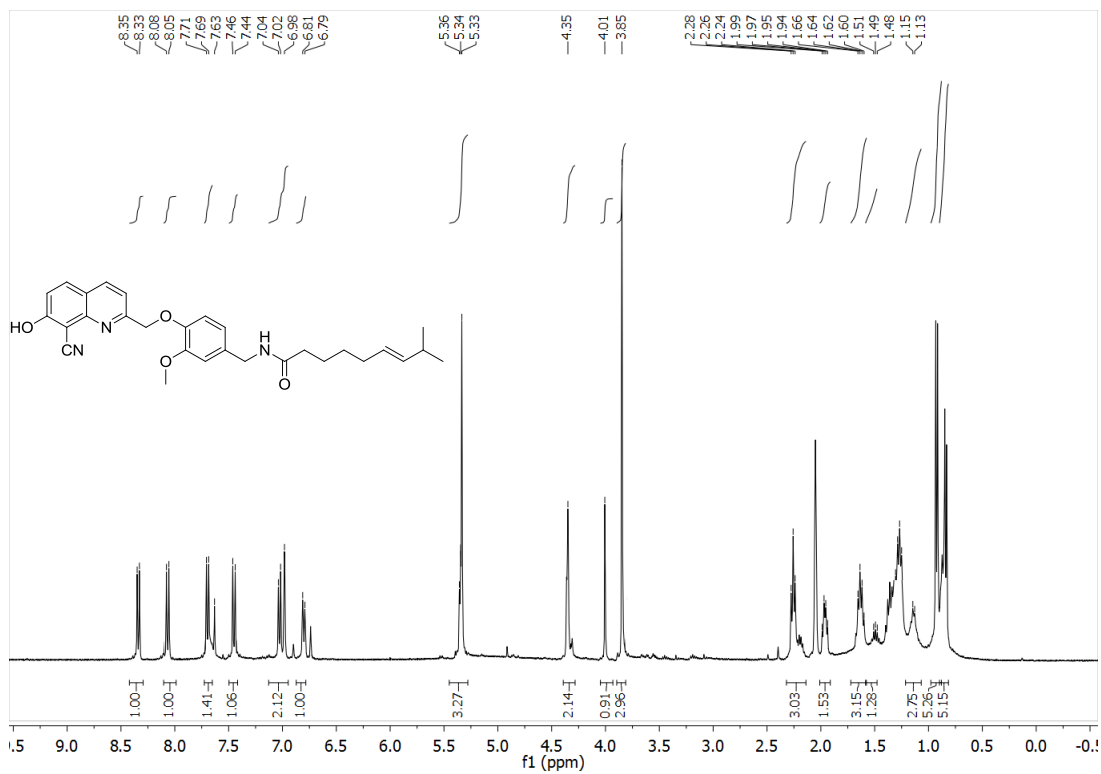


Compound **48** (0.054 g, 0.10 mmol) was dissolved in methylene chloride. Trifluoroacetic acid was added and the reaction stirred at rt for 1 h. The solvent was removed in vacuo and the residue purified by HPLC with 50% CH₃CN/50% H₂O (w/ 0.1 % TFA) to separate isomers. Fractions containing only one peak corresponding to CyHQ-capsaicin were combined and concentrated to provide CyHQ-capsaicin (0.08 g, 0.16 mmol, 17% yield).:

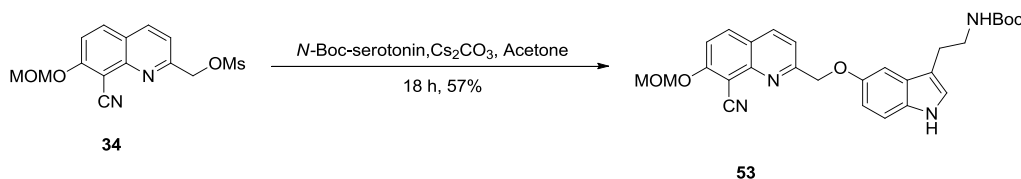
¹H NMR (400 MHz, methanol-*d*₄) δ 8.34 (d, 1H), 8.07 (d, 1H), 7.70 (d, 1H), 7.45 (d, 1H), 7.03 (d, 1H), 6.98 (s, 1H), 6.80 (d, 1H), 5.34 (d, 3H), 4.36 (d, 2H), 3.85 (s, 3H), 1.96 (t, 2H), 1.63 (m, 2H), 1.4 – 1.2 (m, 8 H), 0.92 (d, 3H), 0.84 (d, 3H);

¹³C NMR(126 MHz, chloroform-*d*) δ 162.50, 157.05, 149.60, 137.49, 133.68, 133.42, 131.59, 128.08, 123.09, 118.99, 116.28, 115.42, 114.62, 114.54, 112.46, 111.99, 111.78, 103.34, 95.10, 71.59, 56.98, 56.91, 56.85, 40.70, 38.46, 29.70, 28.44, 27.79, 25.88, 25.67.

HRMS-ESI (*m/z*): [M+H]⁺ calculated for C₂₉H₃₃N₃O₄, 488.2544; found, 488.2579



tert-Butyl (2-(5-((8-cyano-7-(methoxymethoxy)quinolin-2-yl)methoxy)-1H-indol-3-yl)ethyl)carbamate (53)

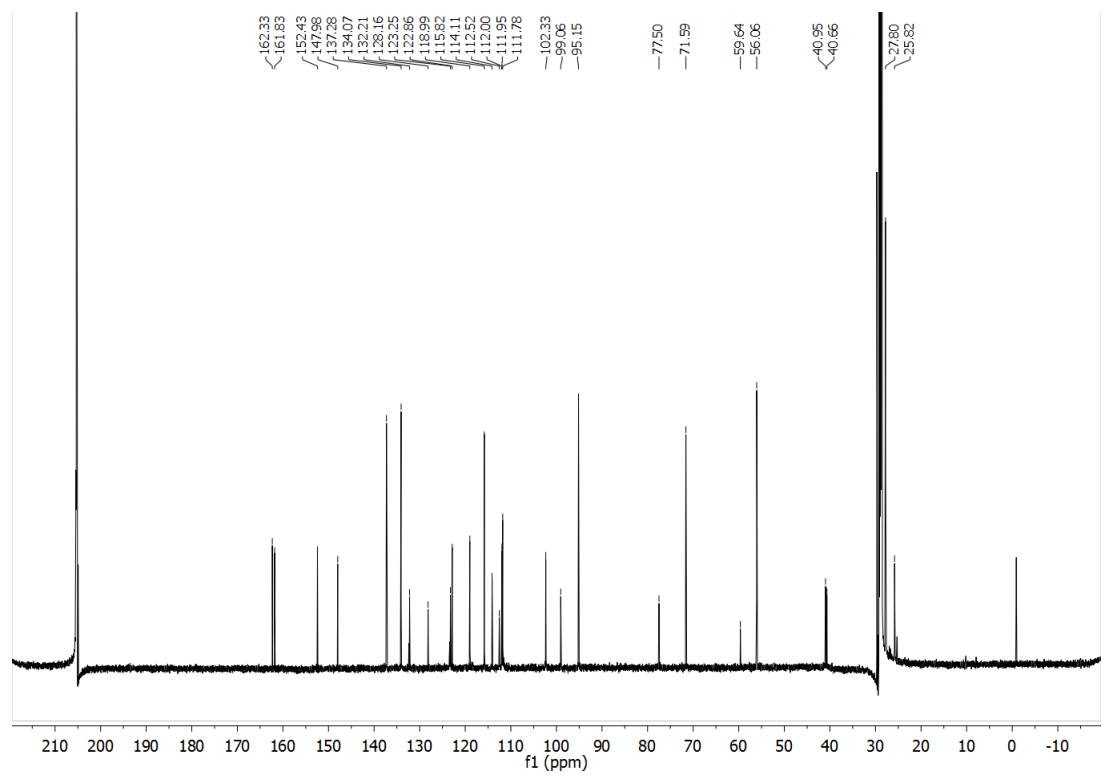
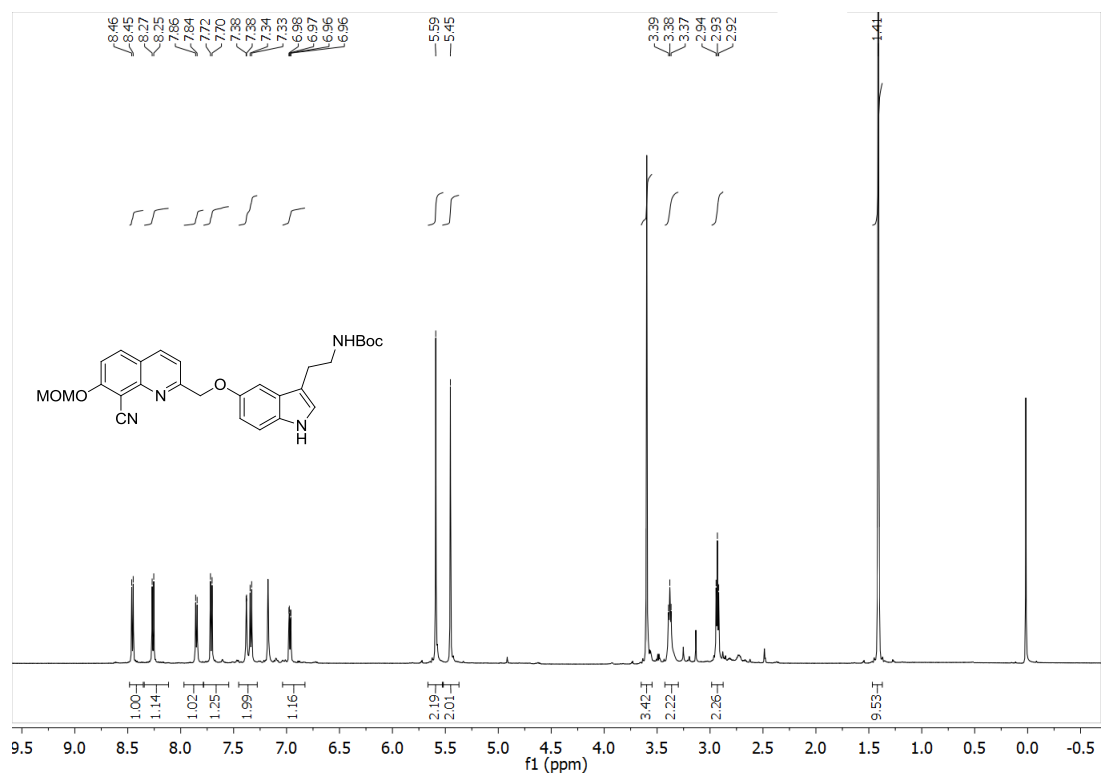


Compound **34** (0.036 g, 0.11 mmol) was dissolved in Acetone (1mL) and *N*-Boc-serotonin (0.046 g, 0.17 mmol), and Cs₂CO₃ (0.072 g, 0.22 mmol) were added. The reaction was stirred overnight and then concentrated in vacuo and the crude product was purified via flash chromatography eluting with EtOAc/hexane (1:2). The solvent was removed in vacuo to provide **53** as a yellow oil (0.035 g, 0.069 mmol, 63% yield).:

¹H NMR (600 MHz, chloroform-*d*) δ 8.42 (d, 1H), 8.25 (d, 1H), 7.85 (d, 1H), 7.71 (d, 1H), 7.38 (s, 1H), 7.34 (d, 1H), 6.97 (d, 1H), 5.59 (s, 2h), 5.45 (s, 2H), 3.59 (s, 3H), 3.38 (t, 2H), 2.93 (t, 3H), 1.41 (s, 9H)

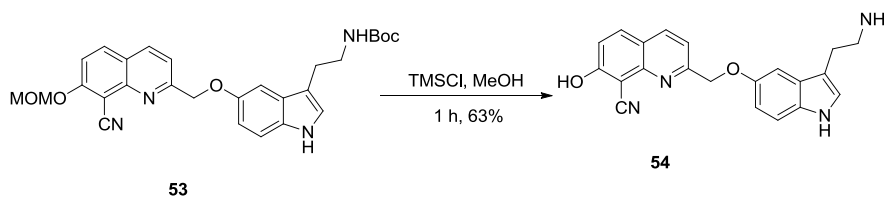
¹³C NMR (151 MHz, acetone-*d*₆) δ 162.33, 161.83, 152.43, 147.98, 137.28, 134.07, 132.21, 128.16, 123.25, 122.86, 118.99, 115.82, 114.11, 112.52, 112.00, 111.95, 111.78, 102.33, 99.06, 95.15, 77.50, 71.59, 59.64, 56.06, 40.95, 40.66, 27.80, 25.82

HRMS-ESI (*m/z*): [M+H]⁺ calculated for C₂₈H₃₀N₄O₅, 503.2289; found, 503.2296



2-(((3-(2-Aminoethyl)-1H-indol-5-yl)oxy)methyl)-7-hydroxyquinoline-8-carbonitrile

(54)

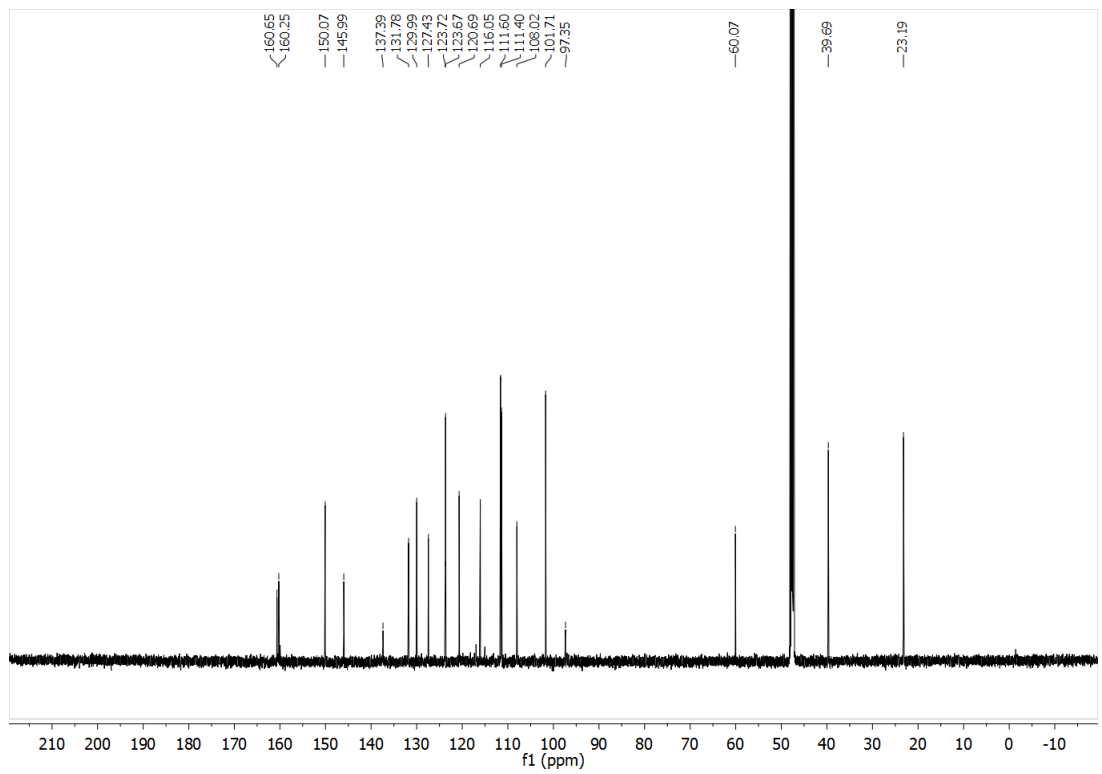
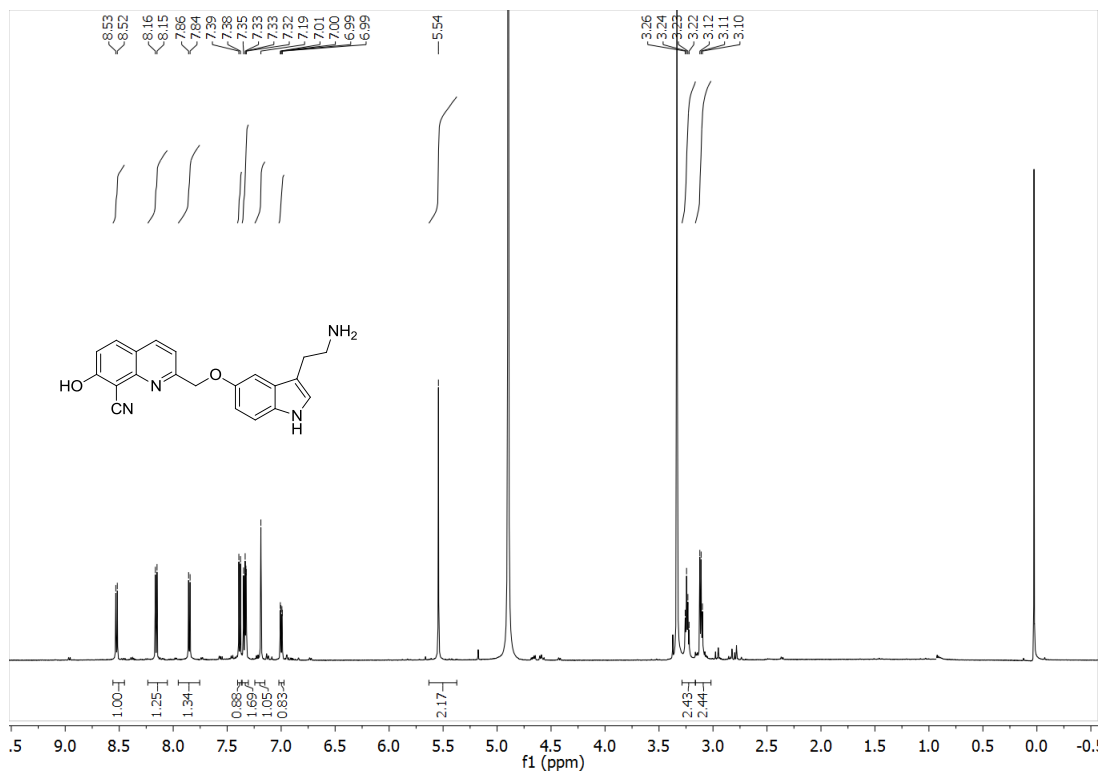


Compound **53** (0.038 g, 0.075 mmol) was dissolved in methanol. Trimethylsilylchloride titrated in until the reaction was complete by uHPLC. The solvent was removed in vacuo and the residue purified by HPLC with a 10 min gradient from 10% MeCN/water (w/ 0.1% TFA) to 100% MeCN. Fractions containing only one peak were combined and concentrated to provide **54** was a yellow oil (0.017g, 0.047 mmol, 63% yield).:

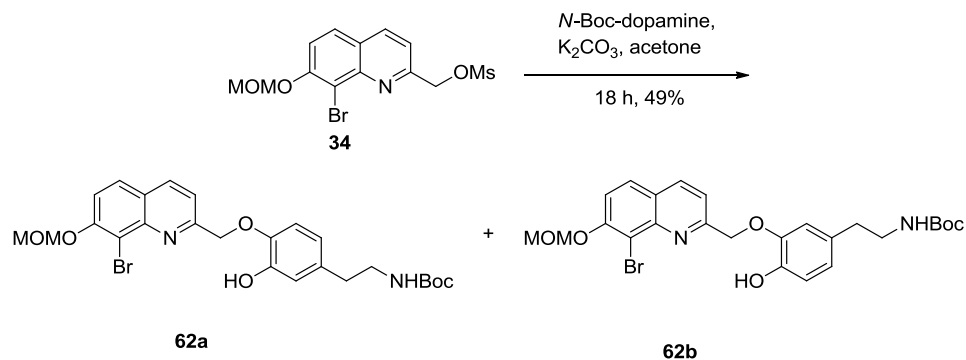
¹H NMR (600 MHz, methanol-*d*₄) δ 8.53 (d, 1H), 8.15 (d, 1H), 7.85 (d, 1H), 7.39 (d, 1H), 7.34 (m, 2H), 7.18 (s, 1H), 7.03 (d, 1H), 5.54 (s, 2H), 3.25 (t, 2H), 3.12 (t, 2H)

¹³C NMR(151 MHz, methanol-*d*₄) δ 160.65, 160.25, 150.07, 145.99, 137.39, 131.78, 129.99, 127.43, 123.72, 123.67, 120.69, 116.05, 111.60, 111.40, 108.02, 101.71, 97.35, 60.07, 39.69, 23.19.

HRMS-ESI (*m/z*): [M+H]⁺ calculated for C₂₁H₁₈N₄O₂, 359.1503; found, 359.15045



tert-Butyl 3-((8-bromo-7-(methoxymethoxy)quinolin-2-yl)methoxy)-4-hydroxyphenethylcarbamate and tert-butyl 4-((8-bromo-7-(methoxymethoxy)quinolin-2-yl)methoxy)-3-hydroxyphenethylcarbamate (54)

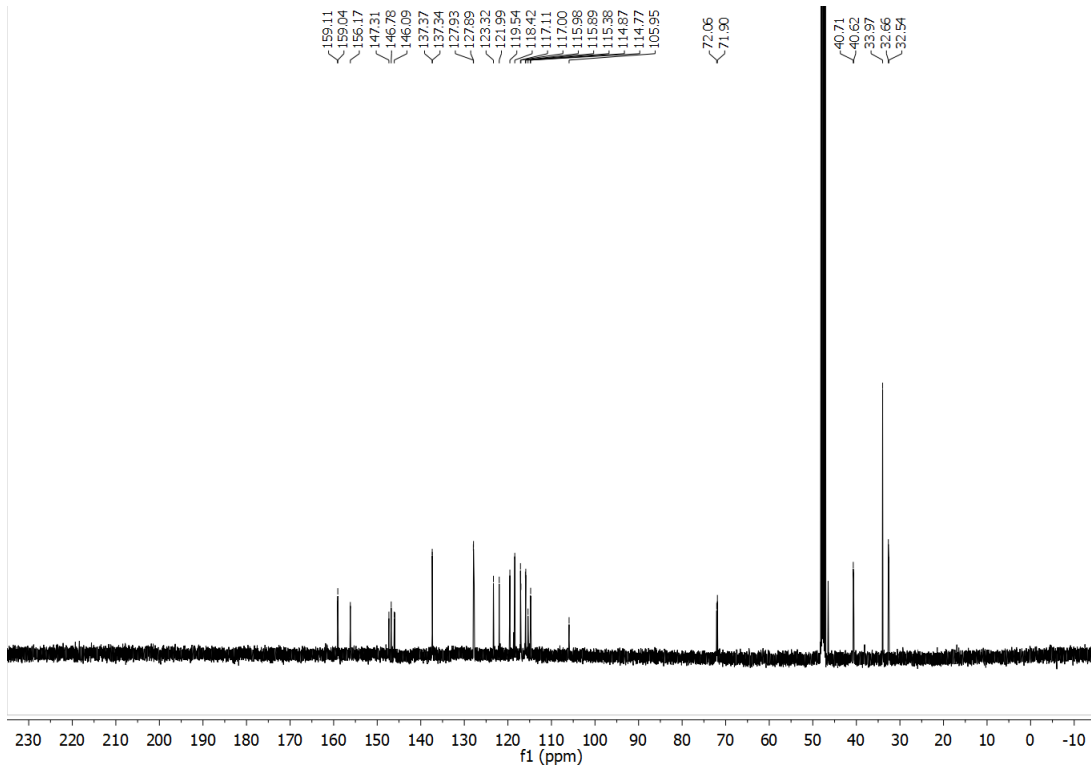
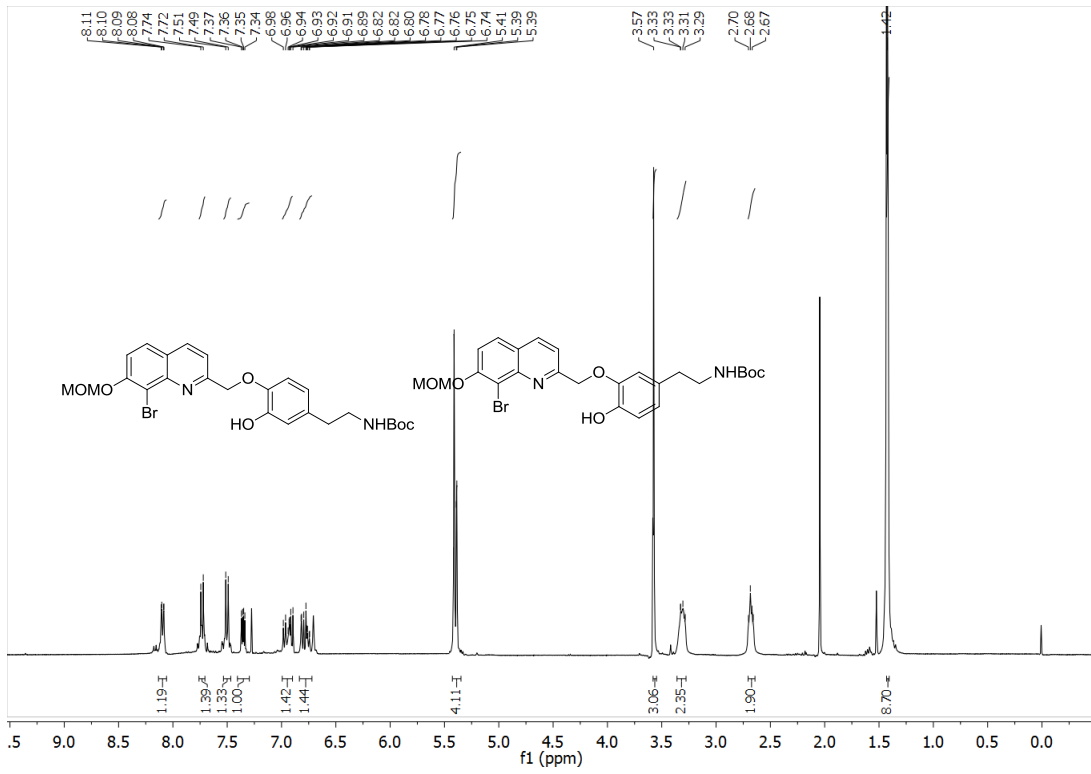


Compound (**34**) (0.396 g, 1.06 mmol) was dissolved in acetone. *N*-Boc-dopamine (0.269 g, 1.06 mmol) and potassium carbonate (0.293 g, 2.13 mmol) were added and the reaction stirred at rt for 3 d. The reaction was concentrated *in vacuo* and the crude product was purified via flash chromatography eluting with EtOAc/hexane (1/2) and dried *in vacuo* to yield the product as a yellow oil (0.176 g, 0.331 mmol, 49% yield):

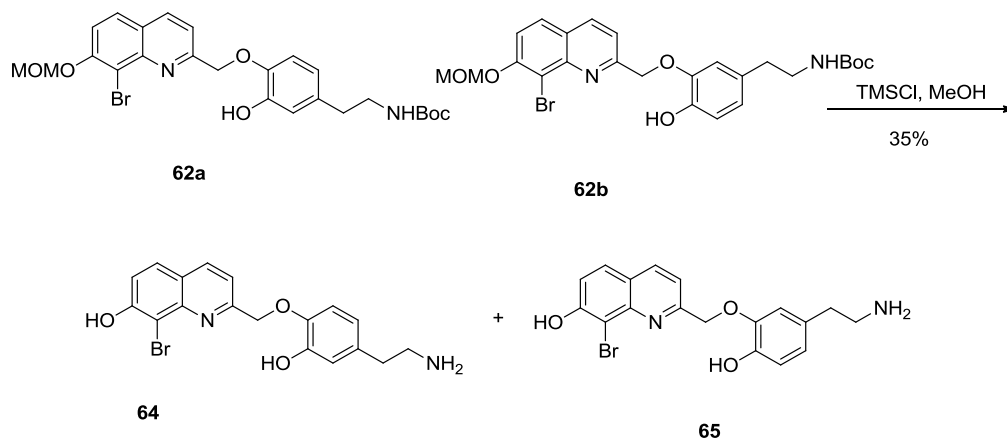
¹H NMR (400 MHz, methanol-*d*₄) δ 8.44 – 8.25 (d, *J* = 8.3 Hz, 1H), 8.05 – 7.84 (d, *J* = 9.0 Hz, 1H), 7.65 – 7.41 (dd, *J* = 12.3, 8.8 Hz, 2H), 6.76 – 6.57 (m, 3H), 5.63 – 5.48 (s, 2H), 5.50 – 5.36 (s, 2H), 3.59 – 3.44 (s, 3H), 3.19 – 3.10 (t, *J* = 6.9 Hz, 2H), 2.64 – 2.47 (t, *J* = 7.5 Hz, 2H), 1.50 – 1.35 (s, 9H).

¹³C NMR (126 MHz, methanol-*d*₄) δ 159.11, 159.04, 156.17, 147.31, 146.78, 146.09, 137.37, 137.34, 127.93, 127.89, 123.32, 121.99, 119.54, 118.42, 117.11, 117.00, 115.98, 115.89, 115.38, 114.87, 114.77, 105.95, 72.06, 71.90, 40.71, 40.62, 33.97, 32.66, 32.54.

HRMS-ESI (*m/z*): [M+H]⁺ calculated for C₂₉H₂₉N₂O₆Br, 533.1282, 535.1262; found, 533.1287, 535.1263



2-((4-(2-Aminoethyl)-2-hydroxyphenoxy)methyl)-8-bromoquinolin-7-ol (64) and 2-((5-(2-aminoethyl)-2-hydroxyphenoxy)methyl)-8-bromoquinolin-7-ol (65)

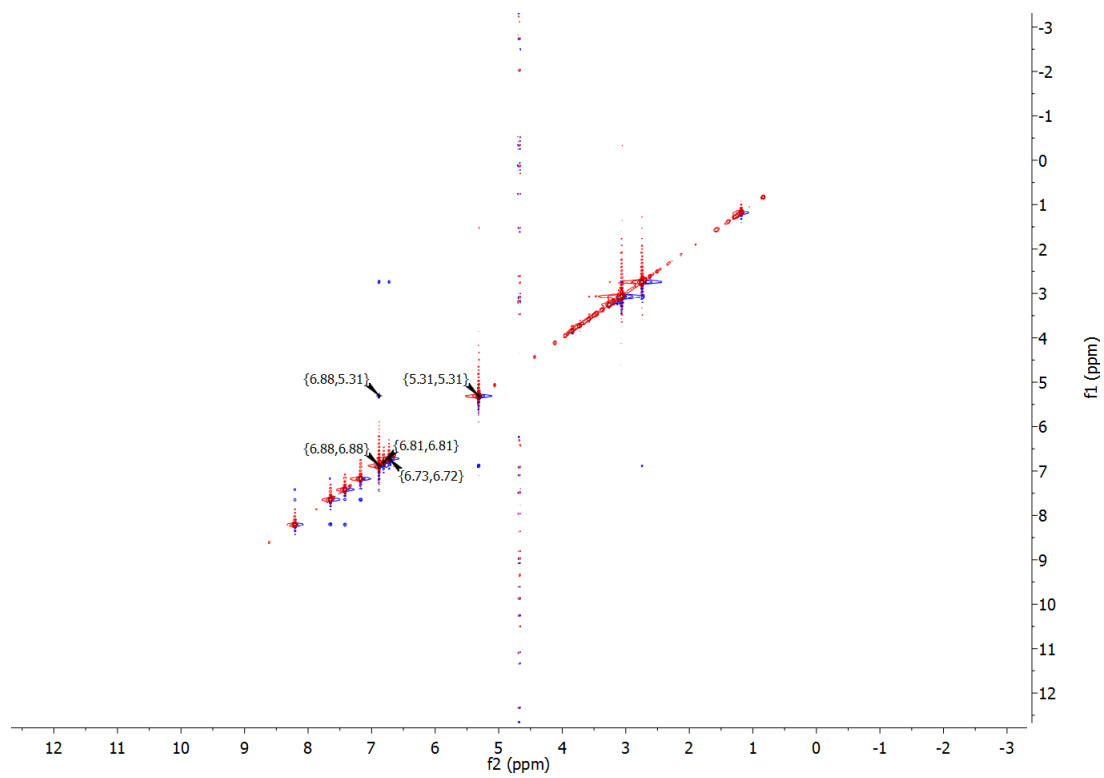
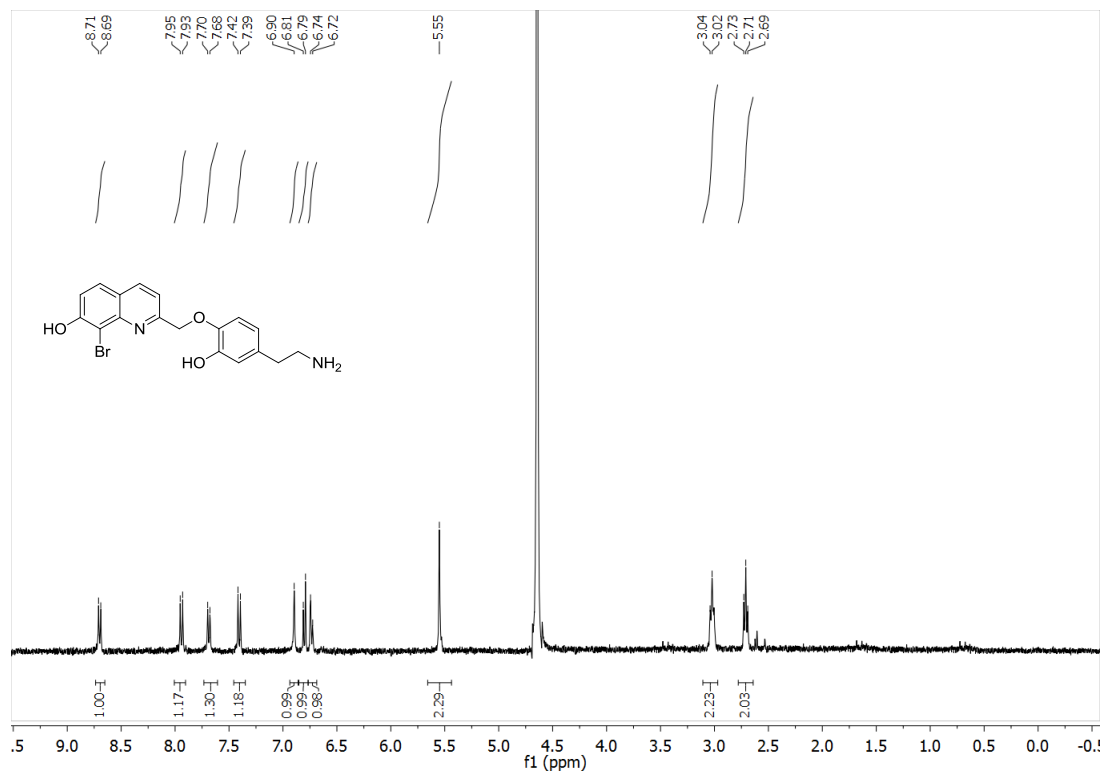


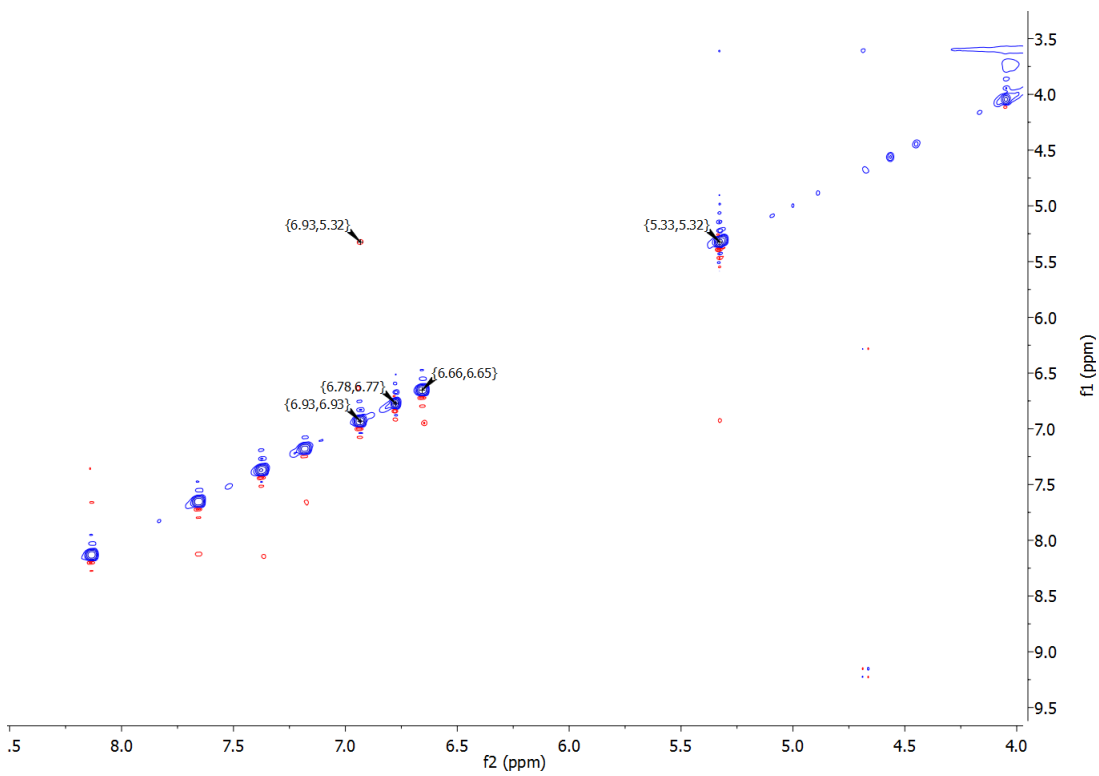
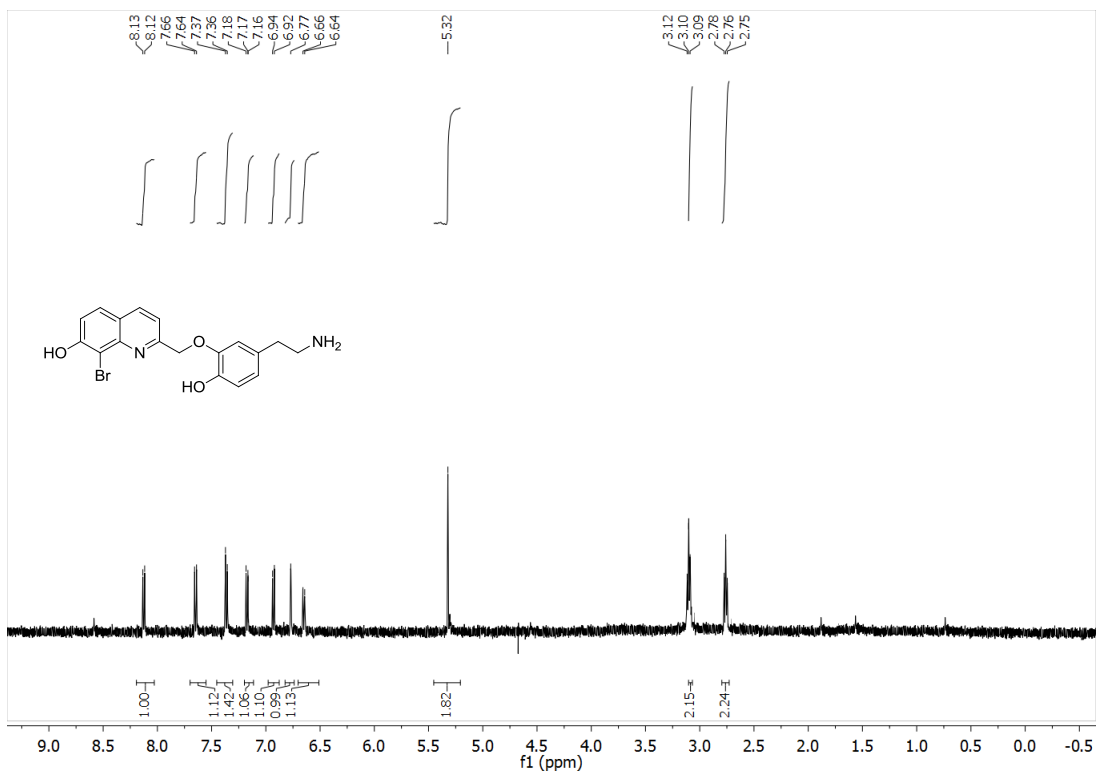
A mixture of **62a** and **62b** (0.180 g, 0.33 mmol) was dissolved in methanol and trimethylsilyl chloride (0.13 mL, 0.99 mmol) was added and the reaction stirred at rt for 18 h. The reaction was concentrated *in vacuo* and the residue was purified over C18 capped silica gel eluting with 100% H₂O, the product was collected as a yellow oil (0.048 g, 0.116 mmol, 35% yield):

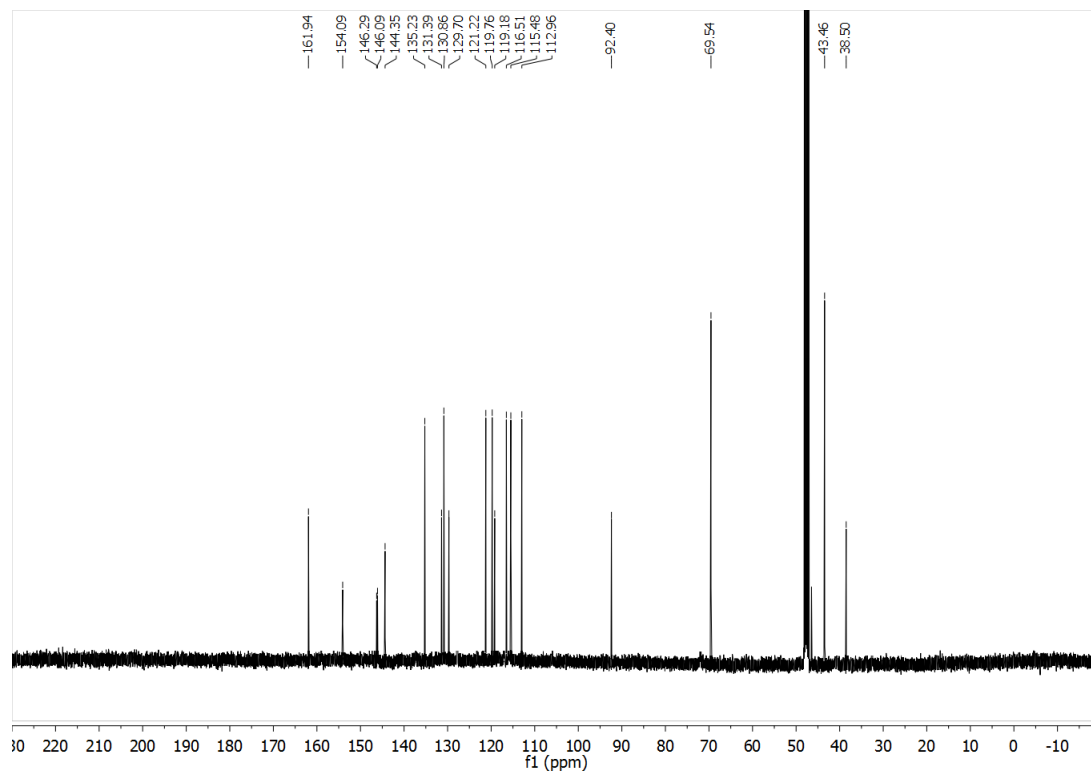
¹H NMR (400 MHz, methanol-*d*₄) δ 8.20 (d, 1H), 7.64 (d, 1H), 7.41 (d, 1H), 7.16 (d, 1H), 6.87 (s, 1H), 6.80 (d, 2H), 6.71 (d, 2H), 3.06 (q, 2H), 2.73 (t, 2H);

¹³C NMR (125 MHz, methanol-*d*₄) δ 161.94, 154.09, 146.29, 146.09, 144.35, 135.23, 131.39, 130.86, 129.70, 121.22, 119.76, 119.18, 116.51, 115.48, 112.96, 92.40, 69.54, 43.46, 38.50.

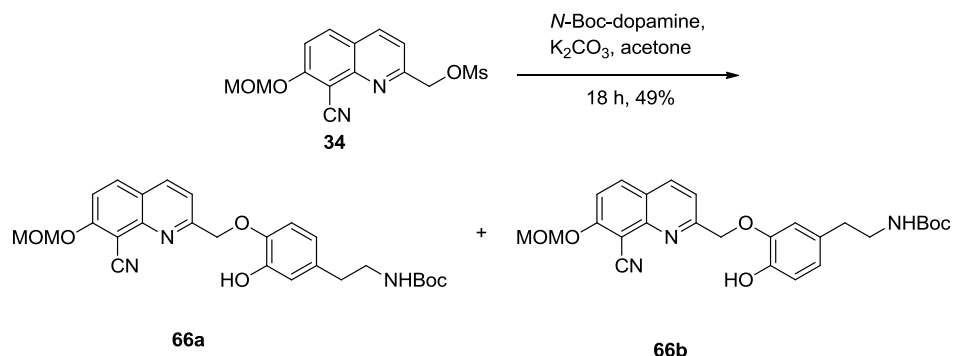
HRMS-ESI (*m/z*): [M+H]⁺ calculated for C₁₈H₁₇N₂O₃Br, 389.0496, 391.0475; found, 389.0495, 391.0478







tert-Butyl 4-((8-cyano-7-(methoxymethoxy)quinolin-2-yl)methoxy)-3-hydroxyphenethylcarbamate (66)

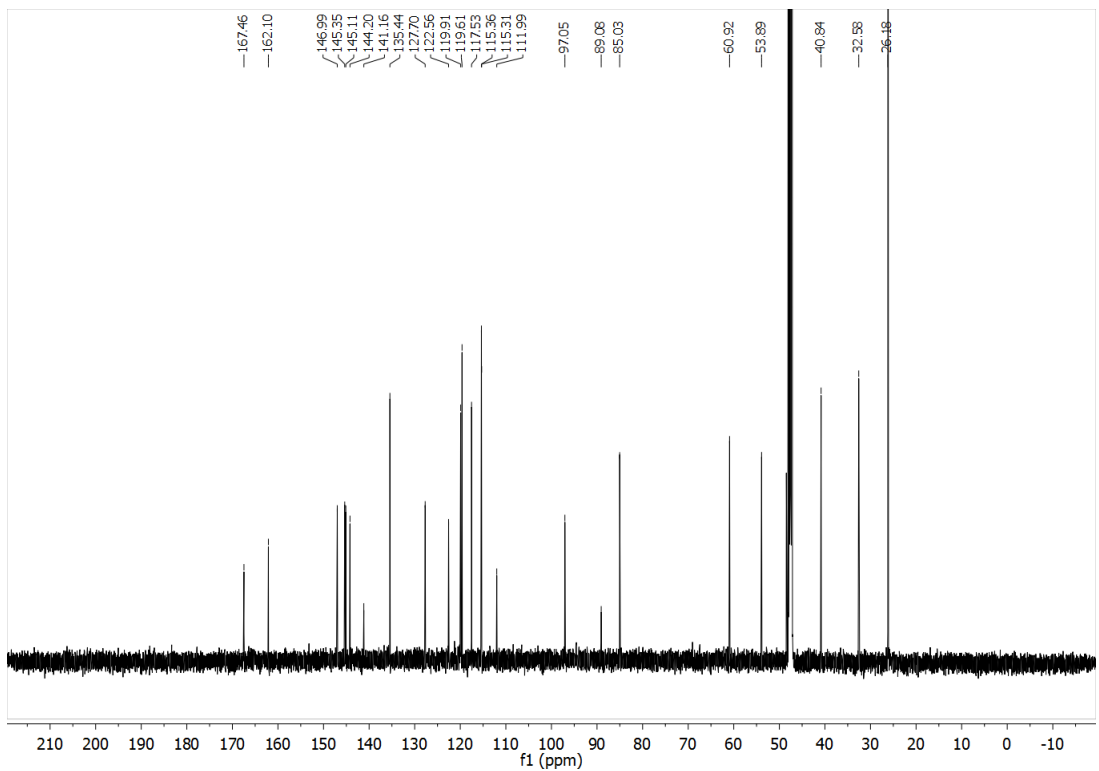
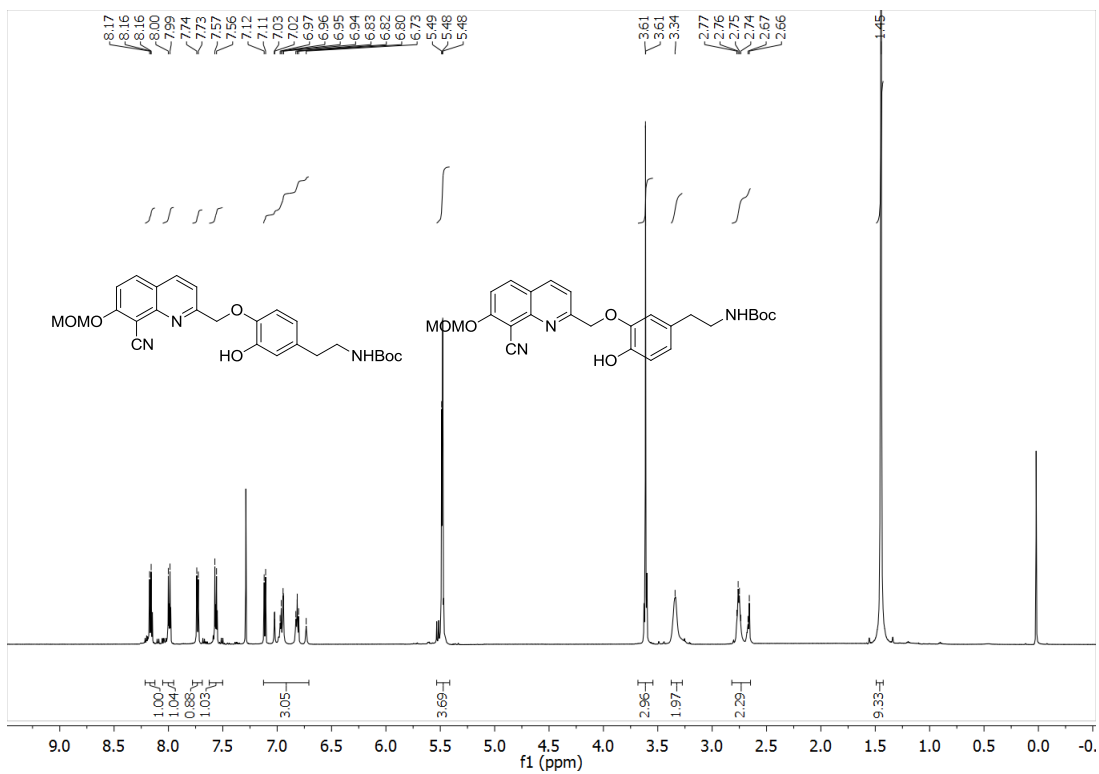


Compound (**34**) (0.050 g, 0.15 mmol) was dissolved in 2 mL acetone. Boc-dopamine (0.039 g, 0.15 mmol) and cesium carbonate (0.100 g 0.308 mmol) were added and the reaction was monitored by uHPLC. Upon completion, the reaction was concentrated *in vacuo* and the residue purified over silica gel eluting with EtOAc/hexanes (2:3) to yield **66** as a yellow oil (0.038 g, 0.079 mmol, 49% yield):

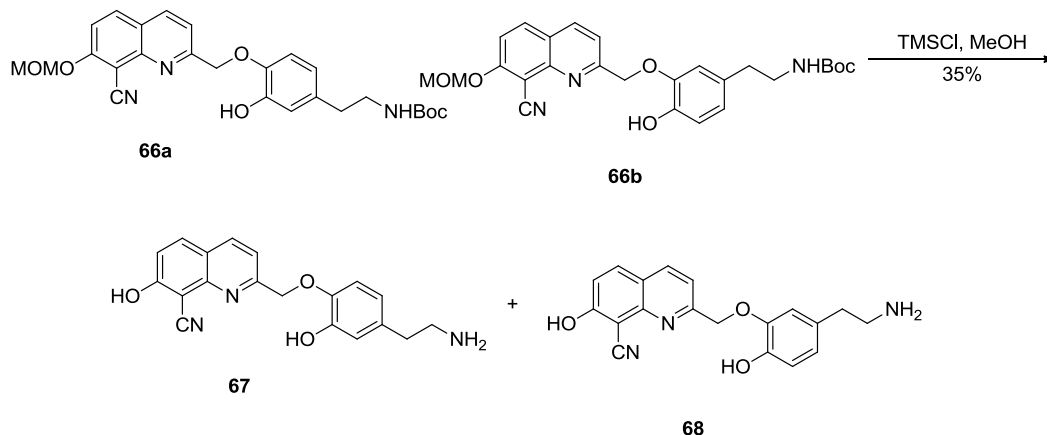
1H NMR (600 MHz, chloroform-*d*) δ 8.23 – 8.10 (m, 1H), 7.99 (d, $J = 9.2$ Hz, 1H), 7.73 (d, $J = 8.4$ Hz, 1H), 7.57 (d, $J = 9.2$ Hz, 1H), 7.15 – 6.67 (m, 3H), 5.73 – 5.23 (m, 4H), 3.61 (d, $J = 0.9$ Hz, 3H), 3.38-3.29 (m, 2H), 2.83 – 2.60 (m, 2H), 1.45 (s, 9H).

^{13}C NMR 13 (151 MHz, methanol-*d*₄) δ 167.46, 162.10, 146.99, 145.35, 145.11, 144.20, 141.16, 135.44, 127.70, 122.56, 119.91, 119.61, 117.53, 115.36, 115.31, 111.99, 97.05, 89.08, 85.03, 60.92, 53.89, 40.84, 32.58, 26.18.

HRMS-ESI (m/z): $[M+H]^+$ calculated for $C_{26}H_{29}N_3O_6$, 480.2129; found, 480.2130



2-((4-(2-Aminoethyl)-2-hydroxyphenoxy)methyl)-7-hydroxyquinoline-8-carbonitrile (67) and 2-((5-(2-aminoethyl)-2-hydroxyphenoxy)methyl)-7-hydroxyquinoline-8-carbonitrile (68)

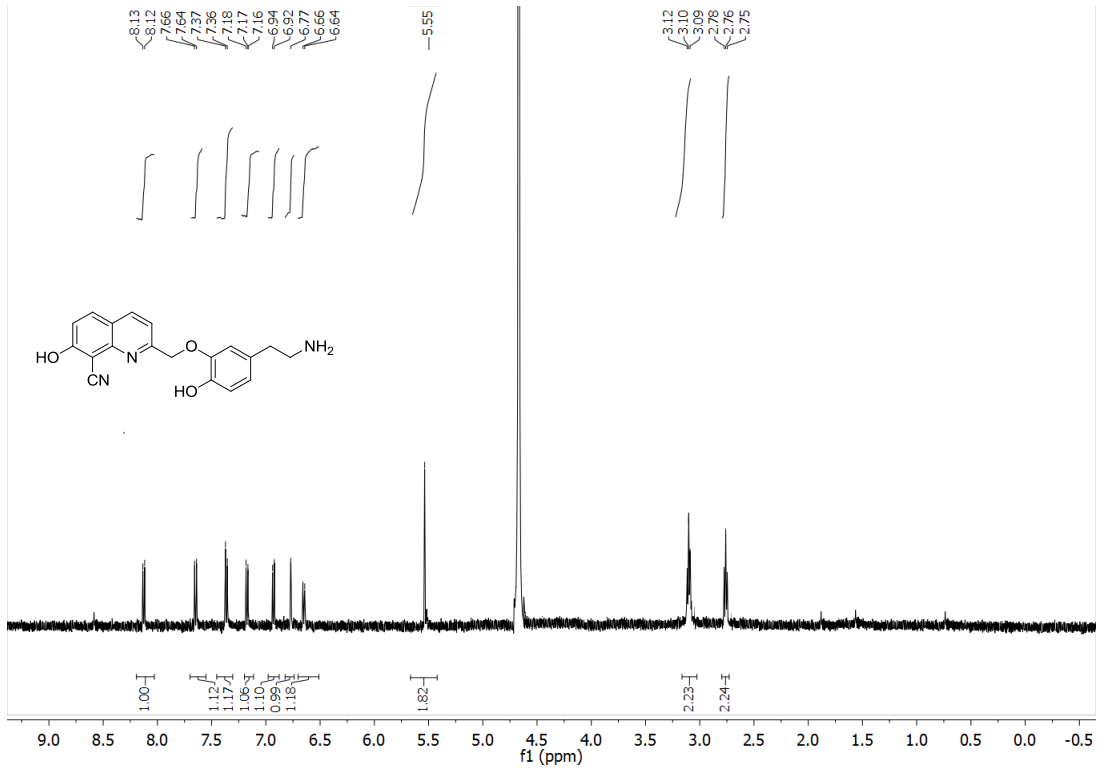
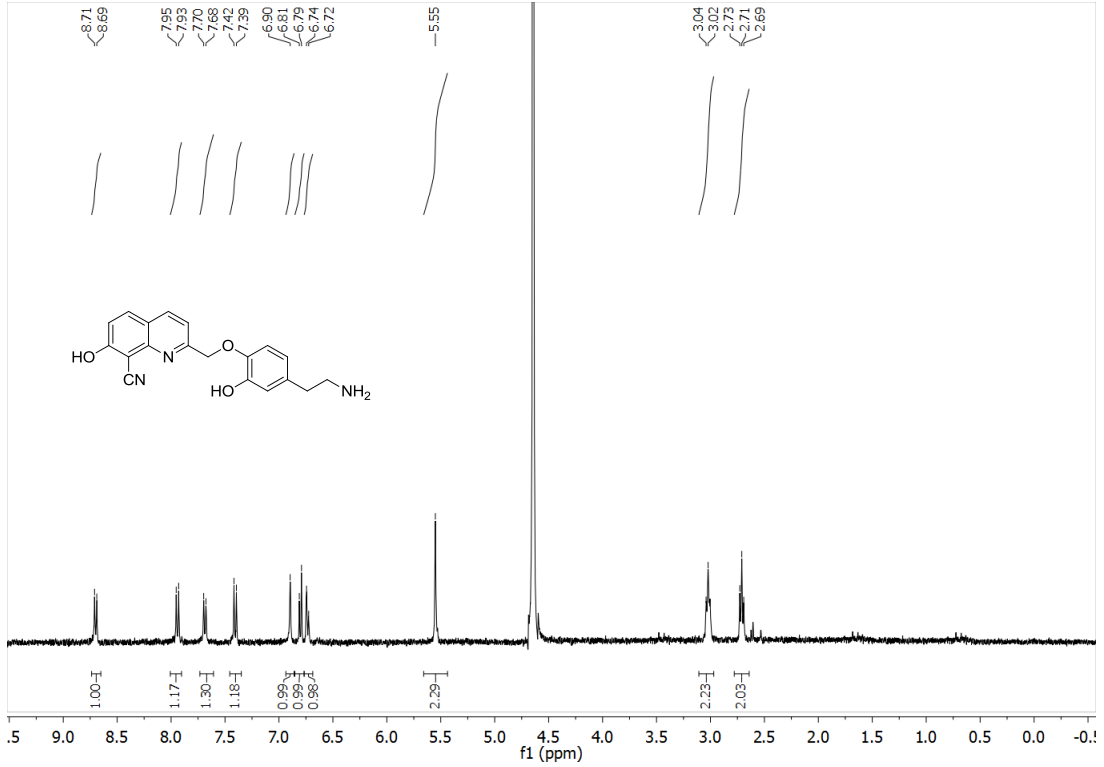


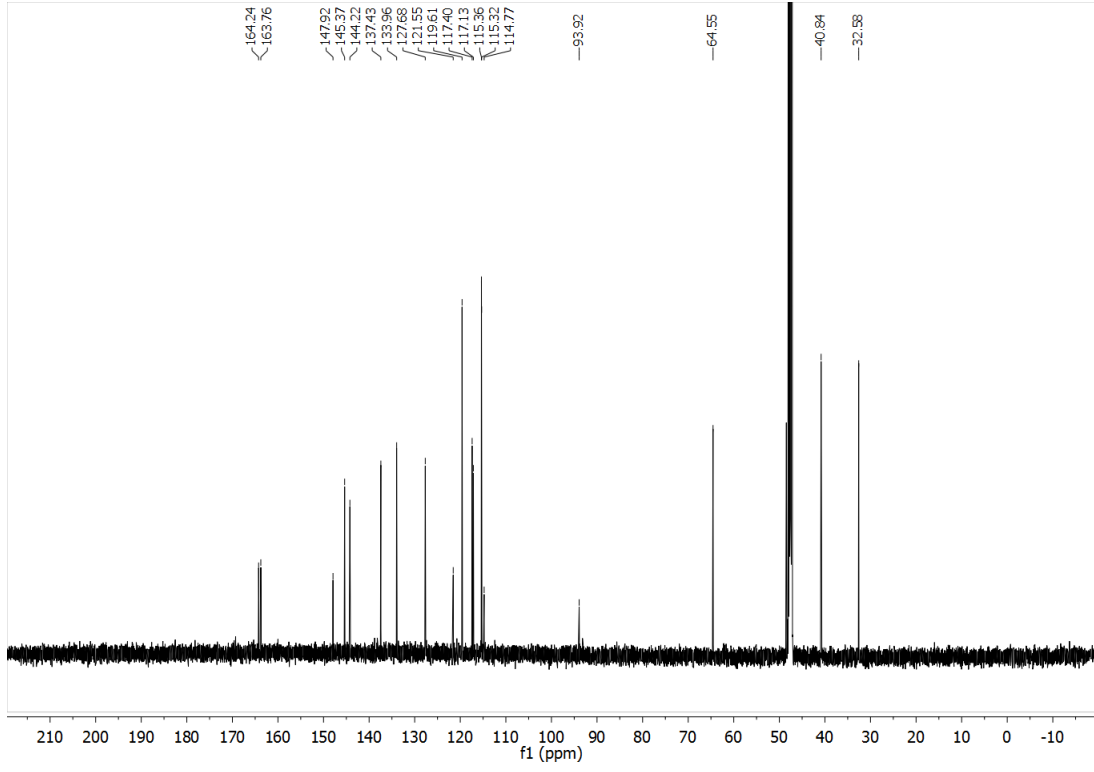
A mixture of **66a** and **66b** (0.038 g, 0.079 mmol) was dissolved in methanol and TMSCl (0.041 mL, 0.32 mmol) was added and the reaction stirred at rt for 18 h. The reaction was concentrated *in vacuo* and the residue was purified over C18 capped silica gel eluting with MeCN/H₂O (3:2). The fractions containing product were concentrated *in vacuo* to provide **67** and **68** as a pale yellow solid (0.022 g, 0.065mmol, 83% yield):

¹H NMR (600 MHz, deuterium oxide) 8.42 (d, *J* = 8.3 Hz, 1H), 7.94 (d, *J* = 9.0 Hz, 1H), 7.69 (dd, *J* = 12.3, 8.8 Hz, 1H), 7.28 (d, *J* = 9.0 Hz, 1H) 6.90 (s, 1H), 6.80 (d, 8.5 Hz, 1H), 6.73 (d, 8.5 Hz, 1H) 5.73 (s, 2H), 3.03 (t, *J* = 6.9 Hz, 2H), 2.70 (t, *J* = 7.5 Hz, 2H).

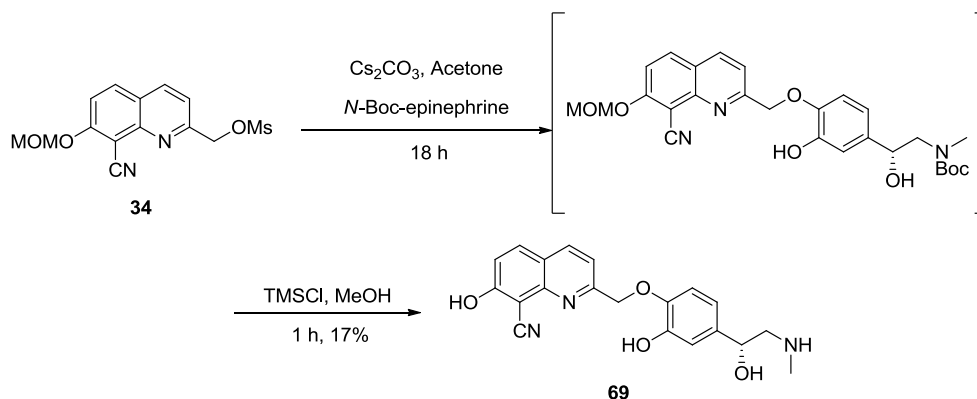
¹³C NMR (151 MHz, methanol-*d*₄) δ 164.24, 163.76, 147.92, 145.37, 144.22, 137.43, 133.96, 127.68, 121.55, 119.61, 117.40, 117.13, 115.36, 115.32, 114.77, 93.92, 64.55, 40.84, 32.58.

HRMS-ESI (*m/z*): [M+H]⁺ calculated for C₁₉H₁₇N₃O₃, 336.1343; found, 336.1347





(R)-7-Hydroxy-2-((2-hydroxy-4-(1-hydroxy-2-(methylamino)ethyl)phenoxy)methyl)quinoline-8-carbonitrile (70)

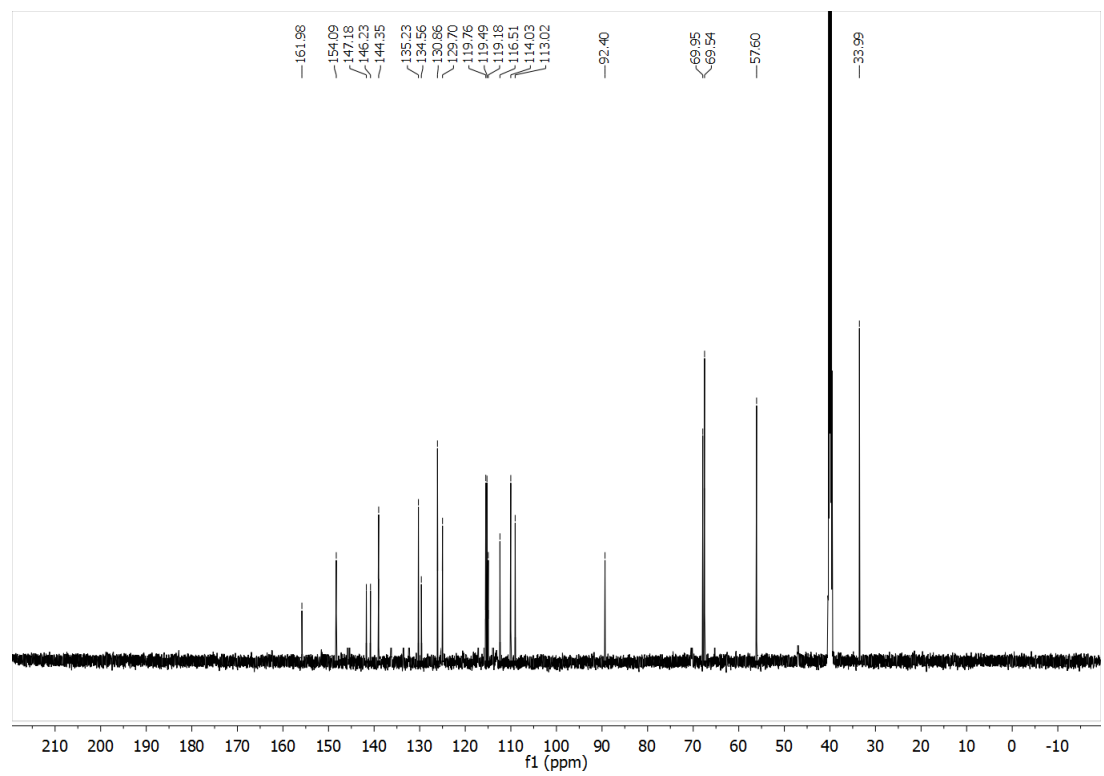
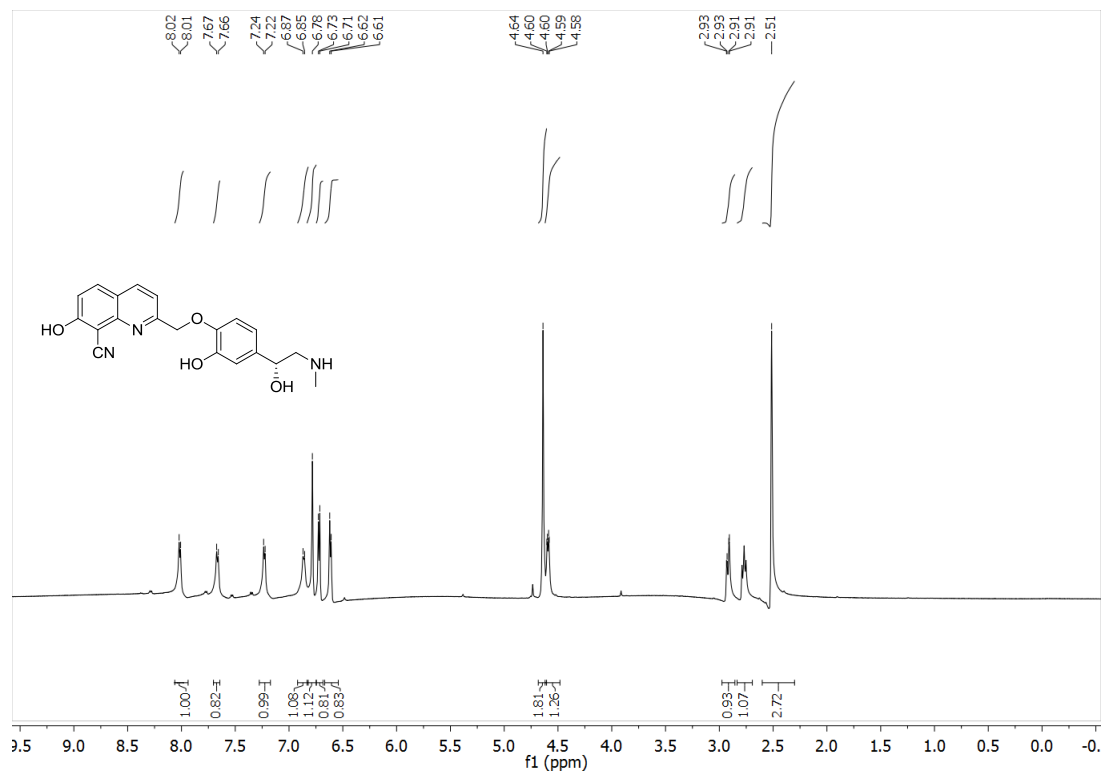


Compound **34** (0.040 g, 0.12 mmol) and *N*-Boc-epinephrine (0.035 g, 0.12 mmol) and were stirred in 2 mL acetone and Cs₂CO₃ (0.080 g, 0.25 mmol) was added. The reaction was monitored by uHPLC and upon completion was filtered over celite and concentrated in vacuo. The crude material was dissolved in methanol (1 mL) and trimethylsilyl chloride was titrated in aliquots (15 μ L) until the reaction was complete by uHPLC. Upon completion, the reaction was concentrated in vacuo and purified by HPLC, 10 min gradient from 5% MeCN/95% H₂O (0.1% TFA) to 100% MeCN. Fractions containing only one peak were combined and concentrated in vacuo to provide **70** as a yellow film (0.008 g, 0.022 mmol, 17% yield)

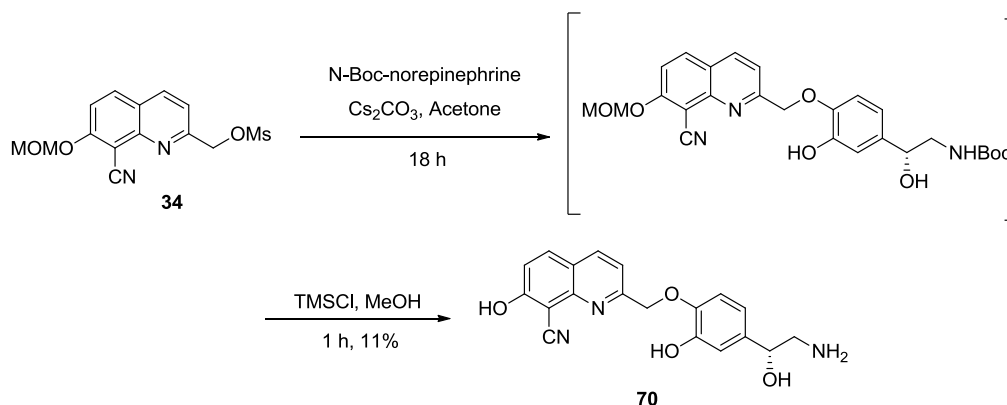
¹H NMR (600 MHz, DMSO-*d*₆) δ 8.01 (d, *J* = 8.4 Hz, 1H), 7.66 (d, *J* = 9.4 Hz, 1H), 7.23 (d, *J* = 8.4 Hz, 1H), 6.86 (d, *J* = 9.4 Hz, 1H), 6.78 (s, 1H), 6.72 (d, *J* = 8.0 Hz, 1H), 6.61 (d, *J* = 8.0 Hz, 1H), 4.64 (s, 2H), 4.59 (dd, *J* = 9.8, 3.3 Hz, 1H), 3.00 – 2.84 (m, 1H), 2.84 – 2.64 (m, 1H), 2.51 (s, 3H).

¹³C NMR: (151 MHz, DMSO-*d*₆) 161.98, 154.09, 147.18, 146.23, 144.35, 135.23, 134.56, 130.86, 129.70, 119.76, 119.49, 119.18, 116.51, 113.02, 92.40, 69.95, 69.54, 57.60, 33.99

HRMS-ESI (*m/z*): [M+H]⁺ calculated for C₂₀H₁₉N₃O₄, 366.1448; found,
366.1447



(R)-2-((4-(2-Amino-1-hydroxyethyl)-2-hydroxyphenoxy)methyl)-7-hydroxyquinoline-8-carbonitrile (71)

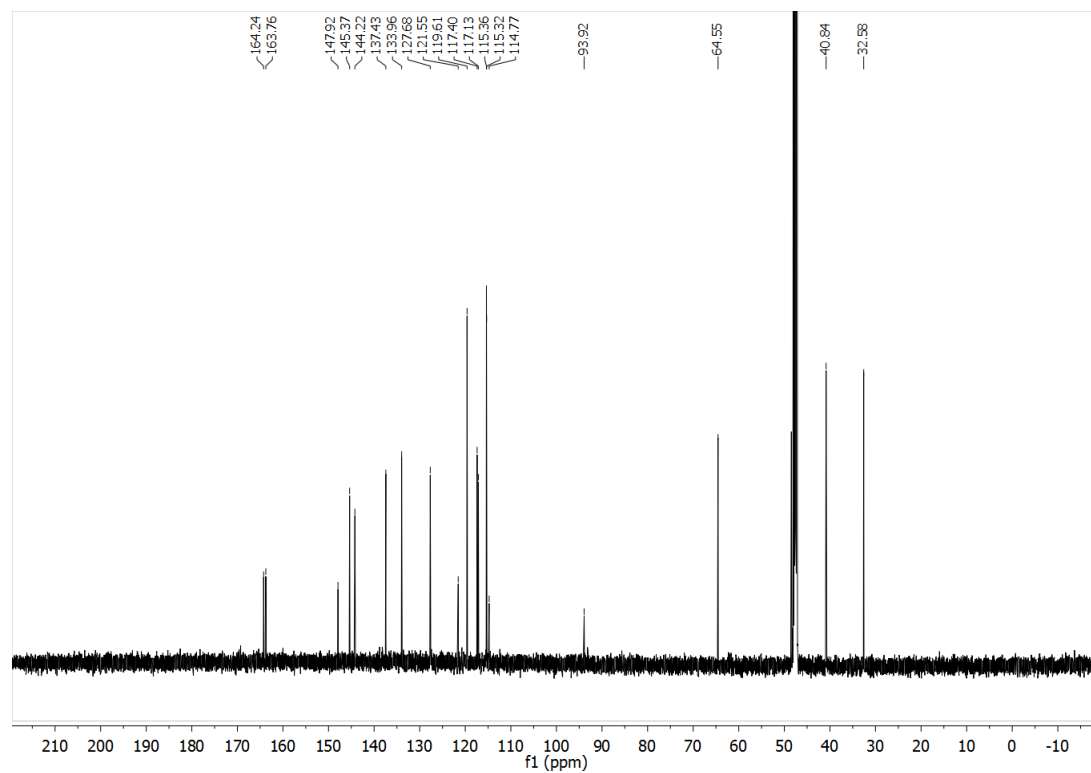
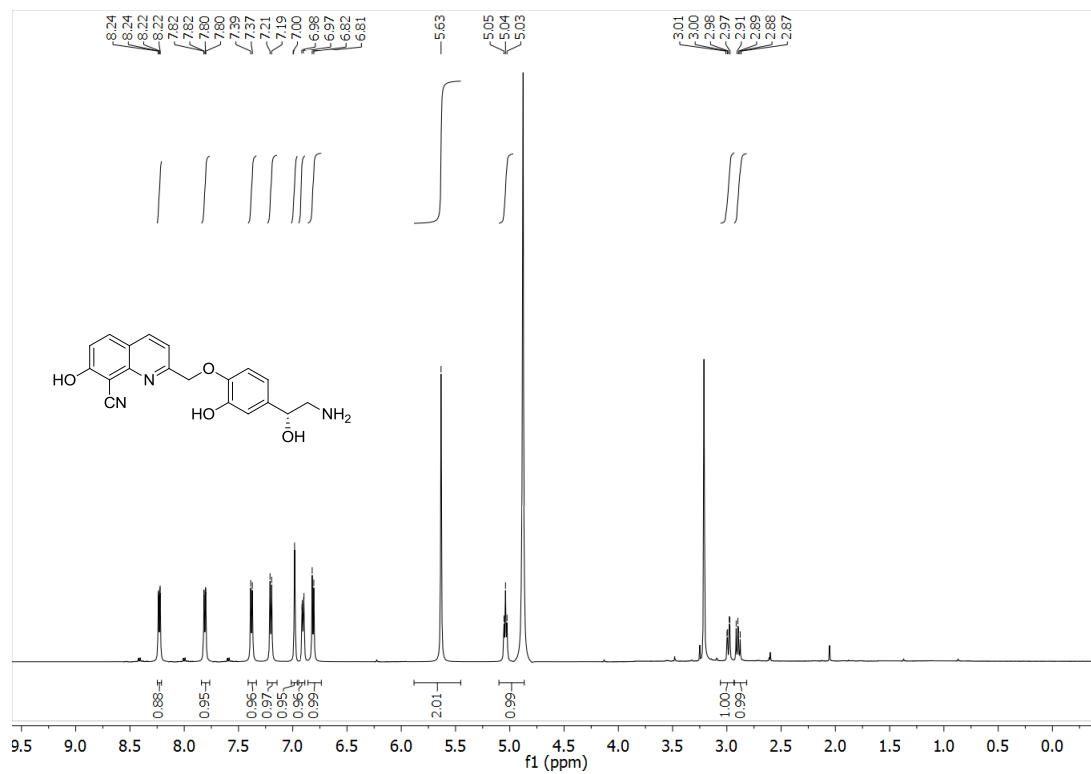


Compound **34** (0.043 g, 0.13 mmol) and *N*-Boc-norepinephrine (0.035 g, 0.13 mmol) and were stirred in 2 mL acetone and Cs_2CO_3 (0.086 g, 0.262 mmol) was added. The reaction was monitored by uHPLC and upon completion was filtered over celite and concentrated in vacuo. The crude material was dissolved in 1 mL methanol and trimethylsilyl chloride was titrated in aliquots (15- μL) until the reaction was complete by uHPLC. Upon completion, the reaction was concentrated in vacuo and purified by HPLC, 10 min gradient from 5% MeCN/95% H_2O (0.1% TFA) to 100% MeCN. Fractions containing only one peak were combined and concentrated in vacuo to provide **71** as a yellow film (0.005 g, 0.014 mmol, 11% yield):

$^1\text{H NMR}$ (600 MHz, methanol- d_4) δ 8.23 (d, $J = 8.4$ Hz, 1H), 7.81 (d, $J = 9.4$ Hz, 1H), 7.38 (d, $J = 8.4$ Hz, 1H), 7.20 (d, $J = 9.4$ Hz, 1H), 7.00 (s, 1H), 6.98 (d, $J = 8.0$ Hz, 1H), 6.82 (d, $J = 8.0$ Hz, 1H), 5.63 (s, 2H), 5.04 (t, $J = 9.8$ Hz, 1H), 3.00 (m, 1H), 2.89 (m, 1H)

¹³C NMR (151 MHz, methanol-*d*₄) δ 164.24, 163.76, 147.92, 145.37, 144.22, 137.43, 133.96, 127.68, 121.55, 119.61, 117.40, 117.13, 115.36, 115.32, 114.77, 93.92, 64.55, 40.84, 32.58.

HRMS-ESI (*m/z*): [M+H]⁺ calculated for C₁₉H₁₇N₃O₄, 352.1292; found, 352.12934



Determination of Quantum Efficiency for One-Photon Photolysis

Solutions (100 μM) of the relevant substrate in KMOPS 7.2 pH were irradiated in quartz cuvettes (21-Q-10, Starna, Atascadero, CA) with an LED (Cairn Optoled Lite) set to 365 ± 10 nm. Aliquots (25 μL) were removed at various timepoints and analyzed by uHPLC (MeCN/H₂O 0.1% TFA: 6 minute gradient 5% MeCN to 100% MeCN, 2 minute gradient 100% MeCN to 5% MeCN), using external standard curves to determine concentrations. Reaction progress was plotted and the data fit to a single exponential curve.¹⁷¹ Quantum efficiencies (Q_u) were calculated using the following equation:

$$Q_u = (I\sigma t_{90\%})^{-1}$$

I : intensity ($\text{ein}\cdot\text{cm}^{-2}\cdot\text{s}$)

σ : decadic extinction coefficient ($\text{mol}^{-1}\cdot\text{cm}^2$)

$t_{90\%}$: time at which 90% of the starting material has been consumed

The intensity of the LED I was measured by potassium ferrioxalate actinometry¹⁹⁴ and calculated according to the following equation:

$$I = \frac{V_3 \Delta D_{510}}{1000 \varepsilon_{510} V_2 \phi_{Fe} t}$$

V_3 : volume of dilution (25 mL)

ΔD_{510} : change in absorption at 510 nm

ε_{510} : extinction coefficient of actinometry solution ($1.11 \times 10^4 \text{ M}^{-1} \text{ cm}^{-1}$)

V_2 : volume of potassium ferrioxalate taken for analysis (2 mL)

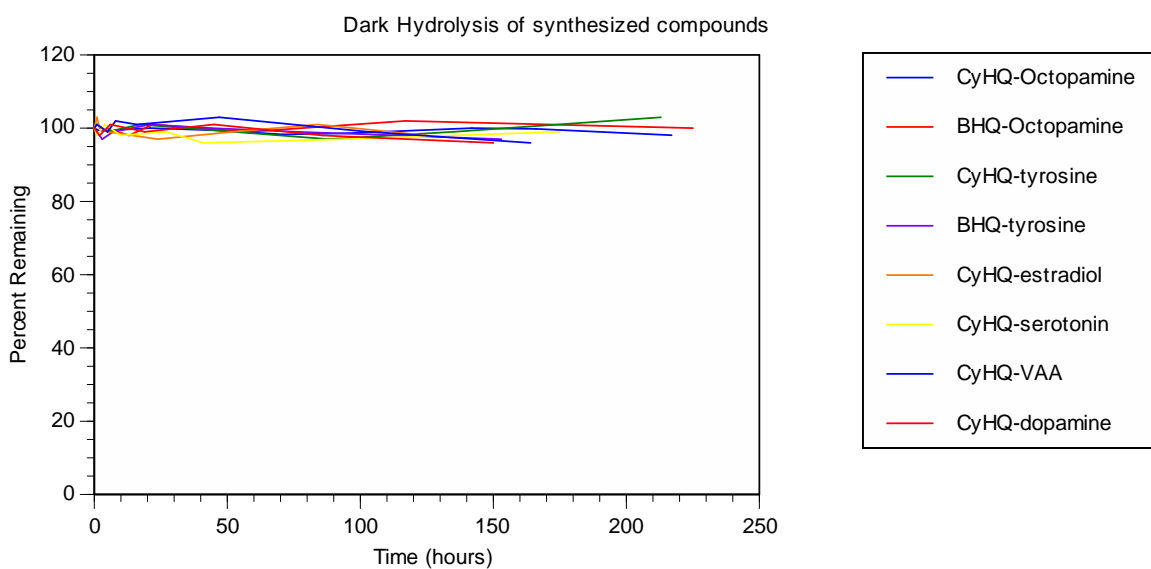
ϕ_{Fe} : quantum yield for the production of ferrous ions from potassium ferrioxalate at 365 nm (1.26)

t : irradiation time (30 s)

Compound	Intensity ($\text{ein}\cdot\text{cm}\cdot\text{s}^{-2}$)	Extinction Coefficient ($\text{M}^{-1}\cdot\text{cm}^{-1}$) (ϵ) at $\lambda =$ 370 nm	Single Exponential Decay Fit	t_{90} (s)	Quantum Efficiency	Retention time of starting material
CyHQ- octopamine 38	7.28E-9	5400	$Y = 100(-3.12E^{-2}X)$	74	0.34	2.9 min
BHQ- octopamine 37	1.55E-8	2700	$Y = 100(-3.24E^{-2}X)$	67	0.36	3.0 min
CyHQ- tyrosine 42	8.96E-9	4900	$Y = 100(-3.83E^{-2}X)$	60	0.38	2.7 min
BHQ- tyrosine 41	1.36E-8	2600	$Y = 100(-2.62E^{-2}X)$	87	0.32	2.8 min
CyHQ- estradiol 46	7.03E-9	6200	$Y = 100(-2.96E^{-2}X)$	78	0.29	5.7 min
BHQ- estradiol 45		3100	$Y = 100(-3.24E^{-2}X)$	N/A	N/A	5.9 min
CyHQ- serotonin 54	6.95E-9	5700	$Y = 100(-3.53E^{-2}X)$	65	0.39	2.4 min
CyHQ-VAA 50	8.75E-9	6100	$Y = 100(-5.05E^{-2}X)$	46	0.41	2.5 min
CyHQ- dopamine 66, 67	4.18E-9	5200	$Y = 100(-9.07E^{-3}X)$	254	0.18	2.6 min

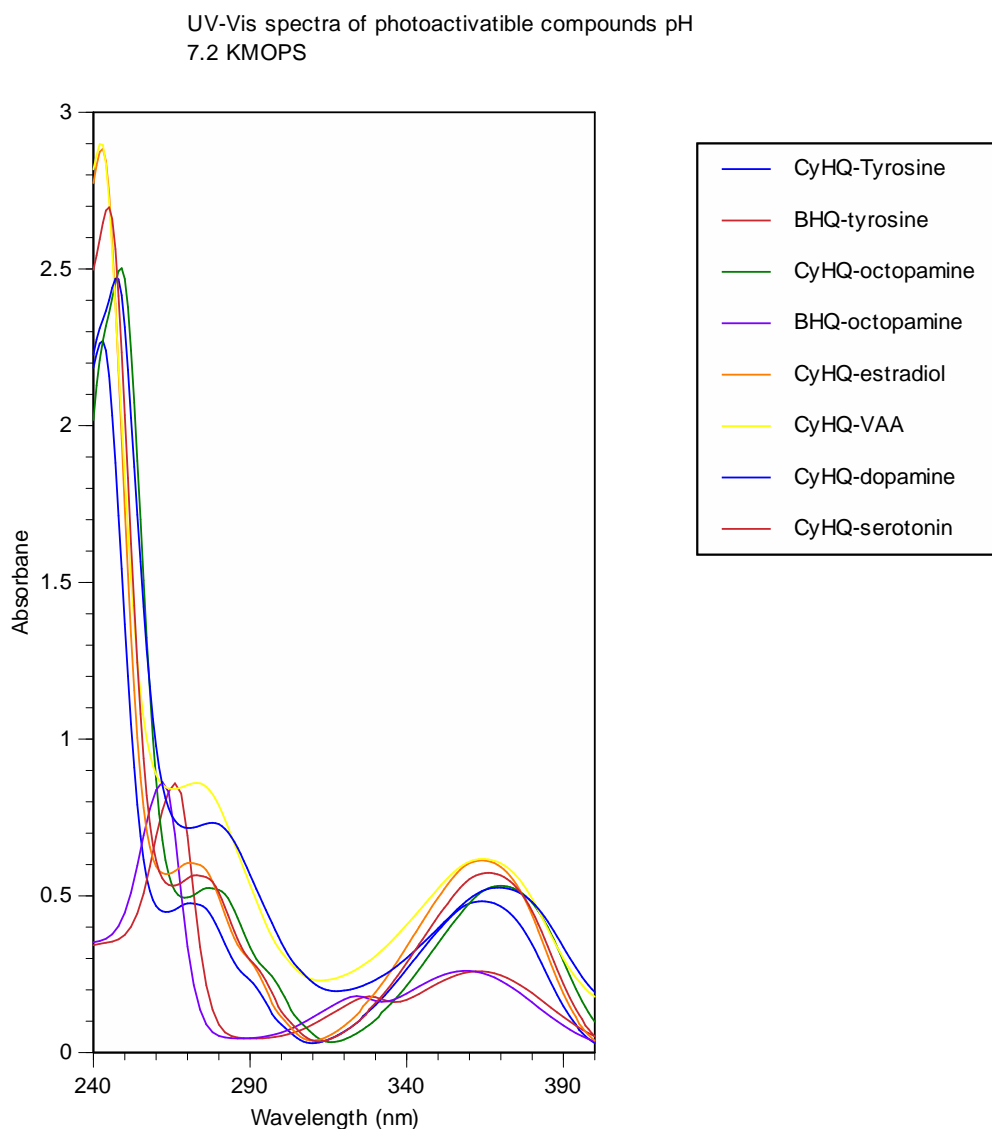
Determination of Dark Hydrolysis Rates

Substrates were dissolved in KMOPS (approximately 100 μ M) and stored in the dark at room temperature. Samples (5 μ L) for uHPLC analysis were removed and analyzed periodically as described for one-photon photolysis. None of the compounds synthesized displayed measurable dark hydrolysis over ~100-h timeframe.



Determination of Molar Absorptivity Coefficient

UV-Vis spectra were acquired by analyzing 100- μ M solutions of the relevant substrate prepared as described for one-photon photolysis with a spectral window measuring from 240 nm to 400 nm. A blank sample of KMOPS 7.2 pH was also prepared for a baseline. This method was repeated three times and the three absorbencies were averaged and the molar absorptivity (ϵ) at $\lambda = 370$ nm was calculated according to Beer-Lambert Law.



Determination of fluorescence emission intensity

Solutions (25 μM) of BHQ-OAc and BHQ-Dopamine in KMOPS 7.2 pH were prepared analogously to the procedure for one-photon photolysis. A blank sample of KMOPS 7.2 pH was also prepared for a baseline. The three samples were analyzed by a Cary Eclipse Fluorescence Spectrophotometer, and the baseline measurement was subtracted from both BHQ samples providing BHQ-OAc with $1.4\text{E}7$ RFU (relative fluorescence units)^{xlvi} and BHQ-Dopamine $1.0\text{E}7$ RFU.¹⁹⁵

^{xlvi} Due to significant technical limitations standardized fluorescence emission spectra are difficult and time consuming to attain. Thus most spectra are recorded relative to one another

Determination of two-photon uncaging cross-section

Solutions (100 μM) of the substrates in KMOPS 7.2 pH were prepared and stored in the dark. 25 μL aliquots of this solution were placed in a microcuvette (10 \times 1 \times 1 mm illuminated dimensions, 25 μL) and irradiated with a fs-pulsed and mode-locked Ti:Sapphire laser (Chameleon Ultra II, Coherent) with 740 nm light at an average power of 220 - 300 mW. Three samples of each substrate were irradiated for various time periods and analyzed by uHPLC as described for one-photon experiments.

A solution of fluorescein at pH 9.0 was prepared to act as a standard because of its well-characterized 2PE cross-section ($\delta_{aF} = 30 \text{ GM}$ at 740 nm) and quantum yield ($Q_{F2} = 0.9$). UV-Vis absorption spectroscopy was used to verify concentration. 25 μL aliquots of fluorescein solution were placed in the microcuvette and irradiated by the laser under the same conditions used for the caged compound. The fluorescence output of the solution was measured with a radiometer before and after the caged compound samples were irradiated and the two values were averaged.

The following equation was used to calculate the two-photon action cross-section for each compound:

$$\delta_u = \frac{N_p \emptyset Q_{F2} \delta_{aF} C_F}{\langle F(t) \rangle C_s}$$

N_p : number of product molecules formed per unit time (molecules/s) determined by uHPLC

\emptyset : is the collection efficiency of the detector (8.77×10^{-4})

Q_{F2} : is the quantum yield of fluorescein at pH 9.0 (0.9)

δ_{aF} : 2PE cross section of fluorescein at 740 nm (30 GM)

C_F : concentration of fluorescein (μM)

$\langle F(t) \rangle$: time averaged fluorescent photon flux (photon/s)

C_s : concentration of substrate (μM)

The collection efficiency of the detector is calculated by the following equation

$$\phi = \frac{Ay}{4\pi R^2 n^2}$$

A: area of detector (0.38 cm²)

y: fraction of integrated emission spectrum transmitted by interference filter (0.465)

R: distance from the center of the cuvette to the detector (2.25 cm)

n: refractive index of water (1.33)

The number of product molecules formed per unit time N_p was calculated by the following equation

$$N_p = \frac{C_s V_s A' - H C_s V_s A'}{t}$$

C_s : concentration of substrate (μM)

V_s : volume of substrate (25 μL)

A : 6.022×10^{23} molecules/mol

H : fraction of substrate remaining

t : time (s)

The time averaged photon flux $\langle F(t) \rangle$ was calculated by the following equation

$$\langle F(t) \rangle = \frac{FA\lambda}{rhc}$$

F : fluorescence reading (A)

A : area of detector (0.38 cm²)

λ : wavelength (535×10^{-9})

r : spectral response of the detector (0.09385 at 535 nm)

h : Planck's constant (6.63×10^{-34} J·s)

c : speed of light (3.00×10^8 m/s)

Compound	Decay Curve Equation	Np	C _s (μM)	C _f (μM)	<F(t)>	GM
BHQ-octopamine 37	$Y = 100(-1.15E^{-2}X)$	1.3E12	98	12	7.37E9	0.49
CyHQ-octopamine 38	$Y = 100(-1.99E^{-3}X)$	2.41E 11	105	12	3.46E9	0.18
CyHQ-tyrosine 42	$Y = 100(-4.49E^{-3}X)$	5.29E 11	102	14	4.62E9	0.36
BHQ-tyrosine 41	$Y = 100(-1.93E^{-2}X)$	2.14E 12	96	14	1.16E10	0.61
CyHQ-estradiol 46	$Y = 100(-3.36E^{-3}X)$	3.88E 11	100	14	5.24E9	0.24
CyHQ-serotonin 54	$Y = 100(-8.66E^{-3}X)$	1.00E 12	100	10	9.85E9	0.23
CyHQ-VAA 50	$Y = 100(-4.54E^{-3}X)$	5.03E 11	96	15	7.54E9	0.24
CyHQ-dopamine 66, 67	$Y = 100(-3.17E^{-3}X)$	3.81E 11	104	12	6.65E9	0.15

References

1. Beaulieu, J.-M.; Gainetdinov, R. R., The Physiology, Signaling, and Pharmacology of Dopamine Receptors. *Pharmacol. Rev.* **2011**, *63* (1), 182-217.
2. Witkovsky, P., Dopamine and retinal function. *Doc. Ophthalmol.* **2004**, *108* (1), 17-39.
3. Aperia, A. C., Intrarenal Dopamine: A Key Signal in the Interactive Regulation of Sodium Metabolism. *Annu. Rev. Physiol.* **2000**, *62* (1), 621-647.
4. Missale, C.; Nash, S. R.; Robinson, S. W.; Jaber, M.; Caron, M. G., Dopamine Receptors: From Structure to Function. *Physiol. Rev.* **1998**, *78* (1), 189-225.
5. NIDA: Dopamine pathways. 2012. Accessed March 2014
http://wikipedia/commons/d/de/Dopamine_pathways.svg
6. Andén, N. E.; Carlsson, A.; Dahlström, A.; Fuxe, K.; Hillarp, N. Å.; Larsson, K., Demonstration and mapping out of nigro-neostriatal dopamine neurons. *Life Sci.* **1964**, *3* (6), 523-530.
7. Iversen, L. L. *Dopamine handbook*; Oxford University Press, 2010.
8. Haggstrom, M. Basal ganglia circuits. May 2010. Accessed March 2014
http://upload.wikimedia.org/wikipedia/commons/c/c9/Basal_ganglia_circuits.png
9. Matsuda, W.; Furuta, T.; Nakamura, K. C.; Hioki, H.; Fujiyama, F.; Arai, R.; Kaneko, T., Single Nigrostriatal Dopaminergic Neurons Form Widely Spread and Highly Dense Axonal Arborizations in the Neostriatum. *J. Neurosci.* **2009**, *29* (2), 444-453.
10. Nair-Roberts, R. G.; Chatelain-Badie, S. D.; Benson, E.; White-Cooper, H.; Bolam, J. P.; Ungless, M. A., Stereological estimates of dopaminergic, GABAergic and glutamatergic neurons in the ventral tegmental area, substantia nigra and retrorubral field in the rat. *Neurosci.* **2008**, *152* (4), 1024-1031.
11. Oorschot, D. E., Total number of neurons in the neostriatal, pallidal, subthalamic, and substantia nigral nuclei of the rat basal ganglia: a stereological study using the cavalieri and optical disector methods. *J. Comp. Neurol.* **1996**, *366*, 580-99.
12. Wickens, J. R.; Arbuthnott, G. W., Chapter IV Structural and functional interactions in the striatum at the receptor level. In *Handbook of Chemical Neuroanatomy*, 21, 199-236.
13. Kawaguchi, Y.; Wilson, C. J.; Emson, P. C., Projection subtypes of rat neostriatal matrix cells revealed by intracellular injection of biocytin. *J. Neurosci.* **1990**, *10*, 3421-38.
14. Tepper, J. M.; Bolam, J. P., Functional diversity and specificity of neostriatal interneurons. *Curr. Opin. Neurobiol.* **2004**, *14* (6), 685-692.
15. Tennyson, V. M.; Barrett, R. E.; Cohen, G.; Cote, L.; Helkkila, R.; Mytilineou, C., Correlation of Anatomical and Biochemical Development of the Rabbit Neostriatum. In *Progress in Brain Research*, Ford, D. H., Ed. Elsevier: 1973; Vol. Volume 40, pp 203-217.
16. Gerfen, C.; Herkenham, M.; Thibault, J., The neostriatal mosaic: II. Patch- and matrix-directed mesostriatal dopaminergic and non-dopaminergic systems. *J. Neurosci.* **1987**, *7* (12), 3915-3934.

17. Gerfen, C.; Baimbridge, K.; Thibault, J., The neostriatal mosaic: III. Biochemical and developmental dissociation of patch-matrix mesostriatal systems. *J. Neurosci.* **1987**, *7* (12), 3935-3944.
18. Lacey, C. J.; Boyes, J.; Gerlach, O.; Chen, L.; Magill, P. J.; Bolam, J. P., GABAB receptors at glutamatergic synapses in the rat striatum. *Neurosci.* **2005**, *136* (4), 1083-1095.
19. Moss, J.; Bolam, J. P., A Dopaminergic Axon Lattice in the Striatum and Its Relationship with Cortical and Thalamic Terminals. *J. Neurosci.* **2008**, *28* (44), 11221-11230.
20. Gerfen, C. R.; Young, W. S., 3rd, Distribution of striatonigral and striatopallidal peptidergic neurons in both patch and matrix compartments: an in situ hybridization histochemistry and fluorescent retrograde tracing study. *Brain Res.* **1988**, *460*, 161-7.
21. Pan, H. S.; Penney, J. B.; Young, A. B., γ -Aminobutyric acid and benzodiazepine receptor changes induced by unilateral 6-hydroxydopamine lesions of the medial forebrain bundle. *J. Neurochem.* **1985**, *45*, 1396-404.
22. Gerfen, C. R.; Engber, T. M.; Mahan, L. C.; Susel, Z.; Chase, T. N.; Monsma, F. J., Jr.; Sibley, D. R., D1 and D2 dopamine receptor-regulated gene expression of striatonigral and striatopallidal neurons. *Science* **1990**, *250*, 1429-32.
23. DeLong, M. R., Primate models of movement disorders of basal ganglia origin. *Trends Neurosci.* **1990**, *13*, 281-5.
24. Haggstrom, M., Basal ganglia in Parkinson's. May 2010.
25. Robbins, T. W.; Weinberger, D.; Taylor, J. G.; Morris, R. G., Dissociating Executive Functions of the Prefrontal Cortex [and Discussion]. *Philos. Trans. R. Soc., B* **1996**, *351* (1346), 1463-1471.
26. Barbas, H.; Medalla, M.; Alade, O.; Suski, J.; Zikopoulos, B.; Lera, P., Relationship of Prefrontal Connections to Inhibitory Systems in Superior Temporal Areas in the Rhesus Monkey. *Cereb. Cortex* **2005**, *15* (9), 1356-1370.
27. Dias, R.; Robbins, T. W.; Roberts, A. C., Dissociable Forms of Inhibitory Control within Prefrontal Cortex with an Analog of the Wisconsin Card Sort Test: Restriction to Novel Situations and Independence from "On-Line" Processing. *J. Neurosci.* **1997**, *17* (23), 9285-9297.
28. Goldman-Rakic, P. S.; Lidow, M. S.; Smiley, J. F.; Williams, M. S., The anatomy of dopamine in monkey and human prefrontal cortex. *J. Neural Trans., Supp.* **1992**, *36*, 163-177.
29. Smiley, J. F.; Goldman-Rakic, P. S., Heterogeneous Targets of Dopamine Synapses in Monkey Prefrontal Cortex Demonstrated by Serial Section Electron Microscopy: A Laminar Analysis Using the Silver-enhanced Diaminobenzidine Sulfide (SEDS) Immunolabeling Technique. *Cereb. Cortex* **1993**, *3* (3), 223-238.
30. Goldman-Rakic, P. S.; Leranth, C.; Williams, S. M.; Mons, N.; Geffard, M., Dopamine synaptic complex with pyramidal neurons in primate cerebral cortex. *Proc. Natl. Acad. Sci. U. S. A.* **1989**, *86* (22), 9015-9019.
31. Pickel, V. M.; Garzón, M.; Mengual, E., Chapter 12 Electron microscopic immunolabeling of transporters and receptors identifies transmitter-specific functional sites envisioned in Cajal's neuron. In *Progress in Brain Research*, 136, 145-155.

32. Andersen, P. H.; Gingrich, J. A.; Bates, M. D.; Dearry, A.; Falardeau, P.; Senogles, S. E.; Caron, M. G., Dopamine receptor subtypes: beyond the D1/D2 classification. *Trends Pharmacol. Sci.* **1990**, *11* (6), 231-236.
33. Tiberi, M.; Jarvie, K. R.; Silvia, C.; Falardeau, P.; Gingrich, J. A.; Godinot, N.; Bertrand, L.; Yang-Feng, T. L.; Fremeau, R. T.; Caron, M. G., Cloning, molecular characterization, and chromosomal assignment of a gene encoding a second D1 dopamine receptor subtype: differential expression pattern in rat brain compared with the D1A receptor. *Proc. Natl. Acad. Sci. U. S. A.* **1991**, *88* (17), 7491-7495.
34. Sibley, D. R., New Insights into Dopaminergic Receptor Function Using Antisense and Genetically Altered Animals. *Annu. Rev. Pharmacol. Toxicol.* **1999**, *39* (1), 313-341.
35. Svenningsson, P.; Nishi, A.; Fisone, G.; Girault, J.-A.; Nairn, A. C.; Greengard, P., DARPP-32: An Integrator of Neurotransmission. *Annu. Rev. Pharmacol. Toxicol.* **2004**, *44* (1), 269-296.
36. Nishi, A.; Snyder, G. L.; Greengard, P., Bidirectional Regulation of DARPP-32 Phosphorylation by Dopamine. *J. Neurosci.* **1997**, *17* (21), 8147-8155.
37. Greengard, P., Review: Neuroscience: The neurobiology of slow synaptic transmission. *Science* **2001**, *294*, 1024-1030.
38. Bibb, J. A.; Snyder, G. L.; Nishi, A.; Yan, Z.; Meijer, L.; Fienberg, A. A.; Tsai, U. H.; Kwon, Y. T.; Girault, J.-A.; Czernik, A. J.; Haganir, R. L.; Hemmings, H. C., Jr.; Nairn, A. C.; Greengard, P., Phosphorylation of DARPP-32 by Cdk5 modulates dopamine signalling in neurons. *Nature* **1999**, *402*, 669-671.
39. Gould, T. D.; Manji, H. K., DARPP-32: A molecular switch at the nexus of reward pathway plasticity. *Proc. Natl. Acad. Sci. U. S. A.* **2005**, *102* (2), 253-254.
40. Berhow, M. T.; Hiroi, N.; Nestler, E. J., Regulation of ERK (Extracellular signal Regulated Kinase), part of the neurotrophin signal transduction cascade, in the rat mesolimbic dopamine system by chronic exposure to morphine or cocaine. *J. Neurosci.* **1996**, *1*, 4707-4715.
41. Chen, J.; Rusnak, M.; Luedtke, R. R.; Sidhu, A., D1 Dopamine Receptor Mediates Dopamine-induced Cytotoxicity via the ERK Signal Cascade. *J. Biol. Chem.* **2004**, *279*, 39317-39330.
42. Beom, S.; Cheong, D.; Torres, G.; Caron, M. G.; Kim, K.-M., Comparative Studies of Molecular Mechanisms of Dopamine D2 and D3 Receptors for the Activation of Extracellular Signal-regulated Kinase. *J. Biol. Chem.* **2004**, *279*, 28304-28314.
43. Valjent, E.; Corvol, J.-C.; Pages, C.; Besson, M.-J.; Maldonado, R.; Caboche, J., Involvement of the extracellular signal-regulated kinase cascade for cocaine rewarding properties. *J. Neurosci.* **2000**, *20*, 8701-8709.
44. Valjent, E.; Pascoli, V.; Svenningsson, P.; Paul, S.; Enslen, H.; Corvol, J.-C.; Stipanovich, A.; Caboche, J.; Lombroso, P. J.; Nairn, A. C.; Greengard, P.; Herve, D.; Girault, J.-A., Regulation of a protein phosphatase cascade allows convergent dopamine and glutamate signals to activate ERK in the striatum. *Proc. Natl. Acad. Sci. U. S. A.* **2005**, *102*, 491-496.
45. Brami-Cherrier, K.; Valjent, E.; Herve, D.; Darragh, J.; Corvol, J.-C.; Pages, C.; Simon, A. J.; Girault, J.-A.; Caboche, J., Parsing molecular and behavioral effects

- of cocaine in mitogen- and stress-activated protein kinase-1-deficient mice. *J. Neurosci.* **2005**, *25*, 11444-11454.
46. Grienberger, C.; Konnerth, A., Imaging Calcium in Neurons. *Neuron* **2012**, *73* (5), 862-885.
 47. So, C. H.; Verma, V.; Alijaniam, M.; Cheng, R.; Rashid, A. J.; O'Dowd, B. F.; George, S. R., Calcium Signaling by Dopamine D5 Receptor and D5-D2 Receptor Hetero-Oligomers Occurs by a Mechanism Distinct from That for Dopamine D1-D2 Receptor Hetero-Oligomers. *Mol. Pharmacol.* **2009**, *75* (4), 843-854.
 48. Zhang, Z.-W.; Burke, M. W.; Calakos, N.; Beaulieu, J.-M.; Vaucher, E., Confocal analysis of cholinergic and dopaminergic inputs onto pyramidal cells in the prefrontal cortex of rodents. *Front. Neuroanatomy* **2010**, *4*.
 49. Hernández-López, S.; Tkatch, T.; Perez-Garci, E.; Galarraga, E.; Bargas, J.; Hamm, H.; Surmeier, D. J., D2 Dopamine Receptors in Striatal Medium Spiny Neurons Reduce L-Type Ca²⁺ Currents and Excitability via a Novel PLCβ1–IP3–Calcineurin-Signaling Cascade. *J. Neurosci.* **2000**, *20* (24), 8987-8995.
 50. Karam, C. S.; Ballon, J. S.; Bivens, N. M.; Freyberg, Z.; Girgis, R. R.; Lizardi-Ortiz, J. E.; Markx, S.; Lieberman, J. A.; Javitch, J. A., Signaling pathways in schizophrenia: emerging targets and therapeutic strategies. *Trends Pharmacol. Sci.* **2010**, *31* (8), 381-390.
 51. Karege, F.; Perroud, N.; Burkhardt, S.; Schwald, M.; Ballmann, E.; La Harpe, R.; Malafosse, A., Alteration in Kinase Activity But Not in Protein Levels of Protein Kinase B and Glycogen Synthase Kinase-3β in Ventral Prefrontal Cortex of Depressed Suicide Victims. *Biol. Psychiatry* **2007**, *61* (2), 240-245.
 52. Zhang, J.; Vinuela, A.; Neely, M. H.; Hallett, P. J.; Grant, S. G. N.; Miller, G. M.; Isacson, O.; Caron, M. G.; Yao, W.-D., Inhibition of the Dopamine D1 Receptor Signaling by PSD-95. *J. Biol. Chem.* **2007**, *282* (21), 15778-15789.
 53. Fiorentini, C.; Gardoni, F.; Spano, P.; Di Luca, M.; Missale, C., Regulation of Dopamine D1 Receptor Trafficking and Desensitization by Oligomerization with Glutamate N-Methyl-D-aspartate Receptors. *J. Biol. Chem.* **2003**, *278* (22), 20196-20202.
 54. Tritsch, Nicolas X.; Sabatini, Bernardo L., Dopaminergic Modulation of Synaptic Transmission in Cortex and Striatum. *Neuron* **2012**, *76* (1), 33-50.
 55. Salgado, H.; Tecuapetla, F.; Perez-Rosello, T.; Perez-Burgos, A.; Perez-Garci, E.; Galarraga, E.; Bargas, J., A Reconfiguration of CaV2 Ca²⁺ Channel Current and Its Dopaminergic D2 Modulation in Developing Neostriatal Neurons. *J. Neurophys.* **2005**, *94* (6), 3771-3787.
 56. Xu, T.-X.; Yao, W.-D., D1 and D2 dopamine receptors in separate circuits cooperate to drive associative long-term potentiation in the prefrontal cortex. *Proc. Natl. Acad. Sci. U. S. A.* **2010**, *107* (37), 16366-16371.
 57. Kohnomi, S.; Koshikawa, N.; Kobayashi, M., D2-like dopamine receptors differentially regulate unitary IPSCs depending on presynaptic GABAergic neuron subtypes in rat nucleus accumbens shell. *J. Neurophys.* **2012**, *107* (2), 692-703.
 58. Centonze, D.; Bracci, E.; Pisani, A.; Gubellini, P.; Bernardi, G.; Calabresi, P., Activation of dopamine D1-like receptors excites LTS interneurons of the striatum. *Eur. J. Neurosci.* **2002**, *15* (12), 2049-2052.

59. Towers, S. K.; Hestrin, S., D1-Like Dopamine Receptor Activation Modulates GABAergic Inhibition But Not Electrical Coupling between Neocortical Fast-Spiking Interneurons. *J. Neurosci.* **2008**, *28* (10), 2633-2641.
60. Taverna, S.; Canciani, B.; Pennartz, C. M. A., Dopamine D1-receptors modulate lateral inhibition between principal cells of the nucleus accumbens. *J. Neurophys.* **2005**, *93* (3), 1816-1819.
61. Gao, W. J.; Goldman-Rakic, P. S., Selective modulation of excitatory and inhibitory microcircuits by dopamine. *Proc. Natl. Acad. Sci. U. S. A.* **2003**, *100* (5), 2836-2841.
62. Wang, W.; Dever, D.; Lowe, J.; Storey, G. P.; Bhansali, A.; Eck, E. K.; Nitulescu, I.; Weimer, J.; Bamford, N. S., Regulation of prefrontal excitatory neurotransmission by dopamine in the nucleus accumbens core. *J. Physiol.* **2012**, *590* (16), 3743-3769.
63. Braithwaite, S. P.; Adkisson, M.; Leung, J.; Nava, A.; Masterson, B.; Urfer, R.; Oksenberg, D.; Nikolich, K., Regulation of NMDA receptor trafficking and function by striatal-enriched tyrosine phosphatase (STEP). *Eur. J. Neurosci.* **2006**, *23* (11), 2847-2856.
64. Gonzalez-Islas, C.; Hablitz, J. J., Dopamine enhances EPSCs in layer II-III pyramidal neurons in rat prefrontal cortex. *J. Neurosci.* **2003**, *23* (3), 867-875.
65. Higley, M. J.; Sabatini, B. L., Competitive regulation of synaptic Ca²⁺ influx by D2 dopamine and A2A adenosine receptors. *Nat. Neurosci.* **2010**, *13* (8), 958-966.
66. Wang, X.; Zhong, P.; Gu, Z.; Yan, Z., Regulation of NMDA Receptors by Dopamine D4 Signaling in Prefrontal Cortex. *J. Neurosci.* **2003**, *23* (30), 9852-9861.
67. André, V. M.; Cepeda, C.; Cummings, D. M.; Jocoy, E. L.; Fisher, Y. E.; William Yang, X.; Levine, M. S., Dopamine modulation of excitatory currents in the striatum is dictated by the expression of D1 or D2 receptors and modified by endocannabinoids. *Eur. J. Neurosci.* **2010**, *31* (1), 14-28.
68. Håkansson, K.; Galdi, S.; Hendrick, J.; Snyder, G.; Greengard, P.; Fisone, G., Regulation of phosphorylation of the GluR1 AMPA receptor by dopamine D 2 receptors. *J. Neurochem.* **2006**, *96* (2), 482-488.
69. Sun, X.; Zhao, Y.; Wolf, M. E., Dopamine receptor stimulation modulates AMPA receptor synaptic insertion in prefrontal cortex neurons. *J. Neurosci.* **2005**, *25* (32), 7342-7351.
70. Sun, X.; Milovanovic, M.; Zhao, Y.; Wolf, M. E., Acute and chronic dopamine receptor stimulation modulates AMPA receptor trafficking in nucleus accumbens neurons cocultured with prefrontal cortex neurons. *J. Neurosci.* **2008**, *28* (16), 4216-4230.
71. Shepherd, J. D.; Huganir, R. L., The cell biology of synaptic plasticity: AMPA receptor trafficking. 2007; Vol. 23, pp 613-643.
72. Bolam, J. P.; Hanley, J. J.; Booth, P. A. C.; Bevan, M. D., Synaptic organisation of the basal ganglia. *J. Anat.* **2000**, *196* (4), 527-542.
73. Parent, M.; Parent, A., Single-axon tracing study of corticostriatal projections arising from primary motor cortex in primates. *J. Comp. Neurol.* **2006**, *496* (2), 202-213.

74. Wilson, C. J., Chapter 18 The generation of natural firing patterns in neostriatal neurons. In *Progress in Brain Research*, Arbuthnott, G. W.; Emson, P. C., Eds. Elsevier: 1993; Vol. Volume 99, pp 277-297.
75. Mahon, S.; Vautrelle, N.; Pezard, L.; Slaght, S. J.; Deniau, J.-M.; Chouvet, G.; Charpier, S., Distinct Patterns of Striatal Medium Spiny Neuron Activity during the Natural Sleep–Wake Cycle. *J. Neurosci.* **2006**, *26* (48), 12587-12595.
76. Surmeier, D. J.; Ding, J.; Day, M.; Wang, Z.; Shen, W., D1 and D2 dopamine-receptor modulation of striatal glutamatergic signaling in striatal medium spiny neurons. *Trends Neurosci.* **2007**, *30* (5), 228-235.
77. Bamford, N. S.; Zhang, H.; Schmitz, Y.; Wu, N.-P.; Cepeda, C.; Levine, M. S.; Schmauss, C.; Zakharenko, S. S.; Zablow, L.; Sulzer, D., Heterosynaptic Dopamine Neurotransmission Selects Sets of Corticostriatal Terminals. *Neuron* **2004**, *42* (4), 653-663.
78. Gao, T.; Yatani, A.; Dell'Acqua, M. L.; Sako, H.; Green, S. A.; Dascal, N.; Scott, J. D.; Hosey, M. M., cAMP-Dependent Regulation of Cardiac L-Type Ca²⁺ Channels Requires Membrane Targeting of PKA and Phosphorylation of Channel Subunits. *Neuron* **1997**, *19* (1), 185-196.
79. Vilchis, C.; Bargas, J.; Ayala, G. X.; Galván, E.; Galarraga, E., Ca²⁺ channels that activate Ca²⁺-dependent K⁺ currents in neostriatal neurons. *Neurosci.* **1999**, *95* (3), 745-752.
80. Bennett, B. D.; Bolam, J. P., Synaptic input and output of parvalbumin-immunoreactive neurons in the neostriatum of the rat. *Neurosci.* **1994**, *62* (3), 707-719.
81. Gage, G. J.; Stoetznner, C. R.; Wiltschko, A. B.; Berke, J. D., Selective Activation of Striatal Fast-Spiking Interneurons during Choice Execution. *Neuron* **2010**, *67* (3), 466-479.
82. Rajakumar, N.; Elisevich, K.; Flumerfelt, B. A., The pallidostriatal projection in the rat: a recurrent inhibitory loop? *Brain Res.* **1994**, *651* (1–2), 332-336.
83. Sciamanna, G.; Bonsi, P.; Tassone, A.; Cuomo, D.; Tschertner, A.; Viscomi, M. T.; Martella, G.; Sharma, N.; Bernardi, G.; Standaert, D. G.; Pisani, A., Impaired striatal D2 receptor function leads to enhanced GABA transmission in a mouse model of DYT1 dystonia. *Neurobiol. Dis.* **2009**, *34* (1), 133-145.
84. Beiser, D. G.; Hua, S. E.; Houk, J. C., Network models of the basal ganglia. *Curr. Opin. Neurobiol.* **1997**, *7* (2), 185-190.
85. Ellis-Davies, G. C. R., Neurobiology with Caged Calcium. *Chem. Rev.* **2008**, *108* (5), 1603-1613.
86. Kao, J. P. Y., Caged Molecules: Principles and Practical Considerations. In *Current Protocols in Neuroscience*, John Wiley & Sons, Inc.: 2001.
87. Huang, Y. H.; Muralidharan, S.; Sinha, S. R.; Kao, J. P. Y.; Bergles, D. E., Ncm-d-aspartate: A novel caged d-aspartate suitable for activation of glutamate transporters and N-methyl-d-aspartate (NMDA) receptors in brain tissue. *Neuropharmacol.* **2005**, *49* (6), 831-842.
88. Cai, X.; Liang, C. W.; Muralidharan, S.; Kao, J. P. Y.; Tang, C.-M.; Thompson, S. M., Unique Roles of SK and Kv4.2 Potassium Channels in Dendritic Integration. *Neuron* **2004**, *44* (2), 351-364.

89. Rossi, F. M.; Kao, J. P. Y., Nmoc-DBHQ, a New Caged Molecule for Modulating Sarcoplasmic/Endoplasmic Reticulum Ca²⁺ ATPase Activity with Light Flashes. *J. Biol. Chem.* **1997**, *272* (6), 3266-3271.
90. Conrad, P. G.; Givens, R. S.; Weber, J. F. W.; Kandler, K., New Phototriggers:1 Extending the p-Hydroxyphenacyl π - π^* Absorption Range. *Org. Lett.* **2000**, *2* (11), 1545-1547.
91. Furuta, T.; Wang, S. S.-H.; Dantzker, J. L.; Dore, T. M.; Bybee, W. J.; Callaway, E. M.; Denk, W.; Tsien, R. Y., Brominated 7-hydroxycoumarin-4-ylmethyls: Photolabile protecting groups with biologically useful cross-sections for two photon photolysis. *Proc. Natl. Acad. Sci. U. S. A.* **1999**, *96* (4), 1193-1200.
92. Papageorgiou, G.; Ogden, D. C.; Barth, A.; Corrie, J. E. T., Photorelease of Carboxylic Acids from 1-Acyl-7-nitroindolines in Aqueous Solution: Rapid and Efficient Photorelease of l-Glutamate1. *J. Am. Chem. Soc.* **1999**, *121* (27), 6503-6504.
93. Papageorgiou, G.; Corrie, J. E. T., Effects of aromatic substituents on the photocleavage of 1-acyl-7-nitroindolines. *Tetrahedron* **2000**, *56* (41), 8197-8205.
94. Lee, C. C.; Sherman, S. M., Glutamatergic Inhibition in Sensory Neocortex. *Cereb. Cortex* **2009**, *19* (10), 2281-2289.
95. Lee, C. C.; Sherman, S. M., Synaptic Properties of Thalamic and Intracortical Inputs to Layer 4 of the First- and Higher-Order Cortical Areas in the Auditory and Somatosensory Systems. *J. Neurophys.* **2008**, *100* (1), 317-326.
96. Canepari, M.; Ogden, D., Kinetic, pharmacological and activity-dependent separation of two Ca²⁺ signalling pathways mediated by type 1 metabotropic glutamate receptors in rat Purkinje neurones. *J. Physiol.* **2006**, *573* (1), 65-82.
97. Diamond, J. S., Deriving the Glutamate Clearance Time Course from Transporter Currents in CA1 Hippocampal Astrocytes: Transmitter Uptake Gets Faster during Development. *J. Neurosci.* **2005**, *25* (11), 2906-2916.
98. Canepari, M.; Auger, C.; Ogden, D., Ca²⁺ Ion Permeability and Single-Channel Properties of the Metabotropic Slow EPSC of Rat Purkinje Neurons. *J. Neurosci.* **2004**, *24* (14), 3563-3573.
99. Pei, W.; Ritz, M.; McCarthy, M.; Huang, Z.; Niu, L., Receptor Occupancy and Channel-opening Kinetics. *J. Biol. Chem.* **2007**, *282* (31), 22731-22736.
100. Frick, A.; Zieglgänsberger, W.; Dodt, H.-U., Glutamate Receptors Form Hot Spots on Apical Dendrites of Neocortical Pyramidal Neurons. *J. Neurophys.* **2001**, *86* (3), 1412-1421.
101. Pettit, D. L.; Augustine, G. J., Distribution of Functional Glutamate and GABA Receptors on Hippocampal Pyramidal Cells and Interneurons. *J. Neurophys.* **2000**, *84* (1), 28-38.
102. (a) Shao, L.-R.; Dudek, F. E., Increased Excitatory Synaptic Activity and Local Connectivity of Hippocampal CA1 Pyramidal Cells in Rats With Kainate-Induced Epilepsy. *J. Neurophys.* **2004**, *92* (3), 1366-1373; (b) Shao, L.-R.; Dudek, F. E., Detection of Increased Local Excitatory Circuits in the Hippocampus during Epileptogenesis Using Focal Flash Photolysis of Caged Glutamate. *Epilepsia* **2005**, *46*, 100-106.
103. (a) Zhang, Y.-P.; Holbro, N.; Oertner, T. G., Optical induction of plasticity at single synapses reveals input-specific accumulation of α CaMKII. *Proc. Natl.*

- Acad. Sci. U. S. A.* **2008**, *105* (33), 12039-12044; (b) Rossi, B.; Collin, T., Presynaptic NMDA receptors act as local high-gain glutamate detector in developing cerebellar molecular layer interneurons. *J. Neurochem.* **2013**, *126* (1), 47-57; (c) Eder, M.; Zieglgänsberger, W.; Dodt, H.-U., Neocortical Long-Term Potentiation and Long-Term Depression: Site of Expression Investigated by Infrared-Guided Laser Stimulation. *J. Neurosci.* **2002**, *22* (17), 7558-7568.
104. (a) Richardson, R. J.; Blundon, J. A.; Bayazitov, I. T.; Zakharenko, S. S., Connectivity Patterns Revealed by Mapping of Active Inputs on Dendrites of Thalamorecipient Neurons in the Auditory Cortex. *J. Neurosci.* **2009**, *29* (20), 6406-6417; (b) Hirtz, J. J.; Braun, N.; Griesemer, D.; Hannes, C.; Janz, K.; Löhrke, S.; Müller, B.; Friauf, E., Synaptic Refinement of an Inhibitory Topographic Map in the Auditory Brainstem Requires Functional CaV1.3 Calcium Channels. *J. Neurosci.* **2012**, *32* (42), 14602-14616; (c) Kam, K.; Worrell, J. W.; Ventalon, C.; Emiliani, V.; Feldman, J. L., Emergence of Population Bursts from Simultaneous Activation of Small Subsets of preBötzinger Complex Inspiratory Neurons. *J. Neurosci.* **2013**, *33* (8), 3332-3338; (d) Auger, C.; Ogden, D., AMPA receptor activation controls type I metabotropic glutamate receptor signalling via a tyrosine kinase at parallel fibre–Purkinje cell synapses. *J. Physiol.* **2010**, *588* (16), 3063-3074.
105. Maiella, P.; Brill, T., Spectroscopy of Hydrothermal Reactions. 10. Evidence of Wall Effects in Decarboxylation Kinetics of 1.00 m HCO₂X (X= H, Na) at 280-330° C and 275 bar. *J. Phys. Chem. A* **1998**, *102* (29), 5886-5891.
106. Klán, P.; Šolomek, T.; Bochet, C. G.; Blanc, A.; Givens, R.; Rubina, M.; Popik, V.; Kostikov, A.; Wirz, J., Photoremovable Protecting Groups in Chemistry and Biology: Reaction Mechanisms and Efficacy. *Chem. Rev.* **2012**, *113* (1), 119-191.
107. Maier, W.; Corrie, J. E. T.; Papageorgiou, G.; Laube, B.; Grewer, C., Comparative analysis of inhibitory effects of caged ligands for the NMDA receptor. *J. Neurosci. Meth.* **2005**, *142* (1), 1-9.
108. Amatrudo, J. M.; Olson, J. P.; Lur, G.; Chiu, C. Q.; Higley, M. J.; Ellis-Davies, G. C. R., Wavelength-Selective One- and Two-Photon Uncaging of GABA. *ACS Chem. Neurosci.* **2013**.
109. Donato, L.; Mourot, A.; Davenport, C. M.; Herbivo, C.; Warther, D.; Léonard, J.; Bolze, F.; Nicoud, J.-F.; Kramer, R. H.; Goeldner, M.; Specht, A., Water-Soluble, Donor–Acceptor Biphenyl Derivatives in the 2-(o-Nitrophenyl)propyl Series: Highly Efficient Two-Photon Uncaging of the Neurotransmitter γ -Aminobutyric Acid at $\lambda=800$ nm. *Angew. Chem., Int. Ed.* **2012**, *51* (8), 1840-1843.
110. Matsuzaki, M.; Hayama, T.; Kasai, H.; Ellis-Davies, G. C. R., Two-photon uncaging of γ -aminobutyric acid in intact brain tissue. *Nat. Chem. Biol.* **2010**, *6* (4), 255-257.
111. Zayat, L.; Noval, M. G.; Campi, J.; Calero, C. I.; Calvo, D. J.; Etchenique, R., A New Inorganic Photolabile Protecting Group for Highly Efficient Visible Light GABA Uncaging. *ChemBioChem* **2007**, *8* (17), 2035-2038.
112. Rial Verde, E.; Zayat, L.; Etchenique, R.; Yuste, R., Photorelease of GABA with visible light using an inorganic caging group. *Front. Neural Circuits* **2008**, *2*.

113. Lopes-dos-Santos, V.; Campi, J.; Filevich, O.; Ribeiro, S.; Etchenique, R., In vivo photorelease of GABA in the mouse cortex. *Braz. J. Med. Biol. Res.* **2011**, *44*, 688-693.
114. Gee, K. R.; Wieboldt, R.; Hess, G. P., Synthesis and Photochemistry of a New Photolabile Derivative of GABA-Neurotransmitter Release and Receptor Activation in the Microsecond Time Region. *J. Am. Chem. Soc.* **1994**, *116* (18), 8366-8367.
115. Khirug, S.; Yamada, J.; Afzalov, R.; Voipio, J.; Khiroug, L.; Kaila, K., GABAergic Depolarization of the Axon Initial Segment in Cortical Principal Neurons Is Caused by the Na-K-2Cl Cotransporter NKCC1. *J. Neurosci.* **2008**, *28* (18), 4635-4639.
116. Yang, X.-F.; Schmidt, B. F.; Rode, D. L.; Rothman, S. M., Optical suppression of experimental seizures in rat brain slices. *Epilepsia* **2010**, *51* (1), 127-135.
117. Dellal, S. S.; Luo, R.; Otis, T. S., GABAA receptors increase excitability and conduction velocity of cerebellar parallel fiber axons. *J. Neurophys.* **2012**, *107* (11), 2958-2970.
118. Dittman, J. S.; Regehr, W. G., Mechanism and Kinetics of Heterosynaptic Depression at a Cerebellar Synapse. *J. Neurosci.* **1997**, *17* (23), 9048-9059.
119. Adams, S. R.; Kao, J. P. Y.; Grynkiewicz, G.; Minta, A.; Tsien, R. Y., Biologically useful chelators that release Ca²⁺ upon illumination. *J. Am. Chem. Soc.* **1988**, *110* (10), 3212-3220.
120. Kaplan, J. H.; Ellis-Davies, G. C., Photolabile chelators for the rapid photorelease of divalent cations. *Proc. Natl. Acad. Sci. U. S. A.* **1988**, *85* (17), 6571-6575.
121. Tsien, R. Y.; Zucker, R. S., Control of cytoplasmic calcium with photolabile tetracarboxylate 2-nitrobenzhydryl chelators. *Biophys. J.* **1986**, *50* (5), 843-853.
122. Zucker, R. S.; Haydon, P. G., Membrane potential has no direct role in evoking neurotransmitter release. *Nature* **1988**, *335* (6188), 360-362.
123. Mulkey, R. M.; Zucker, R. S., Action potentials must admit calcium to evoke transmitter release. *Nature* **1991**, *350* (6314), 153-155.
124. Thomas, P.; Surprenant, A.; Almers, W., Cytosolic Ca²⁺, exocytosis, and endocytosis in single melanotrophs of the rat pituitary. *Neuron* **1990**, *5* (5), 723-733.
125. Thomas, P.; Wong, J. G.; Almers, W., Millisecond studies of secretion in single rat pituitary cells stimulated by flash photolysis of caged Ca²⁺. *EMBO J.* **1993**, *12* (1), 303-306.
126. Thomas, P.; Wong, J. G.; Lee, A. K.; Almers, W., A low affinity Ca²⁺ receptor controls the final steps in peptide secretion from pituitary melanotrophs. *Neuron* **1993**, *11* (1), 93-104.
127. Heinemann, C.; Chow, R. H.; Neher, E.; Zucker, R. S., Kinetics of the secretory response in bovine chromaffin cells following flash photolysis of caged Ca²⁺. *Biophys. J.* **1994**, *67* (6), 2546-2557.
128. Heidelberger, R.; Heinemann, C.; Neher, E.; Matthews, G., Calcium dependence of the rate of exocytosis in a synaptic terminal. *Nature* **1994**, *371* (6497), 513-515.

129. DelPrincipe, F.; Egger, M.; Ellis-Davies, G. C. R.; Niggli, E., Two-photon and UV-laser flash photolysis of the Ca²⁺-cage, dimethoxynitrophenyl-EGTA-4. *Cell Calcium* **1999**, *25* (1), 85-91.
130. Adams, S. R.; Lec-Ram, V.; Tsien, R. Y., A new caged Ca²⁺, azid-1, is far more photosensitive than nitrobenzyl-based chelators. *Chem. Biol.* **1997**, *4* (11), 867-878.
131. Momotake, A.; Lindegger, N.; Niggli, E.; Barsotti, R. J.; Ellis-Davies, G. C., The nitrodibenzofuran chromophore: a new caging group for ultra-efficient photolysis in living cells. *Nat. Meth.* **2006**, *3* (1), 35-40.
132. Walker, J. W.; Somlyo, A. V.; Goldman, Y. E.; Somlyo, A. P.; Trentham, D. R., Kinetics of smooth and skeletal muscle activation by laser pulse photolysis of caged inositol 1,4,5-trisphosphate. *Nature* **1987**, *327* (6119), 249-252.
133. Li, W.-h.; Llopis, J.; Whitney, M.; Zlokarnik, G.; Tsien, R. Y., Cell-permeant caged InsP3 ester shows that Ca²⁺ spike frequency can optimize gene expression. *Nature* **1998**, *392* (6679), 936-941.
134. Sarkisov, D. V.; Wang, S. S.-H., Order-Dependent Coincidence Detection in Cerebellar Purkinje Neurons at the Inositol Trisphosphate Receptor. *J. Neurosci.* **2008**, *28* (1), 133-142.
135. Kato, N.; Isomura, Y.; Tanaka, T., Intracellular calcium releases facilitate induction of long-term depression. *Neuropharmacol.* **2000**, *39* (6), 1107-1110.
136. Doi, T.; Kuroda, S.; Michikawa, T.; Kawato, M., Inositol 1,4,5-Trisphosphate-Dependent Ca²⁺ Threshold Dynamics Detect Spike Timing in Cerebellar Purkinje Cells. *J. Neurosci.* **2005**, *25* (4), 950-961.
137. Kantevari, S.; Buskila, Y.; Ellis-Davies, G. C. R., Synthesis and characterization of cell-permeant 6-nitrodibenzofuranyl-caged IP3. *Photochem. Photobiol. Sci.* **2012**, *11* (3), 508-513.
138. Crowe, S. E.; Kantevari, S.; Ellis-Davies, G. C. R., Photochemically Initiated Intracellular Astrocytic Calcium Waves in Living Mice Using Two-Photon Uncaging of IP3. *ACS Chem. Neurosci.* **2010**, *1* (8), 575-585.
139. Stutzmann, G. E.; Caccamo, A.; LaFerla, F. M.; Parker, I., Dysregulated IP3 Signaling in Cortical Neurons of Knock-In Mice Expressing an Alzheimer's-Linked Mutation in Presenilin1 Results in Exaggerated Ca²⁺ Signals and Altered Membrane Excitability. *J. Neurosci.* **2004**, *24* (2), 508-513.
140. Muralidharan, S.; Nerbonne, J. M., Photolabile "caged" adrenergic receptor agonists and related model compounds. *J. Photochem. Photobiol., B* **1995**, *27* (2), 123-137.
141. Breiting, H.-G. A.; Wieboldt, R.; Ramesh, D.; Carpenter, B. K.; Hess, G. P., Synthesis and Characterization of Photolabile Derivatives of Serotonin for Chemical Kinetic Investigations of the Serotonin 5-HT₃ Receptor†. *Biochem.* **2000**, *39* (18), 5500-5508.
142. Breiting, H.-G. A.; Geetha, N.; Hess, G. P., Inhibition of the Serotonin 5-HT₃ Receptor by Nicotine, Cocaine, and Fluoxetine Investigated by Rapid Chemical Kinetic Techniques†. *Biochem.* **2001**, *40* (28), 8419-8429.
143. Lee, T. H.; Gee, K. R.; Ellinwood, E. H.; Seidler, F. J., Combining 'caged-dopamine' photolysis with fast-scan cyclic voltammetry to assess dopamine

- clearance and release autoinhibition in vitro. *J. Neurosci. Meth.* **1996**, *67* (2), 221-231.
144. Lee, T. H.; Gee, K. R.; Davidson, C.; Ellinwood, E. H., Direct, real-time assessment of dopamine release autoinhibition in the rat caudate-putamen. *Neurosci.* **2002**, *112* (3), 647-654.
145. Araya, R.; Andino-Pavlovsky, V.; Yuste, R.; Etchenique, R., Two-Photon Optical Interrogation of Individual Dendritic Spines with Caged Dopamine. *ACS Chem. Neurosci.* **2013**, *4* (8), 1163-1167.
146. Sjulson, L.; Miesenböck, G., Photocontrol of Neural Activity: Biophysical Mechanisms and Performance in Vivo. *Chem. Rev.* **2008**, *108* (5), 1588-1602.
147. Caterina, M. J.; Schumacher, M. A.; Tominaga, M.; Rosen, T. A.; Levine, J. D.; Julius, D., The capsaicin receptor: a heat-activated ion channel in the pain pathway. *Nature* **1997**, *389* (6653), 816-824.
148. Zemelman, B. V.; Nesnas, N.; Lee, G. A.; Miesenböck, G., Photochemical gating of heterologous ion channels: Remote control over genetically designated populations of neurons. *Proc. Natl. Acad. Sci. U. S. A.* **2003**, *100* (3), 1352-1357.
149. (a) Gilbert, D.; Funk, K.; Dekowski, B.; Lechler, R.; Keller, S.; Möhrlein, F.; Frings, S.; Hagen, V., Caged Capsaicins: New Tools for the Examination of TRPV1 Channels in Somatosensory Neurons. *ChemBioChem* **2007**, *8* (1), 89-97; (b) Van Ryssen, M. P.; Avlonitis, N.; Giniatullin, R.; McDougall, C.; Carr, J. L.; Stanton-Humphreys, M. N.; Borgstrom, E. L. A.; Brown, C. T. A.; Fayuk, D.; Surin, A.; Niittykoski, M.; Khiroug, L.; Conway, S. J., Synthesis, photolysis studies and in vitro photorelease of caged TRPV1 agonists and antagonists. *Org. Biomol. Chem.* **2009**, *7* (22), 4695-4707; (c) Carr, J. L.; Wease, K. N.; Van Ryssen, M. P.; Paterson, S.; Agate, B.; Gallagher, K. A.; Brown, C. T. A.; Scott, R. H.; Conway, S. J., In vitro photo-release of a TRPV1 agonist. *Bioorg. Med. Chem. Lett.* **2006**, *16* (1), 208-212.
150. Zhao, J.; Gover, T. D.; Muralidharan, S.; Auston, D. A.; Weinreich, D.; Kao, J. P. Y., Caged Vanilloid Ligands for Activation of TRPV1 Receptors by 1- and 2-Photon Excitation†. *Biochem.* **2006**, *45* (15), 4915-4926.
151. Fenno, L.; Yizhar, O.; Deisseroth, K., The Development and Application of Optogenetics. *Annu. Rev. Neurosci.* **2011**, *34* (1), 389-412.
152. Hatanaka, Y.; Sadakane, Y., Photoaffinity labeling in drug discovery and developments: chemical gateway for entering proteomic frontier. *Curr. Top. Med. Chem.* **2002**, *2* (3), 271-288.
153. Demchenko, A. P., Advanced Fluorescence Reporters in Chemistry and Biology III. Demchenko, A. P., Ed. Springer Berlin Heidelberg: 2011; pp. 1-352.
154. Mayer, G.; Heckel, A., Biologically Active Molecules with a "Light Switch". *Angew. Chem., Int. Ed.* **2006**, *45* (30), 4900-4921.
155. Kiskin, N.; Chillingworth, R.; McCray, J.; Piston, D.; Ogden, D., The efficiency of two-photon photolysis of a "caged" fluorophore, o-1-(2-nitrophenyl)ethylpyranine, in relation to photodamage of synaptic terminals. *Eur. Biophys. J.* **2002**, *30* (8), 588-604.
156. Davis, M. J.; Kragor, C. H.; Reddie, K. G.; Wilson, H. C.; Zhu, Y.; Dore, T. M., Substituent Effects on the Sensitivity of a Quinoline Photoremovable Protecting

- Group to One- and Two-Photon Excitation. *J. Org. Chem.* **2009**, *74* (4), 1721-1729.
157. Rea, Adam C.; Vandenberg, Laura N.; Ball, Rebecca E.; Snouffer, Ashley A.; Hudson, Alicia G.; Zhu, Y.; McLain, Duncan E.; Johnston, Lindsey L.; Lauderdale, James D.; Levin, M.; Dore, Timothy M., Light-Activated Serotonin for Exploring Its Action in Biological Systems. *Chem. Biol.* **2013**, *20* (12), 1536-1546.
158. Venken, K. J.; Bellen, H. J., Emerging technologies for gene manipulation in *Drosophila melanogaster*. *Nat. Rev. Genet.* **2005**, *6* (3), 167-178.
159. Scott, K.; Brady Jr, R.; Cravchik, A.; Morozov, P.; Rzhetsky, A.; Zuker, C.; Axel, R., A Chemosensory Gene Family Encoding Candidate Gustatory and Olfactory Receptors in *Drosophila*. *Cell* **2001**, *104* (5), 661-673.
160. Vosshall, L. B.; Wong, A. M.; Axel, R., An olfactory sensory map in the fly brain. *Cell* **2000**, *102* (2), 147-159.
161. Wright, N. J., Evolution of the techniques used in studying associative olfactory learning and memory in adult *Drosophila* in vivo: a historical and technical perspective. *Invert. Neurosci.* **2013**, 1-11.
162. Farooqui, T., Review of octopamine in insect nervous systems. *Open Access Insect Physiol.* **2012**, *4*, 1-17.
163. Tse, M. T., Reward: Finding the paths to food reward. *Nat. Rev. Neurosci.* **2012**, *13* (12), 816-817.
164. Fedoryak, O. D.; Dore, T. M., Brominated Hydroxyquinoline as a Photolabile Protecting Group with Sensitivity to Multiphoton Excitation. *Org. Lett.* **2002**, *4* (20), 3419-3422.
165. Chou, C.; Young, D. D.; Deiters, A., Photocaged T7 RNA Polymerase for the Light Activation of Transcription and Gene Function in Pro-and Eukaryotic Cells. *ChemBioChem* **2010**, *11* (7), 972-977.
166. Sivik, M. R., Cesium Carbonate. In *Encyclopedia of Reagents for Organic Synthesis*, John Wiley & Sons, Ltd: 2001.
167. Marshall, C., Specificity of receptor tyrosine kinase signaling: transient versus sustained extracellular signal-regulated kinase activation. *Cell* **1995**, *80* (2), 179-185.
168. Sato, K.; Akaishi, T.; Matsuki, N.; Ohno, Y.; Nakazawa, K., β -Estradiol induces synaptogenesis in the hippocampus by enhancing brain-derived neurotrophic factor release from dentate gyrus granule cells. *Brain Res.* **2007**, *1150*, 108-120.
169. Foy, M. R.; Henderson, V. W.; Berger, T. W.; Thompson, R. F., Estrogen and neural plasticity. *Curr. Dir. Psych. Sci.* **2000**, *9* (5), 148-152.
170. Yamamoto, K. R., Steroid receptor regulated transcription of specific genes and gene networks. *Annu. Rev. Genet.* **1985**, *19* (1), 209-252.
171. Rea, A. C. The Synthesis and Characterization of a Series of Caged Neurotransmitters with Two-Photon Sensitivity for Use In Vivo. University of Georgia, Athens, GA, 2011.
172. Bagdy, G.; Kecskemeti, V.; Riba, P.; Jakus, R., Serotonin and epilepsy. *J. Neurochem.* **2007**, *100* (4), 857-873.
173. Schaal, J.; Dekowski, B.; Wiesner, B.; Eichhorst, J.; Marter, K.; Vargas, C.; Keller, S.; Eremina, N.; Barth, A.; Baumann, A.; Eisenhardt, D.; Hagen, V.,

- Coumarin-Based Octopamine Phototrigger and their Effects on an Insect Octopamine Receptor. *ChemBioChem* **2012**, *13* (10), 1458-1464.
174. Russell, A. G.; Sadler, M. J.; Laidlaw, H. J.; Gutierrez-Loriente, A.; Wharton, C. W.; Carteau, D.; Bassani, D. M.; Snaith, J. S., Photorelease of tyrosine from [small alpha]-carboxy-6-nitroveratryl ([small alpha]CNV) derivatives. *Photochem. Photobiol. Sci.* **2012**, *11* (3), 556-563.
175. Ma, J.; Rea, A. C.; An, H.; Ma, C.; Guan, X.; Li, M.-D.; Su, T.; Yeung, C. S.; Harris, K. T.; Zhu, Y.; Nganga, J. L.; Fedoryak, O. D.; Dore, T. M.; Phillips, D. L., Unraveling the Mechanism of the Photodeprotection Reaction of 8-Bromo- and 8-Chloro-7-hydroxyquinoline Caged Acetates. *Chem. Eu. J.* **2012**, *18* (22), 6854-6865.
176. Szwarc, M.; Williams, D., Studies of the Variations in Bond Dissociation Energies of Aromatic Compounds. II. Substituted Bromobenzenes. *Proc. R. Soc. London, Ser. A* **1953**, *219* (1138), 353-366.
177. Ma, J.; Cheng, S. C.; An, H.; Li, M. D.; Ma, C.; Rea, A. C.; Zhu, Y.; Nganga, J. L.; Dore, T. M.; Phillips, D. L., Comparison of the absorption, emission, and resonance Raman spectra of 7-hydroxyquinoline and 8-bromo-7-hydroxyquinoline caged acetate. *J. Phys. Chem. A* **2011**, *115* (42), 11632-11640.
178. Arias-Carrión, O.; Stamelou, M.; Murillo-Rodríguez, E.; Menéndez-González, M.; Pöppel, E., Dopaminergic reward system: a short integrative review. *Int. Arch. Med.* **2010**, *3*, 24.
179. Fu, Y.; Westenbroek, R. E.; Scheuer, T.; Catterall, W. A., Phosphorylation sites required for regulation of cardiac calcium channels in the fight-or-flight response. *Proc. Natl. Acad. Sci. U. S. A.* **2013**, *110* (48), 19621-19626.
180. Levy, M. N., Brief Reviews: Sympathetic-Parasympathetic Interactions in the Heart. *Circ. Res.* **1971**, *29* (5), 437-445.
181. Reaven, G. M.; Lithell, H.; Landsberg, L., Hypertension and associated metabolic abnormalities--the role of insulin resistance and the sympathoadrenal system. *N. Engl. J. Med.* **1996**, *334* (6), 374-381.
182. Cahill, L.; Gorski, L.; Le, K., Enhanced Human Memory Consolidation With Post-Learning Stress: Interaction With the Degree of Arousal at Encoding. *Learn. Mem.* **2003**, *10* (4), 270-274.
183. Toth, M.; Ziegler, M.; Sun, P.; Gresack, J.; Risbrough, V., Impaired conditioned fear response and startle reactivity in epinephrine-deficient mice. *Behav. Pharmacol.* **2013**, *24* (1), 1-9.
184. Bley, F.; Schaper, K.; Görner, H., Photoprocesses of Molecules with 2-Nitrobenzyl Protecting Groups and Caged Organic Acids. *Photochem. Photobiol.* **2008**, *84* (1), 162-171.
185. McCray, J. A.; Trentham, D. R., Properties and Uses of Photoreactive Caged Compounds. *Annu. Rev. Biophys. Biophys. Chem.* **1989**, *18* (1), 239-270.
186. Salierno, M.; Marceca, E.; Peterka, D. S.; Yuste, R.; Etchenique, R., A fast ruthenium polypyridine cage complex photoreleases glutamate with visible or IR light in one and two photon regimes. *J. Inorg. Biochem.* **2010**, *104* (4), 418-422.
187. Franks, K. M.; Stevens, C. F.; Sejnowski, T. J., Independent Sources of Quantal Variability at Single Glutamatergic Synapses. *J. Neurosci.* **2003**, *23* (8), 3186-3195.

188. Fernández, C.; Nieto, O.; Rivas, E.; Montenegro, G.; Fontenla, J. A.; Fernández-Mayoralas, A., Synthesis and biological studies of glycosyl dopamine derivatives as potential antiparkinsonian agents. *Carbohydr. Res.* **2000**, 327 (4), 353-365.
189. Fino, E.; Araya, R.; Peterka, D. S.; Salierno, M.; Etchenique, R.; Yuste, R., RuBi-Glutamate: Two-photon and visible-light photoactivation of neurons and dendritic spines. *Front. Neural Circuits* **2009**, 3.
190. Mol, N. J. d.; Henegouwen, G. M. J. B. v.; Gerritsma, K. W., Photochemical Decomposition of Catecholamines. The Extent of Aminochrome Formation from Adrenaline, Isoprenaline, and Noradrenaline induced by Ultraviolet Light. *Photochem. Photobiol. Sci.* **1979**, 29 (3), 479-482.
191. Mattok, G. L.; Heacock, R. A., A Simple Preparation of 5,6-Dihydroxy-N-methylindole. *Can. J. Chem.* **1964**, 42 (2), 484-485.
192. Anderson, R.; Brimble, M.; Brimble, M. A.; Nairn, M. R.; Packerá, J. E.; Nairn, M.; Packer, J., Reactions of semiquinones in aqueous solution. A comparison of the one electron reduction of kalafungin and analogues with other semiquinones using pulse radiolysis. *J. Chem. Soc., Perkin Trans. 2* **1999**, (3), 475-480.
193. Wang, L.; Bai, J.; Huang, P.; Wang, H.; Zhang, L.; Zhao, Y., Electrochemical Behavior and Determination of Epinephrine at a Penicillamine Self-assembled Gold Electrode. *Int. J. Electrochem. Sci* **2006**, 1, 238-249.
194. Hatchard, C.; Parker, C. A., A new sensitive chemical actinometer. II. Potassium ferrioxalate as a standard chemical actinometer. *Proc. R. Soc. London, Ser. A* **1956**, 235 (1203), 518-536.
195. Parker, C.; Rees, W., Fluorescence spectrometry. A review. *Analyst* **1962**, 87 (1031), 83-111.

Appendix A: Synthesis of a Warhead Free Acyloxy Methyl Ketone (AOMK)

Post-translational modification is a process of enzyme maturation where a protein is translated from RNA in an inactive form and further modifications render it biologically active. In some cases the modification serves to remove some inhibitory functionality, and in others it enables proper cellular localization.¹ In situations where directly targeting a protein of interest is unfeasible, these post-translational modification steps may be considered as potential targets for drug development.²

One particular target is the Ras GTPase, a membrane bound signaling protein, found on the cytosolic side of the cell membrane.³ Ras function has been observed to modulate the MEK/ERK pathway,⁴ MAP kinase cascades,⁵ mTOR 1 signaling,⁶ and cyclin dependent kinases.⁷ When regarding the wide variety of signaling pathways Ras is involved in, it is no surprise that modulation of Ras activity is an intriguing target for cancer therapy. In fact mutations in any one of the three isoforms of Ras, H-Ras, N-Ras, and K-Ras, have been implicated in 20% - 30% of all human cancers.⁸ Unfortunately efforts to target the active site of Ras have been complicated by the high concentration of its endogenous ligands GTP and GDP.⁹

Since direct targeting of Ras is unlikely to be successful, research shifted to indirectly modulating Ras activity. One potential indirect target is the Ras GTPase activating protein (GAP), which increases the rate of GTP hydrolysis and correspondingly decreases Ras activity.¹⁰ Another potential series of targets are the three proteins involved in Ras maturation: farnesyl transferase, which appends a lipid onto a cysteine located on the C-terminal end of Ras, Ras converting enzyme (Rce1p), which

cleaves off the last three amino acids of the C-termini, and isoprenylated cysteine methyl transferase (ICMT) which methylates the new C-terminal cysteine.³

Farnesyl transferase is a cytosolic protein with a solved crystal structure,¹¹ and as such has received the most interest as a potential drug target.¹² Farnesyl transferase inhibitors (FTIs) have shown some success in treating H-Ras related cancers,¹³ N-Ras and K-Ras related cancers have shown to be resistant due to an alternative isoprenylation enzyme geranylgeranyl transferase.¹⁴ ICMT is another potential therapeutic target, with ICMT inhibition slowly growing in interest.¹⁵

Rce1p is the final potential target on the Ras maturation pathway and was chosen for its selectivity toward Ras over other members of the small GTPase family of proteins, such as Rho or Rheb,² and for its demonstrated ability to modulate Ras activity.¹⁶

AOMKs have demonstrated an ability to inhibit Rce1p.¹⁷ So to probe the efficacy of this system, a series of AOMKs were synthesized in the Dore lab (Figure 51), and tested in a fluorescence based proteolysis assay. The most potent contained the –OBn protected phenylalanine – arginine dipeptide sequence.

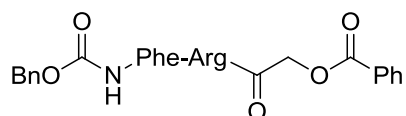
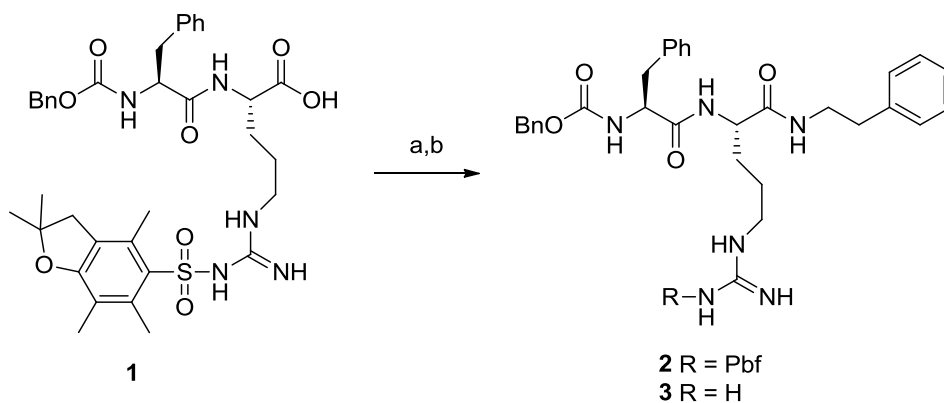


Figure 51 Representative AOMK

To determine whether the AOMK moiety was being displaced and inhibition was occurring through irreversible inactivation of Rce1p, a “warhead free” analogue **3** lacking the AOMK functionality was synthesized (Figure 52). Compound **1** was synthesized in two steps, first coupling the phenethylamine functionality with HOBt and HBTU in DCM

to provide **2**, followed by deprotection of the Pbf group with TFA in water and HPLC purification to provide the desired compound **3**.



Reagents and Conditions: (a) HOBt, HBTU, DIPEA, CH₂Cl₂, 0 °C, then rt overnight, 39%;
(b) TFA/H₂O, 0 °C, 2 h, 33%

Figure 52 Synthesis of warhead free AOMK

The synthesized compound **3** was tested in the same fluorescence based proteolysis assay and exhibited similar levels of inhibition against Rce1p indicating that the inhibition observed was not due to an irreversible binding of the AOMKs to Rce1p.¹⁸

References

1. Basso, A. D., Kirschmeier, P., Bishop, W. R., Thematic review series: lipid posttranslational modifications. Farnesyl transferase inhibitors. *J. Lipid Res.* **2006**, *47*, 15-31.
2. Konstantinopoulos, P. A., Karamouzis, M. V., Papavassiliou, A. G., Post-translational modifications and regulation of the RAS superfamily of GTPases as anticancer targets. *Na. Rev. Drug Disc.* **2007**, *6*, 541-555.
3. Wright, L. P., Philips, M. R., Thematic review series: Lipid Posttranslational Modifications CAAX modification and membrane targeting of Ras. *J. Lipid Res.* **2006**, *47*, 883-891.
4. Kolch, W., Meaningful relationships: the regulation of the Ras/Raf/MEK/ERK pathway by protein interactions. *Biochem. J.* **2000**, *351*, 289-305.
5. Xing, J., Ginty, D. D., Greenberg, M. E., Coupling of the RAS-MAPK pathway to gene activation by RSK2, a growth factor-regulated CREB kinase. *Science.* **1996**, *273*, 959-963.
6. Bodine, S. C., Stitt, T. N., Gonzalez, M., Kline, W. O., Stover, G. L., Bauerlein, R., Zlotchenko, E., Scrimgeour, A., Lawrence, J. C., Glass, D. J., Akt/mTOR pathway is a crucial regulator of skeletal muscle hypertrophy and can prevent muscle atrophy in vivo. *Nat. Cell Biol.* **2001**, *3*, 1014-1019.
7. Leone, G., DeGregori, J., Sears, R., Jakoi, L., Nevins, J. R., Myc and Ras collaborate in inducing accumulation of active cyclin E/Cdk2 and E2F. *Nature.* **1997**, *387*, 422-426.
8. Mascaux, C., Iannino, N., Martin, B., Paesmans, M., Berghmans, T., Dusart, M., Haller, A., Lothaire, P., Meert, A.-P., Noël, S., The role of RAS oncogene in survival of patients with lung cancer: a systematic review of the literature with meta-analysis. *Brit. J. Cancer.* **2004**, *92*, 131-139.
9. Schlichting, I., Almo, S. C., Rapp, G., Wilson, K., Petratos, K., Lentfer, A., Wittinghofer, A., Kabsch, W., Pai, E. F., Petsko, G. A., Time-resolved X-ray crystallographic study of the conformational change in Ha-Ras p21 protein on GTP hydrolysis. *Nature.* **1990**, *345*, 309-315.
10. Bos, J. L., Rehmann, H., Wittinghofer, A., GEFs and GAPs: critical elements in the control of small G proteins. *Cell.* **2007**, *129*, 865-877.
11. Park, H.-W., Boduluri, S. R., Moomaw, J. F., Casey, P. J., Beese, L. S., Crystal structure of protein farnesyltransferase at 2.25 angstrom resolution. *Science.* **1997**, *275*, 1800-1805.
12. Rowinsky, E. K., Windle, J. J., Von Hoff, D. D., Ras prote in farnesyltransferase: a strategic target for anticancer therapeutic development. *J. Clinical Oncology.* **1999**, *17*, 3631-3652.
13. Sun, J., Qian, Y., Hamilton, A. D., Sebti, S. M., Both farnesyltransferase and geranylgeranyltransferase I inhibitors are required for inhibition of oncogenic K-Ras prenylation but each alone is sufficient to suppress human tumor growth in nude mouse xenografts. *Oncogene.* **1998**, *16*, 1467.
14. Lerner, E. C., Zhang, T.-T., Knowles, D. B., Qian, Y., Hamilton, A. D., Sebti, S. M., Inhibition of the prenylation of K-Ras, but not H-or N-Ras, is highly resistant to CAAX peptidomimetics and requires both a farnesyltransferase and a

- geranylgeranyltransferase I inhibitor in human tumor cell lines. *Oncogene*. **1997**, *15*, 1283-1288.
15. Bergo, M. O, Gavino, B. J, Hong, C, Beigneux, A. P, McMahon, M, Casey, P. J, Young, S. G., Inactivation of Icm1 inhibits transformation by oncogenic K-Ras and B-Raf. *J. Clinical Investigation*. **2004**, *113*, 539-550
 16. Kim, E, Ambroziak, P, Otto, J. C, Taylor, B, Ashby, M, Shannon, K, Casey, P. J, Young, S. G., Disruption of the mouse Rce1 gene results in defective Ras processing and mislocalization of Ras within cells. *J. Biol. Chem*. **1999**, *274*, 8383-8390.
 17. Porter, S. B., Hildebrandt, E. R., Breevoort, S. R., Mokry, D. Z., Dore, T. M., & Schmidt, W. K Inhibition of the CaaX proteases Rce1p and Ste24p by peptidyl (acyloxy) methyl ketones. *Biochim. Biophys. Acta* **2007**, *1773*, 853-862.
 18. Dechert, A. M. R., MacNamara, J. P., Breevoort, S. R., Hildebrandt, E. R., Hembree, N. W., Rea, A. C., Mclain, D. E., Porter, S. B., Schmidt, W. K., Dore, T. M.. Modulation of the inhibitor properties of dipeptidyl (acyloxy) methyl ketones toward the CaaX proteases. *Bioorg. Med. Chem*. **2010** *18*, 6230-6237.

Appendix B: Toward the Optimization of the Synthesis of CyHQ

Optimization of HQ

Due to import restrictions on certain chemicals in the United Arab Emirates, our lab was missing one of the key reagents^{xlix} necessary to begin synthesis of the quinoline scaffold **1** (Figure 53). So to address this issue alternative reagents were investigated.

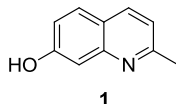


Figure 53 Caging Scaffold

The condensation of pyruvic acid, 3-aminophenol, and acetaldehyde provided the desired 4-carboxy intermediate **2**,¹ but thermal decarboxylation ultimately failed (Figure 54).

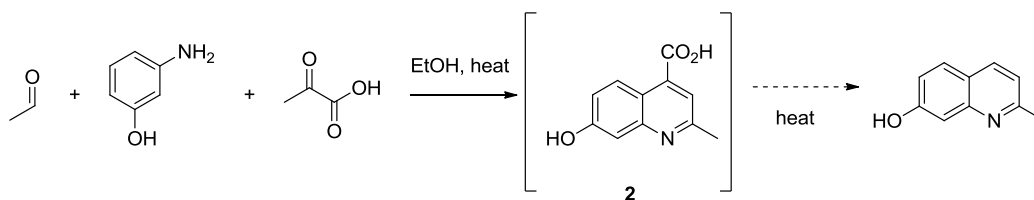


Figure 54 Alternative HQ attempts

Acetaldehyde can undergo a self condensation reaction to form crotonaldehyde, so forming **1** with *in situ* generation of crotonaldehyde was investigated using traditional Skraup quinoline synthesis conditions (Figure 55). The material generated contained a significant number of impurities, most prominently what is likely a polyphenolic

^{xlix}Crotonaldehyde has a greater than 6 month lead time for shipping, and there have been recurrent problems with various suppliers in delivering on time

¹Compound verified by LCMS

species,^{li} however it was deemed pure enough for the moment for downstream chemistry.^{liii}

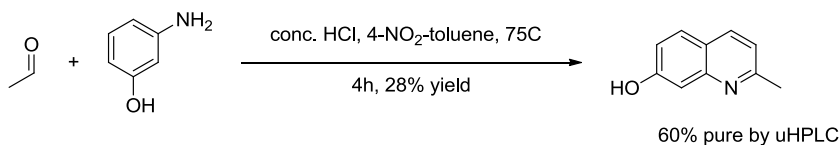


Figure 55 HQ formation from acetaldehyde

4-Nitrotoluene was removed from the reaction conditions in an effort to reduce the impurity profile,^{liii} and due to a pronounced exotherm^{liv} upon the addition of acetaldehyde to the reaction mixture, catalytic HCl was used. These changes slightly increased the overall purity of the product mixture (~50% purity) and reduced difficulty of workup. After a six month delay work could resume with crotonaldehyde,^{lv} and in the hands of a coworker, the synthesis of **1** was solved.^{lvi}

Optimization of CyHQ

According to established protocols at the time, synthesis of CyHQ was a four step process (Figure 56):^{lvii} first a Reimer-Tiemann reaction formylated C-8 of **1** provided intermediate **3**, next condensation with hydroxylamine gave intermediate **4**, followed by the activation with acetic anhydride gave intermediate **5**, and elimination of the acetate with base gave the desired compound **6** in very poor overall yield.^{lviii}

^{li} Based on broad peaks in both LCMS and uHPLC as well as in H NMR

^{liii} Anything of greater than 40% purity by uHPLC was at the time deemed sufficient, due to the requirements of generating the desired final targets

^{liii} 4-Nitrotoluene acts as an oxidant of the intermediate dihydroxyquinoline, but in my hands didn't oxidize sufficiently quickly to be considered useful

^{liv} Exotherm increase from 25°C to 57°C upon addition of acetaldehyde to a stirred solution of 3-aminophenol in conc. HCl

^{lv} Crotonaldehyde is preferable due to the decreased reactivity relative to acetaldehyde

^{lvi} Magnus Widegren put forth considerable effort optimizing the reaction conditions and considerably more effort in optimizing the isolation of pure HQ

^{lvii} Matt O'Conner was primarily responsible for the optimization of this one-pot protocol.

^{lviii} In my hands the four step process resulted in less than 1% of the desired CyHQ

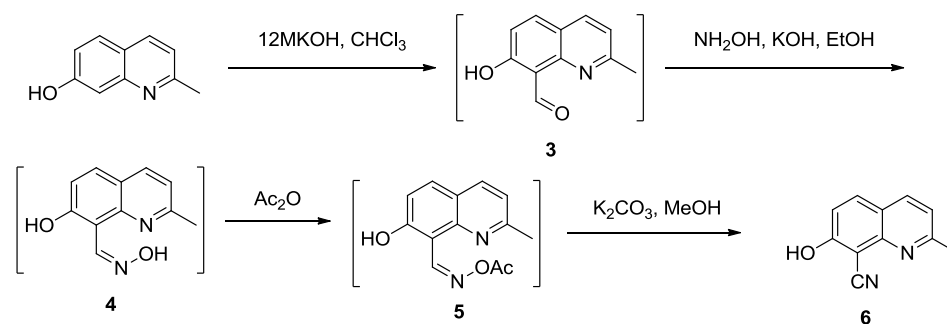


Figure 56 Original CyHQ formation

The Reimer-Tiemann reaction involved extensive gas formation, and the reaction had a tendency to explode out of the top of the condenser, so an alternative reaction would be desirable. The Duff reaction^{lix} is an alternative formylation reaction that uses hexamethyltetraamine (HMTA) as the formyl source. However, regardless of the acid used,^{lix} no conversion to product was observed. There was an initial investigation into potential metal-mediated cross-coupling of BHQ with a cyanide source to generate CyHQ directly,^{lxi} however these investigations were undertaken in DMF and only debromination of the starting material was observed.

Our transition to Abu Dhabi brought with it a great increase in synthetic chemistry experience and access to equipment that hadn't been readily available at the University of Georgia.^{lxii} With these improvements the cross-coupling was investigated in a microwave reactor with dimethylacetamide as a solvent (Figure 57).^{lxiii} LCMS verified that the desired compound **6** was formed, in ~10% yield.

^{lix} Proposed by Magnus Widegren

^{lx} Acetic acid, trifluoroacetic acid, and triflic acid were all used

^{lxi} Matt O'Conner was responsible for the initial investigations as well as the observation of debromination in all of his experiments.

^{lxii} Notably a microwave reactor and quick access to LCMS capabilities

^{lxiii} Boiling point of 165°C vs. the boiling point of DMF 132°C

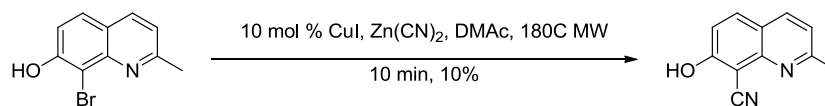


Figure 57 Microwave formation of CyHQ

This led to further investigations, and it was found that cyanation occurred regardless of the cyanide source used,^{lxiv} however the best results were observed when CuCN was used.^{lxv} With the base conditions in hand alternative solvents for the Rosenmund-von Braun reaction were investigated,^{lxvi} DMAc proved to be the best choice. It was during these investigations that the isolation of BHQ changed, and the compound was isolated as a tosylate salt. Fortuitously it was observed that the temperature required for cyanation was reduced from ~180°C to 150°C. This temperature reduction proved invaluable for two reasons. First, the microwave reactor limited reactions to ~100 mg of BHQ at a time, and the temperature reduction allowed us to switch to refluxing DMAc at ambient pressure in a fume hood and increase to 10 g or larger reactions. The second reason was an observation, supported by attempting the cyanation reaction on a variety of BHQ substrates protected at the C-7 -OH^{lxvii} decreasing the electron density of the ring system decreased the extent of thermal debromination observed. This observation eventually led to the development of the current protocol regarding the synthesis of CyHQ. Compound **8** is cyanated via Rosenmund-von Braun conditions in good yield and with minimal^{lxviii} debromination observed by uHPLC.

^{lxiv} NaCN and K[Fe₂(CN)₆] worked with CuI

^{lxv} Yield increase from ~25% for catalytic systems and ~50% for CuCN

^{lxvi} Pyridine, N-methylmorpholine showed no conversion to product, while THF and xylenes showed less than 10% conversion to product

^{lxvii} Methoxymethyl ether protection was investigated by me while pivalate, acetate, and benzenesulphonyl protection were investigated by Magnus Widegren

^{lxviii} Less than 5%

Appendix C: Synthesis of BHQ-ATP Sodium Salt

BHQ-ATP **2** was previously synthesized in our lab from the corresponding phosphate **1** as the ammonium salt (Figure 58).^{lxi} This compound exhibited some dark activity due to the ammonium counter-ion having some neuroactivity, so a sodium salt of **2** that did not possess dark activity was desired.

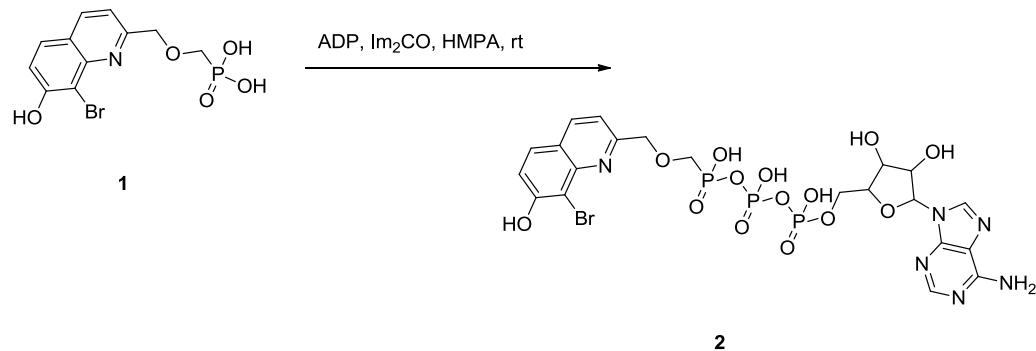


Figure 58 Synthesis of BHQ-ATP

Initial attempts at synthesis^{lxx} were complicated by difficulty in purifying **2**,^{lxxi} but eventually HPLC conditions were set utilizing a 100- μ M triethylammonium acetate (TEAA) buffer and methanol.^{lxxii} The method comprised a 20 minute isocratic portion (100% TEAA buffer) followed by a 50 minute ramp to 100% methanol.^{lxxiii} BHQ-ATP eluted at ~ 40 minutes,^{lxxiv} followed by **1**, and a number of unidentified side products.^{lxxv}

Dowex 50WX2 is a strong ion exchange resin that has a higher affinity for greasy cations than small hard cations. Preloading the resin with Na⁺ ions and then flushing through **2** as the triethylammonium salt swapped the cations, and gave **2** as the sodium

^{lxi} Synthesized by Yue Zhu

^{lxx} Reported isolated yield is 9.4%, however in my hands yields isolated yields were typically 2-4%

^{lxxi} Several batches of BHQ-ATP were consumed in unsuccessful attempts to purify **2**

^{lxxii} A full description of appropriate HPLC conditions and gradients came courtesy of a conversation with Yue Zhu

^{lxxiii} BHQ-ATP has a shoulder in the HPLC UV absorbance trace at 260 nm, this shoulder is not observed for any other products of this reaction

^{lxxiv} Variation in retention time is due to remaking the TEAA buffer after every run and small discrepancies in the exact buffer concentration

^{lxxv} Presumably BHQ-ADP, BHQ-AMP and other alternative phosphate couplings.

salt.^{lxxvi} This was confirmed by comparing the ¹H NMR spectra of the triethylammonium salt to that of the sodium salt (Figure 59)

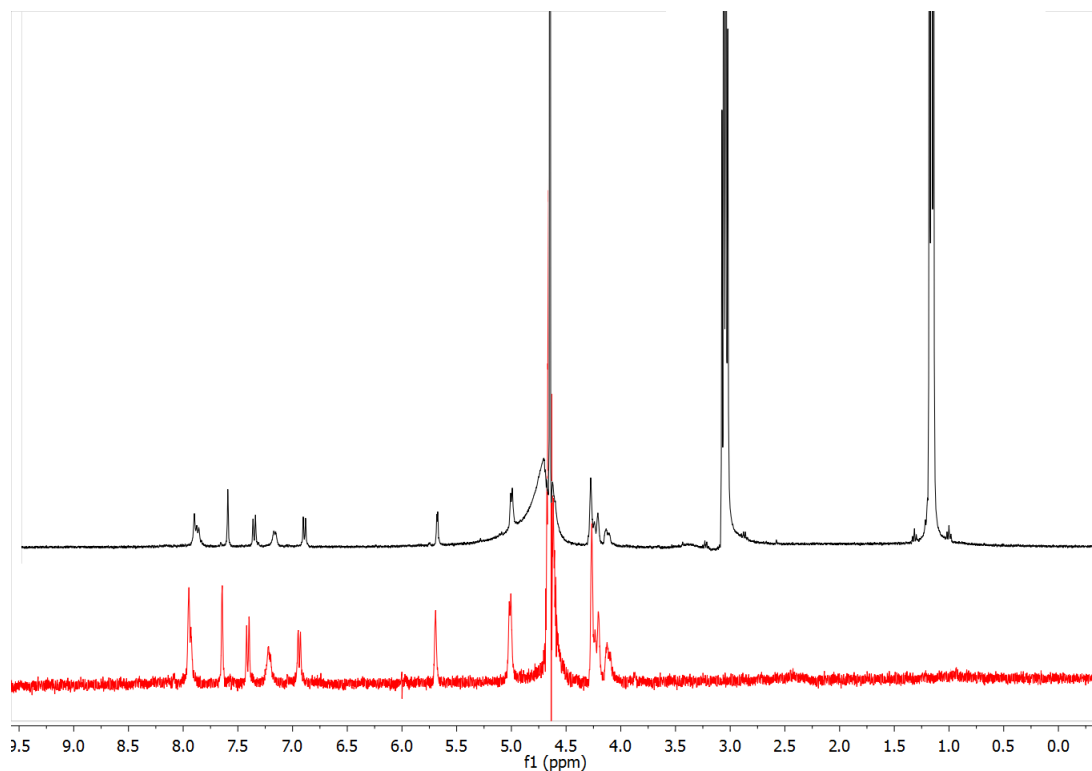


Figure 59 ¹H NMR in D₂O of BHQ-ATP TEA Salt (black) Na Salt (red)

The sodium salt of **2** was then utilized with 2PE to map P2X receptors on a hippocampal pyramidal neuron (Figure 60).^{lxxvii} A dendritic projection from the pyramidal neuron is outlined by a grid of red dots (left), each dot corresponds to a 2PE irradiation point, and to a corresponding electrophysiological readout from the pyramidal neuron (right). Irradiation only provides an electrophysiological response at two points on the upper right of the grid, thus providing a putative location for the P2X receptor.

^{lxxvi} 5 mg of BHQ-ATP as the sodium salt represents several months of synthesis and purification

^{lxxvii} Work done by Michael Tadross while in Richard Tsien's lab

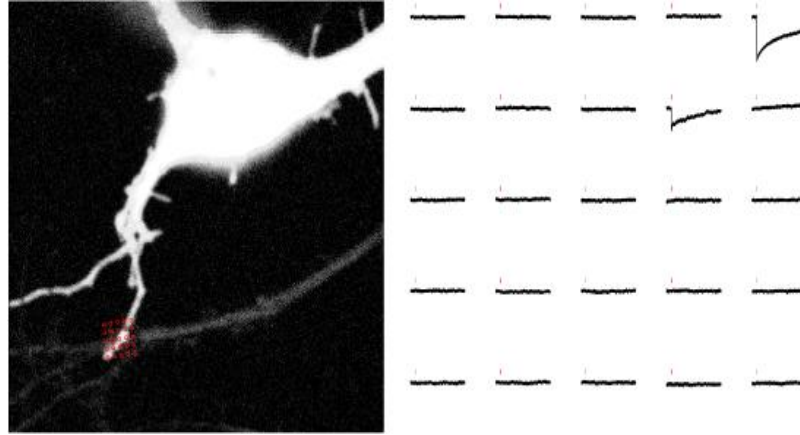


Figure 60 P2X receptor activation with BHQ-ATP, each red dot (left) corresponds to an electrophysiological response (right)

Appendix D: Synthesis of Human Ferrochelatase Ligand

Human Ferrochelatase (HFc) is the final step on the heme synthesis pathway, and is involved in metal chelation into protoporphyrin IX.¹ Studying the mechanism of ferrochelatase has been complicated due to the fact that the enzyme itself is linked to the interior membrane of the mitochondria, and is delivered the necessary substrates: ferrous iron and protoporphyrin IX by chaperone proteins.² This complication has been demonstrated by in vitro crystallography studies that show HFc to be efficient enough at chelating metals into the porphyrin ring to include almost all of the first row transition metals as well as lead and mercury among others.³

The proposed mechanism of HFc is insertion of the porphyrin ring into the active site of the enzyme, deprotonation of the porphyrin nitrogens followed by chelation of the metal into the center of the macrocycle, and finally product release.³ Crystallographic studies by Dr. Lanzilotta have shown that it is product release of the heme macrocycle that is the rate limiting step; this step involves the unwinding of a pi-helix and the corresponding opening of the active site to enable heme to be removed and transported elsewhere.⁴

One of the unresolved issues regarding the mechanism of HFc is which side of the porphyrin ring does the metal approach from. To address this issue, corrole **9** was synthesized according to published protocols (Figure 61).^{lxxviii} Since the corrole possesses a smaller macrocyclic structure than the corresponding porphyrin, it was hypothesized that the chelation mechanistic step would not fully occur. Crystallography

^{lxxviii} I picked up this project on somewhat short notice following a rearrangement of priorities precipitated by the departure of the graduate student that had originally been assigned the project.

experiments would then be able to determine on which side of the corrole the metal “sits” and thus an inference about which side of the ferrochelatase enzyme the iron is chaperoned in from.

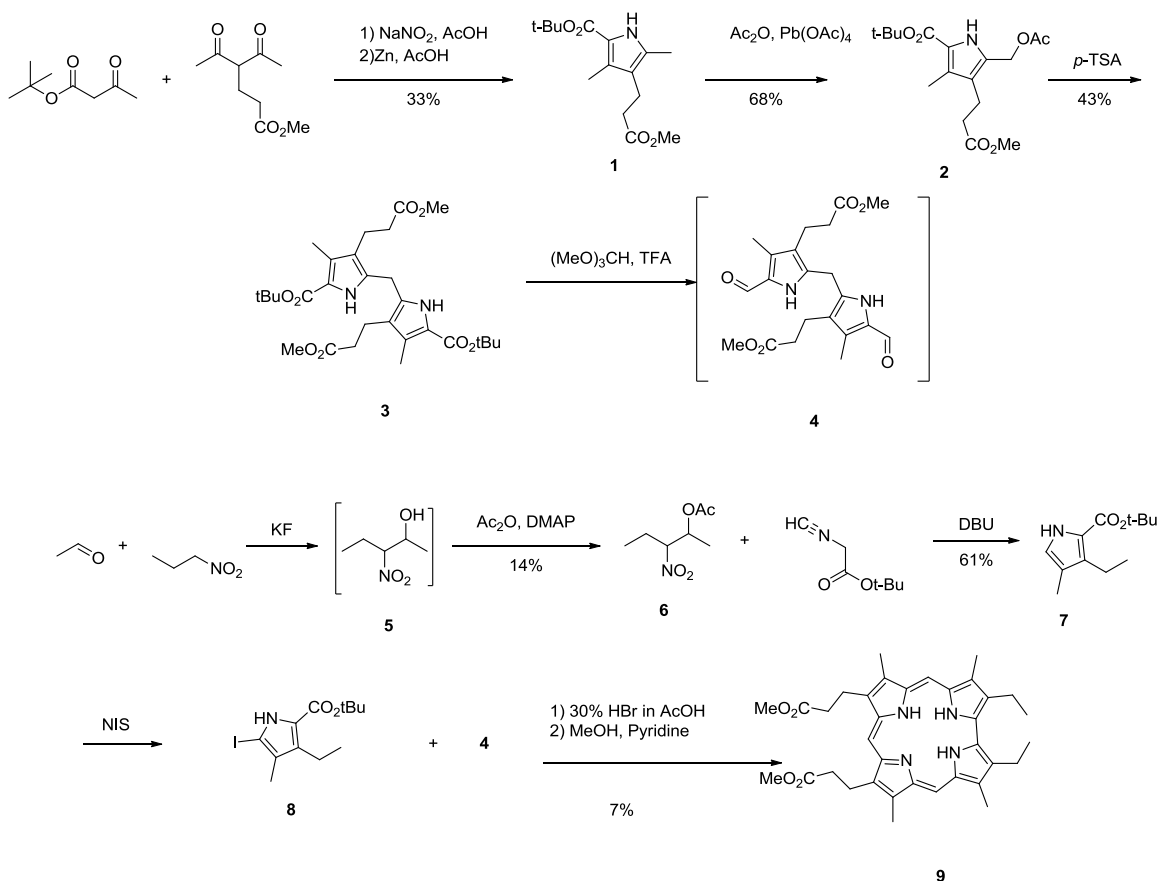


Figure 61 Synthesis of Corrole

Approximately 40 mg of the corrole was eventually synthesized, and I was offered the opportunity to perform some of the follow up biological experiments. So for a semester I attempted to co-crystallize the hFC protein with the corrole inside it, however, all attempts were unsuccessful.

References

1. Ajioka, R. S, Phillips, J. D, Kushner, J. P.: Biosynthesis of heme in mammals. *Biochim. Biophys. Acta.* **2006**, 1763, 723-736.
2. Medlock, A, Swartz, L, Dailey, T. A, Dailey, H. A, Lanzilotta, W. N.: Substrate interactions with human ferrochelatase. *Proc. Natl. Acad. Sci. U. S. A.* **2007**, 104, 1789-1793.
3. Dailey, H, Dailey, T, Wu, C.-K, Medlock, A, Rose, J, Wang, K.-F., Ferrochelatase at the millennium: structures, mechanisms and [2Fe-2S] clusters. *Cell. and Mol. Life Sci.* **2000**, 57, 1909-1926.
4. Medlock, A. E, Carter, M, Dailey, T. A, Dailey, H. A, Lanzilotta, W. N.: Product release rather than chelation determines metal specificity for ferrochelatase. *J. Mol. Bio.* **2009**, 393, 308-319.